



Développement et évaluation d'une plateforme vaccinale novatrice pour le traitement du mélanome

Solène Besson

► To cite this version:

Solène Besson. Développement et évaluation d'une plateforme vaccinale novatrice pour le traitement du mélanome. Biochimie, Biologie Moléculaire. Université Grenoble Alpes [2020-..], 2022. Français. NNT : 2022GRALV072 . tel-04054734

HAL Id: tel-04054734

<https://theses.hal.science/tel-04054734>

Submitted on 1 Apr 2023

HAL is a multi-disciplinary open access archive for the deposit and dissemination of scientific research documents, whether they are published or not. The documents may come from teaching and research institutions in France or abroad, or from public or private research centers.

L'archive ouverte pluridisciplinaire **HAL**, est destinée au dépôt et à la diffusion de documents scientifiques de niveau recherche, publiés ou non, émanant des établissements d'enseignement et de recherche français ou étrangers, des laboratoires publics ou privés.

THÈSE

Pour obtenir le grade de

DOCTEUR DE L'UNIVERSITÉ GRENOBLE ALPES

École doctorale : CSV- Chimie et Sciences du Vivant

Spécialité : Virologie - Microbiologie - Immunologie

Unité de recherche : Institut de Biologie Structurale

Développement et évaluation d'une plateforme vaccinale novatrice pour le traitement du mélanome

Development and evaluation of a novel vaccine platform for the treatment of melanoma

Présentée par :

Solène BESSON

Direction de thèse :

Pascal FENDER

DIRECTEUR DE RECHERCHE, Université Grenoble Alpes

Directeur de thèse

Rapporteurs :

Bernard VERRIER

DIRECTEUR DE RECHERCHE, CNRS délégation Rhône Auvergne

Karim BENIHOUUD

PROFESSEUR DES UNIVERSITES, Université Paris Sud

Thèse soutenue publiquement le **28 novembre 2022**, devant le jury composé de :

Pascal FENDER

DIRECTEUR DE RECHERCHE, CNRS délégation Alpes

Directeur de thèse

Bernard VERRIER

DIRECTEUR DE RECHERCHE, CNRS délégation Rhône Auvergne

Rapporteur

Karim BENIHOUUD

PROFESSEUR DES UNIVERSITES, Université Paris Sud

Rapporteur

Laurence CHAPEROT

Chercheur HDR, Etablissement Français du Sang

Examinatrice

Céline COLACIOS

MAITRE DE CONFERENCES HDR, Université Toulouse 3 - Paul Sabatier

Examinatrice

Franck FIESCHI

PROFESSEUR DES UNIVERSITES, Univeristé Grenoble Alpes

Président

TABLE DES MATIERES

REMERCIEMENTS.....	4
RESUME.....	8
ABSTRACT	10
ABREVIATIONS.....	12
LISTE DES FIGURES.....	15
LISTE DES TABLEAUX	16
CHAPITRE I : INTRODUCTION	17
I. Caractéristiques du mélanome.....	17
1) La peau	17
2) Rôle biologique des mélanocytes et pigmentation de la peau.....	20
3) Pouvoir photo-protecteur de la peau et plus particulièrement de la mélanine..	21
4) Rayonnement UV et mutation de l'ADN : première étape au développement d'un mélanome	22
5) Développement du mélanome suite à exposition UV	25
6) Les différents types de mélanomes cutanés et muqueux ainsi que leurs anomalies moléculaires.....	27
a. Les mélanomes cutanés	28
b. Les mélanomes non cutanés	29
7) Diagnostic du mélanome.....	30
8) Première prise en charge du patient après diagnostic et détermination du stade du mélanome	36
II. Prise en charge « conventionnelle » du mélanome	39
1) Chirurgie	39
2) Radiothérapie.....	40
3) Chimiothérapie.....	41
4) Les thérapies ciblées	42
III. Les immunothérapies.....	45
1) Les inhibiteurs de points de contrôles immunitaires.....	46
a. Les points de contrôle immunitaires (« immune checkpoints »).....	46
b. Les anticorps bloqueurs des points de contrôle immunitaires.....	48
c. Biomarqueurs prédictifs de bonne réponse à l'immunothérapie par anticorps bloqueurs.....	51
2) Le transfert adoptif de lymphocytes T	55
a. La thérapie par lymphocytes infiltrant la tumeur (TIL)	56
b. La thérapie par TCR modifiés	58
c. La thérapie par récepteur antigénique chimérique (CAR-T).....	58
3) Traitement par anticorps bloqueurs ou thérapie cellulaire ? Que choisir en fonction du type de mélanome : cutané ou non cutané	60

IV. Les vaccins thérapeutiques	62
1) Découverte des premiers vaccins thérapeutiques.....	62
a. Vaccins thérapeutiques approuvés	62
b. Echec des essais cliniques des vaccins thérapeutiques	66
2) Anticorps bloqueurs + Vaccins thérapeutiques : « the perfect partners ».....	67
3) Vaccins thérapeutiques en essai clinique utilisant différentes plateformes vaccinales	71
a. Vaccins anticancéreux à base de cellules.....	71
b. Vaccins d'origine virale.....	74
c. Vaccins peptidiques.....	74
d. Vaccins à ADN.....	75
e. Vaccins à ARNm.....	75
f. Vaccins personnalisés.....	76
CHAPITRE II : PRÉSENTATION DE LA PLATEFORME VACCINALE ‘ADDOMER’	79
CHAPITRE III : OBJECTIFS DE LA THÈSE	97
1) Production et optimisation des ADDomers	98
2) Evaluation <i>in vitro</i> des vaccins ADDomers en oncologie	98
3) Evaluation <i>in vivo</i> chez la souris des vaccins ADDomers en oncologie.....	99
CHAPITRE IV : OPTIMISATIONS DE LA PLATEFORME ‘ADDOMER’ POUR L’EXPOSITION D’ÉPITOPE ET D’ANTIGÈNES DU MÉLANOME	100
CHAPITRE V : EVALUATION <i>IN VITRO</i> D’ADDOMERS PRÉSENTANT DES ÉPITOPE ET ANTIGÈNES HUMAINS DU MÉLANOME.....	111
CHAPITRE VI : EVALUATION <i>IN VIVO</i> D’ADDOMERS PRÉSENTANT DES ÉPITOPE ET ANTIGÈNES MODÈLES DU MÉLANOME	143
CONCLUSION GÉNÉRALE ET PERSPECTIVES.....	165
1) Production et optimisation des ADDomers	166
2) Evaluation <i>in vitro</i> des vaccins ADDomers	167
a. Comparaison des vaccins ADD A2L et ADD MelA	167
b. Dé-ciblage et re-ciblage des ADDomers.....	168
3) Evaluation <i>in vivo</i> chez la souris des vaccins ADDomers	170

ANNEXE **176**

RÉFÉRENCES **190**

Remerciements

Je voudrais remercier en premier lieu le Pr Karim Benihoud et le Dr Bernard Verrier de me faire l'honneur d'évaluer ce manuscrit, ainsi que le Pr Franck Fieschi, le Dr Céline Colacios et le Dr Laurence Chaperot pour avoir accepté d'évaluer ce travail en tant qu'examineurs. Je remercie spécifiquement le Pr Franck Fieschi d'avoir assuré la présidence du jury lors de la soutenance.

Merci aux membres de mon Comité de Suivi Individuel (Dalil Hannani, Pascal Poignard, Juliette Treppéau, Peter Lowe et Franck Fieschi) pour avoir accepté de suivre et évaluer mon travail, pour les riches discussions et vos précieux conseils tout au long de cette thèse.

Un immense merci à la Fondation d'Entreprise ‘SILAB Jean Paufique’ pour avoir financé ce projet de recherche. Ce fut un réel plaisir de travailler avec vous et de venir présenter mes résultats à Brive chaque année, j'en garde de très bons souvenirs (malgré quelques mésaventures...). Merci particulièrement à Mme Brigitte Closs-Gonthier et à Mme Hélène Coppin d'avoir suivi mon projet de thèse pendant ces 3 ans.

Pascal, merci de m'avoir fait confiance pour ce sujet ambitieux et complexe. Je ne pensais pas avoir de réponse quand je t'ai envoyé ce premier mail et encore moins un contrat de thèse après tous ces nombreux appels, rendez-vous et répétitions. Merci de m'avoir soutenue pour ce projet qui tu le sais me tient beaucoup à cœur. Cette thèse n'a pas été un long fleuve tranquille mais je suis fière de nos résultats et j'espère que ce projet continuera car moi j'y crois ! Je te souhaite pleins de nouvelles aventures avec ce bel ADDomer et, qui sait, il deviendra peut-être le Dream Vaccine. Merci également à tes parents de m'avoir permis visiter LE plus beau village de France. Vive les adénos !

Caroline, merci infiniment pour ton implication tout au long de ce projet. Merci pour ton temps et tes conseils et merci de m'avoir aidée et formée à toute la partie immuno de cette thèse. Ce fut un plaisir de travailler avec toi.

Un grand merci également à Dalil pour ton implication dans ce projet ainsi qu'en tant que membre de mon CSI. Merci pour ta patience, tes conseils et ta bonne humeur. Merci de m'avoir formée à l'expérimentation animale, je n'aurais pas pu rêver de meilleur professeur.

Ce fut également un plaisir de se rendre aux journées de la SFI ensemble.

Merci à David et Olivier pour m'avoir accompagnée et aidée sur cette fin de thèse. Merci pour votre gentillesse et nos discussions scientifiques ou non devant le FACS... (j'ai pleins de nouveaux projets de voyage maintenant !)

Emilie B, ce fut un plaisir de te rencontrer à la SFI et encore plus de pouvoir travailler avec toi par la suite. Merci infiniment de t'être occupée de mes souris pendant de nombreux mois m'évitant ainsi de parcourir la moitié de la ville. Merci pour ta gentillesse et ta bonne humeur je te souhaite le meilleur pour ta fin de thèse.

Un grand merci à l'équipe adéno et leurs amis : Emilie, Chris, Marie-Claire, Salomé et Marc-André, Caroline et Philippe pour tous les bons moments passés avec vous. Mention spéciale à 'El Binom' Chris pour tes encouragements et ton aide pendant cette thèse, à Emilie pour ton grand soutien et toutes nos discussions et à Philippe pour ta bonne humeur au labo et tes talents de conteur (tu m'auras bien fait rire avec toutes tes histoires).

Merci à mes compagnons thésards de l'IBS et de l'EFS, Ada, Fella, Hussein, Axelle, Eleonora et Camille pour le soutien et les bons moments. Je vous souhaite bon courage pour la fin de vos thèse (you can do it !!) et le meilleur pour la suite. Au plaisir de se revoir. Mention spéciale pour Ada : un grand merci pour ton soutien depuis le 1^{er} jour et tous les bons moments qu'on a passé ensemble au labo et autres (coucou la rando en Chartreuse...). Merci de m'avoir écoutée et encouragée pendant ces 3 ans. J'aurais eu du mal à tenir sans toi. J'espère avoir été autant là pour toi que tu l'as été pour moi. And remember : GO GIRL !!

Merci au studio 'Pole and Aerial box' pour m'avoir permis de m'envoler quelques heures au milieu de cette thèse. J'y ai trouvé bien plus qu'un sport : une passion et des rencontres inoubliables.

Enfin merci infiniment à mes parents pour m'avoir permis de faire ces études et de m'avoir donné le goût et la possibilité de voyager pendant celles-ci. Vous savez combien cela était important pour moi et je vous remercie de m'avoir permis de le faire. Maman, je te remercie de m'avoir transmis ton sens de l'organisation et ta persévérance, j'en ai eu grand besoin pendant ces années. Papa, merci pour ton soutien et pour tous les allers retours que tu as dû faire pour me déménager aux 4 coins de la France. Je vous aime. Merci également à mes frères, cousins, cousines, oncles et tantes et amis pour votre soutien pendant toutes ces années.

Johan...comment t'exprimer toute ma reconnaissance. Merci d'être à mes côtés depuis toutes ces années, de me soutenir et de me supporter. Cette thèse n'aurait pas été la même sans toi tu le sais et je te remercie infiniment de m'avoir soutenue pendant ces 3 ans. Merci également de m'avoir nourrie de tes bons petits plats pendant ces années. On dit que les bons chimistes sont des bons cuisiniers j'imagine donc que tu es un bon chimiste et je te souhaite une belle carrière

remplie de molécules à 20 étapes de synthèse. Un petit coucou également à nos bebous à grandes oreilles.

Résumé

Les particules pseudovirales constituent des plateformes protéiques polyvalentes qui peuvent être utilisées comme plateforme vaccinale, principalement en infectiologie. Dans ces travaux de thèse, nous avons utilisé des dodécaèdres d'adénovirus pour afficher soit des épitopes courts, soit un antigène tumoral de grande taille. Ces particules non infectieuses mais immunogènes sont formées pendant le cycle de réPLICATION de l'adénovirus, et ont été modifiées pour créer une plateforme polyvalente appelée ADDomer (ADenovirus Dodecamer). Récemment, il a été démontré que des ADDomers affichant un épitope du virus Chikungunya induisaient avec succès une réponse anti-épitopique chez la souris.

Sur la base de ces résultats, ce projet vise à adapter la plateforme ADDomer afin de développer un vaccin thérapeutique contre le mélanome. Des ADDomers affichant des épitopes/antigènes de mélanome ont été produits et caractérisés. Les épitopes peuvent être directement insérés génétiquement à l'intérieur des boucles de surface des ADDomers et seront donc affichés à leur surface. Pour l'affichage d'antigènes, le système autocatalytique SpyTag/SpyCatcher a été adapté afin de fixer de manière covalente les antigènes sur la surface des ADDomers.

Une fois les ADDomers produits et caractérisés, nous avons exploré pour la première fois l'immunogénicité de ces ADDomers et leur impact sur des sous-types de cellules dendritiques (DC) humaines. Nous avons d'abord démontré que les ADDomers A2L et MelanA (épitope et antigène de mélanome humain) présentaient un fort potentiel de stimulation immunitaire des sous-types de cellules dendritiques humaines (cDC2s, cDC1s, pDCs), qui étaient capables d'internaliser et de cross présenter l'antigène tumoral, puis d'amorcer l'activation de réponses

cellulaires T spécifiques de l'antigène. De plus, afin d'améliorer l'adressage spécifique des DCs, des ligands spécifiques ont été conçus.

Enfin, nous avons évalué la capacité des ADDomers à contrôler la croissance du mélanome B16-OVA chez la souris. Plusieurs adjuvants ont été testés, montrant ainsi que le Poly I:C était bien adapté pour générer une réponse cellulaire et humorale homogène contre les épitopes souhaités. Dans un schéma prophylactique, la vaccination avec les ADDomers présentant des épitopes d'ovalbumine a entraîné une inhibition totale de la croissance tumorale. De plus, une stratégie de vaccination thérapeutique a montré un retard dans la croissance de la tumeur greffée ou son rejet total. Nous avons remarqué au cours de ces expériences que si l'affichage d'épitopes sur l'ADDomer était suffisant pour empêcher la croissance de la tumeur, l'affichage d'antigènes entiers présente le grand avantage de surmonter la barrière de la restriction allélique permettant d'obtenir une immunothérapie "prête à l'emploi" applicable à une large population.

Mots clés : particules pseudo-virales, adénovirus, vaccin thérapeutique, mélanome

Abstract

Virus like particles (VLPs) are versatile protein-based platforms which can be used as vaccine platform mainly in infectiology. In the present work we used adenoviruses dodecahedrons to display either short epitopes or a large tumor antigen. These non-infectious but immunogenic structures are formed during the adenovirus replication cycle, and have been modified to create a versatile platform named ADDomer (ADenovirus Dodecamer). Recently, it has been shown that ADDomers displaying a Chikungunya virus epitope successfully induced an anti-epitopic response in mice.

Based on these results, this project aims at adapting the ADDomer platform to develop a cancer vaccine for melanoma. ADDomers displaying melanoma epitopes/antigens have successfully been produced and characterized. Epitopes can directly be genetically inserted inside the ADDomers' exposed loops and are therefore exposed on the ADDomers' surface. For antigens, the autocatalytic system SpyTag/SpyCatcher was adapted in order to covalently fix antigens on the ADDomers' surface.

Once the ADDomers were fully produced and characterized, we explored for the first time the immunogenicity of these ADDomers and their impact on human dendritic cell (DC) subsets' features. We first demonstrated that A2L/MelA-ADDomers (ADDomers displaying human melanoma either epitope or antigen) displayed a strong immune-stimulating potential on human DC subsets (cDC2s, cDC1s, pDCs), which were able to internalize and cross-present tumor antigen, and subsequently cross-prime antigen-specific T-cell responses. To further limit off-target effects and enhance DC targeting, we engineered specific ligands to de-target untargeted cells (epithelial cells) and improve DCs' addressing.

Finally, we evaluated the ADDomers' ability to control melanoma B16-OVA growth in mice. A set of adjuvants was screened showing that Poly I:C was well-suited to generate a homogenous cellular and humoral response against the desired epitopes. In a prophylactic setting, vaccination with the ADDomers displaying ovalbumin epitopes resulted in a total inhibition of tumor growth one month after vaccination. Remarkably, a therapeutic vaccination strategy showed a delay in the grafted tumor growth or its total rejection. Interestingly, if the 'simple' epitope display on the ADDomer was sufficient to prevent tumor growth, the improved engineered platform enabling the display of large antigen represents a tool to overcome the barrier of immune allele restriction, broadening the immune response, and paving the way to its potential use in humans as an off-the-shelf vaccine.

Keywords: virus-like-particles, adenoviruses, cancer vaccine, melanoma

Abréviations

ACT : Adoptive Cell Transfer

ADN : Acide DésoxyriboNucléique

ADNc : Acide DésoxyriboNucléique complémentaire

ALCAM : Activated leukocyte cell adhesion molecule

ARN : Acide RiboNucléique

ARNm : Acide RiboNucléique messager

B7 : B lymphocyte activation antigen

B7H3 : B7 homolog 3 protein

BRAF : B-Raf Ser/Thr kinase

CAR : Chimeric Antigenic Receptor

CCND1 : Cycline D1

CD28 : Cluster of Differentiation 28

CD4 : Cluster of Differentiation 4

CD40 : Cluster of Differentiation 40

CD8 : Cluster of Differentiation 8

CD80 : Cluster of Differentiation 80

CD86 : Cluster of Differentiation 86

cDC1 : Conventional type 1 dendritic cell

cDC2 : Conventional type 2 dendritic cell

CDK4 : Cyclin Dependent Kinase 4

CMH : Complexe Majeur d'Histocompatibilité

CSID : Chronically sun induced melanoma

CTLA-4 : Cytotoxic T-Lymphocyte associated protein 4

CTNNB1 : Catenin Beta 1

CYSLTR2 : Cysteinyl Leukotriene Receptor 2

DC : Dendritic cells

DOPA : 3,4-dihydroxyphénylalanine

EZH2 : Enhancer of zeste homolog 2

Fc γ R : Fc-gamma receptor

FDA : Food and Drug Administration

GITR : Glucocorticoid-induced TNFR-related protein

GM-CSF : Granulocyte Macrophage Colony Stimulating Factor

GNA11 : G Protein Subunit Alpha 11

GNAQ : G Protein Subunit Alpha Q

gp100 : Glycoprotein 100

HER2 : Human epidermal growth factor receptor 2

iCAM : InterCellular Adhesion Molecule

IDO : Indoleamine 2,3-dioxygenase

IFN γ : Interféron gamma

IL-8 : Interleukine 8

LAG3 : Lymphocyte-activation gene 3

MAPK : Mitogen-activated protein kinase

MART1/MelanA: melanoma antigen recognized by T-cells

MDSC : Myeloid-Derived Suppressor Cells

MEK : MAPK/ERK activity Kinase

Mel-CAM : Melanoma cell adhesion molecule

MMP : Matrix metalloproteinases

NF1 : Neurofibromatose 1

non-CSID : non-chronically sun induced melanoma

NRAS : Neuroblastoma RAS

PD-1 : Programmed cell Death protein 1

pDC : Plasmacytoid dendritic cell

PDGFRA : Platelet-derived growth factor receptor A

PI3K : Phosphatidylinositol-3 kinase

PLCB4 : Phospholipase C beta 4

PTEN : Phosphatase and Tensin Homolog

RANKL : Receptor activator of nuclear factor kappa-B ligand

RAS : Retrovirus Associated Sequences

RECIST : Response Evaluation Criteria in Solid Tumours

SC: SpyCatcher

scFv : Single-chain variable fragment

SF3B1 : Splicing Factor 3b Subunit 1

ST: SpyTag

TAA : Tumor Associated Antigen

Tc1 : Lymphocytes T cytotoxiques 1

TCR : T cell Receptor

TERT : Telomerase Reverse Transcriptase

Th1 : Lymphocytes T helpers 1

TIGIT : T cell immunoreceptor with Ig and ITIM domains

TIL : Tumor Infiltrating Lymphocytes

TIM3 : T-cell immunoglobulin and mucin containing protein-3

TNF α : Tumor Necrosis Factor alpha

TPR : Translocated Promoter Region

Treg : Lymphocytes T régulateurs

TRP-1 : Tyrosinase-related protein 1

UV : Ultra-violets

VEGF : Vascular Endothelial Growth Factor

Liste des figures

Figure 1: Schéma de la structure de la peau.....	18
Figure 2: Mélanogenèse et influence du type de mélanine sur la couleur de la peau	21
Figure 3: Stades d'évolution du mélanome	25
Figure 4: Différents sous types de mélanome avec leurs mutations génétiques et traitements associés.....	28
Figure 5: (a) observation macroscopique d'un mélanome à extension superficielle (b) vue de la même lésion à travers un dermoscope.....	31
Figure 6: Méthode ABCDEF pour l'identification d'un mélanome	32
Figure 7: Mélanomes présentant des microstructures caractéristiques permettant de les identifier grâce à la méthode de la liste en 7 points	34
Figure 8: Exérèse des ganglions sentinelles.....	40
Figure 9: Impact de l'altération en cas de cancer des voies de signalisation impliquant BRAF, MEK et KIT	44
Figure 10: Régulation des lymphocytes T par CD28 et CTLA-4	46
Figure 11: Rôle des points de contrôles immunitaires PD-L1 et CTLA-4 dans un contexte tumoral	47
Figure 12: Action des anticorps bloqueurs.....	50
Figure 13: Récapitulatif des biomarqueurs prédictifs pour un traitement par anticorps bloqueurs	54
Figure 14: Schéma des différentes thérapies de transfert adoptif de lymphocytes T	56

Figure 15: Schéma du protocole d'expansion des TILs du prélèvement à la réinjection chez le patient	57
Figure 16: Schéma d'un récepteur CAR	59
Figure 17: Schéma des mécanismes d'activation des lymphocytes T d'une part et des CAR T d'autre part	59
Figure 18: Résumé des biomarqueurs en faveur soit d'un traitement par anticorps bloqueurs soit d'un traitement par transfert adoptif de lymphocytes T	61
Figure 19: Proposition de mécanisme d'action du vaccin T-VEC	65
Figure 20 : Mécanismes illustrant le potentiel synergique des vaccins thérapeutiques et des anticorps modulateurs	68
Figure 21: Schéma proposant une explication à la présence d'effets secondaires d'origine immunologique suite à un traitement par anticorps bloqueurs	70
Figure 22: Schéma proposant une explication à la diminution des effets secondaires d'origine immunologique suite à un traitement par anticorps bloqueurs + vaccin thérapeutique	70
Figure 23: Schéma récapitulant les étapes nécessaires au développement d'un vaccin personnalisé	77

Liste des tableaux

Tableau 1: Sensibilité et spécificité des différentes méthodes de diagnostic du mélanome	35
Tableau 2: Différents stades du mélanome et traitements associés.....	38
Tableau 3: Autres molécules ciblées dans les essais en développement.....	50
Tableau 4 : Présentation de vaccins personnalisés actuellement essais cliniques dans le mélanome	78

Chapitre I : Introduction

I. Caractéristiques du mélanome

Dans cette première partie de ce chapitre d'introduction nous allons aborder le mélanome en commençant par présenter la peau et les mélanocytes, respectivement l'organe et les cellules au sein duquel il se développe. Nous nous intéresserons ensuite au développement du mélanome suite à une exposition aux rayons ultraviolets, puis nous détaillerons les méthodes de diagnostiques ainsi que les différents types et stades des mélanomes. Nous finirons enfin par une description de la première prise en charge du patient suite au diagnostic avec les traitements associés. Ces traitements sont ensuite détaillés dans les trois parties suivantes.

1) La peau

Avec un poids moyen de 5kg et une superficie de 2m², la peau constitue le plus grand organe du corps humain¹. Elle assure de nombreuses fonctions vitales pour l'organisme. En effet, elle joue évidemment un rôle de barrière face à l'environnement extérieur (agressions mécaniques, chimiques, biologiques, rayonnement UV) mais elle assure également de nombreuses fonctions immunitaires (première ligne de défense contre les agressions)², neurosensorielles³, thermiques et biochimiques (synthèse vitamine D3, conversion testostérone)²⁻⁴.

Structuellement, la peau est divisée en 3 couches : l'épiderme, le derme et l'hypoderme.

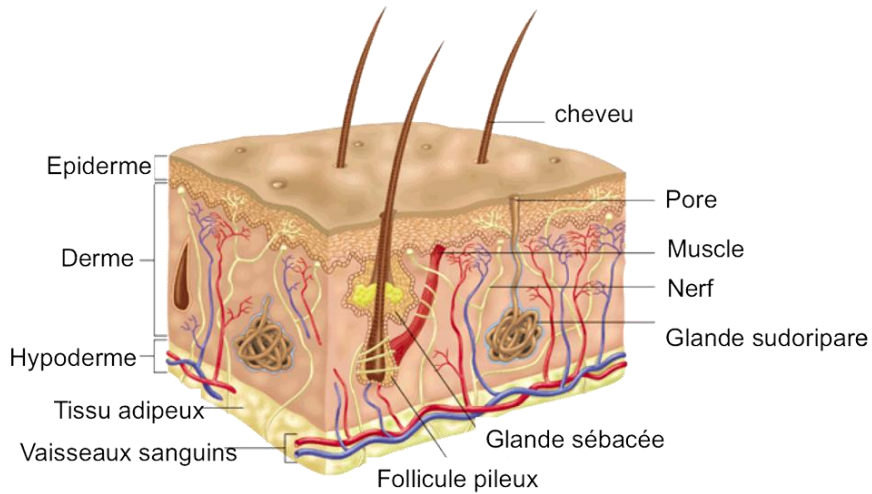


Figure 1: Schéma de la structure de la peau. Schéma issu du site de Dermeal, laboratoire dermatologique

- **L'épiderme**

L'épiderme constitue la couche superficielle de la peau. Cette couche en renouvellement rapide et continu n'est pas vascularisée et doit ainsi compter sur le derme pour se nourrir. L'épiderme comprend 4 à 5 sous couches cellulaires dans lesquelles on trouve 4 types de cellules : les kératinocytes, les cellules de Langerhans, les cellules de Merkel et les mélanocytes.

Les cellules les plus abondantes de l'épiderme sont les kératinocytes qui constituent à eux seuls 80% de l'épiderme. Ceux-ci sont organisés en 4 couches principales (couche cornée, couche granuleuse, couche épineuse et couche basale) formant ainsi des strates conférant à l'épiderme son nom d'épiderme stratifié³. Les kératinocytes sont produits dans la couche basale (couche la plus profonde de l'épiderme) et se différencient au fur et à mesure de leur migration vers la surface de la peau. Cette migration des kératinocytes depuis la couche basale jusqu'à la surface de la peau prend environ 30 jours⁵. La fonction principale des kératinocytes est la synthèse d'une protéine, la kératine qui aide à protéger la peau contre les agressions extérieures. La kératine se dépose progressivement en superficie et est le constituant principal de la couche cornée.

L'épiderme contient également 20% de cellules dendritiques (cellules de Langerhans, cellules de Merkel et mélanocytes) se présentant sous différentes formes. Les cellules de Langerhans découvertes en 1868 par le médecin allemand Paul Langerhans, sont des sentinelles du système immunitaire et participent à la première ligne de défense de l'organisme contre les corps étrangers (virus, bactéries...) ayant pénétrés l'épiderme⁶. Les cellules de Merkel, décrites comme les cellules du toucher par l'histopathologiste allemand Friedrich Merkel en 1875⁷, sont des prolongations du système neuroendocrinien et jouent un important rôle de mécanorécepteur⁸. Ce sont elles qui permettent l'identification de la forme et la matière des objets au contact de la peau.

Enfin les mélanocytes, cellules à l'origine du développement du mélanome sont responsables de la production de la mélanine, pigment donnant sa couleur à la peau. Ces cellules clés pour le développement du mélanome feront l'objet d'une description détaillée dans la partie suivante.

• **Le derme**

Le derme, couche intermédiaire de la peau se situe sous l'épiderme. C'est un tissu conjonctif dense qui confère un rôle de soutien à la peau et assure sa solidité. Comme tout tissu conjonctif, le derme est essentiellement formé de fibroblastes synthétisant et sécrétant du collagène, de l'élastine, de l'acide hyaluronique et des glycoprotéines de structure⁵. Tous ces composants forment un réseau dense appelé matrice extracellulaire ancrée à l'épiderme grâce à des fibres de collagène VII au niveau de la jonction dermo-épidermique. Le derme contient également des vaisseaux sanguins, des vaisseaux lymphatiques, des terminaisons nerveuses, des follicules pileux (qui forment la base du poil) ainsi que des glandes sudoripares (produisant la sueur) et sébacées (produisant le sébum). Tous ces constituants assurent l'hydratation et la nutrition de l'épiderme par diffusion à travers la membrane basale.

- **L'hypoderme**

L'hypoderme, couche la plus profonde de la peau, est un tissu graisseux principalement constitué d'adipocytes. Ces cellules sont regroupées en amas et sont spécialisées dans le stockage des graisses sous forme de triglycérides⁵. Cette couche joue un rôle de stockage énergétique et permet l'isolation thermique et la protection mécanique des tissus sous-jacents.

2) Rôle biologique des mélanocytes et pigmentation de la peau

Il existe 2 types de mélanocytes : les mélanocytes épidermiques intercalés entre les cellules de la couche basale de l'épiderme et étendant leurs dendrites vers les kératinocytes des couches basale et épineuse, et les mélanocytes folliculaires localisés dans les follicules pileux⁹. Les uns participent à la couleur de la peau, les autres à la couleur des poils et des cheveux. Le nombre de mélanocytes par mm² est de 2000 ou plus dans la peau exposée du visage et dans la peau du scrotum ou du prépuce. En revanche sur le reste du corps nous retrouvons entre 1000 à 1500 mélanocytes par mm². Ce nombre de mélanocytes reste constant quelle que soit la couleur de peau de l'individu. Un individu à peau sombre ne comporte donc pas plus de mélanocytes qu'un individu à peau claire¹⁰.

On compte un ratio de 1 mélanocyte pour 36 kératinocytes¹¹. Le principal rôle de ces cellules est de produire la mélanine, pigment naturel de la peau. La mélanine est synthétisée à partir de l'acide aminé tyrosine dans des organites spécifiques des mélanocytes appelés mélanosomes. Cette tyrosine est tout d'abord convertie en DOPA, puis en DOPAquinone. Ces 2 réactions sont catalysées par l'enzyme tyrosinase. Ensuite, 2 composés peuvent être formés à partir de la DOPAquinone en fonction de la présence ou non de cystéine dans le mélanosome. En l'absence de cystéine, de l'indole-5,6-quinone est formé, donnant l'eumélanine, pigment de couleur brun-noir. En présence de cystéine, de la cystéinyldopa est formée, donnant de la phéomélanine, pigment de couleur jaune-rouge¹⁰. C'est la présence et la quantité de ces 2 types de mélanine et

non le nombre de mélanocytes qui explique les différences de pigmentation. Les individus à peau claire synthétisent plus particulièrement la phéomélanine tandis que les individus à peau foncée synthétisent plus particulièrement l'eumélanine. Ces deux pigments participent ainsi à la couleur de la peau mais ils ne sont pas les seuls. D'autres pigments participent également à la couleur de la peau comme l'hémoglobine oxygéné (rouge) des capillaires du derme, l'hémoglobine réduite (bleue) des veinules du derme et enfin les caroténoïdes alimentaires (jaune-orange) présents dans le derme et l'épiderme¹.

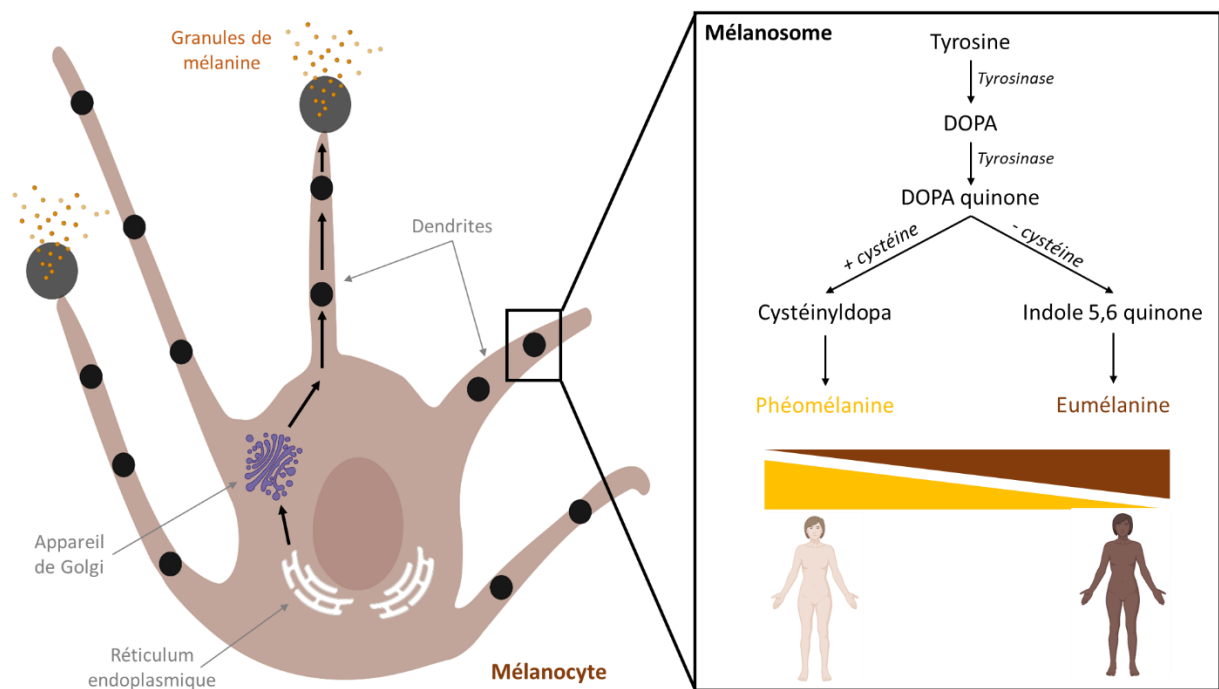


Figure 2: Mélanogenèse et influence du type de mélanine sur la couleur de la peau. Schéma réalisé sur BioRender

3) Pouvoir photo-protecteur de la peau et plus particulièrement de la mélanine

Les mélanosomes sont transportés grâce à des microtubules et des microfilaments vers le bout des dendrites des mélanocytes. Là, ils sont phagocytés par les kératinocytes et la mélanine (eumélanine ou phéomélanine) est ensuite placée au-dessus du noyau cellulaire des

kératinocytes, formant ainsi une calotte qui protège le matériel génétique du rayonnement ultraviolet^{5,12}. En effet la mélanine absorbe fortement dans le domaine UV et visible du spectre, ce qui est à l'origine de sa couleur sombre¹³ (melanos, sombre en grec). La mélanine absorbe également les radicaux libres générés dans les cellules par les radiations UV protégeant ainsi l'ADN des effets nocifs de ces radiations. Les eumélanines ont un pouvoir photo protecteur environ 1000 fois supérieur à celui des phéomélanines ce qui explique pourquoi les sujets clairs ont une peau, qui a plus tendance à brûler au soleil, donnant ainsi naissance aux coups de soleil. La mélanine produite par les mélanocytes joue donc un rôle primordial dans la protection de l'ADN face à l'agression des rayons UV. Par ailleurs, certaines études suggèrent que les caroténoïdes jouent également un rôle photo protecteur non négligeable¹⁴. Enfin, 4 à 7% du rayonnement incident est réfléchi par l'interface air/peau et la couche cornée fournie également une protection contre les rayonnements UV. En effet, son organisation en feuillets parallèles entraîne une importante diffraction protégeant les cellules sous-jacentes. Cette diffraction explique pourquoi il est difficile de provoquer un coup de soleil sur les paumes des mains et les plantes des pieds étant donné la forte épaisseur de l'épiderme au niveau de ces zones corporelles. En effet, l'épaisseur de la couche cornée de l'épiderme est de 80µm à 200µm sur les paumes et les plantes des pieds contre 6µm à 40µm sur le reste du corps.

4) Rayonnement UV et mutation de l'ADN : première étape au développement d'un mélanome

Comme nous l'avons vu, le rayonnement UV solaire peut entraîner des dommages à l'ADN dans les cellules de la peau ce qui peut conduire à la formation de tumeurs. Ce rayonnement endommage également d'autres constituants de la peau comme par exemple les fibres de collagène ce qui entraîne un vieillissement de la peau. Le rayonnement solaire peut être divisé en 3 sous catégories : les UVC (<280nm), les UVB (280-315nm) et les UVA (315-400nm)¹⁵.

Les UVC sont hautement cancérigènes mais heureusement ils sont arrêtés par la couche d'ozone atmosphérique tout comme une partie des UVB (280-290nm).

- **Les UVB**

Les UVB (290-315nm) représentent seulement 5 à 10% des UV atteignant le sol mais ils possèdent un fort potentiel cancérigène de par leurs dommages sur l'ADN et leur interférence avec le système immunitaire. En effet, les photons UVB sont directement absorbés par l'ADN notamment par les bases pyrimidiques (thymine et cytosine). Des réactions photochimiques sont induites dans ces bases qui, si elles sont situées face à face ou adjacentes, se lient ensemble de manière covalente. Cela donne naissance à 2 photo-produits : les dimères cyclobutane et les photo-produits (6,4). Ces dimères pyrimidiques entraînent une distorsion de la double hélice d'ADN ce qui peut donner lieu à des cassures et des arrêts de réPLICATION.

Ainsi, chez l'homme une molécule d'ADN peut subir environ 100, 000 modifications par jour et une heure d'exposition au soleil peut entraîner la formation de 80, 000 dimères de thymine par cellule¹⁶. Heureusement, des mécanismes de réparation de l'ADN existent dans la cellule afin qu'elle puisse en permanence protéger son génome. Ainsi, lorsqu'un dimère pyrimidique apparaît, le brin d'ADN endommagé est localement excisé, éliminé et resynthétisé à partir du brin complémentaire par un mécanisme appelé Nucleotide Excision Repair (NER)¹⁷. Des dommages trop importants peuvent finalement entraîner un programme de mort cellulaire, l'apoptose. Cependant, si ces dommages ne sont pas réparés (car trop nombreux, ou mécanismes de réparation défectueux), l'ADN polymérase insère par défaut une base adénine en face du dimère lorsqu'elle rencontre ce type de lésion qu'elle n'arrive pas à interpréter. Ainsi dans le cas de dimères cytosine-cytosine on obtiendra des mutations de type C→T ou CC→TT. Ces mutations peuvent potentiellement endommager des gènes cruciaux, comme les gènes suppresseurs de tumeur (gène p53 par exemple) régulant les divisions cellulaires et l'apoptose,

et modifier le comportement des cellules (prolifération, adhésion, mobilité, synthèse de molécules aux propriétés particulières).

Par ailleurs, une diminution du nombre ainsi qu'une altération de la forme des cellules de Langerhans ont été observés chez des souris irradiées par des UVB¹⁸. Ainsi en plus d'endommager l'ADN, les UVB diminuent localement l'activité immunitaire favorisant de ce fait l'expansion et la multiplication des cellules mutées.

• Les UVA

Enfin les UVA jouent également un rôle primordial dans le développement de cancers de la peau. L'ADN n'absorbe que très peu les photons UVA mais ceux-ci peuvent provoquer des dommages indirects sur les composés cellulaires (lipides, protéines...) et extracellulaires (matrice extracellulaire du derme) en entraînant la création de radicaux libres. Ces radicaux peuvent aboutir à des cassures dans les brins d'ADN, des réticulations ADN-protéine ainsi que des dommages dans les bases de l'ADN.

Il est intéressant de noter que les UVA, contrairement aux UVB, ne sont pas arrêtés par les vitres et peuvent provoquer des dommages à travers celles-ci. On peut ainsi observer un vieillissement asymétrique du visage chez les personnes étant exposées au soleil de manière prolongée et toujours du même côté sur leur lieu de travail, bien que protégées par une vitre¹⁹. Plus récemment il a été observé qu'une exposition aux UVA via les salons de bronzage augmenteraient de 75% le risque de développer un mélanome.

Ainsi les rayons UV du soleil provoquent des dommages à l'ADN dans les cellules de la peau ce qui peut conduire au développement de cancers de la peau comme les carcinomes et les mélanomes. Dans cette thèse, nous nous focaliserons sur le développement du mélanome.

5) Développement du mélanome suite à exposition UV

La plupart des mélanomes apparaissent suite à une accumulation de mutations génétiques dans les mélanocytes de l'épiderme et d'altérations du micro environnement tumoral²⁰⁻²⁵. En effet, on observe une surexpression de protéines comme les « matrix metalloproteinases » (MMPs) et plus particulièrement les MMP-2 et 9 (Gélatinases A et B) ou encore les MMP-1,8 et 13 (Collagénases 1,2 et 3). Ces MMPs induisent la dégradation des composants de la matrice extracellulaire comme le collagène favorisant ainsi l'infiltration des cellules tumorales à travers le derme et l'hypoderme jusqu'aux vaisseaux sanguins où elles vont pouvoir se disperser dans le reste de l'organisme^{20,22,23} formant ainsi des tumeurs à distance de la tumeur initiale : des métastases.

Tous ces évènements se déroulent en plusieurs phases. Ces phases sont caractérisées par le niveau de Clark qui décrit à quelle profondeur la tumeur a pénétré dans les différentes couches de la peau.

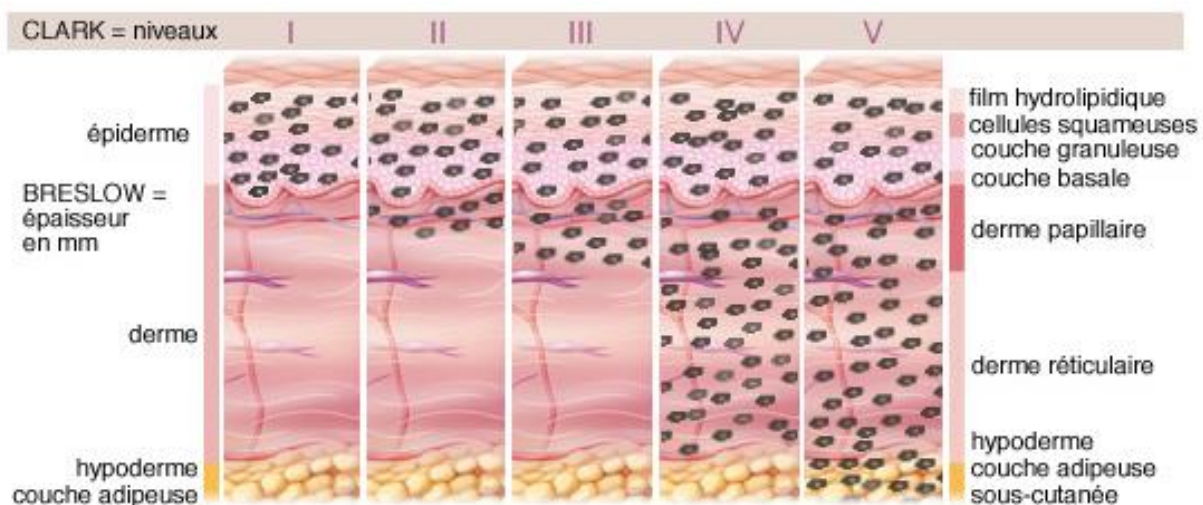


Figure 3: Stades d'évolution du mélanome. Schéma issu du site InfoCancer

Tout d'abord, on assiste à une croissance horizontale de mélanocytes anormaux à partir du mélanocyte muté initiateur. Ces mélanocytes forment une nappe ou des amas le long de la membrane basale de l'épiderme et certains migrent de manière isolée vers les couches supérieures de l'épiderme. Cette première phase est appelée invasion horizontale de l'épiderme et on parle alors de mélanome *in situ*. Vient ensuite une seconde phase de croissance, verticale cette fois, avec envahissement du derme puis une pénétration des vaisseaux sanguins provoquant *in fine* des métastases dans des tissus distants. C'est au cours de cette deuxième phase de progression verticale dermique que les altérations du microenvironnement tumoral et en particulier de la matrice extracellulaire se révèlent fondamentales. Comme cités précédemment, la surexpression de MMPs facilite grandement cette progression, mais on peut également observer une diminution des interactions de contact entre les mélanocytes tumoraux et leurs voisins kératinocytes (diminution de l'expression des E-cadhérines et des desmoglinines ainsi que du nombre de jonctions gaps mélanocyte-kératinocyte) ainsi qu'une augmentation des interactions de contact entre ces mélanocytes tumoraux²⁶ (augmentation de l'expression des N-cadhérines, des Mel-CAM et des ALCAM et du nombre de jonctions gaps mélanocyte-mélanocyte). De plus, on assiste à une modification des interactions paracrines entre les mélanocytes et les autres cellules aux alentours (kératinocytes, fibroblastes, cellules endothéliales et surtout les cellules immunitaires). La croissance des mélanocytes devient ainsi de plus en plus indépendante des facteurs de croissance présents dans le microenvironnement. Les mélanocytes échappent ainsi au contrôle des autres cellules²⁷. Enfin, les molécules d'adhésion et de communication exprimées à leur surface leur permettent d'interagir avec les fibroblastes d'une part (N-cadhérines et jonctions Gap) et les cellules endothéliales d'autre part (N-cadhérines, Mel-Cam, intégrines) permettant ainsi l'invasion du derme et la pénétration dans la circulation sanguine^{26,28-32}. Durant la phase d'invasion verticale on peut observer histologiquement une destruction de la membrane basale due à la synthèse excessive d'enzymes

protéolytiques comme la collagénase par les cellules tumorales ou par les cellules hôtes sous leur contrôle³³.

6) Les différents types de mélanomes cutanés et muqueux ainsi que leurs anomalies moléculaires

De manière générale on classe les mélanomes en 2 grandes catégories : les mélanomes cutanés se développant sur la peau exposée au soleil et les mélanomes non cutanés ou muqueux se développant au niveau des muqueuses non exposées au soleil (uvée de l'œil, tissus muqueux comme la bouche et tissus acraux comme les paumes de mains, plantes de pieds et ongles). Les mélanomes cutanés sont beaucoup plus fréquents que les mélanomes muqueux. En effet, les mélanomes cutanés représentent 91,2% des mélanomes contre moins de 10% pour les mélanomes muqueux³⁴⁻³⁶. Les mélanomes muqueux présentent un moins bon pronostic que les mélanomes cutanés en raison d'un diagnostic tardif de la tumeur primaire, de l'agressivité des tumeurs, d'un fort taux de récidive après traitement et d'une faible survie globale^{37,38}. Cependant un diagnostic post métastatique d'un mélanome cutané ou muqueux conduit à une survie globale similaire³⁷. Enfin, il a été observé que les mélanomes cutanés touchaient préférentiellement les sujets à peaux claires alors que les mélanomes muqueux sont plus répandus chez les sujets à peaux plus sombres³⁹⁻⁴¹.

Ces 2 grands types de mélanome sont très différents et se caractérisent par des anomalies moléculaires différentes. Le mélanome cutané comporte tout d'abord beaucoup plus de mutations (forte charge tumorale) que le mélanome muqueux. On compte environ 179 mutations pour une tumeur exposée au soleil (mélanome cutané) contre seulement 9 mutations pour une tumeur non exposée au soleil (mélanome muqueux)⁴²⁻⁴⁴.

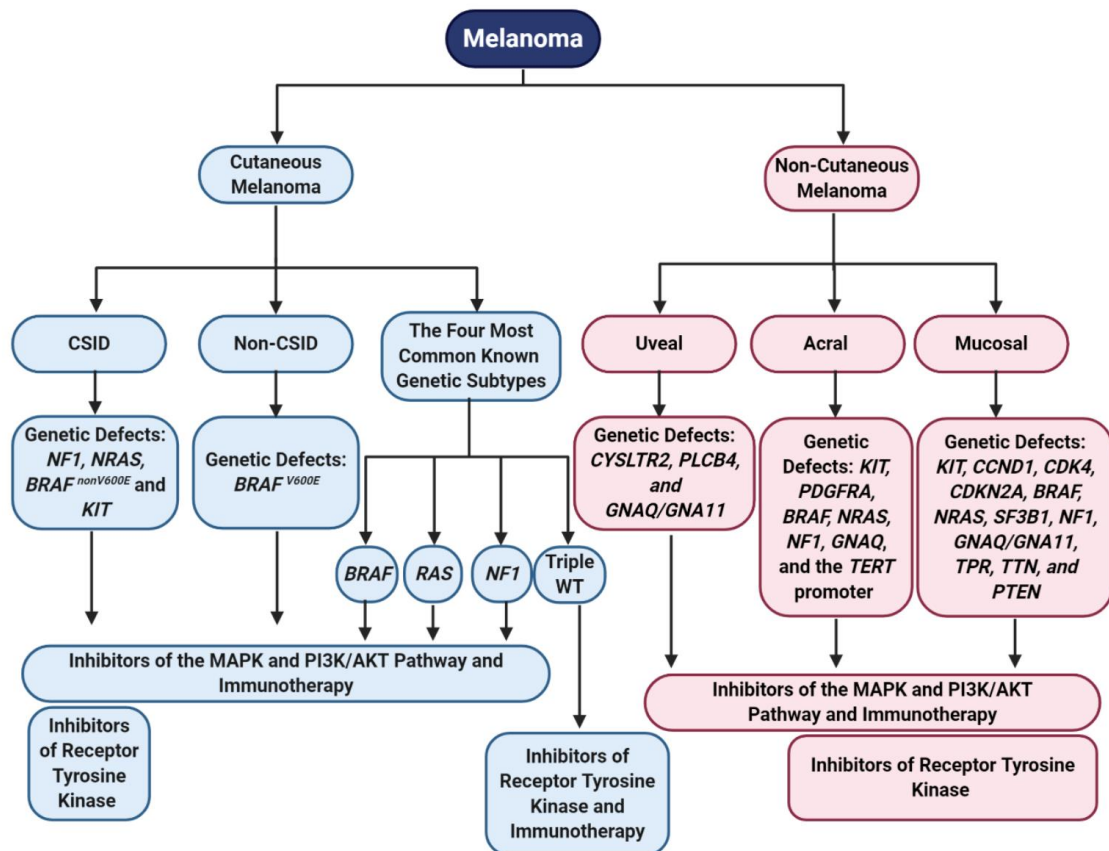


Figure 4: Différents sous types de mélanome avec leurs mutations génétiques et traitements associés. Image tirée de Eddy et Chen 2020⁴⁵

a. Les mélanomes cutanés

Les mélanomes cutanés peuvent être subdivisés en 2 catégories : Mélanomes cutanés induits par exposition chronique au soleil (« chronically sun induced melanoma » soit CSID) et les mélanomes cutanés non induits par exposition chronique au soleil (« non-chronically sun induced melanoma » soit non-CSID). Les mélanomes CSID sont généralement présents chez les individus de plus de 55 ans et se développent sur le visage, le cou et les extrémités distales (mains et pieds par exemple)⁴⁶. Les mélanomes non-CSID quant à eux sont généralement présents chez les individus de moins de 55 ans et se développent sur le torse, et les extrémités

proximales (bras et jambes par exemple)⁴⁶. Les anomalies génétiques associées à ces 2 sous types sont des mutations des gènes NF1, NRAS, BRAF (non V600E) et KIT pour les mélanomes CSID et la mutations BRAF V600E pour les mélanomes non CSID⁴⁶⁻⁴⁸. En plus de ces 2 grandes catégories CSID et non CSID, on trouve aussi 1 autre catégorie où sont regroupés 4 sous types génétiques : BRAF, RAS, NF1 et « triple wild type » (Triple WT)⁴²

Pour le sous type BRAF on retrouve de nombreuses mutations dans le gène BRAF. Da la même manière, on retrouve beaucoup de mutations dans le gène RAS pour le sous type RAS, idem pour NF1⁴². Les mutations de ces 3 sous types entraînent une hyper activation de la voie de signalisation MAPK, impliquée dans la prolifération cellulaire⁴².

Le sous type Triple WT en revanche ne contient de mutations dans aucun de ces 3 gènes. On retrouve cependant des mutations dans les gènes GNAQ, GNA11, KIT, CTNNB1 et EZH2⁴².

b. Les mélanomes non cutanés

On distingue 3 grands types de mélanomes non cutanés : les mélanomes muqueux (bouche par exemple) représentant 1,3% de tous les mélanomes, suivi par les mélanomes acraux (paumes mains, plantes pieds, ongles) représentant 2 à 3% et les mélanomes uvéaux représentant 5,2%^{34,35,49}.

Il est intéressant de noter que même si les **mélanomes acraux** pourraient être considérés comme des mélanomes cutanés, leurs profils génétiques ainsi les facteurs de risques se rapprochent plus des mélanomes non cutanés d'où leur catégorisation de mélanomes non cutanés. Ces mélanomes apparaissent souvent chez des personnes à peau sombre. C'est le mélanome pour lequel le pronostic est le plus mauvais, probablement en raison d'un diagnostic tardif^{49,50}. Ce sous type se caractérise par une amplification ou délétion de certains gènes ainsi

qu'une faible charge mutationnelle^{36,43,51}. Les gènes mutés associés à ce sous type sont les suivants : KIT, PDGFRA, BRAF, NRAS, NF1, GNAQ, et le promoteur TERT⁵¹⁻⁵⁵.

Les **mélanomes uvéaux** se développent au niveau de l'œil notamment chez les personnes avec des yeux et une peau de couleur claire. Ils se caractérisent par une faible charge mutationnelle ainsi que des pertes ou gains chromosomiques^{44,51,56}. Les mutations les plus communes se situent sur les gènes CYSLTR2, PLCB4 et GNAQ/GNA11, induisant l'activation des voies de signalisation de prolifération cellulaire MAPK et PI3K/AKT⁵⁷⁻⁶¹.

Les **mélanomes muqueux** quant à eux, se développent à partir de mélanocytes situés dans les muqueuses des voies gastro-intestinales, urogénitales et respiratoires⁶². On retrouve ici également une faible charge mutationnelle^{36,43,44,63}. Certains gènes sont amplifiés comme les gènes KIT, CCND1 ou encore CDK4^{36,43,55,64}, d'autres sont mutés comme les gènes BRAF, NRAS, SF3B1, NF1, KIT, GNAQ, GNA11, TPR, TTN, et PTEN⁶³⁻⁶⁸. De la même manière que pour les autres mélanomes non cutanés, ces mutations convergent vers une hyperactivation des voies de signalisation MAPK et PI3K/AKT résultant en la progression du cycle cellulaire ainsi que des signaux anti apoptotiques⁶⁸.

7) Diagnostic du mélanome

Dans leur développement précoce les mélanomes peuvent être confondus avec les nævi et nécessitent ainsi des méthodes de diagnostic élaborées. Pour cela des algorithmes de diagnostic différentiel ont été développés et ont pour but de classer les lésions cutanées entre mélanome et non mélanome à partir de critères visuels lors d'un examen clinique à l'œil nu ou à l'aide d'un dermoscope.

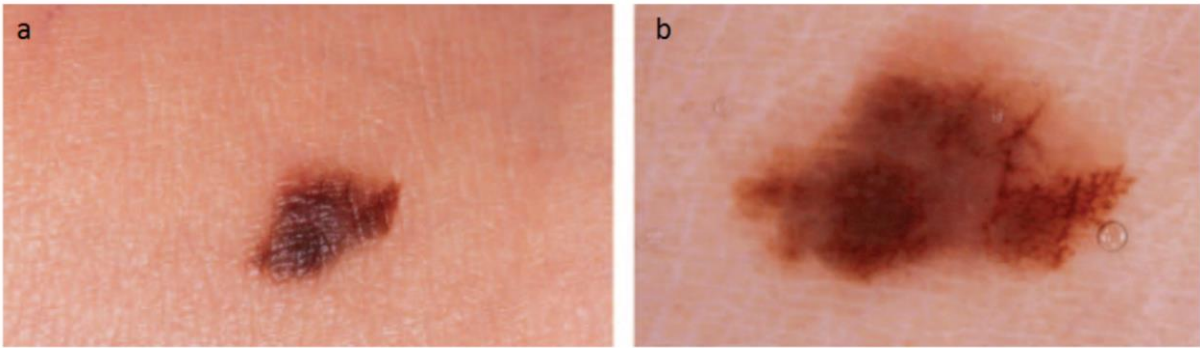


Figure 5: (a) observation macroscopique d'un mélanome à extension superficielle. Une grande partie du rayonnement est réfléchi par la surface de la peau. (b) vue de la même lésion à travers un dermoscope. Les structures de la lésion sont visibles en profondeur. La bulle sur le bord droit de la lésion est une bulle d'air piégée dans le film de liquide placé à la surface de la peau pour diminuer les réflexions dues à la différence d'indice entre l'air et le stratum corneum. Image tirée de Braun et al. 2005⁶⁹.

L'avantage du mélanome contrairement aux autres cancers est qu'il laisse une trace sur la peau facilitant ainsi un diagnostic non intrusif.

Comme le formule le Dr Neville Davis "Malignant melanoma writes its message in the skin with its own ink and it is there for all of us to see. Some see but do not comprehend."

A ce jour il existe 4 types d'algorithmes différentiels couramment utilisé par les dermatologues :

- **La règle ABCDE**

Elaborée par Friedman *et al.* en 1985⁷⁰, la règle ABCDE est l'algorithme différentiel le plus utilisé par les dermatologues français. Il repose sur une liste de critères indiquant un mélanome.

– (A) : lésion Asymétrique : contours, couleurs, structures internes asymétriques. Le dermoscope peut se révéler d'une aide précieuse en rendant visible des asymétries invisibles à l'œil nu.

– (B) : lésion aux Bords irréguliers

– (C) : lésion de Couleur inhomogène

85% des mélanomes possèdent 3 couleurs ou plus, ce qui est le cas de seulement 39% des nævi⁷¹.

– (D) : lésion d'un Diamètre > 6mm

– (E) : lésion présentant une Evolution de sa taille, surface ou couleur

– (F) : lésion « Funny looking » qui est différentes du reste des nævi retrouvés sur le patient

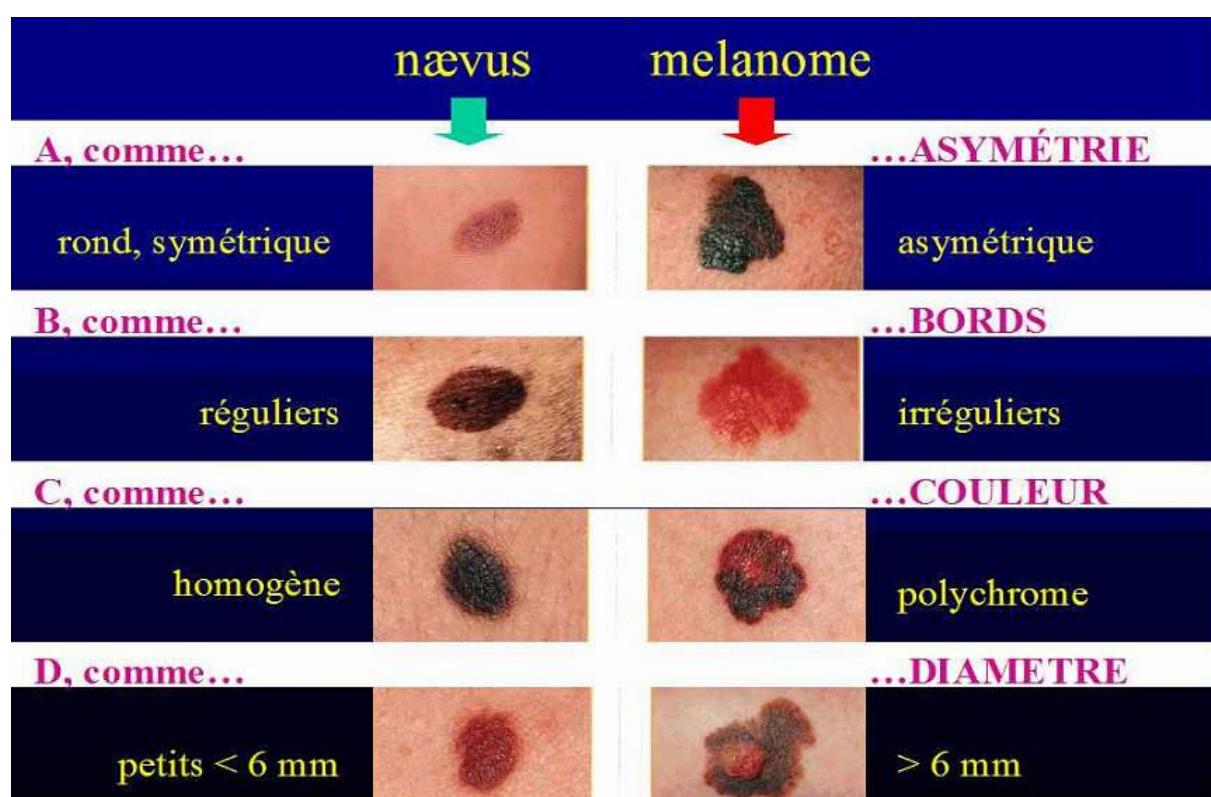


Figure 6: Méthode ABCDEF pour l'identification d'un mélanome. Image issue de la Société Française de Dermatologie

Les critères ABCD sont ensuite quantifiés et moyennés pour obtenir le *Total Dermatoscopy Score* permettant un diagnostic semi-quantitatif. Un score inférieur à 4.75 indique une lésion bénigne et un score supérieur à 5.45 indique la présence probable d'un mélanome⁷².

- **La méthode en 7 points**

Cette méthode initiée par Pehamberger *et al.* en 1987⁷³ est basée sur l'analyse des structures présentes dans la lésion et prend en compte 3 critères majeurs et 4 critères mineurs caractéristiques d'un mélanome⁷¹.

Critères majeurs :

- réseau pigmentaire irrégulier dû à l'invasion des crêtes épidermiques par des mélanocytes malins
- voile blanc-bleu, dû à une hypertrophie des couches supérieures de l'épiderme et à la présence de mélanine dans le derme
- présence d'une vascularisation atypique

Critères mineurs :

- Irrégularités de pigmentation, larges zones sombres irrégulièrement réparties
- présence irrégulière de stries représentant des amas confluents de cellules pigmentées au niveau de l'épiderme ou de la jonction dermoépidermique
- répartition inhomogène de points et de globules
- présence de régressions : zones blanches à forme cicatricielle (fibrose) ou bleu-gris.

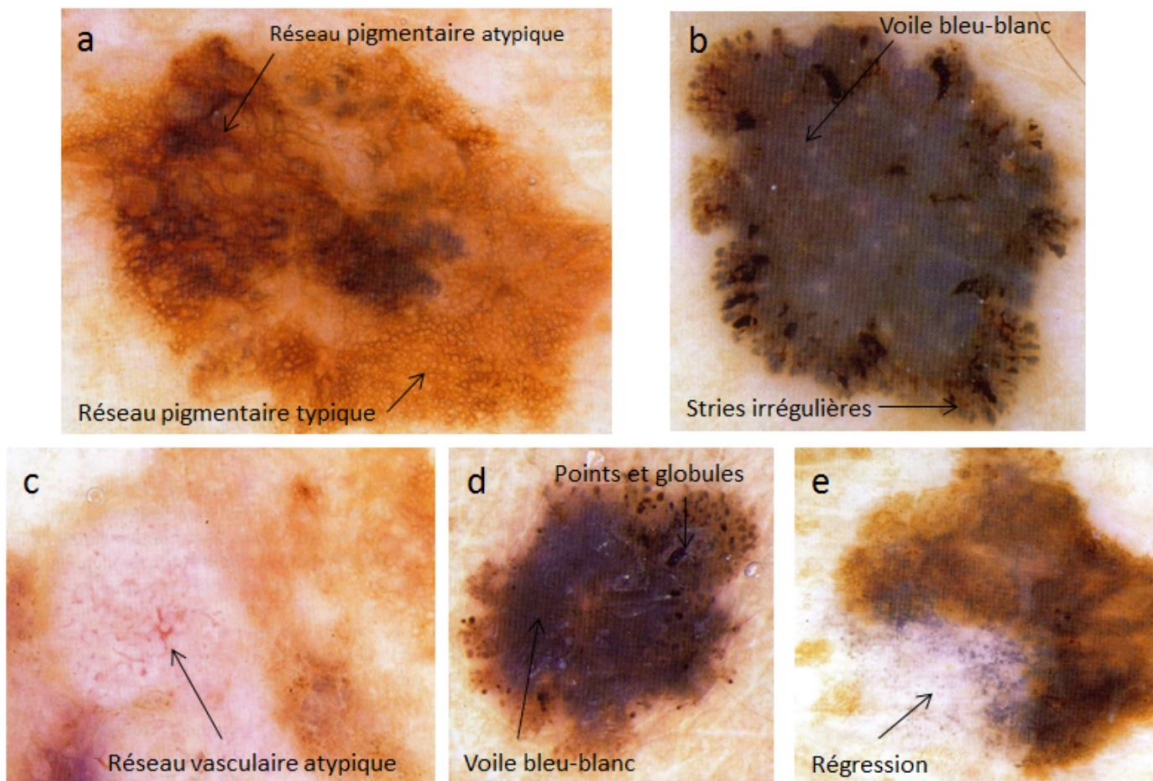


Figure 7: Mélanomes présentant des microstructures caractéristiques permettant de les identifier grâce à la méthode de la liste en 7 points : (a) réseau pigmentaire atypique, et quelques structures de régressions au centre. (b) voile bleu-blanc et stries radiales irrégulières. On peut voir des points et des globules irrégulièrement répartis. (c) réseau vasculaire atypique et irrégulier. On peut voir également des points et des globules irrégulièrement répartis. (d) voile bleu-blanc, points et globules. (e) large structure de régression avec également une répartition irrégulière de points et de globules. Photos tirées de « Atlas of dermoscopy »⁷¹

Un critère majeur + un critère mineur ou un minimum de 3 critères mineurs indique la présence d'un mélanome.

Des critères spécifiques sont utilisés dans le cas de lésions présentes sur le visage, la paume des mains et la plante des pieds à cause de la géométrie particulière de l'épiderme à ces endroits.

- **La méthode de Menzies**

Cette méthode a été établie pour aider les cliniciens peu expérimentés⁴⁸. Elle se base sur l'analyse globale de la lésion et de ses microstructures et consiste en :

- **2 critères négatifs** (on ne les trouve jamais dans un mélanome) : symétrie de la lésion, présence d'une seule couleur (indiquant ainsi que les mélanocytes sont regroupés au niveau d'une même couche)
- **9 critères positifs** (au moins 1 doit être présent pour diagnostiquer un mélanome) : voile bleu-blanc, points bruns multiples, 5 ou 6 couleurs, pseudopodes irrégulièrement répartis, rayonnement pigmentaire radial, dépigmentation cicatricielle, globules ou points noirs à la périphérie, plusieurs points bleus ou gris, réseau pigmentaire élargi.

- **L'analyse du patron de la lésion**

Enfin cette dernière méthode se base sur de nombreux critères morphologiques portant sur le patron global de la lésion (réticulaire, globulaire, pavimenteux, homogène, en éclats d'étoile, parallèle, à composantes multiples) et ses microstructures (stries, points, voile bleu-blanc, régressions, dépigmentation, taches d'encre, patron vasculaire)⁷⁴.

Ces algorithmes amènent chacun à des sensibilités (risque de faux négatif) et leur spécificités (risque de faux positif) différentes comme présenté dans le tableau ci-dessous.

Méthode	Sensibilité (faux négatif)	Spécificité (faux positif)
Règle ABCDEF	82.6	70.0
Liste de 7 points	83.6	71.5
Méthode de Menzies	85.7	71.1
Analyse de patron	83.7	83.4

Tableau 1: Sensibilité et spécificité des différentes méthodes de diagnostic du mélanome⁷⁵

Les valeurs sont indiquées en pourcentage. Plus le pourcentage est élevé, plus la méthode est sensible et spécifique, c'est-à-dire moins il y a de chance d'avoir un faux négatif ou faux positif.

8) Première prise en charge du patient après diagnostic et détermination du stade du mélanome

Suite au diagnostic du dermatologue, une biopsie de la lésion maligne est réalisée afin de confirmer ou réfuter le diagnostic par analyse histopathologique. Le but est également de déterminer le stade de mélanome c'est-à-dire son étendue au moment du diagnostic afin de proposer aux patients le traitement approprié.

Pour déterminer le **stade** du cancer, les médecins s'appuient sur un système international de classification, le système TNM (*Tumor Thickness, Nodal Involvement and Metastasis*)^{76,77}.

Pour évaluer le stade du mélanome, les médecins prennent en compte plusieurs critères.

- **Les caractéristiques de la tumeur primitive (T)**

Son épaisseur

L'épaisseur de la tumeur appelée indice de Breslow, donne une indication du degré d'extension de la maladie dans les couches de la peau, au moment du diagnostic. Une invasion verticale profonde du mélanome est associée à une propagation de la maladie et ainsi à un mauvais pronostic.

Son ulcération

L'ulcération en surface du mélanome donne une information sur l'étendue de mélanome. En effet, l'ulcération permet au mélanome de croître horizontalement et verticalement^{78,79}.

Le nombre de mitoses au mm²

Le nombre de mitoses renseigne sur la vitesse à laquelle les cellules cancéreuses se divisent.

Cet examen est effectué uniquement pour les mélanomes d'épaisseur inférieure ou égale à 1 mm.

- **La présence de métastases en transit et l'atteinte des ganglions lymphatiques (N)**

Les mélanocytes peuvent s'échapper de la tumeur primitive et se disséminer dans les ganglions lymphatiques, situés à proximité de l'endroit où le mélanome est apparu. Ils peuvent ainsi former des métastases en transit dans les vaisseaux lymphatiques, entre le mélanome primitif et les ganglions lymphatiques proches et des métastases ganglionnaires lorsqu'ils atteignent les ganglions.

- **La présence de métastases dans le reste du corps (M)**

Dans le mélanome, les organes le plus souvent touchés par les métastases sont le poumon, la peau, le foie, les os et le cerveau⁸⁰

Tous ces facteurs sont des facteurs pronostiques qui donnent une indication sur l'évolution possible de la maladie. Ils permettent également de définir le stade du mélanome et ainsi de choisir les traitements les plus appropriés. Le tableau ci-dessous résume les différents stades du mélanome ainsi que les traitements qui peuvent être proposés aux patients en fonction du stade.

Stade	Description	Traitements proposés
0 (<i>in situ</i>)	Les cellules cancéreuses sont seulement présentes sur la couche supérieure de la peau.	Chirurgie
IA	Diamètre tumoral > 0,8mm et < 1mm Epaisseur tumorale < 0,8mm Présence ou non d'ulcération	Chirurgie avec éventuellement traitement adjuvant pour éviter des récidives
IB	Diamètre tumoral > 1mm Epaisseur tumorale < 2mm Pas d'ulcération	

IIA	Diamètre tumoral > 2mm et < 4mm Epaisseur tumorale >1mm et < 2mm Présence ou non d'ulcération	
IIB	Epaisseur tumorale > 2mm et < 4mm + ulcération Ou Epaisseur tumorale > 4mm + sans ulcération	
IIC	Epaisseur tumorale > 4mm + ulcération	
III	Métastases dans un ou plusieurs ganglions proches du site tumoral initial	La chirurgie de la tumeur et des ganglions proches de la tumeur (curage ganglionnaire) + traitement adjuvant décidé en RCP (réunion de consultation pluridisciplinaire)
IV	Cancer métastatique avec métastases dans le reste du corps (notamment foie et poumons)	La chirurgie des métastases si accessibles + traitement médicamenteux décidé en RCP

Tableau 2: Différents stades du mélanome et traitements associés. Tableau issu de Naik et al.

2021⁸¹ et du document « Les traitements du mélanome de la peau », Institut National du Cancer, 2016

II. Prise en charge « conventionnelle » du mélanome

1) Chirurgie

La chirurgie reste à ce jour le traitement le plus utilisé pour le mélanome peu importe le stade auquel il est diagnostiqué. Comme énoncé précédemment, une première chirurgie (exérèse diagnostique) est tout d'abord réalisée. Elle permet d'une part la confirmation du diagnostic de mélanome et d'autre part le retrait de la lésion dans un but de contrôle local de la maladie et de prévention de la dissémination des cellules mélanocytaires. Cette première chirurgie permet également de rechercher des mutations de certains gènes comme les gènes BRAF et MEK. Pour les mélanomes *in situ* cette chirurgie est considérée comme curative.

Cette exérèse peut ensuite être compléter par une deuxième chirurgie (exérèse élargie) visant à enlever le reste de la lésion et éventuellement les ganglions touchés. Cette exérèse élargie consiste à retirer une bande plus ou moins large de tissu sain autour de la cicatrice de la première exérèse afin de limiter les risques de rechute. Cette zone est appelée marge de peau saine ou marge de sécurité. Dans le cas où l'exérèse du ganglion sentinelle est nécessaire, 1 à 3 ganglions sont retirés et analysés. En renseignant sur l'envahissement ou non des ganglions, l'exérèse du ganglion sentinelle permet de préciser le stade du cancer, et donne ainsi une indication pronostique pour le patient. En effet, le risque de récidive est plus élevé chez les patients dont le ganglion sentinelle est atteint. Ainsi, si le ganglion sentinelle est envahi, le traitement proposé comprend, dans la plupart des cas, un curage ganglionnaire, parfois associé à un traitement adjuvant (traitement médicamenteux ou radiothérapie). Le curage ganglionnaire a pour but de retirer le plus grand nombre de ganglions lymphatiques de la région drainant la zone où siégeait la tumeur. Malheureusement dans certains cas (environ 20%) le patient peut tout de même rechuter ce qui est associé à un mauvais pronostique⁸².

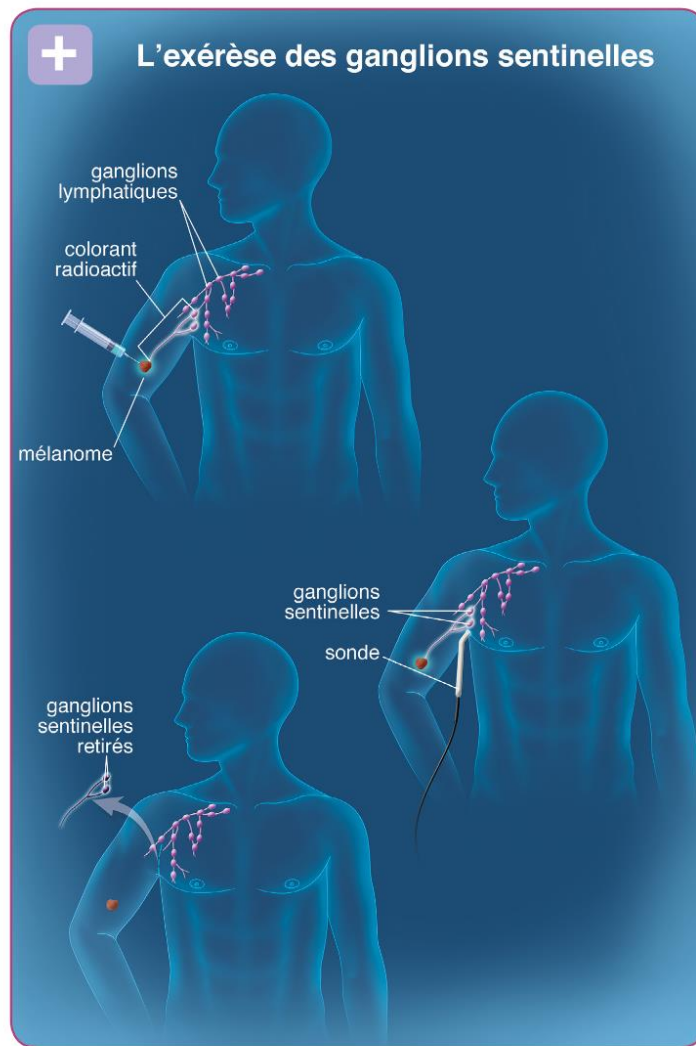


Figure 8: Exérèse des ganglions sentinelles. Illustration issue du document « Les traitements du mélanome de la peau », Institut National du Cancer, 2016

2) Radiothérapie

Un autre traitement également utilisé en thérapie du mélanome est la radiothérapie. Historiquement, le mélanome a toujours été considéré comme étant une tumeur résistante aux radiations à cause de solides mécanismes intrinsèques de réparation des dommages causés à l'ADN⁸³. Cependant, sous certaines conditions (chirurgie non possible, soins palliatifs,

irradiation au niveau du site d'exérèse de la tumeur et/ou des ganglions) la radiothérapie peut être utilisée pour traiter le mélanome^{83,84}.

Il a été non seulement montré que l'irradiation parvenait à tuer les mélanomes ciblés mais induisait également un effet anti tumoral systémique affectant les métastases non ciblées par l'irradiation. Cette capacité des rayonnements localisés à déclencher un effet anti-tumoral systémique est appelé effet abscopal et il a été caractérisé dans de nombreux cancers^{85,86}.

3) Chimiothérapie

La chimiothérapie reste à ce jour encore utilisée pour le traitement du mélanome malgré une efficacité limitée. Les deux chimiothérapies utilisées pour le traitement du mélanome sont les suivantes :

- **La Dacarbazine (DTIC)**

Cet agent alkylant a été approuvé en 1975 pour le traitement du mélanome, cependant, comme la plupart des chimiothérapies, ce traitement n'est pas spécifique et de ce fait endommage beaucoup les cellules saines du patient. De plus, de nombreux essais cliniques ont reporté l'efficacité modeste de cet agent pour le traitement du mélanome. Il reste cependant l'un des principaux traitements de première ligne pour le mélanome métastatique⁸⁷.

- **Le Temozolomide**

Ce traitement est considéré comme un analogue de la dacarbazine mais il a le gros avantage d'être administrable par voie orale. Il est donc particulièrement étudié. De plus, le temozolomide peut atteindre le système nerveux central ce qui représente un point crucial pour le traitement du mélanome avancé, le cerveau étant un des sites de métastases les plus courants⁸⁷.

4) Les thérapies ciblées

Les thérapies ciblées ont révolutionné la prise en charge du mélanome en 2011 lorsque les premiers agents ont été approuvés. On retrouve à ce jour 2 grandes classes de thérapies ciblées : les inhibiteurs de BRAF et les inhibiteurs de MEK.

- **Les inhibiteurs de BRAF**

BRAF étant l'oncogène le plus fréquemment muté dans le mélanome⁸⁸, ses inhibiteurs ont donné des résultats prometteurs dans plusieurs essais cliniques, avec une régression rapide des métastases et des réponses positives chez 50 à 60 % des patients atteints de mélanome^{87,89}. Le premier médicament ayant été approuvé pour le mélanome est le vémurafénib, une molécule inhibitrice sélective du BRAF mutant V600⁸⁸. La mutation activatrice BRAF V600E est responsable de l'hyperactivation de la voie MAPK entraînant une prolifération des cellules cancéreuses. Le vémurafénib inhibe l'activité kinase responsable de l'hyperactivation de cette voie⁹⁰⁻⁹². Dans un essai clinique de phase III (BRIM3), le vemurafenib a montré un taux de réponse objective (ORR) de 48% contre 5% pour la dacarbazine, et une survie médiane sans progression (PFS) de 5,3 mois contre 1,6 mois pour la dacarbazine^{88,93}.

Un deuxième inhibiteur de BRAF, le dabrafenib, a été approuvé peu de temps après et montre également des résultats prometteurs⁸⁸. En termes de toxicités pour ces agents nous retrouvons des éruptions cutanées, de l'arthralgie, de la fatigue, de la fièvre (pour le dabrafenib uniquement) et de la photosensibilité (uniquement pour le vemurafenib). On observe également le développement de lésions cutanées secondaires non mélanoïques, telles que le carcinome spinocellulaire^{94,95}.

- **Les inhibiteurs de MEK**

La deuxième classe de thérapies ciblées sont les inhibiteurs de MEK. Leur développement a été initié lorsqu'il a été découvert que la signalisation de BRAF dépendait de l'activation en aval de MEK1/2^{88,96}.

Le trametinib appartient à cette nouvelle classe de thérapies ciblées et a montré des résultats prometteurs lors d'un essai clinique de phase III (METRIC) dans les mélanomes BRAF mutés V600E/K avancés ou métastatiques. Lors de cet essai, une PFS (« Progression Free Survival » soit survie sans progression) médiane de 4,9 mois dans le groupe trametinib contre 1,5 mois dans le groupe chimiothérapie a été observé. La plupart des patients (65 %) du groupe chimiothérapie sont rapidement passés dans le groupe trametinib. Aucun événement indésirable inattendu n'a été signalé⁹⁷.

L'association d'inhibiteurs de BRAF et de MEK est désormais devenue un des traitements standard des mélanomes avancés comportant la mutation BRAF V600^{88,90}. Des données suggèrent que chez les patients présentant un BRAF muté, l'association d'inhibiteurs de BRAF et de MEK apporte un plus grand bénéfice et retarde le développement de résistance^{98–100}. Récemment, de nouvelles combinaisons d'inhibiteurs de BRAF et de MEK ont été approuvées pour leur utilisation dans le mélanome malin, comme l'inhibiteur de BRAF, encorafenib, et les inhibiteurs de MEK, cobimetinib et binimétinib^{101–104}.

Les **inhibiteurs de KIT**, une tyrosine kinase, sont également une thérapie ciblée utilisée pour le traitement du mélanome. Les mutations et amplifications de KIT sont observées chez moins de 7 % des patients atteints de mélanomes cutanés et chez environ 40 % des patients atteints de mélanomes muqueux et acraux^{55,105}. KIT est une tyrosine kinase clé qui lorsqu'elle est mutée ou stimulée par la liaison du facteur des cellules souches (SCF), active les voies MAPK et PI3K/AKT entraînant la prolifération des cellules cancéreuses¹⁰⁶.

Les patients atteints de mélanome peuvent bénéficier des inhibiteurs imatinib et nilotinib, uniquement après une stratification basée sur leur statut mutationnel de KIT¹⁰⁶. En effet, les amplifications de KIT, à la différence des mutations de KIT, ne confèrent pas de sensibilité à

ces inhibiteurs¹⁰⁶⁻¹⁰⁹. Par ailleurs il a été démontré que suivant le sous-type de mélanome, KIT pouvait agir comme un oncogène ou un suppresseur de tumeur^{110,111}.

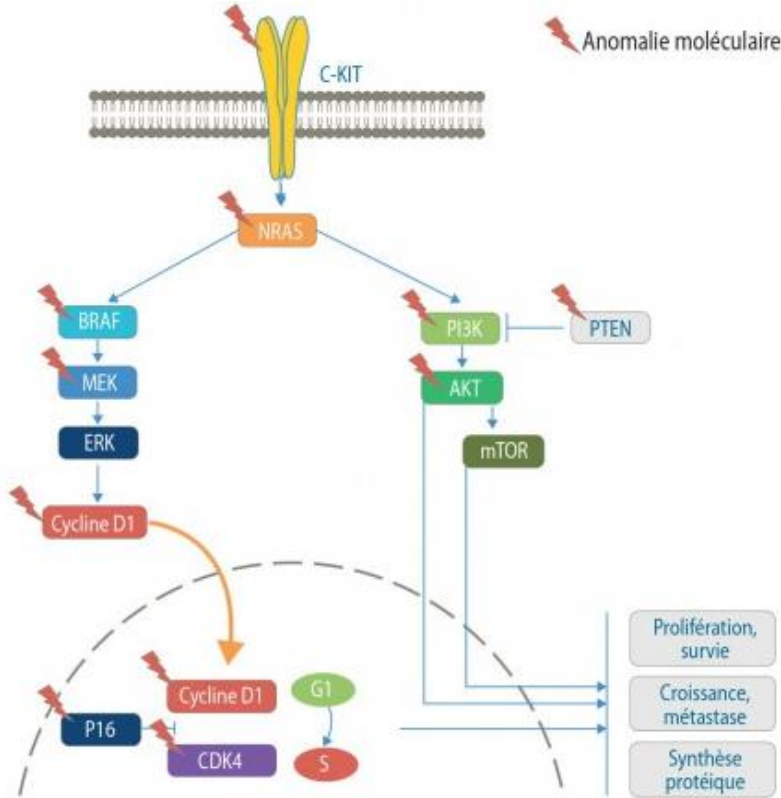


Figure 9: Impact de l'altération, en cas de cancer, des voies de signalisation impliquant BRAF, MEK et KIT. Schéma issu de S. Mourah, C. Lebbé¹¹²

Malheureusement, comme tous les traitements, les patients recevant des inhibiteurs de BRAF et de MEK finissent par développer une résistance et leur maladie progresse, en raison de mécanismes de résistance acquis et intrinsèques à la tumeur. Ces traitements ont été utilisés pendant des années, avant de s'orienter vers de nouvelles stratégies très prometteuses

III. Les immunothérapies

Depuis une dizaine d'années, on assiste à un véritable essor des immunothérapies dans la prise en charge de nombreux cancers. Le mélanome fut l'un des premiers cancers où les immunothérapies (anticorps bloqueurs) ont montré un réel bénéfice clinique à long terme.

De manière générale, les immunothérapies telles que le blocage des points de contrôle immunitaire et la thérapie cellulaire adoptive, ont montré une réponse anti-tumorale remarquable, correspondant à une survie durable à long terme, mais malheureusement tous les patients n'ont pas répondu à ces thérapies^{113,114}.

Le fait que tous les patients ne parviennent pas à bénéficier de ces thérapies suggère qu'une meilleure classification des patients, basée sur leurs caractéristiques, leurs biomarqueurs moléculaires et le sous-type de mélanome, est nécessaire pour améliorer les taux de réponse.

Par ailleurs, suite à l'utilisation de ces nouvelles immunothérapies, les critères d'évaluation de la réponse dans les tumeurs solides (critères RECIST), initialement développés pour déterminer de manière impartiale la réponse de la tumeur aux agents cytotoxiques, ont été modifiés.

Ces nouvelles directives, connues sous le nom de critères RECIST immunologiques (iRECIST) ont pour but prendre en compte les caractéristiques de ces nouvelles thérapies et plus particulièrement le retard de la réponse immunitaire adaptative anti-tumorale associé à ces thérapies. Ces nouveaux critères aident les cliniciens de plusieurs centres à concevoir et à gérer de manière cohérente les données d'immunothérapies, afin de garantir une analyse ainsi qu'une interprétation précise de leur efficacité¹¹⁵⁻¹¹⁷.

1) Les inhibiteurs de points de contrôles immunitaires

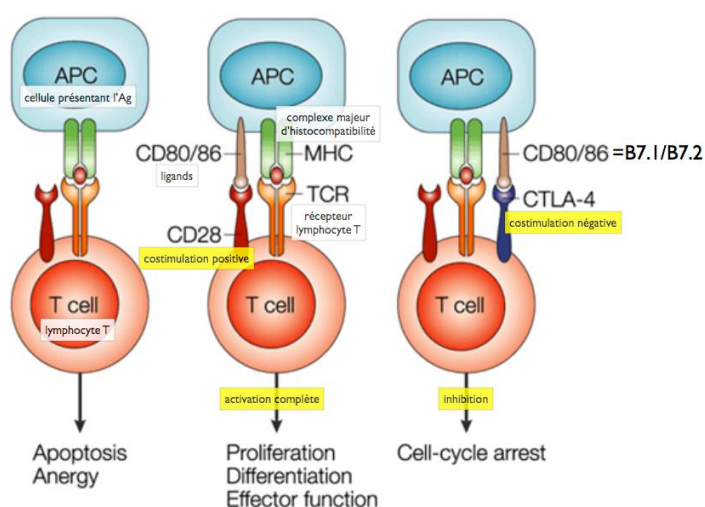
a. Les points de contrôle immunitaires (« immune checkpoints »)

Les deux points de contrôle immunitaire les plus étudiés en immunothérapie sont l'antigène 4 des lymphocytes T cytotoxiques (CTLA-4) et la protéine 1 de mort cellulaire programmée (PD-1). En temps normal, ces molécules régulent le système immunitaire afin d'éviter une suractivation lors d'infections réduisant ainsi le risque de développement d'une maladie autoimmune¹¹⁸⁻¹²⁰.

- **CTLA-4**

CTLA-4 est un récepteur et un membre de la super-famille des immunoglobulines CD28:B7 que l'on retrouve à la surface des cellules T effectrices et des cellules Treg. Sa fonction est de réguler l'intensité de l'activation de ces cellules.

En effet, lorsque les cellules T CD8+ interagissent avec les cellules dendritiques au sein des ganglions lymphatiques, 2 signaux sont nécessaires pour une activation correcte des cellules T : l'interaction du TCR avec le complexe CMH/peptide présent sur les cellules dendritiques et le signal secondaire de CD28 sur les cellules T, qui se lie à CD80/CD86 sur les cellules dendritiques¹²¹.



Source: Alegre et coll. Nature Reviews Immunology 2001;1: 220-228

Figure 10: Régulation des lymphocytes T par CD28 et CTLA-4

En effet, au moment de l'activation des lymphocytes T par les cellules présentatrices d'antigènes (cellules dendritiques par exemple) le CD28 du lymphocyte T se lie au CD80/CD86 de la cellule dendritique. Ce signal de costimulation déclenche l'expansion des cellules T. Le CTLA-4 peut également se lier CD80/CD86 avec une plus grande affinité que le CD28, inhibant ainsi la signalisation TCR en aval et entravant la fonction des cellules T CD8+¹²²⁻¹²⁴. Cela permet de réguler la réponse immunitaire et ainsi d'éviter un emballement de celle-ci. Dans les tumeurs, le CTLA-4 est surexprimé pour supprimer l'activation des cellules immunitaires qui auraient pu réussir à atteindre le site de la tumeur (lymphocytes infiltrant la tumeur - TIL)¹²⁵.

- **PD-1**

PD-1 est également un récepteur inhibiteur comme CTLA-4. Il est exprimé sur les lymphocytes T et B activés, les Tregs ainsi que les cellules NK et exerce sa fonction une fois qu'il est lié à ses deux ligands, PD-L1 et PD-L2. Le ligand PD-L1 est exprimé sur les cellules dendritiques, les macrophages et les lymphocytes B. Dans les tumeurs, le ligand PD-L1 présent à la surface des cellules cancéreuses permet d'inhiber l'activation et la fonction des cellules immunitaires (lymphocytes T notamment) qui auraient pu réussir à atteindre le site de la tumeur¹²⁶.

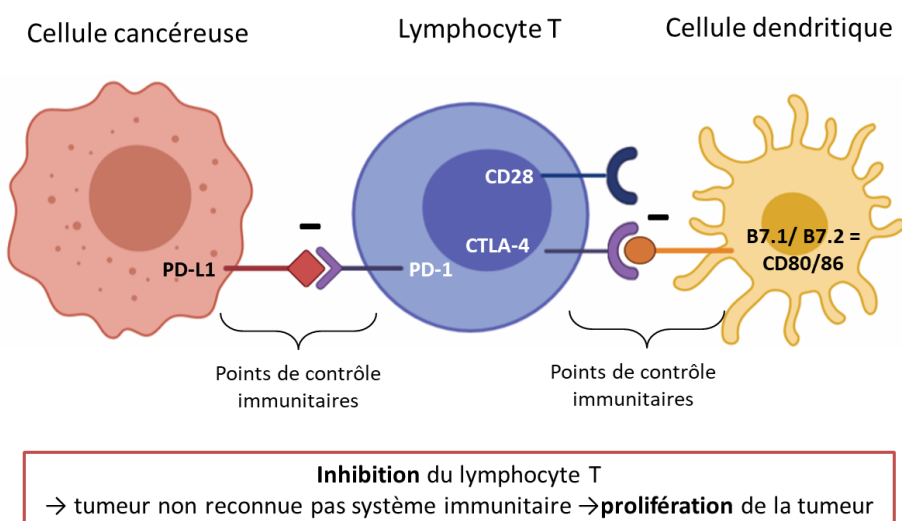


Figure 11: Rôle des points de contrôles immunitaires PD-L1 et CTLA-4 dans un contexte tumoral. Schéma réalisé sur BioRender.

Ces 2 récepteurs font partie de la famille des points de contrôle immunitaires comme ils régulent le système immunitaire. Ces dernières années, ils ont servi de cible au développement d'anticorps se liant à ses récepteurs permettant ainsi la réactivation des cellules immunitaires dans les tumeurs par levée de l'inhibition.

b. Les anticorps bloqueurs des points de contrôle immunitaires

- **L'Ipilimumab : anticorps anti CTLA-4**

Le premier anticorps développé, dirigé contre les points de contrôles immunitaires est l'ipilimumab.

L'ipilimumab se lie à CTLA-4 sur les cellules T, ce qui inhibe sa capacité à se lier à CD80/CD86, et permet l'expansion d'un répertoire de cellules T CD8+ cytotoxiques anti-tumorales spécifiques de l'antigène ainsi que des cellules T CD4+. Il en découle une meilleure réponse immunitaire anti-tumorale¹²⁷⁻¹²⁹. De manière intéressante, il a été montré que la partie Fc de l'anticorps ipilimumab pouvait épuiser les Tregs dans le microenvironnement tumoral, en activant les macrophages exprimant le Fc γ , amplifiant ainsi la réponse immunitaire antitumorale¹³⁰⁻¹³³.

L'ipilimumab a obtenu l'autorisation de la FDA pour le traitement du mélanome après une série d'essais cliniques de phase III (CA184-002 en monothérapie, CA184-024 en association avec la dacarbazine). Le taux de survie à cinq ans était de 18,2 % pour les patients traités par anti-CTLA-4 + dacarbazine contre 8,8 % pour les patients traités par placebo + dacarbazine (CA184-024, NCT00324155)¹³⁴. La toxicité associée à l'ipilimumab comprend de forts effets secondaires liés au système immunitaire tels que la dermatite, la colite, la diarrhée et, plus rarement, l'hépatite, l'uvéite et l'hypophysite¹³⁵.

En France, l'ipilimumab est actuellement accessible uniquement en combinaison avec le nivolumab mais n'est plus utilisé en monothérapie.

- **Le pembrolizumab et le nivolumab : anticorps anti PD1**

Après la preuve de concept de l'ipilimumab, démontrant qu'un blocage des points de contrôle pouvait réellement être une stratégie efficace pour traiter le mélanome, le pembrolizumab et le nivolumab dirigés contre le PD1 ont été étudiés. L'essai clinique de phase III a rapporté une survie globale médiane qui n'a pas été atteinte dans le groupe nivolumab + ipilimumab et qui était de 37,6 mois dans le groupe nivolumab, contre 19,9 mois dans le groupe ipilimumab. Le taux de survie globale à 3 ans était de 58 % dans le groupe nivolumab + ipilimumab et de 52 % dans le groupe nivolumab, contre 34 % dans le groupe ipilimumab (NCT01844505)^{88,136–138}.

- **L'atezolizumab: anticorps anti PD-L1**

L'atezolizumab, un anticorps anti PD-L1 est également exploré en ce moment dans de nombreux essais cliniques¹³⁹.

Cet anticorps se révèle intéressant à étudier car il a été démontré que les anticorps bloquant PD-L1 avaient une efficacité plus élevée pour bloquer la signalisation PD-1/PD-L1 que les anticorps PD1, démontrant ainsi que le pembrolizumab était plus puissant que le nivolumab¹⁴⁰.

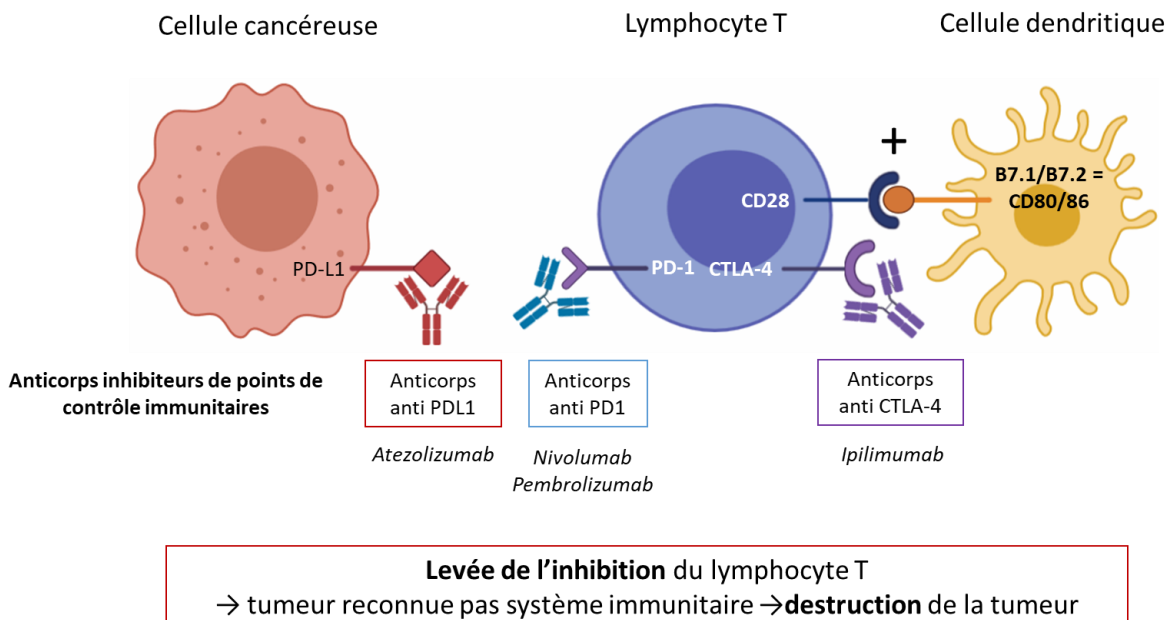


Figure 12: Action des anticorps bloqueurs. Schéma réalisé sur BioRender.

- **Autres cibles et anticorps bloqueurs associés actuellement à étude**

Le succès des résultats obtenus avec les anti-PD1 et les anti-CTLA4 ont motivé le développement des recherches autour d'autres points de contrôle immunitaire. Le tableau ci-dessous présente quelques-unes de ces cibles.

Déverrouillage de freins	Induction de stimulation	Facteurs solubles	Autres
LAG3	41BB	Anti TNF α	Anti intégrine $\alpha 4\beta 7$
TIM3	GITR	Inhibiteur de IDO	Anti RANKL
TIGIT	CD40	Axe A2AR/CD73	Anti VEGF
B7H3	OX40		Ganglioside

Tableau 3: Autres molécules ciblées dans les essais en développement

Devant les résultats très prometteurs de thérapies ciblées et d'immunothérapie, la tendance actuelle est de combiner ces deux approches. La triple combinaison d'atezolizumab, de vemurafenib (inhibiteur de BRAF V600E) et de cobimetnib (inhibiteur de MEK) a ainsi été approuvée par la FDA comme traitement de première ligne du mélanome BRAF V600 non résécable ou métastatique¹⁴¹.

c. Biomarqueurs prédictifs de bonne réponse à l'immunothérapie par anticorps bloqueurs

L'identification de biomarqueurs chez les patients est devenue primordiale de nos jours afin de prédire la réponse au traitement et les résultats en matière de survie¹⁴². Cette identification a pour but d'aider les cliniciens dans leur choix de traitement afin d'administrer à chaque patient un traitement qui lui est le plus approprié en termes de survie, d'effets secondaires etc...

Il est également primordial d'identifier de manière précise quels patients sont susceptibles de répondre à un traitement donné et lesquels ne le sont pas. Cela permet non seulement d'améliorer la qualité de vie des patients mais aussi de réduire la charge financière des patients qui ne répondent pas au traitement.

Différents biomarqueurs ont été étudiés dans le mélanome :

- **L'âge et le sexe**

Une méta-analyse regroupant des essais cliniques impliquant des anticorps bloqueurs a montré un bénéfice clinique plus important chez les hommes que chez les femmes atteints de mélanome¹⁴³. Cette différence s'expliquerait par des différences entre les sexes au niveau des marqueurs moléculaires comme la charge mutationnelle de la tumeur, l'expression de néo

antigènes, l'expression de PD-L1 et enfin le ratio entre cellules immunitaires anti et pro-tumorales¹⁴³.

De plus, une meilleure présentation antigénique a été observée sur les cellules tumorales des patients âgés et des hommes que sur celles des jeunes patients et les femmes, entraînant ainsi une meilleure détection du système immunitaire et une meilleure réponse aux anticorps bloqueurs¹⁴⁴.

- **L'expression de PD-L1**

Ces dernières années, la stratification des patients atteints de mélanome sur la base de l'expression de PD-L1 sur leurs cellules tumorales et immunitaires est devenue cruciale pour identifier les répondeurs aux thérapies anti-PD-1/anti-PD-L1. En effet, les patients traités par anti-PD-1 qui présentent des mélanomes PD-L1 positifs ont des taux de réponse de 50 à 60 %. Leur survie est meilleure que celle des mélanomes PD-L1 négatifs, dont les taux de réponse sont de 10 à 20 %^{145–147}. Cette même tendance a été observée chez les patients traités par atezolizumab, un anticorps anti-PD-L1¹⁴⁵. Cependant, certains patients présentant des tumeurs PD-L1-positives ne répondent pas au traitement anti-PD-1, alors que d'autres patients présentant des tumeurs PD-L1-négatives répondent au traitement, ce qui suggère que d'autres facteurs interviennent dans les réponses au traitement^{148,149}.

Par ailleurs, même si PD-L1 semble être un bon marqueur prédictif de réponse, il ne convient pas de l'utiliser seul. En effet, c'est un biomarqueur dynamique et son expression peut varier en fonction du traitement administré, de la localisation (différents niveaux d'expression entre une tumeur primaire et métastatique et même au sein d'une même tumeur) mais également du temps (différents niveaux d'expression au même endroit mais à deux instants donnés)^{149,150}.

- **Charge mutationnelle de la tumeur**

Il a été observé dans plusieurs cancers dont le mélanome que la charge mutationnelle de la tumeur pouvait jouer un rôle dans la réponse au traitement. Cela s'explique par le fait que les tumeurs ayant une charge mutationnelle élevée, c'est-à-dire comprenant de nombreuses mutations, ont plus de chances de présenter des néo épitopes favorisant ainsi la réponse immunitaire antitumorale^{151,152}.

Dans le mélanome, il a été constaté que les patients présentant un taux de mutation tumorale élevé avaient une meilleure survie suite aux thérapies anti-PD-1/anti-PD-L1. Cependant, certains patients présentant cette forte charge mutationnelle n'ont pas répondu^{153,154}.

- **Présence et quantité de cellules immunitaires pro et anti tumorales**

La présence ou non de cellules immunitaires dans la tumeur est fortement liée à la charge mutationnelle de la tumeur. En effet, plus la tumeur présente des mutations et par conséquent des néo épitopes plus la probabilité qu'elle soit reconnue par le système immunitaire est forte. Certains auteurs¹⁵⁵ ont même proposé l'existence de mutations spécifiques qui rendent une tumeur plus réactive à la thérapie par points de contrôle immunitaires, ce qu'ils définissent comme le " seuil de mutation activant les points de contrôle immunitaires (iCAM) ". Ainsi on observe une augmentation de l'infiltration immunitaire (lymphocytes T CD8+ notamment) dans les tumeurs iCAM positives qui est corrélé à une meilleure réponse au traitement par points de contrôles immunitaires (anti-PD-1/anti-CTLA-4). Cette tumeur infiltrée est donc décrite comme « chaude » contrairement aux tumeurs non infiltrées « froides ».

- **Le microbiote intestinal**

L'étude du microbiote et notamment le microbiote intestinal est un domaine qui s'est extrêmement développé ces dernières années. De nombreux chercheurs partout dans le monde

tentent de comprendre son implication dans le cancer et de découvrir les bactéries favorisants ou non le développement de cancers ou la réponse aux thérapies anticancéreuses^{156–158}.

• Le type de mélanome

Comme décrit précédemment dans ce chapitre, il existe plusieurs types de mélanome qui présentent chacun des charges mutationnelles tumorales, une expression de PD-L1 et des micro-environnements distincts. Ces différences influent donc sur la réponse aux anticorps bloqueurs. Ces sous-types peuvent être divisés en 2 grandes catégories : les mélanomes cutanés (CSID et non-CSID) avec une charge mutationnelle élevée, et les mélanomes non cutanés (mélanome acral, muqueux et uvéal) qui présentent quant à eux une charge mutationnelle plus faible.

Ainsi il a été observé que le mélanome cutané présente de meilleurs taux de réponse aux traitements par blocage des points de contrôle immunitaires que le mélanome non cutané^{56,159–}

¹⁶¹

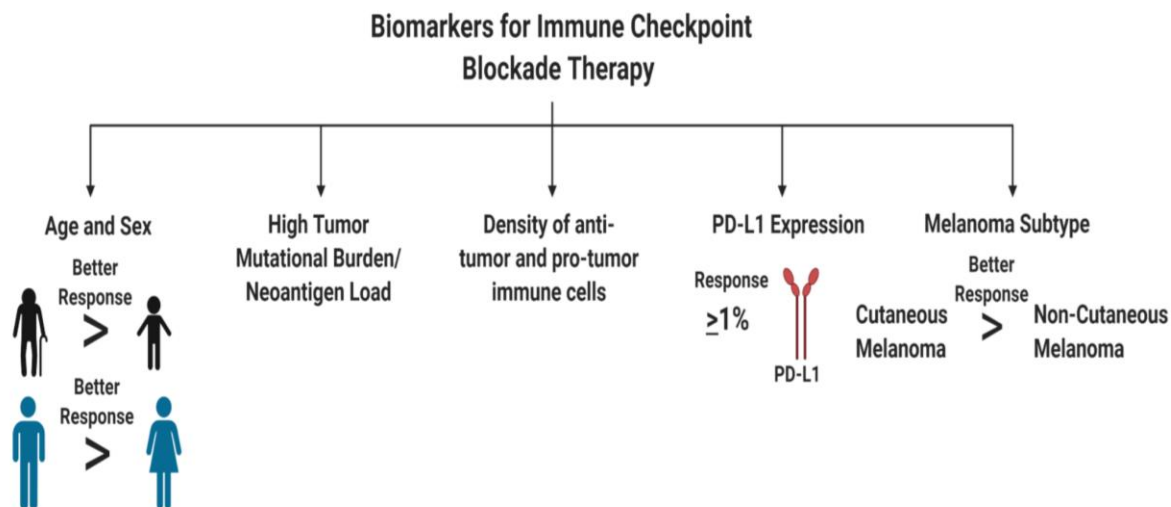


Figure 13: Récapitulatif des biomarqueurs prédictifs pour un traitement par anticorps bloqueurs. Figure issue de Eddy et Chen, 2020⁴⁵

La mise en évidence de ces biomarqueurs a permis de mieux guider les cliniciens dans leur choix de traitement et ainsi permettre aux patients d'obtenir le traitement ayant le plus de chance

de succès thérapeutique. Cependant, ces biomarqueurs sont loin d'être suffisants et comme décrit précédemment, des patients présentant des biomarqueurs en faveur d'un traitement par anticorps bloqueurs (expression de PD-L1) n'ont pas répondu et vice versa.

Idéalement, une caractérisation complète de la tumeur (charge mutationnelle, présence de cellules immunitaires/métabolites inhibiteurs/inhibiteurs solubles, expression de points de contrôle...) serait nécessaire afin de dicter le choix de traitement le plus approprié pour le patient. Malheureusement cette caractérisation est très difficile car la composition de la tumeur peut varier d'une région à l'autre d'une même tumeur, entre 2 tumeurs du même patient et même sur la même zone d'une tumeur à 2 instants donnés. De plus, ces caractérisations ont un coût non négligeable et de ce fait ne sont pas disponibles dans tous les centres de soins. Des solutions alternatives sont actuellement en développement comme les biopsies liquides, permettant la capture de cellules cancéreuses circulantes, ainsi que le PET scan (immuno-positron-emission tomography en anglais) rendant possible la visualisation des lymphocytes T dans la tumeur.

2) Le transfert adoptif de lymphocytes T

Il existe à ce jour 3 types de thérapies adoptives par cellules T : la thérapie par lymphocytes infiltrant la tumeur (TIL), la thérapie par TCR modifié et la thérapie par récepteur antigénique chimérique (CAR)¹⁶².

Ces thérapies diffèrent légèrement les unes des autres, mais leur objectif principal est de renforcer la cytotoxicité des cellules T cytotoxiques (ainsi que d'autres cellules immunitaires) *ex vivo*, puis de les réinjecter aux patients pour induire une régression tumorale^{162,163}.

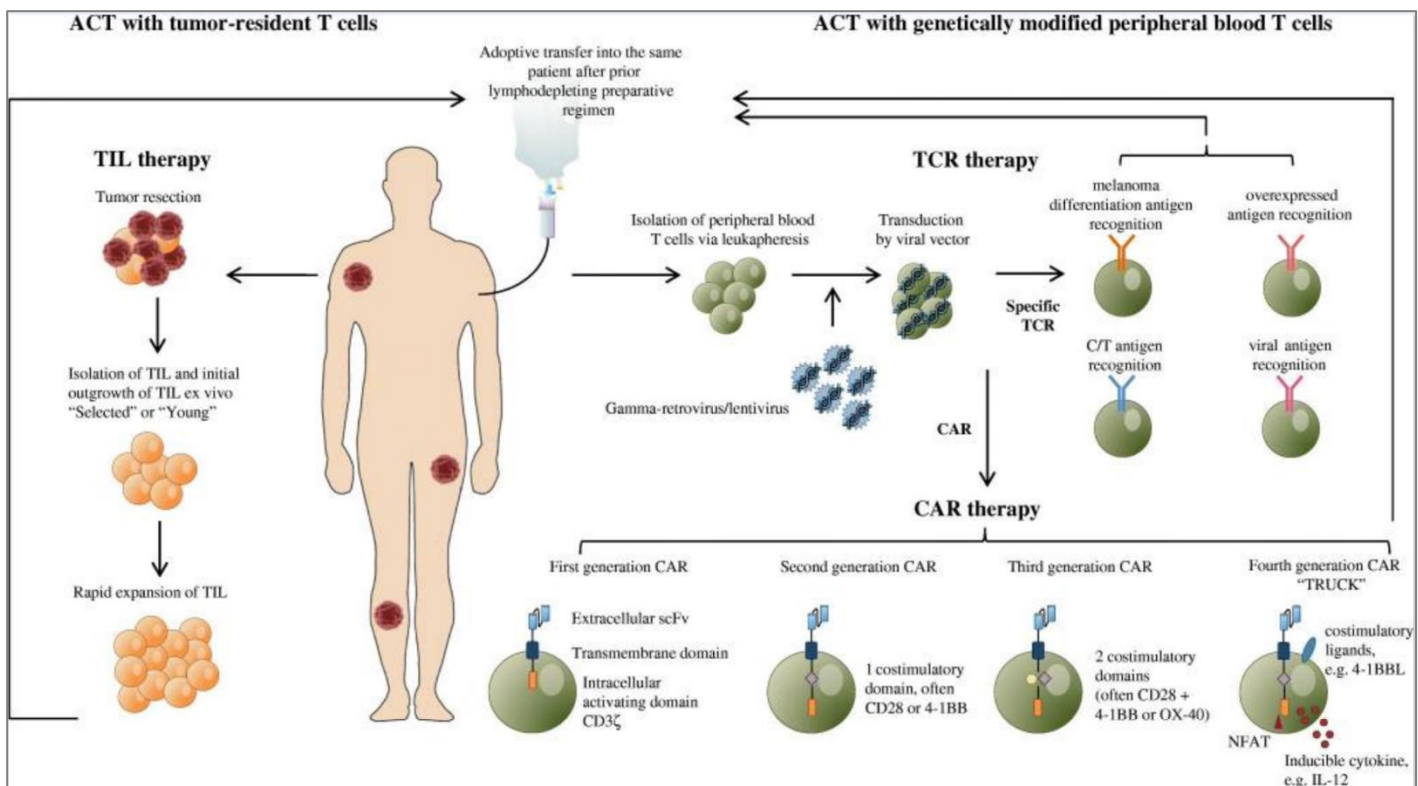


Figure 14: Schéma des différentes thérapies de transfert adoptif de lymphocytes T

(ACT=Adoptive Cell Transfer). Schéma issu de Rohaan et al.¹⁶⁴

a. La thérapie par lymphocytes infiltrant la tumeur (TIL)

Cette première thérapie constitue la base des 2 autres (thérapie par TCR modifiés et thérapie CAR)¹⁶⁵. Elle nécessite tout d'abord l'isolement de lymphocytes infiltrant la tumeur (TIL) à partir de tumeurs excisées, puis, la vérification de la capacité de ces TIL à induire une réponse immunitaire antitumorale^{162,166}. Les TIL isolés sont ensuite multipliés grâce à de l'IL-2, puis réinjectés avec de l'IL-2 à des patients dépourvus de lymphocytes^{162,167,168}. Le traitement par IL-2, associé à la thérapie par TIL, favorise la persistance des TIL réintroduits chez les patients, ainsi que les capacités cytotoxiques des cellules T CD8 + et des cellules NK antitumorales¹⁶⁹.

La thérapie TIL chez les patients atteints de mélanome métastatique a montré des taux de

réponse remarquables supérieurs à 50%, avec 22% de patients présentant une rémission complète^{167,168}.

Cette thérapie présente cependant des inconvénients. En effet, les tumeurs doivent être résécables et contenir des TILs qui pourront être isolés et amplifiés. Ce traitement lourd est souvent accompagné de forts effets secondaires. De plus, le temps d'amplification des lymphocytes peut parfois être long ce qui sous-entend que le patient doit être dans un état général relativement bon pour recevoir ce type de traitement.

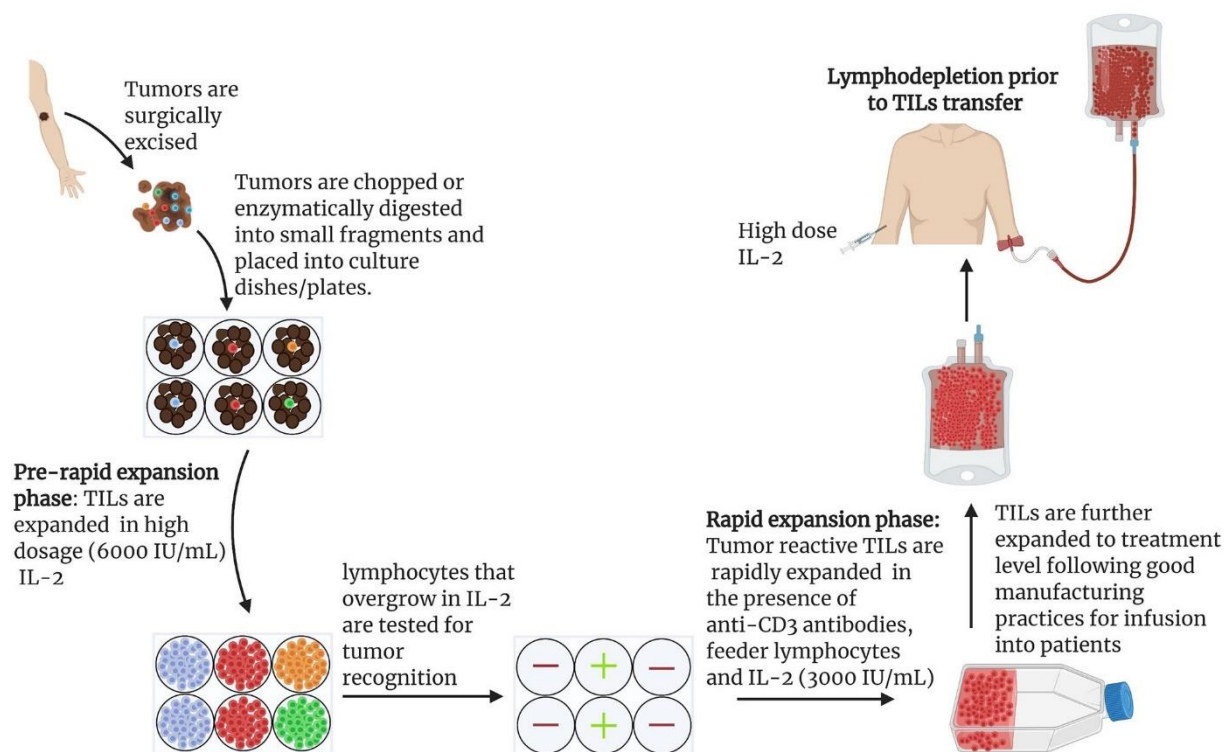


Figure 15: Schéma du protocole d'expansion des TILs du prélèvement à la réinjection chez le patient. Schéma issu de Kumar et al.¹⁷⁰

b. La thérapie par TCR modifiés

Nous avons vu précédemment que l'isolement et la disponibilité des TIL constituaient des obstacles à l'utilisation de la thérapie par lymphocytes infiltrant la tumeur. Pour surmonter ces obstacles la thérapie par TCR modifié a été développée.

Cette thérapie utilise des cellules T isolées chez un patient qui sont ensuite modifiées génétiquement afin qu'elles expriment un TCR spécifique d'un complexe CMH-I/peptide tumoral [431]. Une fois modifiées, ces cellules sont multipliées et réinjectées aux patients [432]. Cette thérapie dépend donc de l'identification d'un peptide tumoral via le CMH-I à la surface des cellules cancéreuses. Malheureusement dans le mélanome, comme dans beaucoup d'autres cancers, non seulement le CMH-I est souvent régulé à la baisse, ce qui rend difficile cette identification mais aussi l'effet anti-tumoral des lymphocytes T réinjectés est en général moindre^{171,172}. Le taux de réponse à une thérapie TCR modifiée est de ce fait assez faible (seulement 13 %)¹⁷³.

Pour surmonter ce problème, la thérapie CAR a été développée pour contourner les barrières imposées par l'expression du CMH I à la surface de la tumeur et permettre aux cellules T de se lier directement aux antigènes de surface de la tumeur¹⁶².

c. La thérapie par récepteur antigénique chimérique (CAR-T)

Cette thérapie repose sur l'insertion d'un récepteur antigénique chimérique (CAR) à surface des cellules T. Ce récepteur est conçu grâce à la fusion du domaine spécifique de l'antigène d'un anticorps monoclonal (scFv), à un domaine transmembranaire se liant aux composants intracellulaires du TCR, ainsi qu'à des molécules de costimulation nécessaires à l'activation des cellules T^{162,174}.

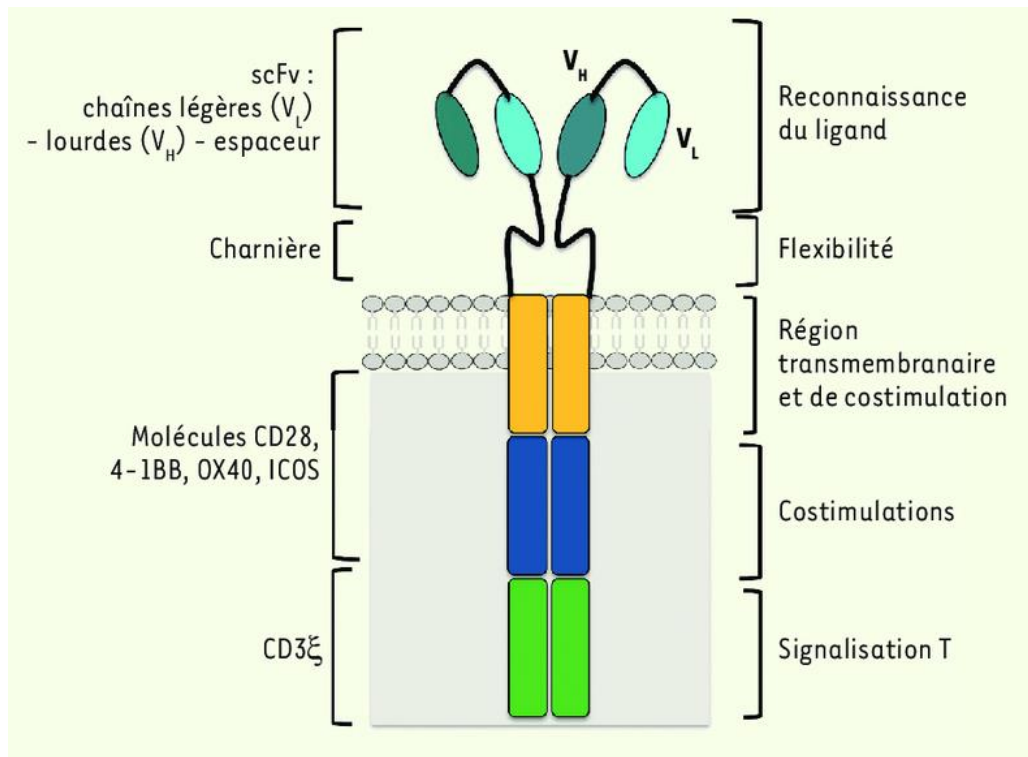


Figure 16: Schéma d'un récepteur CAR. Schéma issu de Catros, 2019¹⁷⁵

Ce récepteur de fusion permet aux cellules T de reconnaître les antigènes tumoraux à la surface de la tumeur, indépendamment de la liaison avec le CMH, ce qui permet aux cellules T CAR d'éliminer les cellules cancéreuses y compris celles régulant à la baisse leur CMH-I^{162,174}.

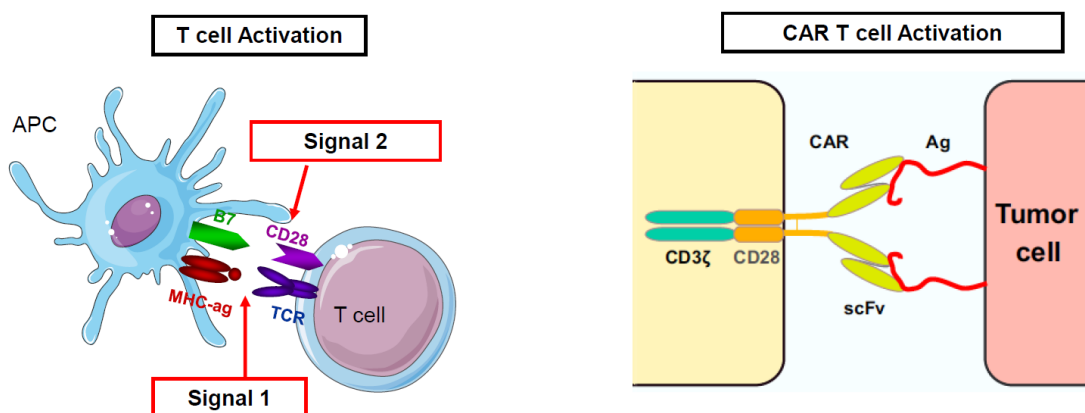


Figure 17: Schéma des mécanismes d'activation des lymphocytes T d'une part et des CAR T d'autre part. Schéma issu d'un cours de DIU « Immunologie et Immunothérapies des Cancers » 2022

La thérapie par cellules T CAR s'est avérée remarquablement efficace pour traiter les patients atteints de tumeurs malignes à cellules B comme la leucémie lymphoblastique aiguë à lymphocytes B, le lymphome B et le myélome plasmocytaire. Cependant, pour les tumeurs solides comme le mélanome, elle s'est heurtée à de faibles taux de réponse (19 % pour les CAR ciblant la gp100 et 30 % pour les CAR ciblant la DMF5) ainsi qu'à des fortes toxicités associées à la destruction des mélanocytes normaux^{162,176}. Cette thérapie présente malheureusement elle aussi les inconvénients des thérapies précédentes à savoir le temps nécessaire au développement des cellules T CAR à partir des cellules T d'un patient, le coût et les toxicités^{162,177}.

3) Traitement par anticorps bloqueurs ou thérapie cellulaire ? Que choisir en fonction du type de mélanome : cutané ou non cutané

Tout comme pour les autres thérapies, la compréhension de la thérapie cellulaire T adoptive s'est améliorée au fur et à mesure de son utilisation. Notamment, il est maintenant possible d'identifier des biomarqueurs pronostiques pouvant prédire si le patient a des chances de répondre ou non au traitement administré et s'il a des chances de développer des résistances. Il a été montré par exemple que les patients atteints de mélanome métastatique n'ayant pas répondu aux traitements antérieurs présentaient une meilleure survie à la thérapie cellulaire T adoptive s'ils avaient une charge mutationnelle tumorale et une charge en néo antigènes élevées¹⁷⁸.

Certains auteurs⁴⁵ suggèrent que les mélanomes non cutanés, avec une faible charge mutationnelle tumorale, une faible charge en néo-antigène et exprimant des niveaux plus élevés en antigènes associés au mélanome (gp100, MART1, tyrosinase, et TRP-1) seraient homogènes au niveau intra tumoral, ce qui les rendrait plus susceptibles d'être éliminées par des cellules T

CAR spécifiques d'un antigène. Au contraire le mélanome cutané, présentant une charge en néo antigènes plus élevée aurait une hétérogénéité intra tumorale plus importante, ce qui le rendrait insensible à un seul type de cellules CAR T spécifiques de l'antigène.

Les profils distincts des sous-types de mélanome suggèreraient donc que le mélanome cutané pourrait plus bénéficier d'une thérapie par blocage des points de contrôle immunitaires, tandis que le mélanome non cutané bénéficierait plus d'une thérapie cellulaire adoptive.

Cependant, comme évoqué précédemment, ces biomarqueurs prédictifs ne sont pas toujours fiables mais ils aident les médecins lors de la prise en charge du patient.

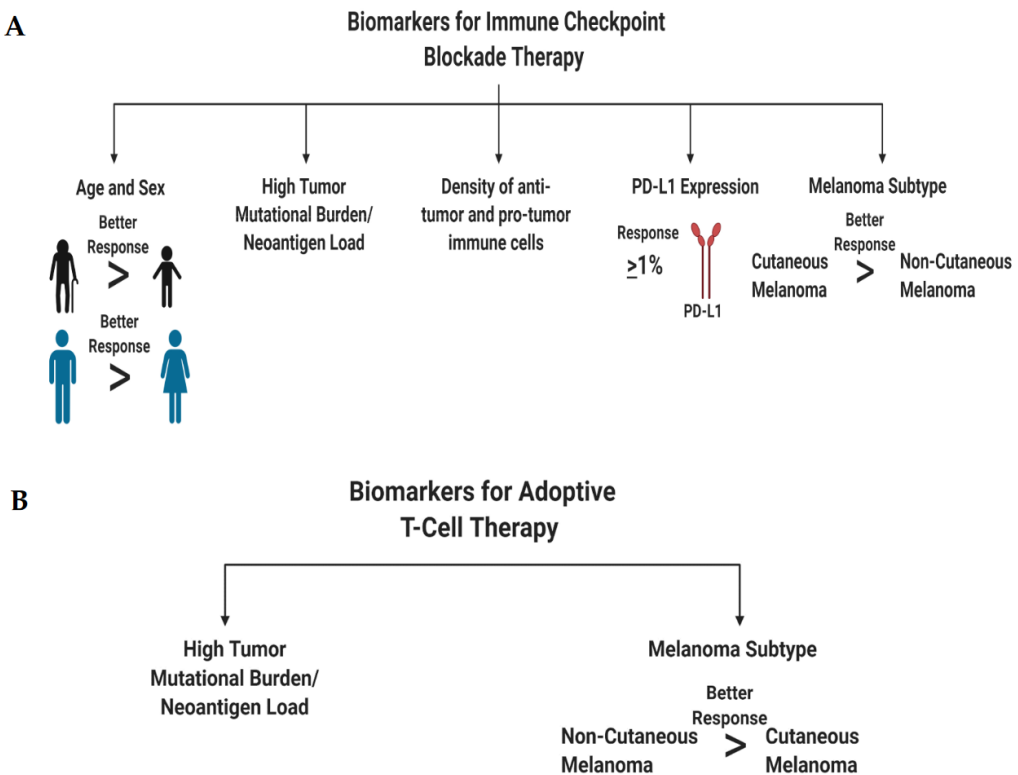


Figure 18: Résumé des biomarqueurs en faveur soit d'un traitement par anticorps bloqueurs soit d'un traitement par transfert adoptif de lymphocytes T. Figure issue de Eddy et Chen,

2020⁴⁵

IV. Les vaccins thérapeutiques

1) Découverte des premiers vaccins thérapeutiques

Dans l'imaginaire populaire, les vaccins sont généralement utilisés à des fins de prévention de maladies infectieuses. Durant les dernières décennies, nous avons vu l'essor de vaccins pour le traitement de cancers que ce soit pour les prévenir ou les traiter. Les vaccins anti-cancéreux les plus connus sont les vaccins ciblant les virus oncogènes : virus du papillome humain et le virus de l'hépatite B. Ces vaccins ont été approuvés par la FDA en tant que vaccins prophylactiques contre ces virus favorisant le développement de cancers, et ils ont connu un franc succès dans la prévention de ces cancers viraux induits¹⁷⁹. Malheureusement, les vaccins anti cancéreux thérapeutiques ont eu moins de succès en clinique.

a. Vaccins thérapeutiques approuvés

La **toxine de Coley** est le tout premier « vaccin anti tumoral » à avoir été découvert à la fin du 19^e siècle¹⁸⁰. Tout commença en 1890. A cette époque, le docteur William Coley était alors un jeune chirurgien à New York. Cette année, une de ces patientes, âgée alors de 17 ans, décède d'un sarcome métastatique. La mort rapide de cette jeune patiente poussa le Dr Coley à consulter les archives de patients atteints de sarcomes au New York Hospital. Un cas attira son attention : 7 ans auparavant un patient de 31 ans avait été admis au New York Hospital avec un sarcome au cou. Après plusieurs tentatives de chirurgie pour retirer cette tumeur qui ne cessait de réapparaître, suivies de greffes de peau inefficaces, le patient contracta une maladie infectieuse de la peau (**l'érysipèle**) due à une bactérie (*Streptococcus pyogenes*). Après avoir attrapé cette maladie, le cancer du patient aurait totalement disparu. D'autres cas similaires avaient également été reportés. En 1891, un patient rendit visite au Dr Coley pour un sarcome récurrent au cou inopérable. L'injection intra-tumorale de la bactérie *Streptococcus pyogenes* responsable de l'érysipèle entraîna une réduction de la tumeur, cependant elle ne disparut pas

totalement. Cela amena Coley à penser qu'il fallait induire une infection plus sévère afin d'avoir une meilleure disparition de la tumeur. Il travailla alors sur un mélange de deux bactéries : *Streptococcus pyogenes* et *Serratia marcescens*. Ce mélange fut par la suite appelé toxine de Coley ou vaccin de Coley et connu un fort succès thérapeutique chez certains patients à l'époque. Le succès thérapeutique restait cependant très aléatoire et ne guérisait qu'une minorité de patients. De plus, la préparation de la toxine était très arbitraire, sans formulation ou concentration standard. Par ailleurs, les toxicités étaient souvent élevées impliquant probablement ce qu'on nomme aujourd'hui des tempêtes cytokiniques. Le directeur du New York Hospital était de ce fait très sceptique sur l'efficacité de la toxine de Coley et était largement plus enthousiasmé par les débuts de la radiothérapie. Les travaux de Coley restèrent donc très controversés et en 1963 la FDA rendit illégale la prescription de la toxine de Coley en dehors d'essais cliniques. Contrairement aux hypothèses de Coley et d'autres médecins qui supposaient que la toxine avait un effet direct de destruction de la tumeur, les hypothèses actuelles reposent plutôt sur le fait que la toxine stimule probablement le système immunitaire du patient ce qui occasionnellement entraînait une destruction tumorale indirecte chez certains patients¹⁸¹.

Près d'un siècle après, en 1977, un nouveau vaccin « anti tumoral », le **Bacille Calmette Guerin (BCG)**, est découvert¹⁸⁰. A cette époque, la tuberculose était encore très présente dans le monde et était de ce fait un problème majeur de santé publique. Cette maladie se développe suite à une exposition à des bactéries : *mycobacterium tuberculosis* et *mycobacterium bovis* qui sont respectivement responsables de la tuberculose humaine et bovine. C'est à partir d'une version atténuee de la souche *mycobacterium bovis* qu'est produit en 1908 le vaccin BCG afin de prévenir les infections humaines et bovines. Le vétérinaire Albert Calmette et le bactériologiste Camille Guerin tous les deux travaillant à l'Institut Pasteur isolèrent une souche virulente de *mycobacterium bovis* chez une vache infectée par la tuberculose bovine. En 1921,

après 13 ans de culture (231 passages) de cette souche ils réussirent à mettre en évidence une version atténuée de la souche. Cette nouvelle souche fut nommée « Bacille de Calmette-Guérin » soit BCG et fut utilisé pour vacciner les jeunes contre la tuberculose.

Ce n'est qu'en 1977 que ce vaccin fut approuvé en tant que vaccin anti cancéreux dans le cancer superficiel de la vessie et du carcinome urothelial *in situ*¹⁷⁹. Le vaccin est délivré via une sonde introduite dans l'urètre libérant ainsi le vaccin à l'intérieur de la vessie permettant une action locale. Cette approbation se base sur les résultats d'un essai clinique de phase 3 montrant une survie sans récidive à 5 ans pour 45% de patients traités avec le BCG¹⁸².

Ces 2 tous premiers « vaccins anti cancéreux » n'ont pas un effet anti tumoral direct mais soulignent l'importance du système immunitaire dans la lutte contre le cancer¹⁸². En effet, ces vaccins stimulent le système immunitaire du patient entraînant par la suite une destruction tumorale indirecte.

Il faut attendre 2010 afin qu'un vaccin anti cancéreux à proprement parlé (c'est à dire ciblant spécifiquement les cellules cancéreuses) soit approuvé¹⁷⁹. Ce vaccin, le **Sipuleucel-T (Provenge)**, a été accepté pour le traitement du cancer de la prostate au stade métastatique résistant au traitement hormonal. Il repose sur l'utilisation de cellules dendritiques autologues, obtenues à partir des cellules souches prélevées sur le patient. *In vitro*, elles sont mises en culture en présence d'une protéine de fusion (PA2024) constituée de l'antigène phosphatase de l'acide prostatique (*Prostatic acid phosphatase*, PAP) qui est présent dans 95 % des cellules cancéreuses de prostate et d'une cytokine (GM-CSF) stimulant la réponse immunitaire. Les cellules sont alors réinjectées au patient et stimulent son système immunitaire contre d'antigène prostatique apporté. L'approbation se base sur les résultats d'un essai clinique de phase 3 montrant notamment une amélioration de la probabilité de la survie à 36 mois chez les patients ayant reçu le vaccin (31,7% contre 23,0% pour le groupe placebo)¹⁸³.

Enfin, en 2015, le **talimogene laherparepvec** (T-VEC), un vaccin basé sur un virus oncolytique est approuvé pour le traitement du mélanome de stade avancé. Ce vaccin dérive d'un virus d'herpès simplex 1 (HSV-1) vivant atténué qui a été modifié pour se répliquer uniquement dans les cellules cancéreuses et pour produire le GM-CSF. Cette approbation se base sur un essai clinique de phase 3 ayant atteint le critère principal à savoir un taux de réponse objective d'une durée supérieure à 6 mois par rapport à du GM-CSF (16,3% pour le vaccin contre 2,1% pour le GM-CSF)¹⁸⁴. Ce vaccin est injecté de manière intra tumorale dans les mélanomes cutanés.

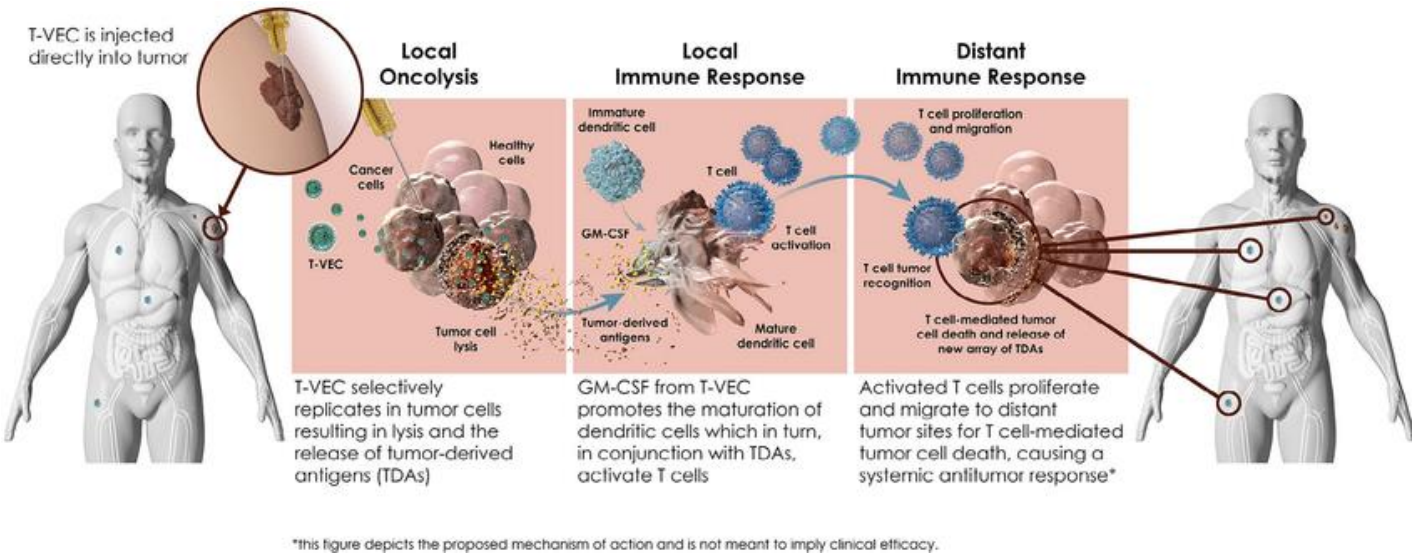


Figure 19: Proposition de mécanisme d'action du vaccin T-VEC. Schéma issu de Hamid et al.¹⁸⁵

Tous ces exemples soulignent l'importance de l'activation du système immunitaire via ces vaccins afin d'avoir une efficacité clinique. Un autre point important pour l'efficacité semble être l'utilisation *in situ* de ces vaccins du moins pour le BCG et le T-VEC ce qui peut parfois être difficile suivant l'accessibilité de la tumeur. De plus, les essais cliniques présentés ci-dessus ne mettent pas en évidence de biomarqueurs prédictifs de réponse et n'expliquent pas les

mécanismes d'action de ces vaccins chez les patients traités¹⁷⁹. Depuis ces premiers vaccins, de nombreux autres ont été testés en clinique sans franc succès et c'est ce que nous allons détailler maintenant.

b. Echec des essais cliniques des vaccins thérapeutiques

De nombreux autres vaccins ont été testés dans des essais cliniques mais les résultats sont beaucoup moins probants¹⁷⁹. Nombre de ces vaccins ont adopté des Tumor-Associated-Antigens (TAA) et des vecteurs microbiologiques (viraux ou bactériens). Ces vaccins, pour la grande majorité, avaient de bons résultats en études précliniques, cependant ce succès n'a malheureusement pas été retrouvé lors des essais cliniques.

Certains suggèrent que le ciblage de ces TAAs qui sont des protéines du soi non mutées mais surexprimées dans les cellules cancéreuses ou encore des protéines onco-foetales (protéines régulées pendant le développement embryonnaire puis inactivées à l'âge adulte) serait en partie responsable du faible succès thérapeutiques de ces vaccins¹⁸⁶. En effet, la régulation par le système immunitaire des lymphocytes T auto réactifs contre ces protéines du soi, mobilisés par ces vaccins, ne laisse souvent en circulation que les lymphocytes T ayant une affinité faible ou modérée pour ces antigènes du soi. De plus, ces TAAs sont exprimés de manière hétérogène au sein d'une même tumeur. Par le phénomène d'immuno-editing, les cellules tumorales n'exprimant pas ces antigènes et donc résistantes vont être sélectionnées par le système immunitaire et aboutir à des tumeurs résistantes au traitement vaccinal entraînant un échec clinique. Cependant malgré ces obstacles, des améliorations des formulations vaccinales ainsi que des protocoles d'administration ont permis d'augmenter la fréquence des lymphocytes T anti tumoraux ciblant ces antigènes. Ces lymphocytes parviennent, suite à ces améliorations, à atteindre 0,1 à 2% de tous les lymphocytes T CD8 périphériques¹⁸⁷⁻¹⁹⁰. Malheureusement ces efforts, même s'ils ont permis le déploiement d'une forte réponse T anti tumorale, n'ont pas

abouti à de réels bénéfices cliniques. Une méta analyse incluant 98 études a conclu d'un taux de réponse de seulement 2,6%¹⁹¹. Par ailleurs, il a été observé que certains vaccins à peptides courts entraînaient un épuisement local (au niveau du site d'injection) des lymphocytes T¹⁹². D'autres causes d'échec ont été proposées : dose de vaccins sous-optimale, voie d'injection et adjuvants non adaptés¹⁷⁹.

Il est devenu de plus en plus clair ces dernières années que les mécanismes d'immunosuppression exercés par la tumeur et son micro-environnement ne peuvent pas simplement être surmontés par une augmentation de la fréquence des lymphocytes T anti-tumoraux comme le proposent les vaccins thérapeutiques actuels.

2) Anticorps bloqueurs + Vaccins thérapeutiques : « the perfect partners »

Selon certains auteurs¹⁸⁶, les vaccins thérapeutiques et les modulateurs de points de contrôle immunitaires des lymphocytes T constituaient les « perfect partners ». En effet, dans le cas d'un cancer non traité, on observe une faible fréquence de lymphocytes T ainsi qu'un fort niveau d'inhibition des points de contrôles immunitaires. Dans le cas d'un cancer traité uniquement par vaccination anti-cancéreuse nous observons une forte fréquence des lymphocytes T périphériques mais qui sont rapidement inhibés par les points de contrôle de la tumeur. Si l'on traite le cancer avec uniquement des modulateurs de points de contrôle immunitaires nous obtenons l'effet inverse c'est-à-dire une levée de l'inhibition des points de contrôles et une faible proportion de lymphocytes T anti-tumoraux. Cette proportion est trop faible pour échapper à la suppression des MDSC (cellules myéloïdes suppressives) et des Tregs. Enfin, la combinaison vaccins/anticorps modulateurs entraîne une haute fréquence de lymphocytes qui grâce aux modulateurs ne sont plus inhibés par la tumeur et peuvent ainsi détruire les cellules tumorales. De plus, les anticorps peuvent également favoriser la costimulation des lymphocytes T en améliorant le potentiel cytolytique des lymphocytes T ainsi que leur prolifération et leur

survie dans le micro environnement tumoral. Ils permettent également d'augmenter la production de cytokines effectrices ainsi que la polarisation de la réponse vers un phénotype pro-inflammatoire de type Th1/Tc1^{193,194}. On assiste alors à un effet anti tumoral synergique des vaccins et anticorps bloqueurs. Ces principes sont illustrés dans le schéma suivant :

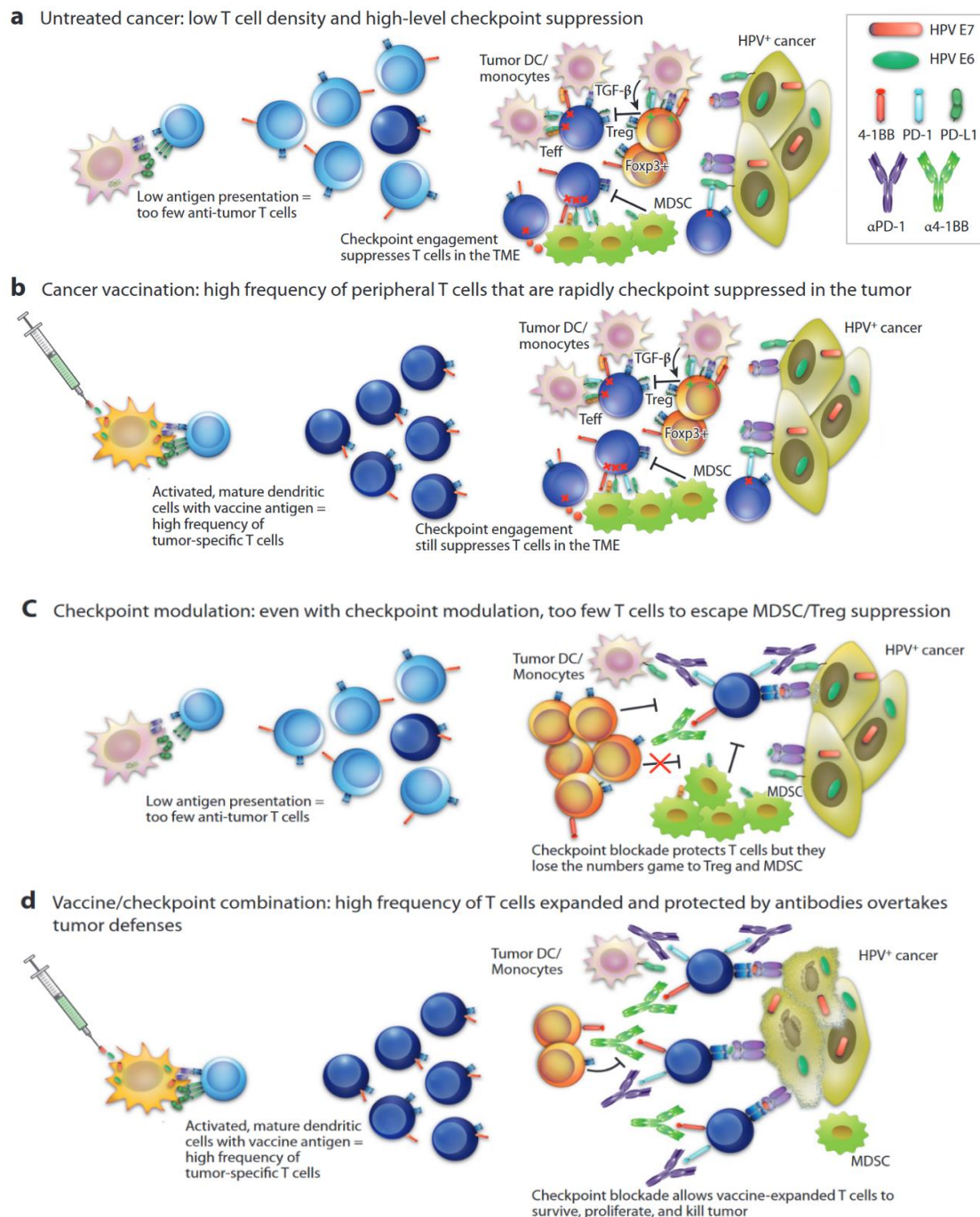


Figure 20 : Mécanismes illustrant le potentiel synergique des vaccins thérapeutiques et des

anticorps modulateurs. Figure extraite de *Curran et al.*¹⁸⁶

Il a également été observé que la combinaison vaccins/ anticorps bloqueurs pourrait diminuer le nombre d'effets indésirables d'origine immunologique (immune related Adverse Events soit irAEs en anglais) couramment observés à différents degrés lors des traitements avec les anticorps bloqueurs imposant ainsi une limitation des doses¹⁹⁵. Dans un essai clinique combinant le vaccin ISA101 et le nivolumab aucun effet secondaire de grade 4 n'a été observé et seulement 2 patients ont eu des effets secondaires de grade 3. Cependant ces effets étaient asymptomatiques et uniquement visible en sérologie.

La théorie qui a été proposée pour expliquer ce phénomène est la suivante : quand les lymphocytes T deviennent activés ils expriment les molécules CTLA-4 et PD-1 à leur surface. Dans le cas d'un traitement uniquement par anticorps, la fréquence de lymphocytes T étant faible (comme évoqué précédemment) nous nous retrouvons avec trop d'anticorps par rapport à la quantité de ligands disponibles sur le faible nombre de lymphocytes T. Les anticorps non liés à des ligands sont donc plus disponibles pour circuler dans l'organisme et se lier à des ligands présents sur des lymphocytes T auto réactifs. Ces lymphocytes normalement inactivés se retrouvent alors activés et peuvent ainsi être responsable d'irAEs. Dans le cas d'une combinaison vaccin/anticorps bloqueurs, une plus grande fréquence de lymphocyte T anti tumoral est générée ce qui limite l'effet hors cible des anticorps qui ont donc plus de ligands à disposition sur la plus grande quantité de lymphocytes T anti tumoraux générés.

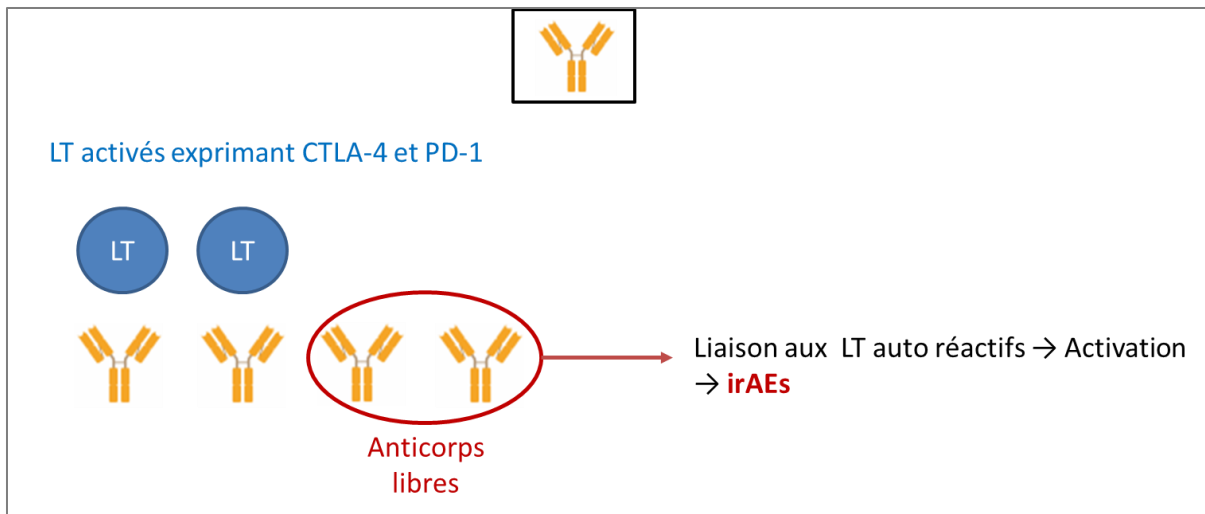


Figure 21: Schéma proposant une explication à la présence d'effets secondaires d'origine immunologique suite à un traitement par anticorps bloqueurs. Schéma réalisé sur BioRender.

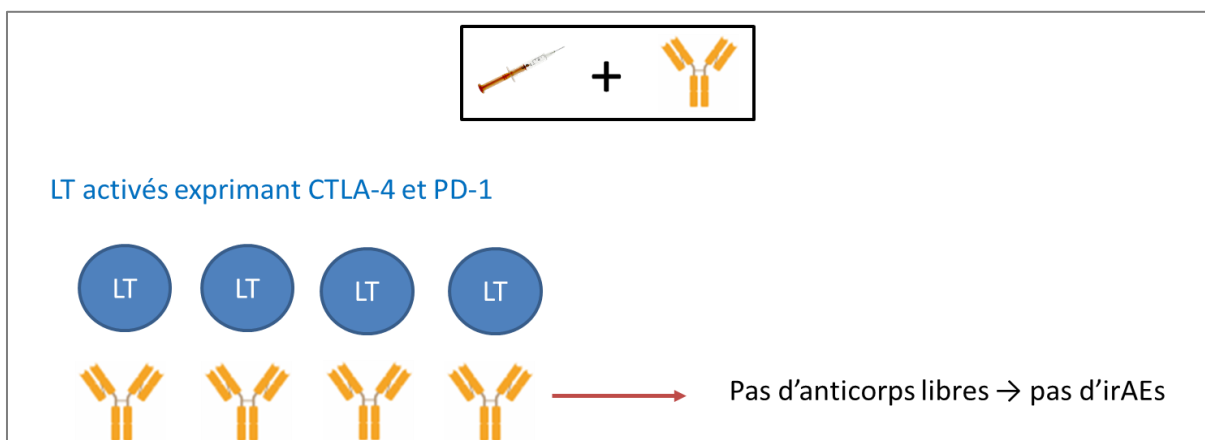


Figure 22: Schéma proposant une explication à la diminution des effets secondaires d'origine immunologique suite à un traitement par anticorps bloqueurs + vaccin thérapeutique.

Schéma réalisé sur BioRender.

3) Vaccins thérapeutiques en essai clinique utilisant différentes plateformes

vaccinales

Les vaccins thérapeutiques semblent donc aujourd’hui commencer à trouver une place dans le traitement des cancers en combinaison avec d’autres thérapies comme les anticorps bloqueurs de points de contrôle immunitaires. En effet, de nombreuses études précliniques combinant des vaccins et des anticorps bloqueurs comme les inhibiteurs de CTLA-4 et PD-1/PD-L1 ont montré l’effet synergique de ces deux approches^{196–202}. Des premiers essais cliniques sur des combinaisons ont également été réalisés et nous allons en présenter quelques-uns ci-dessous. Ces essais de combinaisons se focaliseront principalement sur le cancer du pancréas, le cancer de la prostate et le mélanome et feront intervenir différentes plateformes vaccinales.

a. Vaccins anticancéreux à base de cellules

Il existe 2 grandes sortes de vaccins anticancéreux à base de cellules actuellement utilisés en essais cliniques : les vaccins à base de cellules cancéreuses modifiées et les vaccins à base de cellules dendritiques²⁰³.

Vaccins anti cancéreux à base de cellules cancéreuses modifiées

Le vaccin à base de cellules cancéreuses le plus représentatif est le **GVAX**. Ce vaccin cellulaire allogénique a été développé à l’université John Hopkins (Baltimore, Etats Unis). Il dérive de 2 lignées cellulaires d’adénocarcinome pancréatique qui ont été transfectées afin d’exprimer la cytokine GM-CSF et a été testé sur des patients résistants à la chimiothérapie²⁰⁴. L’expression du GM-CSF a pour but d’augmenter l’efficacité anti tumorale en régulant l’activité des cellules immunitaires comme les cellules dendritiques et les Natural Killers²⁰³. Une revue de 2005 a témoigné de l’efficacité de ce vaccin sur certains patients atteints de mélanome, cancer de la prostate, du pancréas, des cellules rénales et enfin de cancer du poumon non à petites cellules^{205,206}. Ce vaccin était utilisé dans des essais de phases I ou II en

monothérapie ou couplé à de la chimio ou radio thérapie. Des réponses durables et complètes ont été observées chez des patients présentant un cancer du poumon non à petites cellules à un stade avancé. En 2013, une étude de phase Ib a montré une amélioration de la survie globale dans l'adénocarcinome pancréatique en combinant l'ipilimumab (inhibiteur de CTLA-4) et le vaccin GVAX en comparaison avec l'ipilimumab seul²⁰⁷.

En 2015, une autre étude de phase II sur le cancer du pancréas a montré une amélioration de la survie des patients. Le bras A recevait une combinaison cyclophosphamide/GVAX/CRS-207 contre seulement cyclophosphamide/GVAX pour le bras B²⁰⁸. Le cyclophosphamide est une chimiothérapie utilisée en traitement standard contre le cancer du pancréas. Le CRS-207 est un vaccin réalisé à base d'une souche atténuée de *Listeria monocytogenes* modifiée afin qu'elle exprime la mesothéline, antigène associé aux tumeurs notamment pancréatiques.

Deux autres essais sont actuellement en cours (NCT03190265, NCT02451982). Ces essais combinent le GVAX et le CRS-207 avec l'ipilimumab (anti CTLA-4), le nivolumab (anti PD-1), l'urelumab (anti CD137) et le HuMax-IL8 (anti IL8).

L'association de vaccins thérapeutiques avec les anticorps bloqueurs s'est révélée être une stratégie efficace pour traiter les cancers. En effet, en combinant les anti PD-1/CTLA-4 avec le vaccin GVAX le ratio CD8+/Treg ainsi que la présence de lymphocytes T CD8 fonctionnels dans la tumeur (IFN- γ + TNF- α + CD8+) augmentent significativement¹⁹⁷.

Un autre exemple de vaccin cellulaire pouvant être cité est le **AGI101H**. Ce vaccin est composé de 2 lignées cellulaires de mélanome transduites par un ADNc codant pour la protéine de fusion H6 suivante : IL-6 fusionnée avec son récepteur soluble (sIL-6R). Cette protéine de fusion modifie les lignées cellulaires en allant vers un phénotype de cellules souches de mélanome²⁰⁹. Ce vaccin s'est montré bénéfique pour certains patients lors d'une étude phase II en augmentant leur survie à long terme²¹⁰.

Vaccins anti cancéreux à base de cellules dendritiques

Des nombreux essais cliniques impliquant des vaccins à cellules dendritiques ont montré des résultats encourageants. Par exemple, nous pouvons citer une étude de phase IIb publié en 2021. Cette étude démontre une nette amélioration de la survie sans maladie à 24 mois dans le bras vacciné (62.9%) par rapport au bras placebo (34.8%) chez des patients présentant un mélanome de stade III/IV ayant déjà été retiré par chirurgie avant le traitement vaccinal²¹¹. L'objectif de ce vaccin **TLP CDC** (Tumor Lysate, Particle-loaded, Dendritic Cell en anglais) est de prévenir une réapparition du mélanome suite à la chirurgie. Ce vaccin est composé de cellules dendritiques qui ont été chargées avec du lysat tumoral via des particules de paroi cellulaire de levure. Les parois cellulaires des levures *Saccharomyces cerevisiae* se composent de mannoprotéines, de β-glucane et de chitine, liées entre elles de manière covalente. Par un processus d'hydrolyse alcaline à chaud, le contenu alcalin-soluble de la levure (une partie de la paroi cellulaire ainsi que le matériel intracellulaire) peut être éliminé ne laissant que la partie de la paroi cellulaire non soluble dans les alcalins. Cela aboutit à des sphères de β-glucane creuses avec une cavité interne où il est possible de piéger des molécules comme du lysat tumoral par exemple. Ces particules, de par leur riche constitution en β-glucane, sont reconnus de façon efficace et rapide par les macrophages et les cellules dendritiques via une endocytose médiée par le récepteur dectin-1²¹². Cela en fait donc des vecteurs de choix pour charger des cellules dendritiques avec un lysat tumoral. Ces particules sont chargées avec le lysat tumoral du patient obtenu après plusieurs cycles de congélation/décongélation de la tumeur chirurgicalement retirée du patient. Elles sont mises en contact avec les cellules dendritiques du patient, récupérées par prélèvement sanguin²¹³, qui sont ensuite réinjectées au patient. Dans le cas du placebo, le process est identique à l'exception du fait que les particules de paroi cellulaire de levure sont vides c'est-à-dire non chargées avec les antigènes du lysat tumoral. Un essai clinique de phase III est actuellement en cours de développement. L'efficacité

de ce vaccin combiné à des anticorps bloqueurs versus les anticorps seuls va être évaluée dans le mélanome de stade avancé réséqué par chirurgie²¹¹.

Par ailleurs, la combinaison de cellules dendritiques pulsées avec des peptides MART-1 et avec le Tremelimumab s'est montré efficace lors d'un essai de phase I sur des patients présentant un mélanome métastatique²¹⁴.

De plus, une autre combinaison vaccin cellules dendritiques TriMix-DC-MEL/Ipilimumab a montré quelques réponses chez des patients préalablement traités pour un mélanome métastatique lors d'un essai de phase II²¹⁵.

b. Vaccins d'origine virale

En exemple de vaccin d'origine virale nous trouvons le **VRP-HER2**. Ce vaccin est élaboré à partir de particules dérivées d'alphavirus contenant un réplicon d'ARN capable de s'auto amplifier et de coder la protéine HER2, cible principale du cancer du sein. Ce vaccin a montré des résultats encourageants lors d'essais précliniques et cliniques²¹⁶ et est actuellement testé en comparaison et combinaison avec le pembrolizumab dans le cancer du sein (NCT03632941).

Nous pouvons également citer le **PROSTVAC®**. Ce vaccin, dirigé contre l'antigène spécifique de la prostate PSA (Prostate Specific Antigen en anglais), s'est avéré sûr d'utilisation en combinaison avec des anticorps bloqueurs lors d'un essai de phase I²¹⁷. Son efficacité est en cours d'évaluation dans le cancer de la prostate métastatique résistant à la castration (mCRPC) au cours de différents essais de phases II (NCT02506114, NCT02933255).

c. Vaccins peptidiques

En vaccin peptidique nous pouvons citer le **DSP-788** contenant des peptides dérivés du gène tumoral Wilms 1 (WT1). Celui-ci est surexprimé dans de nombreuses tumeurs. Ce vaccin est bien toléré par les patients et il n'a pas été observé de toxicité liée à la dose²¹⁸. De nombreux

essais cliniques sont en cours pour ce vaccin notamment une étude de phase III en combinaison avec le bevacizumab dans le glioblastome récidivant (NCT03149003).

d. Vaccins à ADN

En termes de vaccin à ADN nous pouvons citer le **GX-188E**. Ce vaccin contient plusieurs épitopes fusionnés et est capable d'activer spécifiquement les cellules dendritiques. Ce vaccin a montré en combinaison avec l'anti PD-1 pembrolizumab, un taux de réponse global de 42% pour le traitement du cancer du col de l'utérus de stade avancé. On observe également une nette amélioration du bénéfice thérapeutique de la combinaison GX-188E/ pembrolizumab par rapport au pembrolizumab seul^{219,220}.

e. Vaccins à ARNm

Les vaccins à ARN messagers sont également beaucoup utilisés en recherche clinique en oncologie. Par exemple, le vaccin **TriMixDC-MEL** est composé de 3 ARN messagers codant respectivement pour CD70, CD40L ainsi qu'une forme active du TLR4. Ces 3 ARN sont incorporés dans des cellules dendritiques obtenues directement auprès des patients. Ce vaccin a montré une bonne tolérance et immunogénicité lors de premiers essais cliniques²¹⁵ ainsi que de bons taux de réponses tumorales chez des patients présentant un mélanome de stade III ou IV^{221,222}.

Nous pouvons également citer le vaccin liposomal **BNT111** codant pour 4 antigènes (TAA) du mélanome : NY-ESO-1, MAGE-A3, tyrosinase, et TPTE. Un essai de phase I (NCT02410733) a montré que le vaccin seul ou en combinaison avec des anticorps anti PD-1 entraîne des réponses objectives durables chez des patients atteints de mélanome non opérable et ayant déjà subi un traitement au anticorps bloqueurs. Ces réponses cliniques s'accompagnent de fortes réponses CD4 et CD8 contre les antigènes vaccinaux²²³. Le BNT111 est actuellement

testé en combinaison avec le cemiplimab (anti PD-1) dans le mélanome avancé (NCT04526899).

f. Vaccins personnalisés

Les vaccins anti cancéreux sont généralement dirigés contre des TAAs (Tumor Associated Antigens) sur-exprimés par les cellules cancéreuses mais tout de même exprimés faiblement dans les tissus sains. Cette expression même faible entraîne souvent une tolérance immunitaire centrale ou périphérique ainsi que de l'auto-immunité, entravant ainsi le bénéfice clinique du vaccin. C'est ce manque de spécificité des antigènes qui a été suggéré comme une des causes principales de l'échec des vaccins en clinique par le passé¹⁷⁹. Au cours des dernières années, grâce aux progrès des techniques de Next Generation Sequencing (NGS) et de bio-informatique, le développement de vaccins s'est focalisé sur des vaccins personnalisés dirigés contre des néo-antigènes propres à chaque tumeur de chaque patient²²⁴⁻²²⁶. L'intérêt de cibler ces néo-antigènes est d'augmenter la spécificité du vaccin permettant ainsi d'augmenter le bénéfice clinique ainsi que de diminuer les effets secondaires auto-immuns. En effet, au cours de son développement, la tumeur accumule des mutations qui peuvent modifier les protéines qu'elle exprime et ainsi en former de nouvelles aboutissant ainsi à la formation de néo-antigènes et néo-épitopes spécifiques de cette tumeur. Ces néo-antigènes peuvent varier d'un patient à l'autre mais également d'une tumeur à l'autre chez le même patient et voire même d'une région à l'autre de la même tumeur. Des études montrent que certains néo-antigènes sont retrouvés chez différents patients mais la plupart sont spécifiques à chaque patient²²⁷.

La préparation d'un vaccin personnalisé comprend différentes étapes que nous allons détailler ci-dessous. Tout d'abord, la tumeur du patient est prélevée par chirurgie puis séquencée par séquençage d'ARN afin d'identifier les néo-antigènes et les néo-peptides associés. Des tests bio-informatiques sont ensuite réalisés afin de vérifier *in silico* que les néo-peptides identifiés

se lient bien aux molécules CMH du patient. L'immunogénicité du complexe CMH/néo-peptide est ensuite vérifié par des tests *in vitro* comme les ELISPOT. Les néo-antigènes ou néo-peptides sont ensuite incorporés sous forme de protéine, ARNm ou ADN dans un vecteur (cellules dendritiques pulsées, nanoparticules, particule virale...) puis injectés au patient²²⁸. Certains peptides peuvent également être injectés directement sans utiliser de vecteur. Ces traitements présentent de nombreux inconvénients comme leur coût et la longue durée de fabrication du vaccin personnalisé. Ils ont cependant fait leurs preuves notamment dans le mélanome.

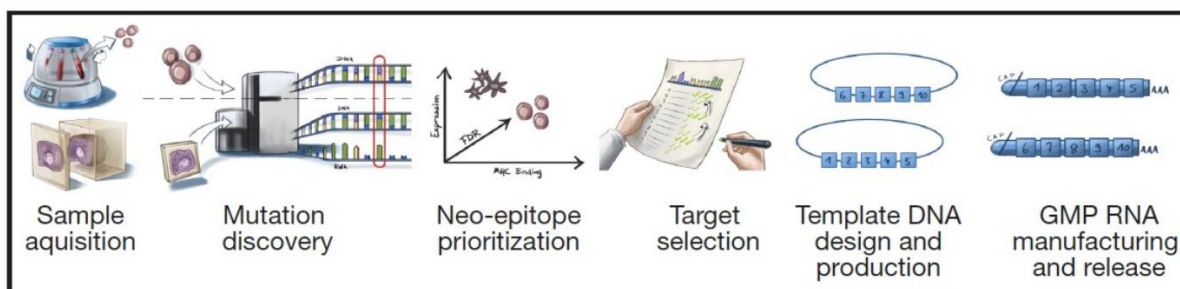


Figure 23: Schéma récapitulant les étapes nécessaires au développement d'un vaccin personnalisé. Schéma issu d'un cours de DIU « Immunologie et Immunothérapies des Cancers » 2022

Le premier vaccin personnalisé que nous pouvons citer dans le cas du mélanome est le **NEO-PV-01**. Ce vaccin contient un mélange de 20 peptides spécifiques à chaque patient qui sont administrés par voie sous cutanée dans 4 sites d'injection. (1 injection à chaque extrémité du corps). Le poly-ICLC (Hiltonol) est utilisé comme adjuvant de ce vaccin. Ce vaccin est actuellement testé dans le mélanome en combinaison avec plusieurs autres agents, ce qui est résumé dans le tableau ci-dessous.

De plus nous pouvons également citer le vaccin **RO7198457**. Ce vaccin contient également un mélange de 20 peptides spécifiques à chaque patient. Ces peptides sous forme d'ARN sont

encapsulés dans une particule liposomale. Ce vaccin est également testé dans le mélanome en combinaison avec plusieurs autres agents (voir tableau ci-dessous).

Vaccin	Agents en combinaison	Numéro NCT	Pathologie	Phase clinique
NEO-PV-01	Anticorps agoniste du CD40 (APX005M) ou ipilimumab + nivolumab	NCT03597282	Mélanome	I
NEO-PV-01	nivolumab	NCT02897765	Mélanome	I
RO7198457	atezolizumab	NCT03289962	Mélanome	I
RO7198457	pembrolizumab	NCT03815058	Mélanome	II

Tableau 4 : Présentation de vaccins personnalisés actuellement essais cliniques dans le mélanome (tableau extrait de *Roy et al.*)¹⁷⁹

Malgré des débuts hésitants, les nouveaux vaccins à l'étude semblent très prometteurs. Même si de nombreuses questions restent encore à résoudre, les prochaines années verront les résultats de nombreux essais cliniques faisant intervenir des vaccins thérapeutiques, qui nous l'espérons apporteront une nouvelle piste thérapeutique efficace pour le traitement des cancers.

Chapitre II : Présentation de la plateforme vaccinale ‘ADDomer’

Introduction du chapitre :

Au laboratoire, nous développons une plateforme vaccinale, d'origine « virale » basée un dodécaèdre d'adénovirus appelé ADDomer.

Cette publication décrit la découverte du dodécaèdre de l'adénovirus en détaillant sa structure et ses fonctions biologiques avant de finir sur ses applications en biotechnologie.

Review

The Adenovirus Dodecahedron: Beyond the Platonic Story

Solène Besson ^{1,†}, Charles Vragniau ^{1,2,†}, Emilie Vassal-Stermann ¹, Marie Claire Dagher ¹ and Pascal Fender ^{1,*} 

¹ Centre National de la Recherche Scientifique, Université Grenoble Alpes, Commissariat Énergies Alternatives, Institut de Biologie Structurale, 41 rue des Martyrs, 38042 Grenoble, France; solene.besson@ibs.fr (S.B.); charles.vragniau.phd@gmail.com (C.V.); emilie.stermann@ibs.fr (E.V.-S.); marie-claire.dagher@ibs.fr (M.C.D.)

² Centre National de la Recherche Scientifique, Université Grenoble Alpes, Institut National Polytechnique Grenoble, Technique de l'ingénierie Médicale et de la Complexité, TIMC-IMAG Bât Jean Roget Faculté de Médecine et Pharmacie, 38700 La Tronche, France

* Correspondence: pascal.fender@ibs.fr

† These authors contributed equally to work.

Received: 11 June 2020; Accepted: 30 June 2020; Published: 2 July 2020



Abstract: Many geometric forms are found in nature, some of them adhering to mathematical laws or amazing aesthetic rules. One of the best-known examples in microbiology is the icosahedral shape of certain viruses with 20 triangular facets and 12 edges. What is less known, however, is that a complementary object displaying 12 faces and 20 edges called a ‘dodecahedron’ can be produced in huge amounts during certain adenovirus replication cycles. The dodecahedron was first described more than 50 years ago in the human adenovirus (HAdV3) viral cycle. Later on, the expression of this recombinant scaffold, combined with improvements in cryo-electron microscopy, made it possible to decipher the structural determinants underlying their architecture. Recently, this particle, which mimics viral entry, was used to fish the long elusive adenovirus receptor, desmoglein-2, which serves as a cellular docking for some adenovirus serotypes. This breakthrough enabled the understanding of the physiological role played by the dodecahedral particles, showing that icosahedral and dodecahedral particles live more than a simple platonic story. All these points are developed in this review, and the potential use of the dodecahedron in therapeutic development is discussed.

Keywords: adenovirus; dodecahedron; platonic solids; virus like particles; receptors; vaccines; structure; viral spreading

1. Introduction to Adenoviruses

Adenoviruses are non-enveloped viruses with a diameter between 70 and 90 nm, presenting an icosahedral capsid. They possess linear double stranded DNA with inverse repeated sequences at each end and an encapsidation sequence. The *Adenoviridae* family is divided into 5 genera: Mastadenoviruses, Aviadenoviruses, Atadenoviruses, Siadenoviruses, and Ichtadenoviruses. They can infect a large variety of species, such as cows, dogs, ducks, horses, snakes, fish, and humans (<https://sites.google.com/site/adenoseq/>). The human adenoviruses (HAdVs) are part of the Mastadenovirus group. These human serotypes have been sorted into seven species from A to G depending on their biological, genetic, biochemical, and structural properties (<http://hadvwg.gmu.edu>). Human adenoviruses are responsible for fever, infections of respiratory tracks, gastroenteritis, and conjunctivitis. In most cases, the symptoms are not visible in healthy persons [1]. However, some serotypes can cause

more severe infections leading in some cases to death in immune-deficient patients and infants. For example, HAdV3, HAdV5, and HAdV7 are responsible for acute respiratory tract infections, and a recent outbreak of HAdV7 in a New Jersey rehabilitation center resulted in eleven deaths (<https://www.nj.gov/health/cd/topics/adenovirus.shtml>). HAdV40 and HAdV41, on the other hand, are known to cause acute and persistent gastroenteritis in children [2]. Subgroup D adenovirus serotypes are known for their ocular tropism resulting in conjunctivitis or epidemic Keratoconjunctivitis (EKC) [3].

All adenoviruses are composed of three main capsid proteins or ‘capsomers’: the hexon, the penton base, and the fiber (Figure 1). The main protein is the hexon, with 240 trimeric capsomers forming the 12 triangular facets of the icosahedral viral capsid [4,5]. The hexon protein is therefore the most abundant structural protein of the adenovirus since 720 hexon copies of the monomer (~110 kDa) are displayed on the virus surface, and it represents 80% of the virus total mass [6]. The penton base is an homopentamer composed of five ~60 kDa monomers displayed on each of the 12 viral capsid apexes. Therefore, each monomer is presented 60 times on the viral capsid. The penton base contains 2 hypervariable loops exposed at the virus surface and named variable loop and RGD (Arginin-Glycin-Aspartic Acid) loop [7]. The highly conserved RGD motif has been described to interact with the $\alpha v \beta 3$ and $\alpha v \beta 5$ integrins, inducing virus internalization [8–10]. However, some adenoviruses, such as HAdV40 and HAdV41, lack this motif, although this does not prevent them from infecting cells [11]. Recently, it has been shown that those serotypes nevertheless interact with 6-containing integrins with a similar affinity [12].

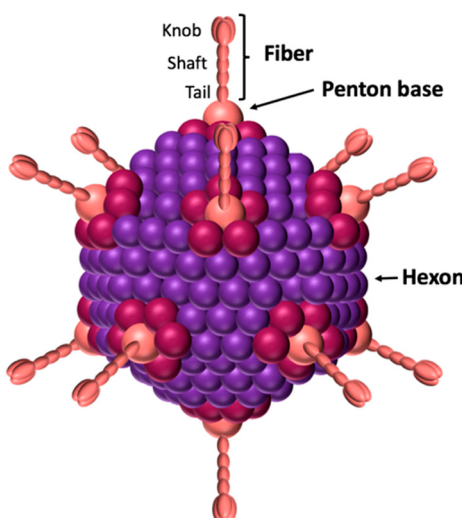


Figure 1. Schematic view of adenovirus. The icosahedral capsid is formed by the hexon. The penton base is located at the 12 vertices and forms a non-covalent complex with the trimeric fiber. The fiber’s knob domain is responsible for the interaction with the receptors.

The fiber, like the penton base, is present on each of the 12 viral capsid apexes. It is an homotrimer composed of a tail, a shaft and a knob domain (Figure 1). The tail, corresponding to the N-terminal of the fiber, forms a non-covalent interaction with the penton base. The shaft contains repeated patterns of 15 amino acids [13,14]. The number of repetitions gives the shaft a length which varies from one serotype to another. For example, the shaft measures 9 nm for HAdV3 and 36 nm for l’HAdV40. The knob corresponds to the globular C-terminal of the fiber and interacts with receptors, allowing virus attachment to the cells [15]. Therefore, the fiber’s knob dictates the viral tropism. To date, three main protein receptors have been identified: CAR, CD46, and desmoglein (DSG)2 [16–18]. In addition to CAR, most of the subgroup D adenoviruses can also use non-protein receptors, such as sialic acids or the GD1-glycan [19,20].

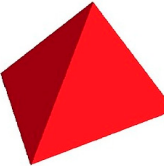
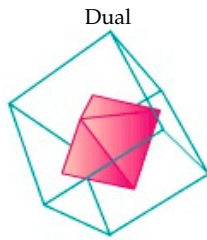
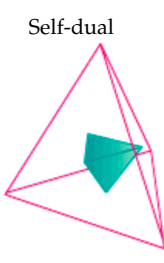
The non-covalent complex formed by the penton base and the fiber is called the penton. This complex contains all the information needed for virus attachment and internalization. Its formation

is due to the interaction between a conserved motif (FNPVYPY) present in the fiber's tail, and a complementary sequence located at the interface between two neighboring penton base monomers [7]. This penton is the building block of the adenovirus dodecahedron described below.

2. The Platonic Solids

A platonic solid is a regular convex polyhedron meaning that all angles are the same and all the sides are equal in length. It is made of congruent (identical in shape and size), regular polygonal faces, such as equilateral triangles, squares, or pentagons, meeting at each vertex (Table 1). Furthermore, these solids can be inscribed into a sphere. Five solids meet these criteria: the tetrahedron (4 triangular faces), the cube (6 square faces), the octahedron (8 triangular faces), the dodecahedron (12 pentagonal faces), and the icosahedron (20 triangular faces). These solids are named after the Greek philosopher Plato, who theorized that the classical elements of the world were made of these 5 solids. Plato associated each solid with each of the 4 basic elements (earth, air, fire, water) and reserved the fifth for the universe or heaven (<https://www.britannica.com/science/Platonic-solid>). They can be associated in dual pairs, where the solids in a dual pair have the same number of edges, and the number of vertexes of one corresponds to the number of faces of another. Therefore, the tetrahedron is self-dual, while the cube and the octahedron form a dual pair, and the dodecahedron and icosahedron form another (Table 1).

Table 1. The five platonic solids. Their shapes and features are reported, as well as their duality and symbolic meanings.

Name	Cube	Octahedron	Tetrahedron	Icosahedron	Dodecahedron
Shape					
Features	6 faces 8 vertices 12 edges	8 faces 6 vertices 12 edges	4 faces 4 vertices 6 edges	20 faces 12 vertices 30 edges	12 faces 20 vertices 30 edges
Facets	Squares	Equilateral triangles	Equilateral triangles	Equilateral triangles	Pentagons
Duality	 			 	
Symbol	Earth	Air	Fire	Water	Universe/Heaven

The two solids forming a dual pair can be inserted into one another. These solids manifest in the world around us, for example in crystals and in viruses. Indeed, some viruses, like the adenoviruses, possess an icosahedral viral capsid. Moreover, during the adenoviral natural replication cycle, dodecahedrons can be produced depending on the adenovirus serotype. Dodecahedrons and

icosahedrons are dual, therefore the adenovirus dodecahedron being an icosahedron when focusing on the vertices and a dodecahedron when focusing on the faces (Table 1).

3. Discovery of the Adenovirus Dodecahedron

3.1. Discovery and Spontaneous Production

The adenovirus dodecahedrons were first discovered in Sweden in 1964. While purifying soluble antigens produced during an HAdV3 infection of human cells, Erling Norrby observed a homogenous population of particles sedimenting by centrifugation at a rate corresponding to 50–60 S. They appeared as six- or five-pointed ‘stars’ composed of identical tubular, capsomer-like structures, each associated with a thin club-shaped projection [21]. The overall diameter between the points surrounding the star was assessed between 40 and 50 nm. These points were later attributed to the fiber’s knobs, and the tubular capsomer was ascribed to the penton base forming the core (star) of the dodecahedron. These particles do not contain hexons, but are exclusively made of penton base and fiber proteins.

Other studies have shown that not all HAdV serotypes are able to produce dodecahedrons. This has been shown to be the case during the replication cycle of serotypes 4, 7, 9, 11, and 15 [22–25]. In contrast, there is no evidence that serotypes 1, 2, 5, 6, 12, 16, 40, and 41 can produce such dodecahedrons [26–29]. It is also worth noticing that none of the well-studied subgroup C serotypes are able to produce dodecahedrons and that, in subgroup B, dodecahedron production is serotype-dependent (Table 2).

Table 2. Subgroups and dodecahedron formation. Human adenovirus (HAdV) serotypes belonging to different subgroups are classified according to dodecahedron formation. Note that dodecahedrons have never been observed in the well-studied subgroup C and that subgroup B contains both dodecahedron-forming and non-dodecahedron forming serotypes.

Subgroup	A	B	C	D	E	F	G
Dd forming		3, 7, 11		9, 15	4		
Non Dd forming	12	16	1, 2, 5, 6			40, 41	

The most studied adenovirus dodecahedron (Ad-Dd) is derived from HAdV3. Like all adenoviral capsid proteins, the penton base is synthesized in the cytoplasm (Figure 2a). This was shown by immunofluorescent of the penton base (i.e., the dodecahedron): the signal can be detected about 12 h after the virus internalization. The penton base protein is then transported to the nucleus, where it accumulates and likely dodecamerizes [30]. At 20 h post infection, immunofluorescence indicates a substantial concentration around the internal nuclear membrane, whereas the progeny virions crystalize randomly in the nucleus as observed by electron microscopy on ultrathin sections. No function has been attributed yet to dodecahedrons in the nucleus, but it would be interesting to investigate whether this specific internal perinuclear location could be associated with a physiological process, such as viral mRNA export. Nevertheless, the number of dodecahedral particles produced per human cell infected by HAdV3 in culture was estimated to be about 7.5×10^5 , which is much more than the number of infectious virions, reinforcing the idea that this particle does play a role in the viral cycle. This point is further discussed later in this review (see Section 6).

3.2. Recombinant Dodecahedrons

The adenovirus dodecahedron was ‘rediscovered’ in 1997 by co-expressing the penton base and the fiber of HAdV3 in insect cells using the baculovirus expression system. Insect cells lysates were then subjected to a sucrose gradient and the heavy fractions were analyzed by negative stain electron microscopy, highlighting spherical particles arranged into regular dodecahedrons by their bases [31]. These particles display two-fold, three-fold, and five-fold symmetry axes. It is worth noticing that, as expected, the HAdV-2 penton base expressed in a similar way did not form dodecahedrons but only pentameric penton bases, as HAdV-2 does not form dodecahedrons under ‘natural’ conditions.

This confirms that not all adenovirus serotypes are able to generate such particles. The recombinant dodecahedron made of 12 pentons (12 penton bases with 12 protruding trimeric fibers) was called the Penton Dodecahedron (Pt-Dd) (Figure 2b). Since only those two genes were cloned in the baculovirus vector, it proved that no other adenoviral component was needed for the formation of this particle. Moreover, the authors showed that the expression of the penton base alone resulted in the production of the dodecameric core, called the Base Dodecahedron (Bs-Dd). This observation showed that the penton base itself contains all the structural information required for dodecamerization and that the fiber was not required. An important feature of these two particles (Pt-Dd and Bs-Dd) is their high capacity to enter cells (Figure 2c). It was also shown that, if the internalization of the Pt-Dd containing the two proteins involved in adenovirus entry was reported as expected, then the fiber-devoid Bs-Dd could also efficiently enter into cells, but a 10-times higher concentration was needed to achieve a similar level [32].

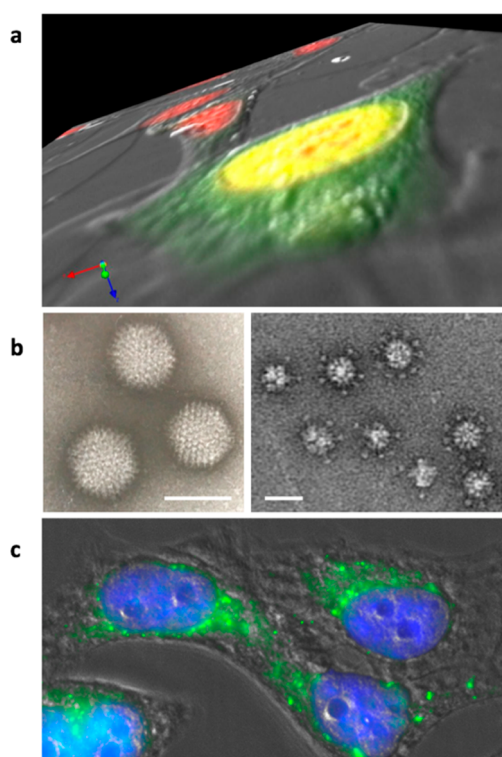


Figure 2. Adenovirus dodecahedron formation and internalization. (a) Z-series of HeLa cells infected for 16 h by wt-HAdV3. Nuclei are stained in red and the penton base is detected in green. The penton base is synthesized in the cytoplasm and transported to the nucleus (yellow results from superposition of the red and green signals) where dodecahedron assembly takes place. (b) Electron microscopy images of the purified adenovirus and (Pt-Dd) ‘penton dodecahedrons’ (bars: 90 and 30 nm, respectively). (c) HeLa cells incubated with recombinant Pt-Dd for 1 h. Cell shapes were observed by DIC, nuclei are stained in blue, and Pt-Dd are detected in green.

Pseudotyping involves adding a viral component onto another viral or pseudoviral scaffold. Since the penton base/fiber interaction mechanism is conserved between several adenovirus serotypes [7], fiber-pseudotyped dodecahedrons are produced. This has been demonstrated by the in vitro addition of the long HAdV2 fiber on Bs-Dd [31] or by coexpression of the HAdV3 Bs-Dd with the ‘short’ fiber of the enteric serotype HAdV41 in insect cells [29]. This result elegantly showed that fibers from serotypes, for which the penton base cannot dodecamerize (HAdV2, HAdV41), can be artificially dodecamerized on the HAdV3-derived Bs-Dd scaffold (Figure 3).

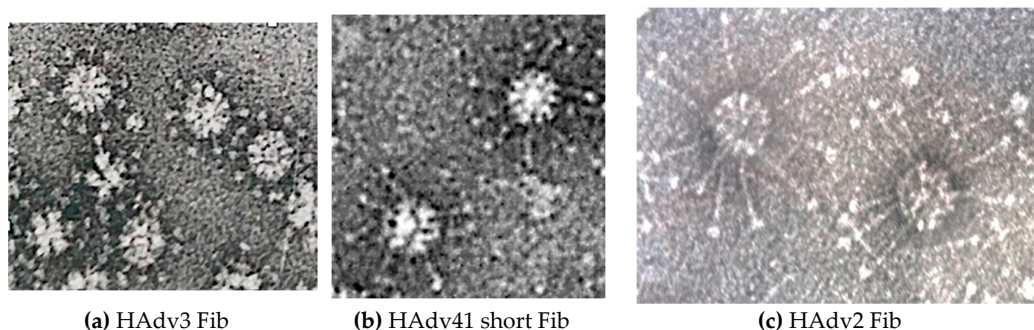


Figure 3. Recombinant HAdV3 dodecahedrons pseudotyped with different fibers. (a) Base Dodecahedron (Bs-Dd) coexpressed with its corresponding HAdV3 fibers, (b) the enteric HAdV41 short fiber, or (c) co-incubated with the HAdV2 fiber are observed by negative staining at the same scale (Bars: 30 nm).

4. Structural Determinants of Dodecamerization

When they form a dodecahedral morphology, the penton bases interact with each other, whereas, when they are on the viral facets, they are separated by the hexons. To the best of our knowledge, this is an exception in virus-like particles (VLPs) [33], which are generally made up of proteins that interact in the same way as they do in the viral capsid. Moreover, as mentioned above, not all serotypes are capable of producing such particles, suggesting that there must be a particular molecular pattern that is responsible for the dodecamerization phenomenon. Several structural studies on dodecahedrons have been undertaken in order to understand the molecular basis for this. Preliminary work was carried out using cryo-microscopy in 1996 using dodecahedrons with and without the fiber. Despite the low resolution accessible by cryo-EM at that time (20–25 Å), the existence of an internal cavity of ~350 nm³ in the center of the particle was revealed [34]. In addition, it was reported that the fixation of the fiber caused a minor density change at the surface of the penton bases.

In 2005, the structure of the Ad2 base was reported by X-ray crystallography at 3.3 Å [7]. Remarkably, this protein, which is unable to dodecamerize under physiological conditions, crystallized in a dodecahedral arrangement in the presence of 1.6 M ammonium sulfate and 10% dioxane. By combining this discovery with an improvement in the dodecahedral resolution of HdAdV3 dodecahedrons by cryo-EM (9 Å), a quasi-atomic structure of the Ad3 dodecahedral particle was reconstructed [35]. In this work, three critical regions involved in dodecamerization were identified in the primary penton base sequence. The first one is located close to the N-terminal (58-SELS-61) and allows homotypic interaction in the two-fold axis with the same sequence from another monomer from an adjacent pentamer. The two other regions (98-NNDFT-102 and 424-FRSTSQ-429, Figure 4a) are distant from each other in the monomer primary sequence but form heterophilic interactions with their counterpart in the monomer of an adjacent pentamer (Figure 4b). Later on, the first crystallographic structure of the Ad3 dodecahedron at 3.8 Å confirmed these data and showed that the charged residues D100 and R425 (highlighted in bold above) formed a salt bridge, as well as an additional network involving hydrogen bonds with N98 and T427 (underlined above), thus stabilizing the structure [36]. Unexpectedly, those residues were not exclusive to HAdV3 but were also present in the non-dodecahedron forming (HAdV2) penton bases. This suggested that, even though those regions are involved in dodecahedron formation, another critical mechanism is required for particle stabilization. The authors elegantly showed that an N-terminal strand-swapping between neighboring HAdV3 penton bases occurred, thus locking the particle. HAdV2 penton bases, on the other hand, were not capable of this. This N-terminal interlocking is controlled by region A (58-SELS-61) since its mutation results in a drastic decrease of dodecahedron stability [36].

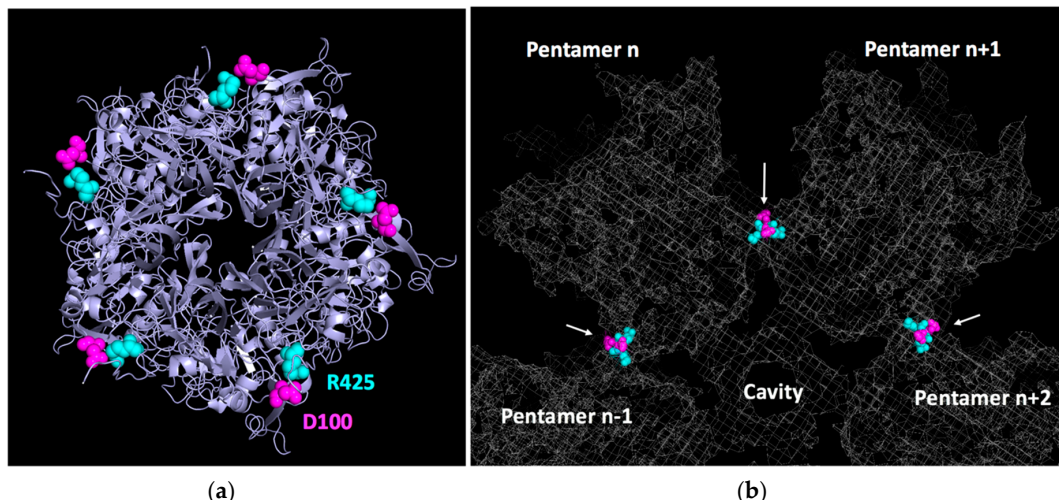


Figure 4. Contact between adjacent pentamers of a dodecahedron. **(a)** Bottom view of a single pentamer with D100 highlighted in magenta and R425 in light blue. **(b)** Zoomed-in slab view of a dodecahedron (grey mesh) showing contacts made by D100 and R425 from adjacent pentamers (PDB 6HCR.).

5. A Tool for Receptor Identification and Characterization

The particle size and multivalency of dodecahedrons make them extremely interesting tools for identifying and characterizing receptors or cellular partners interacting specifically with the penton base or the fiber. The first example was provided with heparan sulphate proteoglycans (HSPGs). Using cells which either expressed or did not express HSPGs, it was shown that both Pt-Dd and Bs-Dd could interact specifically with these cell surface glycoproteins [37]. This result was unexpected since it had previously been reported that, unlike other adenoviral serotypes, HAdV3 could not use these molecules in the same way [38]. This observation suggested either that the penton bases create electrostatic surfaces by stacking in the dodecamers, therefore allowing the interaction with HSPGs, or that the presence of hexons in the viral capsid has a negative effect on this interaction. In any case, it is interesting to note that these particles, partly mimicking the virus, acquire a different property from the virus from which they are derived. The fiber does not seem to be involved in the interaction with HSPGs, since both Bs-Dd and Pt-Dd interact with an apparent affinity on the nanomolar scale. These data obtained by surface plasmon resonance (SPR) on immobilized heparin probably reflect the high avidity due to the multivalency of these particles. A few years later, it was shown by cryo-EM that an extra density was indeed visible on the RGD loop of dodecahedron incubated with an HS oligosaccharide (dp8 = 4 sulfated di-saccharides). A basic BxBB pattern (where B stands for basic, and x for any other amino acids) close to the RGD sequence could play a role in the regulation of the interaction with integrins [39]. The mechanism by which HSPGs regulate this interaction was not fully addressed, but a ‘click to fit’ mechanism was proposed, meaning that a structural change triggered by HSPG could modulate the affinity of the penton base for integrins.

A second example is the identification of several intracellular partners interacting with these dodecahedral particles. By screening a gt11 phage library encoding cDNAs from human lung cells with dodecahedrons, the authors identified a series of partners, all of which have common structural patterns called “WW domains” [40]. These domains get their name from two conserved tryptophans (W) and are known to interact with PP_xY patterns. Remarkably, two PP_xY motifs (x meaning any amino acid) are conserved in the N-terminal of human penton bases, thus explaining why these partners interacted both with Pt-Dd and with Bs-Dd in the previous study. These cellular partners (WP1, WP2, and AIP4) are part of the ubiquitin ligase family, suggesting for the first time that these enzymes could play a role in the cycle of non-enveloped viruses. Previously, these enzymes were only reported in the budding of enveloped viruses [41]. Although dodecahedrons were used for the

identification of these ubiquitin ligases, the dodecamerization is not necessary for the interaction since the HAdV2 penton base alone is also capable of recognizing these partners.

The last example to date is the use of dodecahedrons to identify the missing receptor for the subgroup B adenoviruses. Indeed, although it has been known for a long time that certain subgroup-B adenoviruses interact with CD46, it was also obvious that a certain number of them also interacted with an unidentified receptor X [17,42]. In 2011, Pt-Dd with 12 fibers (as in the native Ad3 virus) was used to fish for this missing receptor [18]. By affinity capture of HeLa cell proteins solubilized by Brij 96V detergent, it was possible to show that a high molecular weight band interacted specifically with the fiber. This interaction required the presence of calcium as already reported in 1995 [43]. The identification of this high molecular weight band by mass spectrometry demonstrated that desmoglein 2 (DSG2), a component of desmosomes, was the receptor for serotypes 3, 7, 11, and 14 [18]. Desmosomes are located at cellular junctions. However, the presence of this receptor in a region that is difficult for the virus to reach is far from an isolated case (for review, see Mateo et al. [44]). Interestingly, identification of desmoglein 2 highlighted a role played by Pt-Dd in the adenoviral replication cell cycle described below.

6. Biological Functions of the Dodecahedron ‘Pseudovirus’

While recombinant dodecahedrons can be produced with or without the fiber, only dodecahedrons displaying the fiber have been reported during the viral lifecycle [21]. As stated above, it has been reported that HAdV3 dodecahedrons are produced in large excess compared to progeny virions [30]. Therefore, the vast majority of penton bases going back to the nucleus after translation are used for dodecahedron formation, and only a small portion is used for neo-virion formation. Such an energy expenditure suggests that dodecahedrons must be involved to some extent in the viral replication strategy and could even be critical. Inside the cell, little is known except that these particles tend to accumulate on the inner side of the nuclear membrane away from the neo-synthesized virions [30]. During synthesis, they could also interact with several members of the ubiquitin ligase family, but this field remains to be studied further.

Outside the cell, the role of dodecahedrons may seem counter-intuitive at first glance. Indeed, Pt-Dd are composed of the two proteins involved in viral entry, and therefore represent a competitor for neo-synthesized virions. This competitor role could be demonstrated on A549 pneumocytes cells in culture infected with the HAdV3-GFP virus, where it was demonstrated that the dodecahedrons had an inhibitory effect on the infection in a dose-dependent manner [18]. However, in this study, the effect of the particles on cells was not limited to a simple competitive role. Rather, they also induced a significant transient cellular remodeling. This effect was measured by real-time cell impedance experiments. The magnitude of the impedance is dependent on the number of cells (cell index), as well as on the shape of the cells, and the cell-substrate attachment quality. When Pt-Dd were added to A549 cell cultures, a rapid and significant drop in impedance could be measured, thus demonstrating a rapid remodeling of the cell shape upon binding. In a similar experiment carried out with Bs-Dd, no effect was detected, thus shedding light on the role of the fiber in inducing this remodeling [45]. Moreover, when the experiment was done with the isolated Ad3 fiber (i.e., not on the dodecahedrons), no remodeling could be induced. This experiment shows, for the first time, the critical role of dodecamerization in inducing physiological effects—the constellated fibers on the dodecahedron produce an effect that cannot be mimicked without this scaffolding. This effect was also visualized by immunofluorescence studies on both fixed and live cells confirming that Pt-Dd induces a rapid (first effect visible in 10–20 min) and specific cell remodeling. Strikingly, both Bs-Dd and Pt-Dd were internalized in this experiment, suggesting that the event triggering cell remodeling is not induced by particle internalization but more likely earlier, when the fibers interact with DSG2. These results are in accordance with experiments made during the identification of DSG2 showing that Pt-Dd induces an epithelial to mesenchymal transition (EMT), resulting in the loss of epithelial markers, such as E-cadherin, and the gain of mesenchymal properties, like cytoskeleton rearrangement, migratory

potential, and matrix metalloproteases (MMPs) expression [18,46]. The mechanism underlying this process was investigated later on. A MAP kinase activation triggered by either Pt-Dd or HAdV3 binding to DSG2, results in the activation of the ADAM17 matrix-metalloproteinase and in the shedding of DSG2 (Figure 5a) [47]. In the scenario where cell disruption by excess capsomer has already been reported for HAdV upon ‘isolated’ fiber binding to the CAR receptor (a member of “tight junctions” between the cells) [48], the HAdV3 fiber must be dodecamerized to exert such an effect. This was demonstrated with an HAdV3 mutant (*mu-Ad3GFP*) where the penton bases were modified to suppress decodecamerization (D100 and R425 mutations). The latter mutation was unable to trigger cell remodeling and featured a worse spreading towards the center of cellular spheroids [49].

Another role of the dodecahedrons upon release from the infected cell, is to trap defensins and, more specifically, the Human Defensin 5 (HD5). HD5 is a small antimicrobial peptide which is able to neutralize the HAdVs from the A, B, C, and E species. To do so, HD5 binds to the HAdV’s capsids, creating a bridge that stabilizes the penton base and the fiber, therefore blocking the pVI protein exposition during the virus uncoating [50,51]. This impairs pVI presentation to the membrane of the endosome, which traps the virus after internalization [52]. The virus is then unable to replicate and is therefore neutralized. The involvement of dodecahedrons in this mechanism has also been studied. It has been shown that HAdV3 dodecahedrons are able to trap and neutralize HD5 secreted by cancer cells, thus acting as a decoy (Figure 5b) [53]. This allows HAdV3 to spread, whereas, in the same conditions the non-dodecahedron forming HAdV5 spreading was limited. Like HAdV5, ‘*mu-Ad3GFP*’ expressing non-dodecamerizing HAdV3 penton bases was also unable to trap defensins, showing that dodecamerization is critical in this process.

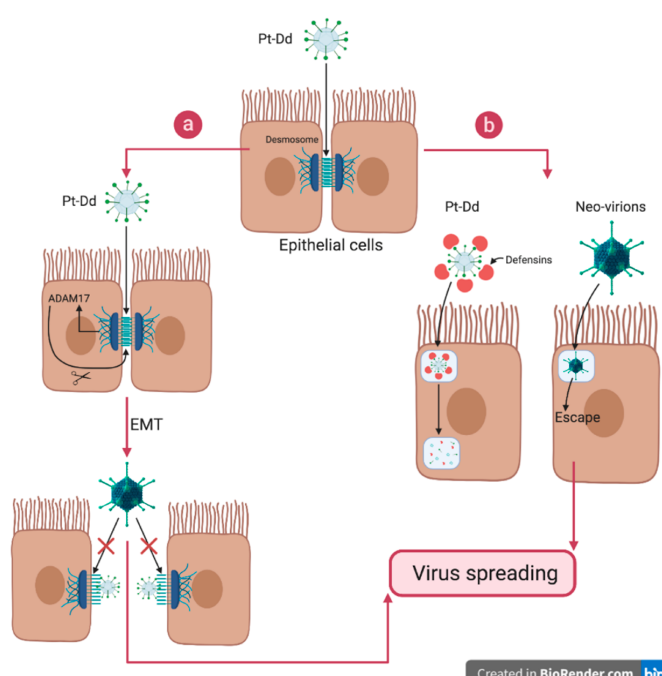


Figure 5. Biological function of the dodecahedron ‘pseudovirus’. Pt-Dd facilitates virus spreading by both interacting with DSG2 and acting as a decoy. (a) Pt-Dd binds to the virus receptor desmoglein 2 located in desmosomes and induces an epithelial to mesenchymal transition (EMT) through MAP kinase signaling and activation of the ADAM17 matrix-metalloproteinase. Moreover, competition between Pt-Dd and virions for DSG2 forces virions to spread in the tissue. (b) At the same time, Pt-Dd traps Human Defensin (HD5), which is known to block adenovirus infection by stabilizing the capsid, thus preventing pVI release and subsequent endosomolysis. By acting as a decoy, Pt-Dd protects neo-virions from defensin attack. Figure created with BioRender.com.

7. Biotechnological Applications

7.1. DNA Delivery

As stated above, dodecahedrons can be rapidly internalized in cells and do not contain any pre-existing nucleic acids. Therefore, they can be excellent vectors for delivering a gene of interest into cells. However, dodecahedrons do not possess an internal cavity large enough to incorporate nucleic acids. Indeed, this central cavity of around 350 nm^3 cannot theoretically enable the packing of more than 100 nucleotides. To overcome this issue, a bifunctional peptide has been designed [31]. This peptide mimics the first 20 amino acids of the trimeric HAdV3 fiber and has a polylysine tail of 20 residues. This peptide can interact with the penton base via the fiber amino acids, as well as with DNA via an electrostatic interaction between the lysine NH_3^+ groups and the DNA PO_3^- groups.

Pt-Dd and Bs-Dd were incubated with the bifunctional peptide and a DNA plasmid carrying the luciferase gene (Figure 6a). It was demonstrated that these complexes could efficiently enter cells and transfer the DNA plasmid into the cell where it reached the nucleus and resulted in gene expression. It is worth noticing that the level of gene expression (and thus of gene transfer) was higher with the penton base dodecahedron. This is probably due to the fact that 3 out of the 5 fiber binding sites on each pentameric penton base are blocked when the trimeric fiber is present, thus limiting access to the fiber-mimicking peptide. However, unlike the use of a ‘classical’ viral vectors, in this kind of approach, the genetic material is not protected. In a similar work using the non-dodecamerizing HAdV5 penton base fused to a decalsine (called 3PO), it has been clearly shown that addition of protamine protected DNA from serum nucleases [54]. Such system has been further explored by adding a heregulin ligand to bind with high affinity Her2/3 or Her2/4 overexpressed on certain aggressive breast cancers [55] and a recent work reported the delivery of RNAi in HER3+ tumors *in vivo* [56].

7.2. Protein Delivery

For the same reasons enounced previously, dodecahedrons represent serious candidates for protein delivery. A study conducted in 2003 demonstrated that dodecahedrons are able to vectorize proteins inside cells [32]. HAdV3 Bs-Dd and Pt-Dd decorated with non-neutralizing monoclonal antibodies (MAbs) directed against the penton base were incubated with cells. In only a few min, antibodies could be delivered inside the cells with both Bs-Dd and Pt-Dd, although the latter was more efficient. Since the MAb alone was not able to be internalized by cells, this data highlights the capacity of dodecahedrons to allow transduction of a high molecular weight protein into cells. However, this promising technique only applies to monoclonal antibodies directed against a component of the dodecahedron. In order to transport any protein of interest into the cells, a more versatile system was necessary.

Therefore, a more universal system has been developed using the interaction properties of the highly-conserved motif “PPxY” motif of the penton base and its “WW” domains (described in Section 5). Three out of the four “WW” domains of the ubiquitin ligase Nedd4 were expressed in fusion with the reporter protein Maltose Binding Protein (MBP), and this protein was efficiently delivered to cells via dodecahedrons (Figure 6a) [57]. This system paved the way to the development of new vaccine technologies described below (cf. ‘vaccination’).

8. Therapeutic “Junction” Opener Effect Improving Anti-Tumor Drugs Efficiency

When the DSG2 was first identified in 2011, it was observed that Pt-Dd binding to DSG2 triggered an epithelial-to-mesenchymal transition (EMT) on breast cancer cells (B474), leading to transient opening of intercellular junctions [18]. This transient opening allowed exposition of poorly accessible receptors, which could be of therapeutic importance but are partially hidden between two adjacent cells. This is the case for Her2/neu, which is targeted by the widely used monoclonal antibody (Mab) ‘Herceptin’ in breast cancer treatment (Figure 6b). It has been shown that the EMT triggered by recombinant Pt-Dd allowed a better exposition of the Her2/neu receptor in tumors. Indeed, a stronger and faster decrease of the tumor size was observed in the group of mice treated with Herceptin

combined with Pt-Dd, compared with the group injected with the therapeutic MAb alone. This study demonstrates that dodecahedrons could be used as therapeutic adjuvants in order to improve the efficiency of anti-tumor treatments. This work served as the basis for the development of a new set of molecules with multimerized HAdV3 fibers called ‘junction openers’ (JO). These have been tested in preclinical studies with other therapeutic MAbs, like the anti-EGF ‘cetuximab’ and chemotherapeutic agents, such as the liposomal doxorubicin ‘Doxil’ [58–60].

Vaccine Development

Most of the preventive vaccines against viral diseases currently in use against are inactivated (chemically or thermally) or attenuated (natural or artificial virulence loss) live viruses. As they are real viruses, there is always a possibility of reactivation. This is not the case for dodecahedrons, which do not contain any viral genetic material. Additionally, the multivalency of dodecahedrons makes them a good tool to trigger an efficient immune response as previously reported for other virus-like particles (VLPs) [61,62].

Several studies have been conducted to evaluate the potential of dodecahedrons as vaccines. In a first approach, 3 out of the 4 Nedd4 “WW” domains were fused to the ovalbumin model antigen 248OVA₃₇₆ cargo. This fusion protein was then attached to the dodecahedrons through the WW-PPxY interaction, so that the cargo was presented in high numbers of copies (Figure 6c) [63,64]. Naive mice were then immunized with the WW-OVA dodecahedrons, which lead to a specific CD8+ T lymphocyte response against OVA. These CD8+ T lymphocytes showed a specific cytotoxic effect against melanoma cells expressing the OVA antigen on their surface (B16-OVA). These promising results paved the way to more experiments with ovalbumin antigens. Mice were immunized with 2 injections of WW-OVA dodecahedrons 14 and 7 days before injection of melanoma cells B16 expressing the OVA antigen (B16-OVA). The tumor growth was evaluated and only one mouse out of 10 developed a tumor. However, it is worth noticing that, for this mouse, the tumor development was delayed (D25 post injection) compared to B16-OVA non-immunized group (around 10 days post injection). The other 9 mice survived several months after the tumor injection, whereas, in the negative control group, the overall survival did not exceed 20 days.

These first results with the model antigen ovalbumin highlighted the strong potential of using dodecahedrons *in vivo* in the vaccine field and in cancer immunotherapy. A similar *in vitro* study was later performed in infectiology with the influenza hemagglutinin attached, showing that several applications could be addressed by using this strategy [65]. However, this kind of approach suffered from two major shortcomings: (i) the presence of an adapter of human origin (the WW domain) and (ii) the need for two different expression systems. To overcome these issues, a new system has recently been reported. The HAdV3 penton base gene was engineered by insertion of restriction sites to create three independent sites for epitope display: one in the VL loop and two others in the RGD loop (flanking the preserved RGD motif) of the penton base sequence. Therefore, various antigenic epitopes of choice could be inserted into this plug-and-play multiepitope display platform named ADDomer (Figure 6c). To illustrate the potential of such a system, the chikungunya major neutralizing epitope E2EP3 (Epitope 3 of the chikungunya E2 protein, 18 amino acids), which is linearly displayed at the new N terminus of E2 glycoprotein created after furin cleavage, was inserted into the ADDomer. This created a virus-like-particle (VLP) vaccine candidate named ADDomer-tevCHIK. To loosen this conformation, a highly specific protease site (Tobacco Etch virus: TEV) was inserted upstream of the epitope. Upon cleavage, the epitope can readopt its native-like conformation comprising an exposed N-terminal serine. After injection in mice, no E2EP3-specific antibodies were obtained with the uncleaved ADDomer-tevCHIK. On the contrary, cleaved ADDomer-tevCHIK exposing the native-like E2EP3 led to a very strong humoral response in absence of adjuvant [66]. In comparison, a nanoparticle scaffold made of polylactic acids (PLA) displaying the same amount of the E2EP3 epitope did not lead to an anti-E2EP3 immune response. This suggests that the ADDomer itself has an adjuvant effect. It is worth noticing that ADDomers rapidly drain to lymph nodes upon injection in mice and are

efficiently internalized in immune blood cells, which is essential for a vaccine candidate. In this study, it was also shown that the ADDomer is remarkably thermostable, which represents a crucial asset for the deployment of ADDomer-based vaccines in remote countries. In summary, all of these results involving a real antigen from a pathogen confirmed the strong potential of dodecahedrons in the vaccine field.

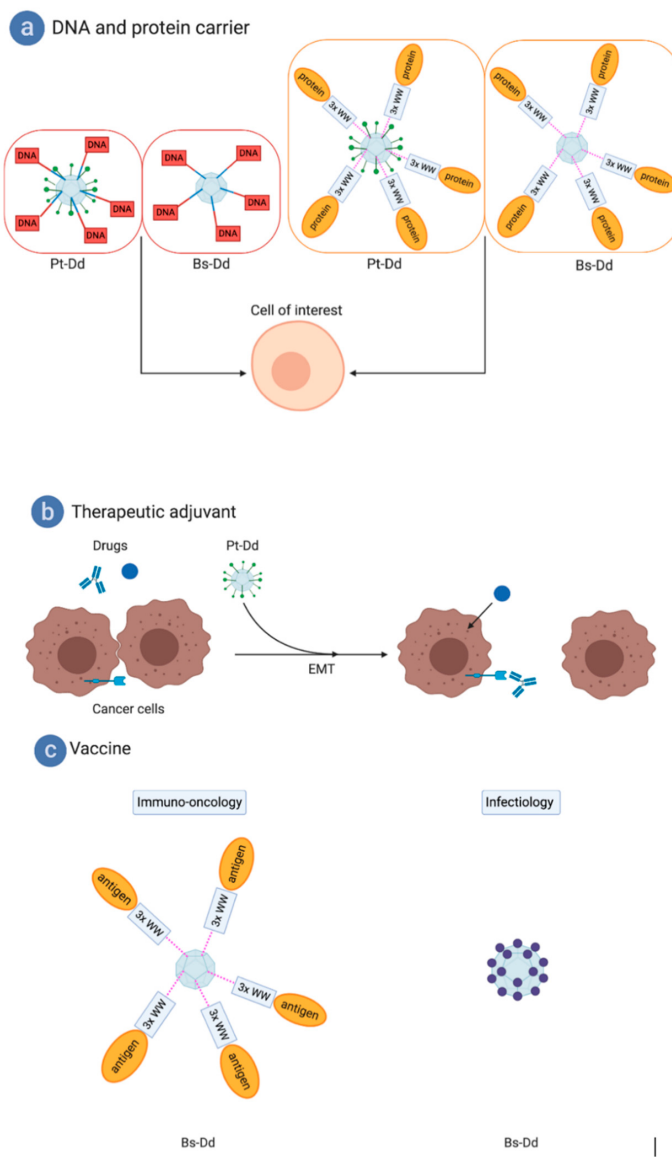


Figure 6. Biotechnological applications of the dodecahedron ‘pseudovirus’. (a) The dodecahedron ‘pseudovirus’ can be used to deliver DNA due to a bispecific peptide or proteins of interest fused to the WW domains. (b) The dodecahedron ‘pseudovirus’ can be used as a therapeutic adjuvant by triggering cell remodeling by making hidden targets accessible to therapeutic monoclonal antibodies (MAbs) or by enabling better access to chemotherapeutic compounds. (c) For vaccine purposes, cancer antigens fused to WW domains can be grafted to Bs-Dd. Alternatively, a single particle can be produced to display epitopes from pathogens, such as emergent viruses. Figure created with BioRender.com.

9. Concluding Remarks

In this review, multiple facets of the adenovirus dodecahedron were detailed. It is interesting to note that these particles, identified in the late 60s by Erling Norrby, were not studied again until their recombinant expression 30 years later. One unique property of the dodecahedrons relies on the ability of the penton bases to interact together symmetrically while they are not in contact in the virion.

The structural mechanisms underlying the formation of dodecahedrons have been elucidated over time, but certain aspects remain to be determined formally, such as where their assembly takes place in the cell and whether chaperone proteins help their assembly. Their production in large numbers suggests that these particles play a role in the viral lifecycle, and it has been confirmed that they favor spreading of the virus after lysis of the infected cells. However, it would be necessary to further explore their putative intracellular role in the infected cell before their dispersion in the extracellular medium. The strong internalization properties of these particles, which interact with the same receptors as the virus but also with other molecules, such as HSPGs, have been used for biotechnological applications. Their use could be further improved by increasing their endosomolysis capacity. Their applications in vaccinology seem promising, as these particles are particularly stable and the 60-mer controlled multimerization, allowing good recognition by the immune system. From a purely geometric point of view, it is interesting to note that an icosahedral virus is capable of producing its dual dodecahedral form. These forms, which intrigued Leonardo da Vinci because of their aesthetics and underlying mathematical relationships since the golden ratio intervenes in the calculation of their radius, their volume, and their coordinates, probably still have a lot to teach us.

Author Contributions: Conceptualization S.B., C.V. and P.F.; software E.V.-S.; investigation S.B., C.V., E.V.-S., M.C.D. and P.F.; writing—original draft preparation S.B., C.V. and P.F.; writing—review and editing S.B., C.V., E.V.-S., M.C.D. and P.F.; project administration P.F.; funding acquisition M.C.D. and P.F. All authors have read and agreed to the published version of the manuscript.

Funding: This research was funded by the ‘Agence Nationale de la Recherche’, grant number ANR18-CE11-0001” and the ‘Région Auvergne Rhône-Alpes’, grant number 20-009070-01.

Acknowledgments: We are grateful to Martyna Judd for the English corrections and for her advice and to Valentin Dettling for his work and support.

Conflicts of Interest: The authors declare no conflict of interest.

References

1. Lion, T. Adenovirus infections in immunocompetent and immunocompromised patients. *Clin. Microbiol. Rev.* **2014**, *27*, 441–462. [[CrossRef](#)]
2. Uhnoo, I.; Wadell, G.; Svensson, L.; Johansson, M.E. Importance of enteric adenoviruses 40 and 41 in acute gastroenteritis in infants and young children. *J. Clin. Microbiol.* **1984**, *20*, 365–372. [[CrossRef](#)]
3. Chandra, N.; Frängsmyr, L.; Imhof, S.; Caraballo, R.; Elofsson, M.; Arnberg, N. Sialic Acid-Containing Glycans as Cellular Receptors for Ocular Human Adenoviruses: Implications for Tropism and Treatment. *Viruses* **2019**, *11*, 395. [[CrossRef](#)] [[PubMed](#)]
4. Grütter, M.; Franklin, R.M. Studies on the molecular weight of the adenovirus type 2 hexon and its subunit. *J. Mol. Biol.* **1974**, *89*, 163–178. [[CrossRef](#)]
5. Boulanger, P.A.; Puvion, F. Adenovirus Assembly. *Eur. J. Biochem.* **1974**, *43*, 465–470. [[CrossRef](#)] [[PubMed](#)]
6. Rux, J.J.; Burnett, R.M. Adenovirus structure. *Hum. Gene Ther.* **2004**, *15*, 1167–1176. [[CrossRef](#)]
7. Zubieta, C.; Schoehn, G.; Chroboczek, J.; Cusack, S. The Structure of the Human Adenovirus 2 Penton. *Mol. Cell* **2005**, *17*, 319–320. [[CrossRef](#)]
8. Belin, M.-T.; Boulanger, P. Involvement of cellular adhesion sequences in the attachment of adenovirus to the HeLa cell surface. *J. Gen. Virol.* **1993**, *74*, 1485–1497. [[CrossRef](#)]
9. Wickham, T.J.; Mathias, P.; Cheresh, D.A.; Nemerow, G.R. Integrins alpha v beta 3 and alpha v beta 5 promote adenovirus internalization but not virus attachment. *Cell* **1993**, *73*, 309–319. [[CrossRef](#)]
10. Bai, M.; Harfe, B.; Freimuth, P. Mutations that alter an Arg-Gly-Asp (RGD) sequence in the adenovirus type 2 penton base protein abolish its cell-rounding activity and delay virus reproduction in flat cells. *J. Virol.* **1993**, *67*, 5198–5205. [[CrossRef](#)]
11. Albinsson, B.; Kidd, A.H. Adenovirus type 41 lacks an RGD alpha(v)-integrin binding motif on the penton base and undergoes delayed uptake in A549 cells. *Virus Res.* **1999**, *64*, 125–136. [[CrossRef](#)]
12. Rajan, A.; Persson, B.D.; Frängsmyr, L.; Olofsson, A.; Sandblad, L.; Heino, J.; Takada, Y.; Mould, A.P.; Schnapp, L.M.; Gall, J.; et al. Enteric Species F Human Adenoviruses use Laminin-Binding Integrins as Co-Receptors for Infection of Ht-29 Cells. *Sci. Rep.* **2018**, *8*, 1–14. [[CrossRef](#)] [[PubMed](#)]

13. Green, N.M.; Wrigley, N.G.; Russell, W.C.; Martin, S.R.; McLachlant, A.D. Evidence for a repeating cross-sheet structure in the adenovirus fibre. *EMBO J.* **1983**, *2*, 1357–1365. [[CrossRef](#)] [[PubMed](#)]
14. Van Raaij, M.J.; Mitraki, A.; Lavigne, G.; Cusack, S. A triple beta-spiral in the adenovirus fibre shaft reveals a new structural motif for a fibrous protein. *Nature* **1999**, *401*, 935–938. [[CrossRef](#)]
15. Louis, N.; Fender, P.; Barge, A.; Kitts, P.; Chroboczek, J. Cell-binding domain of adenovirus serotype 2 fiber. *J. Virol.* **1994**, *68*, 4104–4106. [[CrossRef](#)]
16. Bergelson, J.M.; Cunningham, J.A.; Drogue, G.; Kurt-Jones, E.A.; Krithivas, A.; Hong, J.S.; Horwitz, M.S.; Crowell, R.L.; Finberg, R.W. Isolation of a common receptor for Coxsackie B viruses and adenoviruses 2 and 5. *Science* **1997**, *275*, 1320–1323. [[CrossRef](#)] [[PubMed](#)]
17. Gaggar, A.; Shayakhmetov, D.M.; Lieber, A. CD46 is a cellular receptor for group B adenoviruses. *Nat. Med.* **2003**, *9*, 1408–1412. [[CrossRef](#)] [[PubMed](#)]
18. Wang, H.; Li, Z.-Y.; Liu, Y.; Persson, J.; Beyer, I.; Möller, T.; Koyuncu, D.; Drescher, M.R.; Strauss, R.; Zhang, X.-B.; et al. Desmoglein 2 is a receptor for adenovirus serotypes 3, 7, 11 and 14. *Nat. Med.* **2011**, *17*, 96–104. [[CrossRef](#)]
19. Nilsson, E.C.; Storm, R.J.; Bauer, J.; Johansson, S.M.C.; Lookene, A.; Ångström, J.; Hedenström, M.; Eriksson, T.L.; Frängsmyr, L.; Rinaldi, S.; et al. The GD1a glycan is a cellular receptor for adenoviruses causing epidemic keratoconjunctivitis. *Nat. Med.* **2011**, *17*, 105–109. [[CrossRef](#)]
20. Baker, A.T.; Mundy, R.M.; Davies, J.A.; Rizkallah, P.J.; Parker, A.L. Human adenovirus type 26 uses sialic acid-bearing glycans as a primary cell entry receptor. *Sci. Adv.* **2019**, *5*, eaax3567. [[CrossRef](#)]
21. Norrby, E. The relationship between the soluble antigens and the virion of adenovirus type 3. I. Morphological characteristics. *Virology* **1966**, *28*, 236–248. [[CrossRef](#)]
22. Norrby, E.; Wadell, G. Soluble components of adenovirus type 4. *Virology* **1967**, *31*, 592–600. [[CrossRef](#)]
23. Norrby, E.; Nyberg, B.; Skaaret, P.; Lengyel, A. Separation and characterization of soluble adenovirus type 9 components. *J. Virol.* **1967**, *1*, 1101–1108. [[CrossRef](#)] [[PubMed](#)]
24. Norrby, E. Identification of soluble components of adenovirus type 11. *J. Gen. Virol.* **1968**, *2*, 123–133. [[CrossRef](#)] [[PubMed](#)]
25. Neurath, A.R.; Rubin, B.A. Interaction of p-chloromercuribenzoate with adenoviruses. Inactivation of haemagglutinins and degradation of virions of types 3, 4 and 7. *J. Gen. Virol.* **1968**, *2*, 215–229. [[CrossRef](#)] [[PubMed](#)]
26. Wadell, G.; Norrby, E. Immunological and Other Biological Characteristics of Pentons of Human Adenoviruses. *J. Virol.* **1969**, *4*, 671–680. [[CrossRef](#)] [[PubMed](#)]
27. Norrby, E.; Ankerst, J. Biological Characterization of Structural Components of Adenovirus type 12. *J. Gen. Virol.* **1969**, *5*, 183–194. [[CrossRef](#)]
28. Norrby, E.; Skaaret, P. Comparison between soluble components of adenovirus types 3 and 16 and of the intermediate strain 3–16 (the San Carlos agent). *Virology* **1968**, *36*, 201–211. [[CrossRef](#)]
29. Siqueira-Silva, J.; Fenel, D.; Gout, E.; Yeda, F.P.; Marinheiro, J.C.; Barrella, K.M.; Silva, M.L.; Schoehn, G.; Harsi, C.M.; Fender, P. Generation and biological properties of a recombinant dodecahedron containing the short fiber protein of the human adenovirus 41. *Intervirology* **2012**, *55*, 349–355. [[CrossRef](#)]
30. Fender, P.; Boussaid, A.; Mezin, P.; Chroboczek, J. Synthesis, cellular localization, and quantification of penton-dodecahedron in serotype 3 adenovirus-infected cells. *Virology* **2005**, *340*, 167–173. [[CrossRef](#)]
31. Fender, P.; Ruigrok, R.W.; Gout, E.; Buffet, S.; Chroboczek, J. Adenovirus dodecahedron, a new vector for human gene transfer. *Nat. Biotechnol.* **1997**, *15*, 52–56. [[CrossRef](#)] [[PubMed](#)]
32. Fender, P.; Schoehn, G.; Foucaud-Gamen, J.; Gout, E.; Garcel, A.; Drouet, E.; Chroboczek, J. Adenovirus dodecahedron allows large multimeric protein transduction in human cells. *J. Virol.* **2003**, *77*, 4960–4964. [[CrossRef](#)] [[PubMed](#)]
33. Zeltins, A. Construction and characterization of virus-like particles: a review. *Mol. Biotechnol.* **2013**, *53*, 92–107. [[CrossRef](#)] [[PubMed](#)]
34. Schoehn, G.; Fender, P.; Chroboczek, J.; Hewat, E.A. Adenovirus 3 penton dodecahedron exhibits structural changes of the base on fibre binding. *EMBO J.* **1996**, *15*, 6841–6846. [[CrossRef](#)]
35. Fuschiotti, P.; Schoehn, G.; Fender, P.; Fabry, C.M.S.; Hewat, E.A.; Chroboczek, J.; Ruigrok, R.W.H.; Conway, J.F. Structure of the dodecahedral penton particle from human adenovirus type 3. *J. Mol. Biol.* **2006**, *356*, 510–520. [[CrossRef](#)]

36. Szolajska, E.; Burmeister, W.P.; Zochowska, M.; Nerlo, B.; Andreev, I.; Schoehn, G.; Andrieu, J.-P.; Fender, P.; Naskalska, A.; Zubieta, C.; et al. The structural basis for the integrity of adenovirus Ad3 dodecahedron. *PLoS ONE* **2012**, *7*, e46075. [[CrossRef](#)]
37. Vivès, R.R.; Lortat-Jacob, H.; Chroboczek, J.; Fender, P. Heparan sulfate proteoglycan mediates the selective attachment and internalization of serotype 3 human adenovirus dodecahedron. *Virology* **2004**, *321*, 332–340. [[CrossRef](#)]
38. Dechechchi, M.C.; Melotti, P.; Bonizzato, A.; Santacatterina, M.; Chilosì, M.; Cabrini, G. Heparan Sulfate Glycosaminoglycans Are Receptors Sufficient To Mediate the Initial Binding of Adenovirus Types 2 and 5. *J. Virol.* **2001**, *75*, 8772–8780. [[CrossRef](#)]
39. Gout, E.; Schoehn, G.; Fenel, D.; Lortat-Jacob, H.; Fender, P. The adenovirus type 3 dodecahedron’s RGD loop comprises an HSPG binding site that influences integrin binding. *J. Biomed. Biotechnol.* **2010**, *2010*, 541939. [[CrossRef](#)]
40. Galinier, R.; Gout, E.; Lortat-Jacob, H.; Wood, J.; Chroboczek, J. Adenovirus Protein Involved in Virus Internalization Recruits Ubiquitin–Protein Ligases. *Biochemistry* **2002**, *41*, 14299–14305. [[CrossRef](#)]
41. Shepley-McTaggart, A.; Fan, H.; Sudol, M.; Harty, R.N. Viruses go modular. *J. Biol. Chem.* **2020**, *295*, 4604–4616. [[CrossRef](#)] [[PubMed](#)]
42. Wang, H.; Tuve, S.; Erdman, D.D.; Lieber, A. Receptor usage of a newly emergent adenovirus type 14. *Virology* **2009**, *387*, 436–441. [[CrossRef](#)] [[PubMed](#)]
43. Di Guilmi, A.M.; Barge, A.; Kitts, P.; Gout, E.; Chroboczek, J. Human adenovirus serotype 3 (Ad3) and the AD fiber protein bind to a 130-kDa membrane protein on HeLa cells. *Virus Res.* **1995**, *38*, 71–81. [[CrossRef](#)]
44. Mateo, M.; Generous, A.; Sinn, P.L.; Cattaneo, R. Connections matter—how viruses use cell–cell adhesion components. *J. Cell. Sci.* **2015**, *128*, 431–439. [[CrossRef](#)]
45. Fender, P.; Hall, K.; Schoehn, G.; Blair, G.E. Impact of human adenovirus type 3 dodecahedron on host cells and its potential role in viral infection. *J. Virol.* **2012**, *86*, 5380–5385. [[CrossRef](#)]
46. Weinberg, R.A. Twisted epithelial-mesenchymal transition blocks senescence. *Nat. Cell Biol.* **2008**, *10*, 1021–1023. [[CrossRef](#)]
47. Wang, H.; Ducournau, C.; Saydaminova, K.; Richter, M.; Yumul, R.; Ho, M.; Carter, D.; Zubieta, C.; Fender, P.; Lieber, A. Intracellular signaling and desmoglein 2 shedding triggered by human adenoviruses Ad3, Ad14, and Ad14P1. *J. Virol.* **2015**, *89*, 10841–10859. [[CrossRef](#)]
48. Walters, R.W.; Freimuth, P.; Moninger, T.O.; Ganske, I.; Zabner, J.; Welsh, M.J. Adenovirus fiber disrupts CAR-mediated intercellular adhesion allowing virus escape. *Cell* **2002**, *110*, 789–799. [[CrossRef](#)]
49. Lu, Z.-Z.; Wang, H.; Zhang, Y.; Cao, H.; Li, Z.; Fender, P.; Lieber, A. Penton-dodecahedral particles trigger opening of intercellular junctions and facilitate viral spread during adenovirus serotype 3 infection of epithelial cells. *PLoS Pathog.* **2013**, *9*, e1003718. [[CrossRef](#)]
50. Smith, J.G.; Silvestry, M.; Lindert, S.; Lu, W.; Nemerow, G.R.; Stewart, P.L. Insight into the Mechanisms of Adenovirus Capsid Disassembly from Studies of Defensin Neutralization. *PLoS Pathog.* **2010**, *6*, e1000959. [[CrossRef](#)]
51. Flatt, J.W.; Kim, R.; Smith, J.G.; Nemerow, G.R.; Stewart, P.L. An Intrinsically Disordered Region of the Adenovirus Capsid Is Implicated in Neutralization by Human Alpha Defensin 5. *PLoS ONE* **2013**, *8*, e61571. [[CrossRef](#)] [[PubMed](#)]
52. Staring, J.; Raaben, M.; Brummelkamp, T.R. Viral escape from endosomes and host detection at a glance. *J. Cell Sci.* **2018**, *131*, jcs216259. [[CrossRef](#)] [[PubMed](#)]
53. Vragniau, C.; Hübner, J.-M.; Beidler, P.; Gil, S.; Saydaminova, K.; Lu, Z.-Z.; Yumul, R.; Wang, H.; Richter, M.; Sova, P.; et al. Studies on the Interaction of Tumor-Derived HD5 Alpha Defensins with Adenoviruses and Implications for Oncolytic Adenovirus Therapy. *J. Virol.* **2017**, *91*, e02030-16. [[CrossRef](#)] [[PubMed](#)]
54. Medina-Kauwe, L.K.; Kasahara, N.; Kedes, L. 3PO, a novel nonviral gene delivery system using engineered Ad5 penton proteins. *Gene Ther.* **2001**, *8*, 795–803. [[CrossRef](#)]
55. Medina-Kauwe, L.K.; Maguire, M.; Kasahara, N.; Kedes, L. Nonviral gene delivery to human breast cancer cells by targeted Ad5 penton proteins. *Gene Ther.* **2001**, *8*, 1753–1761. [[CrossRef](#)]
56. Alonso-Valenteen, F.; Pacheco, S.; Srinivas, D.; Rentsendorj, A.; Chu, D.; Lubow, J.; Sims, J.; Miao, T.; Mikhael, S.; Hwang, J.Y.; et al. HER3-targeted protein chimera forms endosomolytic capsomeres and self-assembles into stealth nucleocapsids for systemic tumor homing of RNA interference in vivo. *Nucleic Acids Res.* **2019**, *47*, 11020–11043. [[CrossRef](#)]

57. Garcel, A.; Gout, E.; Timmins, J.; Chroboczek, J.; Fender, P. Protein transduction into human cells by adenovirus dodecahedron using WW domains as universal adaptors. *J. Gene Med.* **2006**, *8*, 524–531. [[CrossRef](#)]
58. Beyer, I.; van Rensburg, R.; Strauss, R.; Li, Z.; Wang, H.; Persson, J.; Yumul, R.; Feng, Q.; Song, H.; Bartek, J.; et al. Epithelial junction opener JO-1 improves monoclonal antibody therapy of cancer. *Cancer Res.* **2011**, *71*, 7080–7090. [[CrossRef](#)] [[PubMed](#)]
59. Wang, H.; Yumul, R.; Cao, H.; Ran, L.; Fan, X.; Richter, M.; Epstein, F.; Gralow, J.; Zubietta, C.; Fender, P.; et al. Structural and functional studies on the interaction of adenovirus fiber knobs and desmoglein 2. *J. Virol.* **2013**, *87*, 11346–11362. [[CrossRef](#)]
60. Richter, M.; Yumul, R.; Wang, H.; Saydaminova, K.; Ho, M.; May, D.; Baldessari, A.; Gough, M.; Drescher, C.; Urban, N.; et al. Preclinical safety and efficacy studies with an affinity-enhanced epithelial junction opener and PEGylated liposomal doxorubicin. *Mol. Ther. Methods Clin. Dev.* **2015**, *2*, 15005. [[CrossRef](#)]
61. Kanekiyo, M.; Wei, C.-J.; Yassine, H.M.; McTamney, P.M.; Boyington, J.C.; Whittle, J.R.R.; Rao, S.S.; Kong, W.-P.; Wang, L.; Nabel, G.J. Self-assembling influenza nanoparticle vaccines elicit broadly neutralizing H1N1 antibodies. *Nature* **2013**, *499*, 102–106. [[CrossRef](#)] [[PubMed](#)]
62. Kanekiyo, M.; Bu, W.; Joyce, M.G.; Meng, G.; Whittle, J.R.R.; Baxa, U.; Yamamoto, T.; Narpala, S.; Todd, J.-P.; Rao, S.S.; et al. Rational Design of an Epstein-Barr Virus Vaccine Targeting the Receptor-Binding Site. *Cell* **2015**, *162*, 1090–1100. [[CrossRef](#)] [[PubMed](#)]
63. Villegas-Mendez, A.; Garin, M.I.; Pineda-Molina, E.; Veratti, E.; Bueren, J.A.; Fender, P.; Lenormand, J.-L. In vivo delivery of antigens by adenovirus dodecahedron induces cellular and humoral immune responses to elicit antitumor immunity. *Mol. Ther.* **2010**, *18*, 1046–1053. [[CrossRef](#)]
64. Villegas-Méndez, A.; Fender, P.; Garin, M.I.; Rothe, R.; Liguori, L.; Marques, B.; Lenormand, J.-L. Functional characterisation of the WW minimal domain for delivering therapeutic proteins by adenovirus dodecahedron. *PLoS ONE* **2012**, *7*, e45416. [[CrossRef](#)] [[PubMed](#)]
65. Naskalska, A.; Szolajska, E.; Andreev, I.; Podsiadla, M.; Chroboczek, J. Towards a novel influenza vaccine: Engineering of hemagglutinin on a platform of adenovirus dodecahedron. *BMC Biotechnol.* **2013**, *13*, 50. [[CrossRef](#)]
66. Vragniau, C.; Bufton, J.C.; Garzoni, F.; Stermann, E.; Rabi, F.; Terrat, C.; Guidetti, M.; Josserand, V.; Williams, M.; Woods, C.J.; et al. Synthetic self-assembling ADDomer platform for highly efficient vaccination by genetically encoded multiepitope display. *Sci. Adv.* **2019**, *5*, eaaw2853. [[CrossRef](#)]



© 2020 by the authors. Licensee MDPI, Basel, Switzerland. This article is an open access article distributed under the terms and conditions of the Creative Commons Attribution (CC BY) license (<http://creativecommons.org/licenses/by/4.0/>).

Conclusion du chapitre :

Dans cette publication la découverte du dodécaèdre de l'adénovirus avec sa structure, ses fonctions biologiques et ses applications en biotechnologie a été détaillée. Comme présenté, ce dodécaèdre d'adénovirus peut être utilisée pour des applications biotechnologiques comme plateforme vaccinale. Au cours de cette thèse nous allons montrer que ce dodécaèdre constitue une plateforme vaccinale prometteuse en oncologie du mélanome.

Chapitre III : Objectifs de la thèse

L’Institut National du Cancer a évalué à plus de 15 500 les nouveaux cas de mélanomes cutanés en 2018 en France métropolitaine. Il est estimé qu’au sein de la population occidentale, 1 individu sur 50 développera un mélanome²²⁹. Le mélanome représente seulement 4 % de l’ensemble des cancers ainsi que 1,2 % des décès par cancer, cependant c'est l'un des cancers pour lequel l'incidence ainsi que la mortalité ont significativement augmenté depuis 40 ans. Le mélanome cutané est de bon pronostic s'il est détecté assez tôt (indice de Breslow < 2 mm et pas de métastases), en revanche un diagnostic tardif réduit fortement les chances de survie étant donné le fort potentiel métastatique de ce cancer. Les chances de survie dépendent donc très largement du stade d’avancement du cancer au moment du diagnostic. Ainsi, selon le programme américain SEER la survie relative à 5 ans est de 98% pour un mélanome localisé, 62% pour un mélanome présentant une extension loco-régionale et de 15% pour un mélanome métastatique. Au vu de ces chiffres, il apparaît donc primordial de poursuivre des recherches de nouvelles thérapies pour traiter ce cancer et les vaccins thérapeutiques constituerait une piste prometteuse.

La thématique de l’équipe du Dr Fender à Grenoble est l’adénovirus. Cette famille de virus à large tropisme a récemment suscité un regain d’intérêt pour son utilisation en tant que vaccin contre le coronavirus SARS-CoV-2 (VAXZEVRIA®, Astra Zeneca-Université d’Oxford ou encore JCOVDEN® du laboratoire Janssen). Les adénovirus peuvent également servir de virus oncolytiques chez l’homme comme le ‘Gendicine’ (Shenzhen SiBiono GeneTech) qui a été approuvé en Chine pour le traitement des tumeurs cancéreuses. De plus, c'est actuellement le vecteur viral le plus utilisé dans les essais cliniques chez l’homme. L’approche novatrice de l’équipe consiste à ne pas utiliser d’adénovirus répliquatifs, en raison

des problèmes réglementaires qui leur sont associés, mais une pseudo-particule immunogène dérivée de l'adénovirus. Cette particule pseudo-virale non-infectieuse mimant l'adénovirus pour les étapes d'entrée dans les cellules est nommée ADDomer (ADenovirus Dodecamer). Cette technologie a été brevetée par le CNRS en 2017 et a déjà fait ses preuves dans le domaine de l'infectiologie²³⁰.

L'objectif du projet est d'utiliser cette technologie de stimulation immunitaire novatrice développée dans l'équipe et de l'appliquer en cancérologie et plus particulièrement au domaine de l'immunothérapie du mélanome. Dans ce but, un consortium a été établi avec les équipes des Dr Chaperot et Aspord à l'EFS de Grenoble, toutes deux spécialistes de l'immunothérapie des mélanomes.

La thèse s'est donc déroulée autour de trois axes principaux :

1) Production et optimisation des ADDomers

Cette première partie du projet de thèse réalisée à l'Institut de Biologie Structurale (IBS, Grenoble) a consisté à produire, purifier et optimiser le design des vaccins ADDomers présentant des épitopes et antigènes modèles et humains du mélanome.

2) Evaluation *in vitro* des vaccins ADDomers en oncologie

Une fois produits et purifiés, les différents ADDomers présentant des épitopes et antigènes humains du mélanome ont été évalués *in vitro* sur des cellules dendritiques (DC) humaines de donneurs sains. Cette partie de la thèse s'est déroulée à l'Etablissement Français du Sang (EFS) ainsi qu'à l'Institute for Advanced Biosciences (IAB) à Grenoble. Ce travail nous a amené à évaluer la capacité des DC à internaliser ces ADDomers, à présenter les épitopes/antigènes

associés et à déclencher des réponses cellulaires T spécifiques de l'antigène. De plus, afin d'améliorer l'adressage spécifique des DCs, des ligands spécifiques ont été conçus.

3) Evaluation *in vivo* chez la souris des vaccins ADDomers en oncologie

Enfin, les différents ADDomers présentant soit des épitopes soit des antigènes modèles du mélanome ont été évalués *in vivo* chez des souris C57bl6J inoculées avec des cellules tumorales de la lignée B16 OVA, lignée communément utilisée dans l'évaluation *in vivo* du mélanome chez la souris. Cette partie d'expérimentation animale de la thèse s'est déroulée à la Plateforme de Haute Technologie Animale (PHTA) à Grenoble. L'immunogénicité des ADDomers ainsi que leur effet préventif et thérapeutique sur la tumeur ont été évalués.

Ces travaux ont pour but d'appliquer la technologie ADDomer au domaine de l'immunothérapie du mélanome dans une optique de développement de vaccin thérapeutique.

Chapitre IV : Optimisations de la plateforme ‘ADDomer’ pour l’exposition d’épitopes et d’antigènes du mélanome

Introduction du chapitre :

Dans ce premier chapitre, nous allons développer les optimisations qui ont été réalisées sur la plateforme ADDomer afin qu'il soit possible d'exposer non seulement des épitopes mais surtout des antigènes entiers de grande taille. L'exposition d'antigènes entiers par un vaccin est primordiale afin de maximiser les chances de destruction tumorale et de s'affranchir de la restriction allélique imposée par l'utilisation d'épitopes. L'exposition d'épitopes à la surface de l'ADDomer est réalisée par insertion génétique. Cependant, cette technique n'est pas applicable pour des antigènes entiers longs et structurés (protéine insoluble). Pour surmonter cet obstacle nous avons décidé d'utiliser le système SpyTag/SpyCatcher, développé par Zakeri et al. en 2012 à l'université d'Oxford. Dans ce chapitre nous montrerons comment ce système a été adapté et optimisé pour l'ADDomer afin d'exposer un mais également plusieurs antigènes de diverses longueurs et structures à sa surface.

Dans l'optique de faciliter la valorisation future de ces résultats par le laboratoire, cette partie sera rédigée en anglais.

ADDomers' design for human tumor epitope and antigen display

The ADDomer is a non-infectious nanoparticle formed of 12 bricks of the homo-pentameric penton base from the human adenovirus type 3. Two exposed loops can be used for the insertion of epitopes, namely the variable loop (VL) and the RGD loop (RGD-L). In order to get rid of the allelic restriction and to elicit a multi-specific anti-tumor response, the display of large antigens rather than small epitopes on the ADDomer surface would be desirable. At the Oxford University, Mark Howarth's group developed a system called SpyTag/SpyCatcher (ST /SC)²³¹. This system derived from the Cnab2 domain of the FbaB protein from the bacteria *Streptococcus pyogenes*, allows the formation of a covalent isopeptidic bond between the aspartate 117 of the SpyTag and the Lysine 31 of the SpyCatcher. This reaction involves a third amino-acid Glutamate 77 which catalyses the reaction (Figure 1A). Commonly the ST (13 amino-acids) is added on either the C or the N terminus of the protein to facilitate the interaction with the SC fused to the protein of interest. In the case of the ADDomer, both C and N termini are buried inside the ADDomer inner cavity and are therefore inaccessible for protein fusion. Therefore, we adapted this system to the ADDomer platform by genetic insertion of the ST inside the exposed variable loop. This ST is then displayed 60 times on the ADDomer's surface and is available for SC binding (Figure 1B).

Figure 1

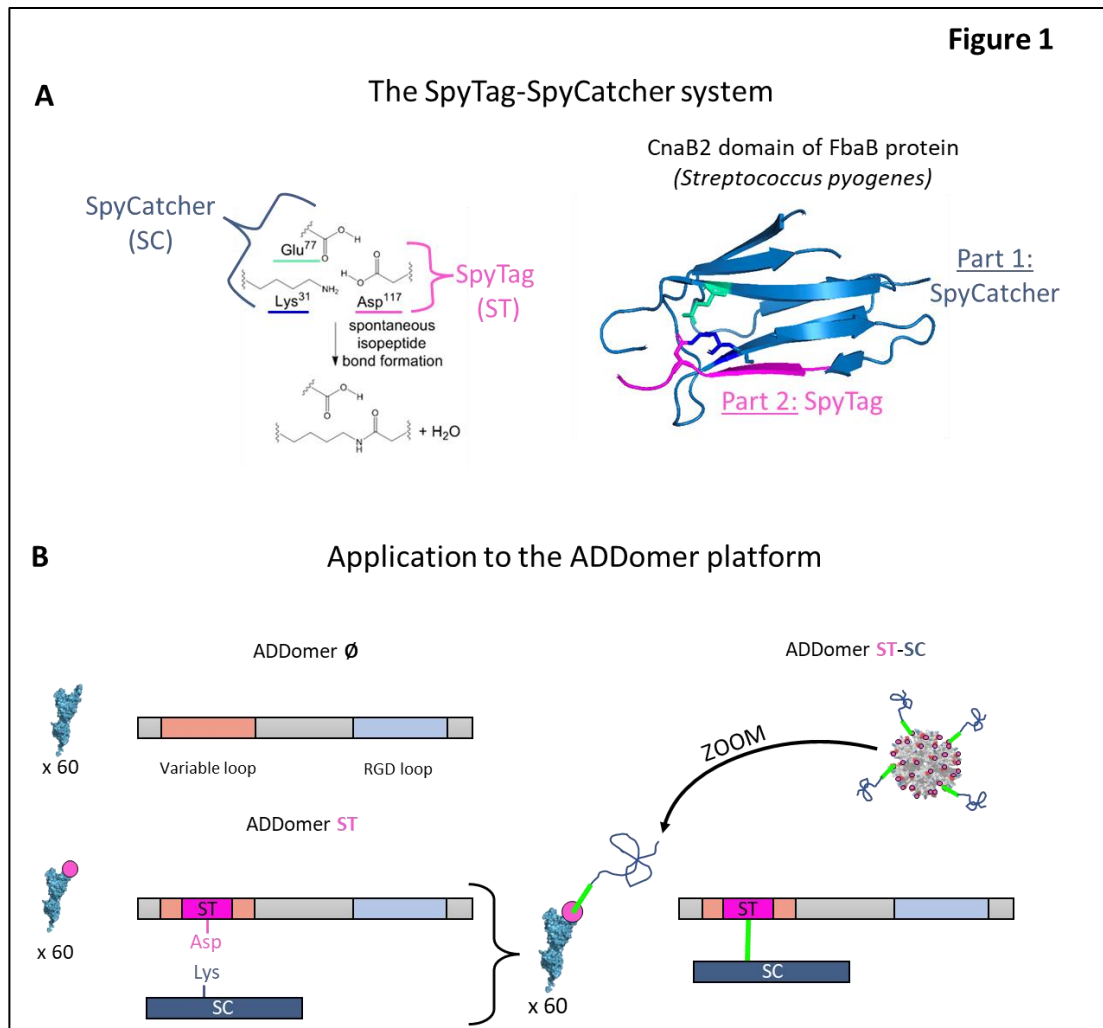


Figure 1: The SpyTag/SpyCatcher system and its application to the ADDomer

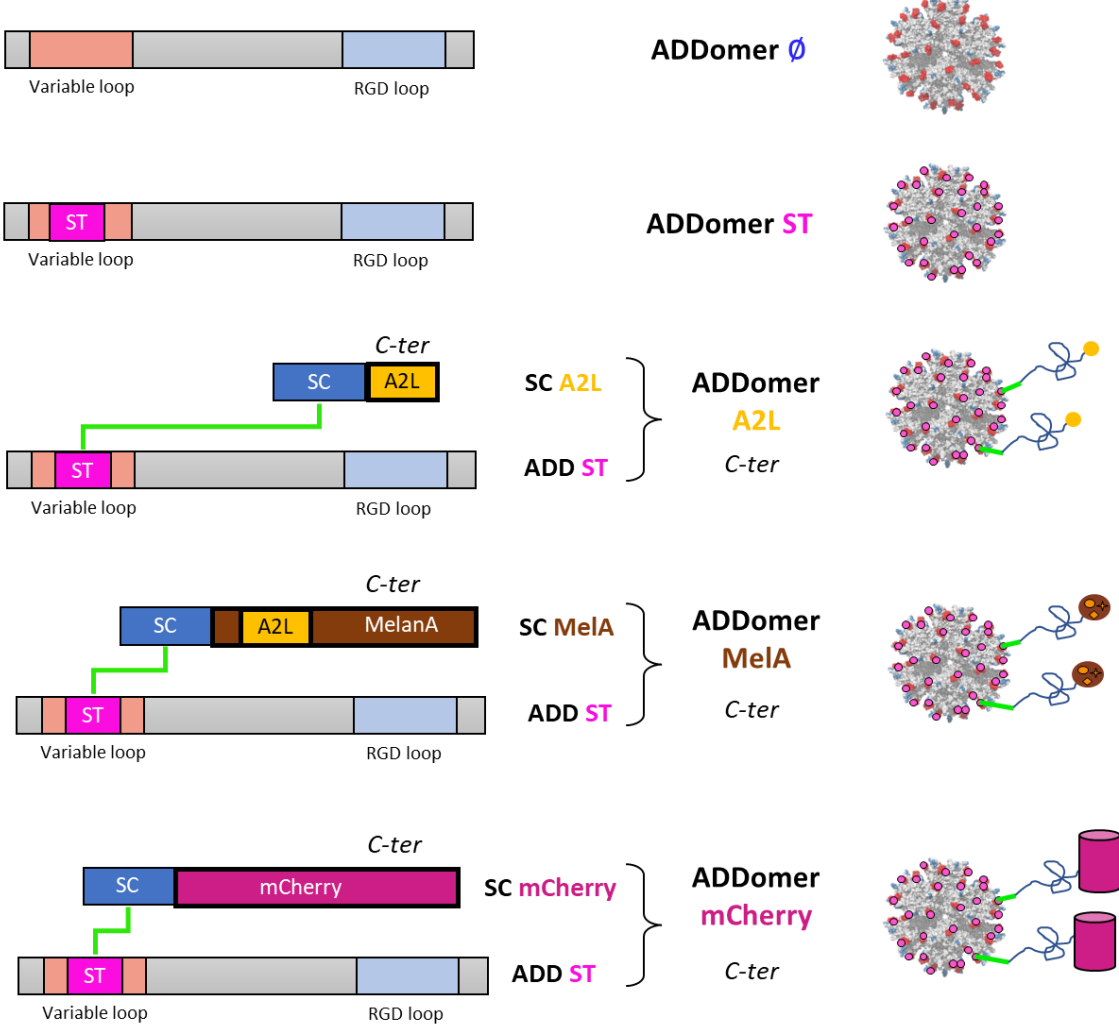
(A) Representation of the 3 residues involved in the interaction between the ST and the SC resulting in the formation of a spontaneous isopeptide bond. (B) Genetic insertion of the ST inside the ADDomer's variable loop allowing its decoration with the SC.

In order to display a human melanoma tumor antigen (MelanA), an ADDomer displaying the SpyTag peptide (ADD-ST) on its surface was used in order to spontaneously make an isopeptidic bond with a SpyCatcher fused to the MelanA protein containing the MelanA₂₆₋₃₅ ‘A2L’ epitope (Figure 2A, 2C). SpyCatcher fused to the A2L sequence epitope

(ELAGIGILTV) was also designed and attached on the ADD-ST. The A2L sequence would have been genetically inserted directly inside the variable loop, so, in this case, the system ST/SC would not have been needed to display this epitope. However, the choice has been made to investigate the SC liaison to the ADD-ST with SC displaying cargos of different sizes. Therefore, both MelanA (13 kDa) and A2L (1 kDa) sequences were genetically fused at the SpyCatcher's C-terminus which led to the following constructions SC-A2L and SC-MelA. The SpyCatcher (SC) was prolonged with a histidine tag on the N terminus (Figure 2C) and a 5 amino acid linker (ASGGT) was used to separate the MelanA and SpyCatcher sequences. SC-A2L and SC-MelA attached to the ADDomer are presented on the Figure 2A. In order to broaden our panel of various sized-proteins fused to the SC, large barrel-shaped protein mCherry was also attached to the SpyCatcher's C-terminus ends (SC-mCherry) (Figure 2A). ADD-ST, SC-A2L, SC-MelA and SC-mCherry were produced separately in insect cell using the baculovirus expression system. Negative stain electron microscopy showed that both non-decorated or particle decorated with the A2L epitope were well-folded (Figure 2B). Similar negative stain electron microscopy images were obtained for the ADDomers displaying the SC-MelA and SC-mCherry.

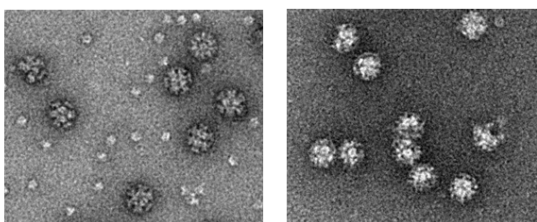
Figure 2

A



B

ADDomer ST ADDomer A2L



C

C-ter
SC MelA

VDTLSGLSSEQGQSGDMTIEEDSATHIKFSKRDEDGKEL
AGATMELRDSSGKTISTWISDGQVKDFLYPGKYTFVE
TAAPDGYEVATAITFTVNEQQQVTVNGKATKGDAHIAS
GGTPREDAHFIYGYPKKGHGHSYTAEELAGIGILT**ILG**
VLLLIGCWYCRRNGYRALMDKSLHVGTQCALRRCP
QEGFDHRDSKVSLQEKNCEPVPNAPPAYEKLSAEQSP
PPYSPGSGHHHHHH

Figure 2: Design and characterization of the different ADDomers (C-ter)

(A) Representation of the different ADDomers produced. Cargos were fused to the C terminus of the SpyCatcher. (B) Negative stain electron microscopy images of ADD ST and ADD A2L. (C) Sequence of SC-MelA (C-ter). The MelanA tumor antigen is coloured in brown (A2L epitope is highlighted in yellow), SpyCatcher is coloured in blue and additional linkers and histidine tag are coloured in black.

Controlled cleavage of Spytag displayed on ADDomer by TEV protease enhances binding of SC-cargos while keeping the overall architecture of the particle.

To produce functionalized ADDomers, SC-A2L and SC-MelA were incubated overnight at RT under agitation with the ADD ST. Binding to the ADD ST via the SpyTag/SpyCatcher system was achieved however the yield was very low. Indeed, the covalent binding of SC-A2L and SC-MelA to ADD-ST was assessed by SDS-PAGE (Figure 3B, lanes 3 and 4). SC-A2L and SC-MelA attachment to the ADD Ø was performed as a negative control (Figure 3B, lanes 1 and 2). As expected, an adduct of a higher molecular weight corresponding to the SC-A2L and SC-MelA bound to the ADD-ST monomer was seen but with low intensity demonstrating that the yield of assembly was very weak.

To overcome this issue, we hypothesized that the ST epitope in the ADDomer's variable loop was not accessible enough or too constricted inside the loop for a proper interaction with the SC-A2L and SC-MelA. Therefore, a new construct was designed (ADD TEV) which presented a tobacco etch virus protease (TEV) cleavage site upstream of the ST (Figure 3A). ADD TEV was then incubated 4h at RT under agitation with the TEV protease. TEV cleavage unconstrained ST, which would make it more relaxed and better accessible on the ADDomer's surface (Figure 3A). Obviously, this internal cleavage split the ADDomer monomer (65kDa) in two bands of about 50 and 15kDa upon denaturation on SDS-PAGE. The cleaved ADD TEV

was then incubated with the SC-A2L and SC-MeA and covalent binding was assessed by SDS-PAGE (Figure 3B, lanes 5 and 6). As expected, an adduct of a higher molecular weight corresponding to the SC-A2L and SC-MeA bound to the ADD-TEV ‘50kDa fragment’ was seen with a much higher intensity compared to the binding to the uncleaved ADD ST (Figure 3B, lanes 5 and 6 for ADD TEV versus lanes 3 and 4 for ADD ST). This result showed that releasing the ST with TEV protease had a beneficial impact on the binding efficiency of both SC-A2L and SC-MeA. Moreover, negative stain electron microscopy showed that ADD TEV displaying the SC-MeA on its surface were well-folded and that the structural integrity was intact despite the internal cleavage of the loop encompassing the ST. (Figure 3C).

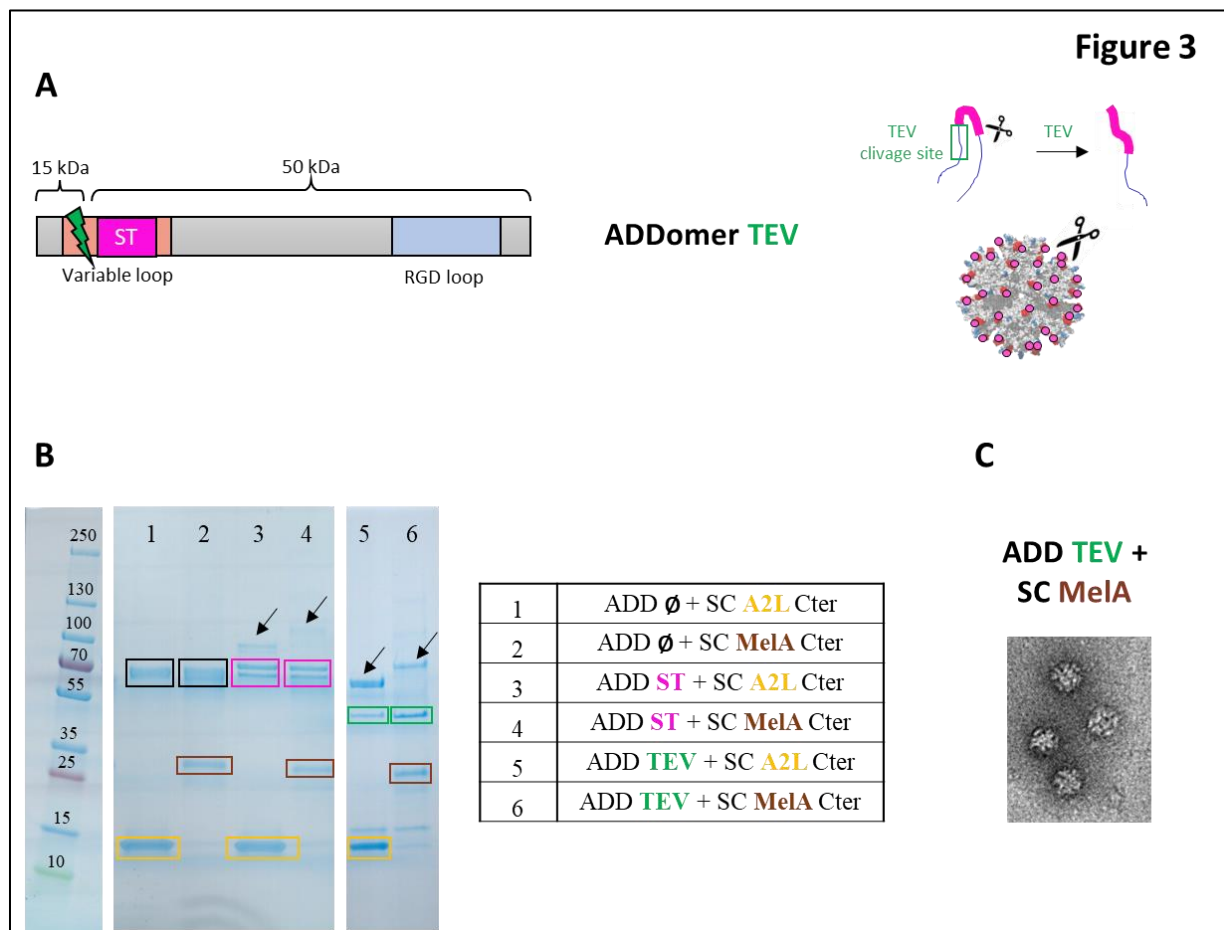


Figure 3: Controlled cleavage of SpyTag displayed on ADDomer by TEV protease

(A) Representation of the ADDomer TEV encompassing a tobacco etch virus protease (TEV) cleavage site upstream of the ST. Upon incubation with the TEV protease the ST is released

which makes it more accessible on the ADDomer's surface. (B) SDS PAGE profile of reduced and boiled samples showing the binding of SC-A2L and SC-MelA to ADD ST (low binding) as well as to ADD TEV (high binding). (C) Negative stain electron microscopy image of ADD TEV displaying the SC-MelA, showing no impact of the TEV protease on the ADDomer's folding and integrity.

Switching the cargo from the SpyCatcher's C-terminus to N-terminus resulted in more efficient binding to the ADD ST

We showed that the binding on epitope/antigen on the ADDomer could be optimized by adding a TEV splicing site upstream of the ST. However, this site makes the ADDomer less stable and more easily degraded, which is a major drawback for a vaccine platform. To overcome this issue and based on the structure of the interaction between SpyCatcher and SpyTag, we hypothesized that putting the epitope/antigen at the N-terminus end of the SpyCatcher rather than at the C-terminus would reduce steric hindrance and therefore facilitate binding without the need for a TEV slicing site (Figure 4A). The antigens MelanA and mCherry were then fused upstream of the SpyCatcher (N terminus) which led to the following constructions MelA-SC and mCherry-SC (Figure 4B). ADD ST was then incubated with the mCherry and MelA proteins fused to either the N or C terminus of the SpyCatcher and covalent binding was assessed by SDS-PAGE (Figure 4C). An adduct of a higher molecular weight corresponding to the mCherry-SC and MelA-SC bound to the ADD-ST monomer was clearly seen with a much higher intensity compared to the binding to SC-mCherry and SC-MelA (Figure 4C). This result showed that switching the antigen position from SpyCatcher's C-terminus to N-terminus leads to beneficial impact on the binding efficiency to ADD ST. Therefore, with cargos on the N-terminus of SC, the TEV cleavage of ADDomer is no longer required which facilitate the manufacturing process and usage of this versatile vector.

Figure 4

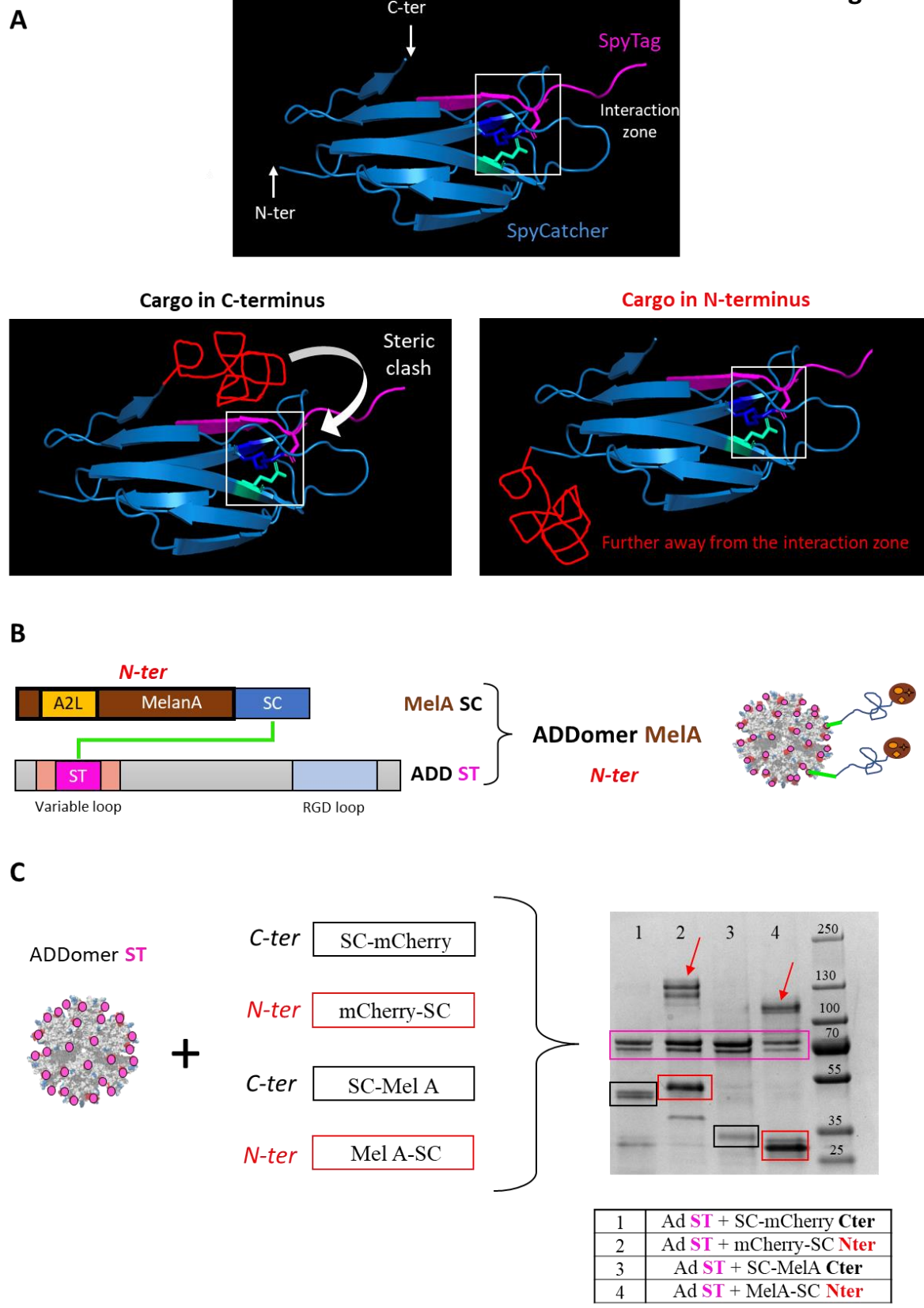


Figure 4: Switching the cargo from the SpyCatcher's C-terminus to N-terminus

(A) Structural images of SpyTag and SpyCatcher interacting together showing that switching the cargo from the C-terminus to the N-terminus of the SpyCatcher could reduce steric hindrance and therefore improve binding. (B) Representation of MelA-SC (N-ter). (C) SDS PAGE profile of reduced and boiled samples showing the binding to ADD ST is improved when the cargo is at the N-terminus end of the SpyCatcher.

Mosaic vectors harbouring cargos from different sizes, origins or structural complexities can be generated

Here, we investigated the capacity of the ADDomer platform to display different cargos simultaneously on its surface. MelA-SC, mCherry-SC and SC-A2L were incubated simultaneously with the ADD ST with a ratio of 1 monomer for 0,3 of each Cargo-SpyCatcher. The binding was assessed by SDS-PAGE (Figure 5). Three adducts of a higher molecular weight each of them corresponding to the mCherry-SC, MelA-SC and SC-A2L bound to the ADD-ST monomer were clearly seen (Figure 5). This result showed that the ADDomer can simultaneously display three different proteins with structural complexity going from a small 17 amino acid peptide to a large barrel-shaped 50kDa protein.

Figure 5

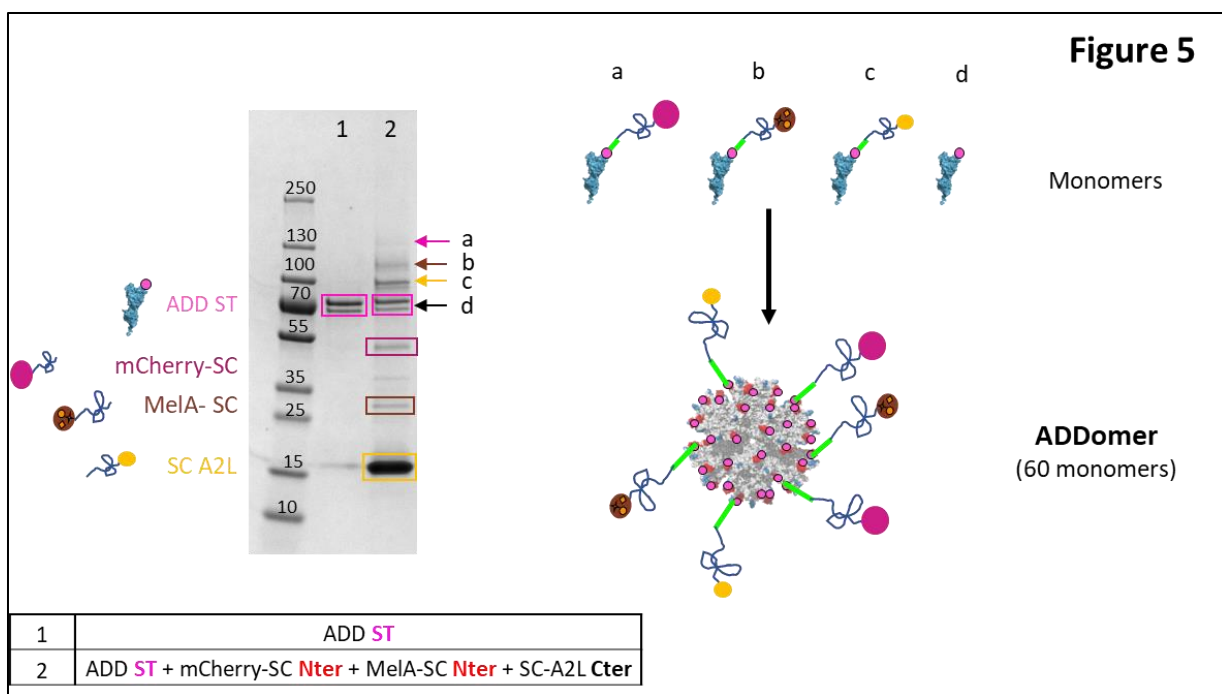


Figure 5: Mosaic vectors harbouring cargos from different sizes, origins or structural complexities

SDS PAGE profile of reduced and boiled samples showing the binding of different cargos (mCherry-SC, MelA-SC, SC-A2L) to the ADD ST.

Conclusion du chapitre :

Pour conclure, dans ce chapitre nous avons vu qu'en utilisant le système d'accroche SpyTag/SpyCatcher il était possible de fixer de manière covalente un ou plusieurs antigènes de taille et structure différentes sur l'ADDomer. La plateforme ADDomer exposant des épitopes par insertion génétique a ainsi été améliorée afin d'exposer également des antigènes entiers par le système SpyTag/SpyCatcher. Nous avons vu que ces antigènes devaient être placés en amont du SC afin de favoriser leur fixation à l'ADDomer. La capacité de ces ADDomers (présentant des épitopes/antigènes du mélanome) à induire une réponse immunitaire anti-tumorale peut ainsi être évaluée *in vitro*.

Chapitre V : Evaluation *in vitro* d'ADDomers présentant des épitopes et antigènes humains du mélanome

Introduction du chapitre :

Dans ce chapitre, nous présenterons les caractérisations *in vitro* qui ont été réalisées sur les ADDomers présentant des épitopes et antigènes du mélanome. Cette publication explore l'immunogénicité des ADDomers présentant un épitope (A2L) ou un antigène (MelanA) humains du mélanome sur des cellules dendritiques humaines issues de donneurs sains.

L'internalisation ainsi que le potentiel activateur des ADDomers a été évalué sur les différents sous-types de cellules dendritiques humaines (cDC2, cDC1, pDC). La capacité des ADDomers à induire une présentation croisée des antigènes/épitopes tumoraux (cross présentation) ainsi que l'activation de lymphocytes T CD8+ dirigés contre ces antigènes/épitopes (cross priming) a également été reportée. Dans une seconde partie, des modifications spécifiques permettant un meilleur adressage des DCs ont été réalisées et évaluées. Ces modifications visent à cibler spécifiquement les cellules dendritiques afin de favoriser l'internalisation des ADDomers dans celles-ci tout en diminuant l'internalisation dans d'autres cellules non ciblées comme les cellules épithéliales par exemple.

Article

Adenovirus-Inspired Virus-like-Particles Displaying Melanoma Tumor Antigen Specifically Target Human DC Subsets and Trigger Antigen-Specific Immune Responses

Solène Besson ¹, David Laurin ^{2,3}, Cyrielle Chauvière ^{2,3}, Michel Thépaut ¹, Jean-Philippe Kleman ¹, Mylène Pezet ², Olivier Manches ^{2,3}, Franck Fieschi ¹, Caroline Aspord ^{2,3,*} and Pascal Fender ^{1,*}

¹ Institut de Biologie Structurale, CEA, CNRS, University Grenoble Alpes, UMR5075, 38042 Grenoble, France

² Immunobiology and Immunotherapy in Chronic Diseases, Institute for Advanced Biosciences, Inserm U 1209, CNRS UMR 5309, University Grenoble Alpes, 38000 Grenoble, France

³ R&D Laboratory, Etablissement Français du Sang Auvergne-Rhône-Alpes, 38000 Grenoble, France

* Correspondence: caroline.aspord@efs.sante.fr (C.A.); pascal.fender@ibs.fr (P.F.)

† These authors contributed equally to this work.

Abstract: Virus-like particles constitute versatile vectors that can be used as vaccine platforms in many fields from infectiology and more recently to oncology. We previously designed non-infectious adenovirus-inspired 60-mer dodecahedric virus-like particles named ADDomers displaying on their surface either a short epitope or a large tumor/viral antigen. In this work, we explored for the first time the immunogenicity of ADDomers exhibiting melanoma-derived tumor antigen/epitope and their impact on the features of human dendritic cell (DC) subsets. We first demonstrated that ADDomers displaying tumor epitope/antigen elicit a strong immune-stimulating potential of human DC subsets (cDC2s, cDC1s, pDCs), which were able to internalize and cross-present tumor antigen, and subsequently cross-prime antigen-specific T-cell responses. To further limit off-target effects and enhance DC targeting, we engineered specific motifs to de-target epithelial cells and improve DCs' addressing. The improved engineered platform making it possible to display large antigen represents a tool to overcome the barrier of immune allele restriction, broadening the immune response, and paving the way to its potential utilization in humans as an off-the-shelf vaccine.

Keywords: adenovirus; vaccine platform; immunotherapy; melanoma; C-type lectin receptors



Citation: Besson, S.; Laurin, D.; Chauvière, C.; Thépaut, M.; Kleman, J.-P.; Pezet, M.; Manches, O.; Fieschi, F.; Aspord, C.; Fender, P. Adenovirus-Inspired Virus-like-Particles Displaying Melanoma Tumor Antigen Specifically Target Human DC Subsets and Trigger Antigen-Specific Immune Responses. *Biomedicines* **2022**, *10*, 2881. <https://doi.org/10.3390/biomedicines10112881>

Academic Editor: Juan Gambini

Received: 13 September 2022

Accepted: 2 November 2022

Published: 10 November 2022

Publisher's Note: MDPI stays neutral with regard to jurisdictional claims in published maps and institutional affiliations.



Copyright: © 2022 by the authors. Licensee MDPI, Basel, Switzerland. This article is an open access article distributed under the terms and conditions of the Creative Commons Attribution (CC BY) license (<https://creativecommons.org/licenses/by/4.0/>).

1. Introduction

Recent years have seen the development of a variety of immunotherapies in oncology with various success depending on the cancer type and state [1–3]. In 2013, Chen DS and Mellman I [4] presented a cancer-immunity cycle explaining the fundamental steps by which the immune system manages to kill cancer cells. This cycle highlights the fundamental role of dendritic cells in the triggering of the anti-tumoral immune response. The aim of any immunotherapies is to drive this cycle and increase one of those steps.

For instance, the blocking of the immune checkpoint PD-1 occurs at the last step of this cycle when cytotoxic T cells destroy cancer cells. On the other hand, cancer vaccines can have an action at the very beginning of this cycle by activating the DCs, leading to the differentiation of T cells into tumor-specific cytotoxic T lymphocytes (CTL), triggering the death of cancerous cells [5]. Indeed, a cancer vaccine's goal is to stimulate the patient's immune system against the vaccine's carried epitopes or antigens. Vaccines are captured by DCs and epitopes/antigens are internalized and presented (cross-presentation) through peptide/HLA complexes to naive T cells triggering their activation and differentiation into antigen-specific CD4+ or CD8+ T cells in lymph nodes (cross priming). Both subsets have different roles: CD4+ T cells are required for CD8+ T cells activation, which will then exhibit their cytotoxic activity. Once activated, CD8+ T cells will travel from the lymph

node to the tumor site through the blood circulation. At the tumor site, activated CD8+ T infiltrate the tumor and recognize the cancer cells thanks to the antigens expressed at their surface through peptide/HLA complexes. Then, they can kill the cancer cells thanks to their cytotoxic activity [4]. Many cancer vaccines are currently under evaluation at preclinical or clinical stages using different strategies, from tumor cell vaccines to genetic vaccines [6,7]. Among genetic vaccines there are viral vectors, such as adenovirus. They can be used in two different manners: either as oncolytic viruses, meaning that they would replicate only inside tumor cells, triggering their death, or as a component of a vaccine to stimulate both innate and adaptive immunity, thus triggering an anti-tumoral response [8]. Adenoviruses are widely used in the clinic; more than 100 clinical trials in Europe and almost 300 in the USA are ongoing. Most of them use the full adenovirus as the vector either encoding a tumor antigen, a cytokine or just engineered as oncolytic viruses [9–11]. We have previously reported that a non-infectious virus-like particle (VLP) derived from the human Adenovirus of type 3 and consisting of 60 identical penton base monomers could be exploited to display epitopes of interest on its surface [12–14]. In this vaccine platform named ADDomer, exposed loops of the penton base protein were engineered to allow insertion of small peptides such as a linear neutralizing epitope from Chikungunya virus [12]. However, this design did not permit the insertion of structurally complex antigens. To overcome this limitation while keeping the immunogenic advantage of ADDomer, we redesigned this platform by genetically inserting a SpyTag. Thanks to that, spontaneous display of large and structurally complex antigens with potential post-translational modifications such as the SARS-CoV-2 Receptor Binding Domain (RBD) or a model antigen ovalbumin fused to the SpyCatcher was achieved. In infectiology, this system displaying the RBD has proven to be highly effective to elicit potent neutralizing antibodies against SARS-CoV-2 in mice [15]. In oncology, ADDomers exhibiting the ovalbumin antigen have also proven to be of great efficiency in controlling melanoma B16-OVA in mice [16].

In this study, we explored *in vitro* the interactions of a cancer vaccine platform ADDomer displaying human melanoma tumor antigen (MelanA) and epitope (A2L) with human DC subsets (cDC2s, cDC1s, pDCs). We deciphered the ability of DCs to internalize such ADDomers, to cross-present associated epitopes/antigens, and to subsequently trigger antigen-specific T-cell responses. To further limit off-target effects and enhance DC targeting, we engineered specific motifs to de-target un-targeted cells (epithelial cells) and improve DCs' addressing.

2. Materials and Methods

2.1. Baculovirus Production

The baculovirus expression system was used for the production of different ADDomers (ADD A2L, ADD ST, ADD KGE, and ADD RGD), as well as for the Spike Receptor Binding Domain of SARS-CoV-2 fused to the SpyCatcher (RBD-SC) and the MelanA tumor antigen fused to the SpyCatcher (MeLA-SC). Synthetic DNA (Genscript, Rijswijk, The Netherlands) was cloned in the pACEBac1 using the restriction sites BamH I and Hind III. For RBD-SC, the RBD sequence (320–554) was cloned upstream of the SC, and a 6His-Tag was added in the C-terminus of SC. The same was performed for the MeLA-SC. The RBD-SC was secreted using the melittin signal peptide present in the vector. Recombinant baculoviruses were made by transposition with an in-house bacmid expressing yellow fluorescent protein, as previously described [12]. Baculoviruses were amplified on Sf21 cells at low multiplicity of infection (MOI) and after two amplification cycles were used to infect insect cells for 64 to 72 h at high MOI. For all proteins except for RBD-SC, the infected cells were pelleted and recovered. For RBD-SC, cells were discarded, and the supernatant was saved.

2.2. Protein Purification

2.2.1. ADDomers' Purification

The ADDomers were purified according to classical protocol [15]. Briefly, after lysis of the insect cell pellet by three cycles of freeze-thaw in the presence of complete protease

inhibitor cocktail (Roche, Paris, France) and removal of debris, the lysate was loaded onto a 20% to 40% sucrose density gradient. The gradient was centrifuged for 18 h at 4 °C on an SW 41 Ti rotor in a Beckman XPN-80 ultracentrifuge. The dense collected fractions at the bottom of the tubes were dialyzed against HEPES 10 mM pH 7.4, NaCl 150 mM, and then loaded onto a Macroprep Q cartridge (Bio-Rad, Paris, France). After elution by a 150 to 600 mM linear NaCl gradient in HEPES 10 mM pH 7.4, ADDomer-containing fractions were checked by SDS-PAGE and concentrated on Amicon (MWCO: 100 kDa) with buffer exchange to HEPES 10 mM pH 7.4, NaCl 150 mM.

2.2.2. RBD-SC Purification

The insect cell supernatant was centrifuged after thawing for 15 min at 7500×*g* and loaded onto a HEPES 10 mM pH 7.4 preequilibrated Heparin column (Cytiva, Paris, France) of 5 mL for 500 mL of supernatant. The column was washed with HEPES 10 mM pH 7.4 for 25 mL then eluted for 10 mL with 0 to 500 mM linear NaCl gradient in HEPES 10 mM pH 7.4. The eluate was supplemented with 30 mM imidazole-HCl (pH 7.4) and incubated with Ni-NTA beads (Qiagen, Paris, France), 2 mL of beads for 500 mL culture, for at least 1 h at 4 °C under gentle agitation. The beads were then poured into an empty column and the protein was eluted by two column volumes (CV) of 250 mM imidazole in HEPES 10 mM pH 7.4, NaCl 150 mM. It was then submitted to buffer exchange using an Amicon device (MWCO 30 kDa).

2.2.3. MelA-SC Purification

Insect cell pellet was lysed by three cycles of freeze-thaw in the presence of a complete protease inhibitor cocktail (Roche, Paris, France), and the lysate containing the His-tagged MelA-SC was loaded to a 1 mL His GraviTrap prepak column (GE Healthcare, Paris, France), pre-equilibrated with 20 CV of 150 mM NaCl, 10 mM HEPES pH 7.4 and 10 mM imidazole. Columns were then washed with 20 CV of the same buffer to remove non-specifically bound material. Proteins were eluted with 10 CV of buffer containing 200 mM imidazole. MelA-SC containing fractions were checked by SDS-PAGE and concentrated on Amicon (MWCO: 30 kDa) with buffer exchange to HEPES 10 mM pH 7.4, NaCl 150 mM.

2.3. Complex Formation and Labelling

2.3.1. ADD-ST + MelA/RBD-SC (ADD-MelA, ADD KGE RBD and ADD RGD RBD) Complex Formation for Cross Priming and Cross Presentation Experiments

Covalent complex formation was obtained by incubation of purified ADD-ST with purified MelA/RBD protein fused to SC (i.e. MelA/RBD-SC). Incubation was performed at 25 °C under agitation on a ThermoMixer (Eppendorf, Paris, France) at 300 rpm. RBD-SC ratio and MelA-SC per ADD-ST was fixed to 1:1 (1 MelA/RBD-SC for 1 monomer) in order to avoid steric hindrance between the MelA/RBD-SC proteins on the ADDomer surface.

Left over RBD-SC/MelA-SC which did not bind to the ADDomers were removed thanks to a 20% to 40% sucrose density gradient. The gradient was centrifuged for 6 h at 60,000 rpm, 4 °C on an SW 60 Ti rotor in a Beckman XPN-80 ultracentrifuge. The dense collected fractions at the bottom of the tubes (complex containing fractions i.e., ADD-MelA/ADD KGE RBD/ADD RGD RBD) were checked by SDS-PAGE and concentrated on Amicon (MWCO: 100 kDa) with buffer exchange to HEPES 10 mM pH 7.4, NaCl 150 mM for sucrose removal. (Supplementary Figure S1).

2.3.2. ADD-ST AF647 + MelA/RBD-SC (ADD-Mela AF647, ADD KGE/RGD +/- RBD AF647) Complex Formation for Internalization Experiments

Covalent complex formation was obtained by incubation of purified ADD-ST with purified MelA/RBD protein fused to SC (MelA/RBD-SC). ADD ST, ADD KGE and ADD RGD were first incubated with the fluorochrome NHS-Alexa Fluor 647 (ThermoFisher, Paris, France) overnight at 25 °C under agitation on a Thermomixer at 300 rpm. The NHS moiety forms a covalent bond with the ADDomers' lysins terminal NH₂ moiety. ADDomers AF647 were then incubated with ethanolamine (1 mM final concentration) for 4 h at 25 °C

under agitation on a Thermomixer at 300 rpm. Finally, incubation with the MelA/RBD-SC was performed overnight at 25 °C under agitation on a Thermomixer at 300 rpm. RBD-SC ratio and MelA-SC per ADD-ST was fixed to 1:1 (1 MelA/RBD-SC for 1 monomer) in order to avoid steric hindrance between the MelA/RBD-SC proteins on the ADDomer surface. Ethanolamine allows the blockage of left-over NHS-AF647 in order to prevent its fixation to RBD-SC/MelA-SC (Supplementary Figure S2). Left-over RBD-SC/MelA-SC were removed as described above.

2.4. Cell Preparation and Culture

2.4.1. Transformed Cell Lines

All experiments were performed in complete RPMI medium (RPMI-1640 Glutamax (Gibco®, Paris, France) enriched with 20 µg/mL Gentamicin, 1% non-essential amino-acids both from (Invitrogen™, France) and 1 mM sodium pyruvate (Sigma, Paris, France)) supplemented with 10% decomplemented fetal calf serum (FCS) (Invitrogen™).

2.4.2. Peripheral Blood Mononuclear Cells (PBMCs) Isolation

Peripheral Blood Mononuclear Cells (PBMCs) were isolated from healthy donor blood and purified by the Ficoll-Hypaque density gradient centrifugation ($800 \times g$, 20 min) technique (Eurobio, Paris, France). The ring of PBMCs formed at the interface between the plasma and the Ficoll is washed in phosphate buffer saline (PBS), centrifuged at $400 \times g$ for 8 min before de-plaquettement at $200 \times g$ for 10 min at 4 °C. PBMC were then numerated and stored frozen at –196 °C in liquid nitrogen until use.

2.5. Fixation, Internalization of ADDomer

2.5.1. Evaluation of the Fixation of ADDomers AF647 on DC Subsets by Flow Cytometry

PBMC (2.10^6 in 250 µL) were incubated with 0.15 µM (1×), 0.5 µM (3×) or 1.5 µM (10×) of each ADDomer AF647 in FACS tubes for 1 h at 37 °C, 5% CO₂ in RPMI supplemented with 10% FCS or in PBS 1× for tubes treated with EDTA (ADD KGE RBD + EDTA and ADD RGD RBD + EDTA). For tubes treated with EDTA, PBMC (2.10^6 in 250 µL) were first incubated with EDTA in PBS 1× (20 mM final concentration) for 30 min at RT. Cells were then washed, incubated with the ADDomers AF647 in PBS 1×, and washed with PBS 1× supplemented with 2% FCS. Next, cells were resuspended in 100 µL PBS 2% FCS and incubated for 20 min in the dark with a mixture of Abs conjugated to fluorochromes (anti-human CD45, Lin, HLA-DR, CD11c, BDCA1, BDCA2, Clec9a antibodies) and live&dead staining, allowing us to detect the ADDomers AF647 fixed or internalized by the three alive DCs subsets. Then, cells were washed in 2 mL PBS 2% FCS before being fixed in 300 µL FACS lysing solution 1×. Analyses were performed using LSR II and analyzed with DIVA 8.3 software from BD.

2.5.2. Determination of the Internalization of ADDomers AF647 by DC Subsets by Confocal Microscopy

To determine whether the ADDomers are internalized or just fixed through surface adhesion by the DC subsets, confocal microscopy was performed on panDCs pre-incubated with ADDomers AF647. PanDCs were purified from PBMC using the kit PanDC pre-enrichment kit (StemCell, Paris, France). PanDCs ($1.2.10^6$ in 600 µL) were incubated with 0.15 µM of each ADDomer-AF647 in FACS tubes for 1 h 30 at 37 °C, 5% CO₂ in RPMI supplemented with 10% FCS. Next, cells were washed in PBS 1× and deposited on 3 poly-lysin coated slides (400,000 cells in 200 µL per slide, 1 slide for each three DC subset). Slides were then placed 20 min at 37 °C in the dark for panDC adhesion. Upon removing the medium, slides were incubated with 100 µL of an antibody mix for 10 min at 37 °C in the dark, comprising CD11c, HLA-DR, and either BDCA1, BDCA2 or BDCA3 antibodies. Slides were then washed with 200 µL of PBS 1×, then cells were fixed with 200 µL of PFA 4% for 10 min at 37 °C in the dark. Slides were then washed twice with 200 µL of PBS 1× before being mounted with 10 µL anti-fade mounting medium

(Invitrogen). The localization of ADDomers was assessed with a laser spinning disk Andromeda-IMIC inverted microscope (Till-Photonics FEI, Paris, France) equipped with an alpha-Plan-Apochromat 63x/1.46 objective (Zeiss, Paris, France). Images were acquired with an iXon U897 EMCCD camera (Andor, Paris, France) controlled with Live Acquisition Software (FEI). Z series optical sections were collected with a step size of 300 nm over 10 microns. Equatorial section was used to represent internalization. Images were denoised with denoise.ai NIS-Element (Nikon, Paris, France) software and then analyzed with FIJI. Intensities of CD11c (Brilliant Violet 421) and HLA-DR (Brilliant Violet 510) markers as well as the subset marker stained with FITC (BDCA 1, 2 or 3) on the cell surface were used to discriminate between the three subsets.

2.6. DC Subsets' Activation and Cytokine Production upon Incubation with ADDomers

2.6.1. PBMCs Preparation/Cell Culture Conditions

PBMCs from two healthy donors were thawed in medium RPMI 20% FCS, centrifuged at $400 \times g$ for 8 min, then resuspended in medium RPMI 10% FCS and plated (2.10^6 cells in 1 mL). PBMCs were incubated either in control conditions, with TLR-ligand (TLR-L) mix (Poly IC 30 $\mu\text{g}/\text{mL}$, R848 1 $\mu\text{g}/\text{mL}$ and CpGA 1 μM), with peptide MelA_{26–35} (10 μM), ADD Ø or ADDomer A2L (1 μM) for 24 h.

2.6.2. Cell Viability and Costimulatory Molecules Expression Analysis by Flow Cytometry

Supernatants (SN) of each condition were taken and stored at -20°C for further cytokine production analysis by Luminex. Cells were harvested and wells washed twice with 1 mL RPMI 10% FCS, then centrifuged at $400 \times g$ for 8 min and resuspended in 100 μL PBS 2% FCS. Cells were then incubated for 20 min in the dark with a mixture of Abs conjugated to fluorochromes allowing us to detect costimulatory molecules (CD40, CD80, CD86), as well as the cell viability (Live & dead marker) on DCs subsets depicted by using anti-human CD45, HLA-DR, Lin, CD11c, BDCA1, 2 and 3 antibodies. Cells were then fixed in 300 μL FACS lysing solution 1×, washed in 2 mL PBS 2% FCS and centrifuged at $600 \times g$ for 5 min. Cells were next resuspended in 300 μL PBS 2% FCS and stored at 4°C until acquisition. Analyses were performed using LSR II and analyzed with DIVA 8.3 software from BD-Biosciences.

2.6.3. Cytokine Secretion Analysis by Luminex

IL12p70, IFN α , IFN β , IFN $\lambda 1$ /IL29 and IFN $\lambda 2$ /IL28 cytokine secretions were measured in culture supernatants by LUMINEX technology using MAGPIX®200 Instrument with xPONENT® software (Bio-Rad).

2.7. Analysis of DCs' Ability to Perform the Cross-Presentation of ADDomers-Associated Epitopes/Antigens

2.7.1. PanDC Incubation with ADDomers

PanDCs (mixture of cDC2s, cDC1s and pDCs) were purified from PBMC from two HLA-A0201+ donors using the kit PanDC pre-enrichment kit (StemCell.) PanDCs (20,000 cells in 100 μL) were incubated with 1 μM of each ADDomer (empty, A2L, MelA, KGE, KGE RBD, RGD, RGD RBD) or the restricted peptide MelA_{26–35} at 1 μM overnight at 37°C , 5% CO₂ in RPMI supplemented with 10% FCS in a 96 well plate.

2.7.2. Conditions of Cross-Presentation

In order to explore if the ADDomers were processed by DCs, a cross presentation assay was performed. Pre-amplified anti-MelA_{26–35} T cells were co-cultured with panDCs pre-incubated with ADDomers in a ratio 5:1 (100,000 pre-amplified anti-MelA_{26–35} T cells for 20,000 panDCs) in 96 wells plate for 20 h in incubator at 37°C , and 5% CO₂. Controls were carried out by incubating the anti-MelA_{26–35} T cells with either RPMI 10% FCS or activation cocktail (PMA/iono). SNs were collected and analyzed by Cytometric Bead Array (CBA provided by BD) to measure the concentration of IFN γ .

2.7.3. Measurement of Cytokines Production by CBA

To determine the amount of IFN γ produced by cells which reflect their ability to recognize the complex HLA/peptide on the antigen presenting cells such as dendritic cells, SNs of the cross-presentation assay were analyzed by CBA. Standard range was prepared from 2500 pg/mL to 0 pg/mL of recombinant IFN γ by cascade dilution 2 by 2. Fluorescent beads (labeled with AlloPhycoCyanin fluorophores APC or APC-Cy7) covered with anti IFN γ Ab were incubated with SN or standard (0.5 μ L of bead with 50 μ L of capture diluent per tube) for 1 h at room temperature (RT) in the dark. Then, an anti IFN γ Abs coupled to PE (0.5 μ L of Abs with 50 μ L of PE detection per tube) was added for 2 h at RT in the dark. Then, tubes were washed with 1 mL of wash buffer and centrifuged at 600 \times g for 5 min. After discarding SN, the acquisition was carried out on Canto II (at least 500 events/cytokine) and analysis using FCAP Array software. The use of standard allowed determining the relationship between the PE intensity and the concentration of cytokines, allowing us then to calculate the concentration of IFN γ in the SN.

2.8. Cross-Priming of Antigen (A2L) Specific CD8 T Cells Using ADDomers

2.8.1. Conditions of Cross-Priming

HLA-A2+ PBMCs were thawed in complete medium RPMI 20% FCS, centrifuged at 400 \times g for 8 min, then resuspended in complete medium RPMI 10% FCS. Cells were plated at 1.10⁶ cells/mL in a 24 well plate and cultured for 7 days at 37 °C 5% CO₂ in different conditions: control, or immunodominant HLA-A2 restricted peptide MelA_{26–35} at 10 μ M, or ADD Ø (without peptide)/ADDomer A2L (containing MelA_{26–35} peptide) at 0.15 μ M. All these conditions were performed with or without a mixture of TLR-L (mix Poly IC (TLR3L) 30 μ g/ mL, R848 (TLR7/8L) 1 μ g/mL and CpGA (TLR9L) 1 μ M). At day 7, cells were harvested, washed, numerated and resuspended at 1.10⁶ cells/mL. Then, 200,000 cells were taken from each condition for dextramer staining (to evaluate the proportion of anti-MelA_{26–35} CD8+ T cells); the remaining cells were restimulated in the same conditions as at day 0. At day 13, the same protocol was performed. At day 20, all cells were collected for dextramer staining and analyzed by flow cytometry using a Canto II.

2.8.2. Determination of Anti-MelA_{26–35} CD8+ T Cells by Dextramer Staining

Dextramer staining was performed at day 0 on 2.10⁶ cells, and at day 7, 13 and 20 on 200,000 cells harvested from the cultures. Cells were washed with 2 mL PBS 2% FCS, resuspended in 100 μ L PBS 2% FCS, and stained for 20 min at RT with 5 μ L of MHC dextramer MelA_{26–35} A*0201/ ELAGIGILTV (PE) from Immudex® according to the manufacturer's instructions. Cells were then stained with 5 μ L of anti-human CD3 (labeled with the fluorophore PC7) and 5 μ L of anti-human CD8 (labeled with the fluorophore APC) both from Beckman Coulter® for 15 min according to the manufacturer's instructions. Cells were washed with 2 mL PBS 2% FCS, resuspended in 300 μ L of FACS lysing solution 1× and stored at 4 °C until acquisition. The proportion of dextramer+ CD8+ T cells together with the intensity of the dextramer labeling were analyzed using a Canto II and DIVA 6.0 software from BD.

2.8.3. Amplification of Antigen Specific CD8+ T Cells

Calculation of absolute numbers of CD8+ T cells was carried out based on the percentage of CD8. Cells number in wells and the percentage of dextramer+ within CD8+ T cells allowed us then to calculate the absolute number of dextramer+ CD8+ T cells. The amplification of antigen specific CD8+ T cells was calculated based on the ratio of absolute numbers of dextramer+ CD8+ T cells at day X/day 0.

2.8.4. Determination of the Affinity of Antigen Specific CD8+ T Cells

The affinity of the amplified dextramer+ CD8+ T cells was measured thanks to the Mean Fluorescence Intensity (MFI) of the dextramer labelling.

2.9. Detargeting Retargeting Experiments

2.9.1. Evaluation of the Interactions between the ADDomers and CLR by Surface Plasmon Resonance

DC-SIGN Biot-ECD and MGL Biot-ECD, used in these SPR measurements, were overexpressed and purified according to previously published protocol [17,18]. A surface plasmon resonance experiment was performed on a T200 instrument. Streptavidin (Ref.: S4762; SIGMA-ALDRICH) diluted at 100 µg/mL in 10 mM NaOAc pH 4 was immobilized on sensor chips sensor chip S Serie CM3 (Cytiva, France). Biotinylated version of DC-SIGN ECD and MGL ECD (called, respectively, DC-SIGN Biot-ECD and MGL Biot-ECD) were used for their capture onto the streptavidin functionalized surfaces. These Biot-ECD version of both CLRs results from a site directed N-terminal biotinylation that allow a uniform orientation of the CLRs ECD on the surface mimicking the natural presentation at the cell surface. This site specific biotinylation on the N-termini are performed in house thanks to a sortagging procedure previously described in Achilli et al. [19]. DC-SIGN Biot-ECD and MGL Biot-ECD were diluted, respectively, at 0.5 µg/mL and 1 µg/mL in HBS P+ (Cytiva), injected at 5 µL/min until a capture level around 1250 RU (1264.4 RU for DC-SIGN Biot-ECD and 1254.0 RU for MGL Biot-ECD) was achieved. For interaction measurements, ADD KGE and ADD KGE RBD were prepared in HEPES 10 mM pH 7.4, NaCl 150 mM, CaCl₂ 4 mM, 0.05% P20. They were injected at concentrations ranging from 0.3 nM to 136.5 nM over DC-SIGN Biot-ECD or a MGL Biot-ECD oriented surface using HBS P+ buffer supplemented with 4 mM CaCl₂ as running buffer at 100 µL/min. RBD-SC was in HEPES 10 mM pH 7.4, NaCl 150 mM, CaCl₂ 4 mM, 0.05% P20) and was injected over a DC-SIGN Biot-ECD or MGL Biot-ECD oriented surface at a concentration ranging from 56 nM to 28.75 µM using HBS P+ buffer supplemented with 4 mM CaCl₂ at 100 µL/min. Streptavidin flow cell surface was used as reference for correction of the binding response. Regeneration of the surfaces was achieved by 50 mM EDTA, pH 8. Binding curves were analyzed using Biacore T200 Evaluation Software 3.2.1 (GE Healthcare) and data were fit using Steady State Affinity model. For ADD KGE RBD, only sensorgram comprised between 8.5 nM down to 0.2 nM were considered for determining the K_{Dapp} for DC-SIGN. In this range of concentrations, a nice saturation curve could be observed in steady state analysis. The higher concentration tested from 8.5 nM up to 136 nM still contributes to higher binding to the surface but in a non-specific mode (linear increase) and thus were not considered in the analysis.

2.9.2. De-Targeting Evaluation Using ADD KGE versus ADD RGD on A549 Cell Line

A549 cells were grown as monolayers in RPMI-1640 Glutamax (Gibco®, France) containing 10% fetal bovine serum (Gibco®), 5,000 U/100 mL of penicillin-streptomycin (Gibco®, France) at 37 °C in 5% CO₂ using T75 flasks, or culture dishes as specified.

2.9.3. ADD KGE and RGD Labeling with AF 488

ADD KGE and ADD RGD were first incubated with the fluorochrome NHS-Alexa 488 (ThermoFisher, France) overnight at 25 °C under agitation on a ThermoMixer (Eppendorf, France) at 300 rpm. The NHS moiety forms a covalent bond with the ADDomers' lysine terminal NH₂ residues.

2.9.4. ADD KGE and ADD RGD Internalization by A549 Evaluated by Flow Cytometry

A549 cells were seeded at 5.10⁴ cells per cm² in a nunclon delta surface 4 wells of 1.9 cm² multidish (ThermoFisher Scientific, France) and incubated overnight at 37 °C, 5% CO₂. The next day medium was replaced with 300 µL of fresh culture medium containing 1 µg of each ADDomer (ADD KGE AF488 or ADD RGD AF488) and cells were further incubated for 1 h at 37 °C, 5% CO₂. Cells were then washed in PBS 1× and were detached by the addition of 100 µL of trypsin in each well for 5 min at 37 °C. This step aims at removing the ADDomers fixed on the cells' surfaces while not affecting the ADDomers internalized by the cells. 900 µL of fresh medium were added and the suspension transferred into

1.5 mL tubes. Cells were pelleted by centrifugation, washed in 500 μ L of PBS 1 \times , then resuspended in 1 mL of PBS, 1% PFA for cell fixation. Analysis was performed directly after fixation by flow cytometry (M4D platform, VYB, Miltenyi biotech, Paris, France). The time between ADDomer's removal and the analysis was estimated to be 20 min.

2.9.5. ADD KGE and ADD RGD Internalization by A549 Evaluated by Time-Lapse Confocal Microscopy

A549 cells were seeded at 5.10^4 cells per cm 2 in a coverglass bottom 4 compartments 35 mm dish (Cellview™ Greiner, Paris, France) and incubated overnight at 37 °C, 5% CO $_2$. The next day, medium was replaced with 300 μ L of fresh culture medium containing 10 μ g of each ADDomer (ADD KGE AF488 or ADD RGD AF488) and cells were further incubated for 1 h at 37 °C, 5% CO $_2$. The dish was then immediately imaged using a spinning disk confocal microscope with a 100 \times 1.49NA apochromatic oil immersion objective. Imaging was performed using an iXon Ultra EMCCD (16bits per pixel, IQ bioimaging software, Andor) for 1 h, acquired every 15 s for AF488 fluorescence, and every 150 s for transmission using differential interference contrast (M4D platform, IX83 Olympus; CSU-XI Yokogawa; Okolab incubation chamber kept at 28 °C, 5% CO $_2$). Both conditions were imaged in parallel. Analysis was generated using Imaris (Bitplane, Paris, France) and Fiji open-source software [20]. The time between ADDomer's removal and the analysis was estimated to be 1 or 2 min.

3. Results

3.1. Human Melanoma Epitope A2L Can Be Displayed on the ADDomer Surface by Genetic Insertion

The ADDomer is a non-infectious nanoparticle formed of 12 bricks of the homo-pentameric penton base from the human adenovirus type 3. Two exposed loops can be used for the insertion of epitopes, namely the variable loop (VL) and the RGD loop (RGD-L) (Figure 1A). A sequence containing the A2L epitope from the tumor associated antigen MelanA (MelanA_{26–35}) was genetically inserted into the VL. This epitope has been chosen to initiate a CD8 + T lymphocyte immune response via the epitope A2L presented to the CD8 by DCs. Due to the spontaneous homo-oligomerization of the 12-pentameric penton bases, 60 copies of each epitope are exposed on the surface of the ADDomer particle named ADDomer-A2L (ADD-A2L) (Figure 1A). The ADD-A2L was successfully produced in a baculovirus expression system and purified in two steps (Figure 1B, upper panel).

3.2. The Large Human Tumor Associated Antigen MelanA Can Be Displayed on the ADDomer's Surface Using the SpyTag/SpyCatcher System

In order to get rid of the allelic restriction and to elicit a multi-specific anti-tumor response, the display of large antigens rather than small epitopes on the ADDomer surface is desirable. To do this, an ADDomer displaying the SpyTag peptide (ADD-ST) on its surface (Figure 1A,C) was used to spontaneously establish an isopeptidic bond with a SpyCatcher (SC) fused to the MelanA protein containing the A2L epitope. The MelanA protein was genetically fused at the SpyCatcher N-terminus (MelanA-SC) and a 5 amino acid linker was used to separate the MelanA and SpyCatcher sequences. The SpyCatcher was extended with a histidine tag on the C-terminus (Figure 1C). ADD-ST and MelanA-SC were produced separately in insect cells using the baculovirus expression system.

The covalent binding of MelanA-SC to ADD-ST was assessed by SDS-PAGE. As expected, a higher molecular weight corresponding to an adduct of the MelanA-SC bound to the ADD-ST monomer was clearly seen (Figure 1B, lower panel). This ADDomer displaying the MelanA antigen was named ADD MelA.

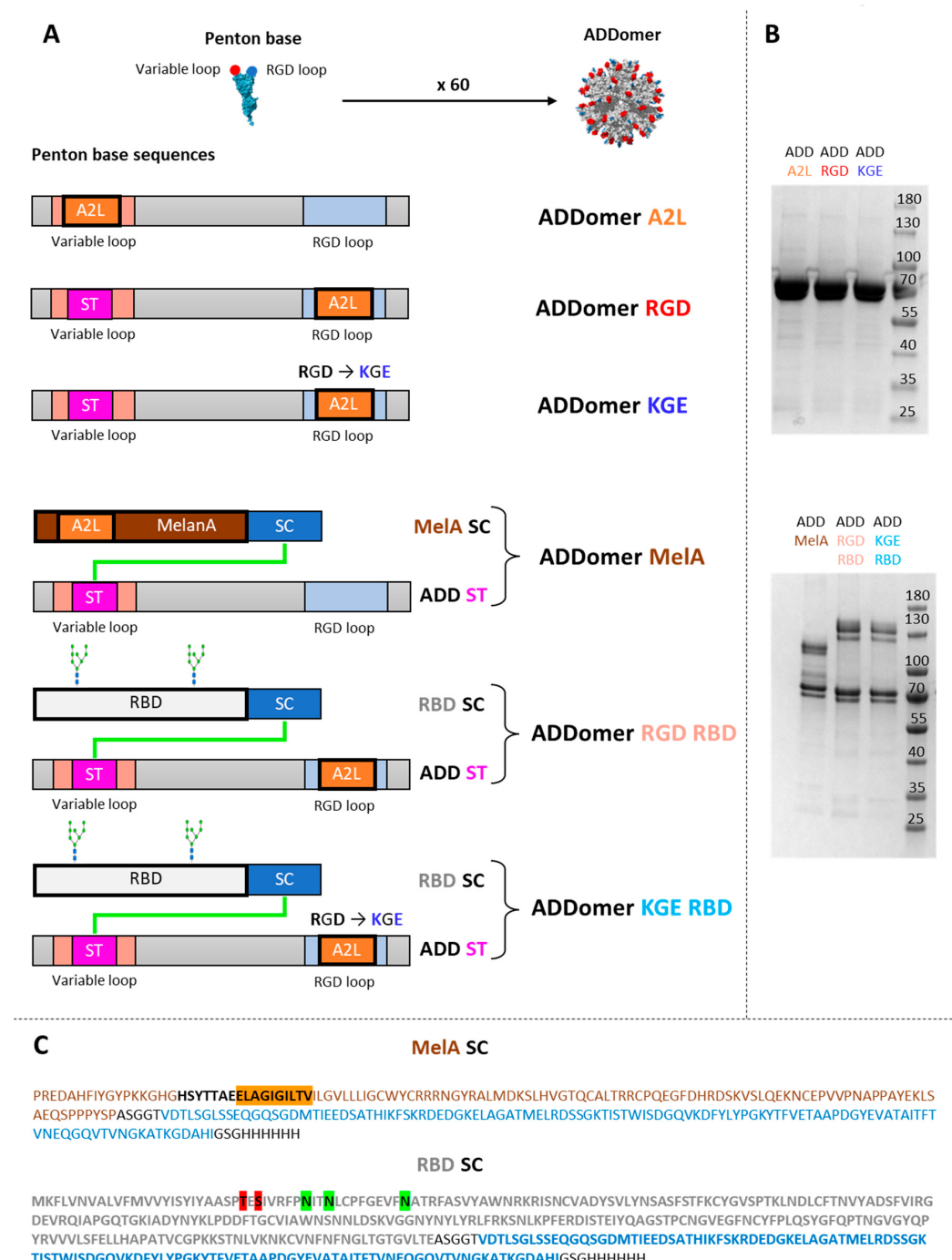


Figure 1. Design and characterization of the different ADDomers. (A) Diagram showing the insertion of the A2L epitope (A2L in orange) and SpyTag (ST in pink) in the 2 loops of the ADDomer monomer. SpyTag can make an isopeptidic bond with SpyCatcher (SC in blue) fused to the RBD protein (in grey) or the MelanA protein (MelA in brown). (B) SDS-PAGE profiles of reduced and boiled samples of the different ADDomers showing the apparition of a higher MW covalent adduct for the ADD-MelA (ADD-ST/MelA-SC), ADD KGE RBD (ADD-KGE/RBD-SC) and ADD RGD RBD (ADD-RGD/RBD-SC). (C) Sequences of the MelA-SC and RBD-SC. In the MelA-SC sequence, the MelanA tumor antigen is colored in brown (A2L epitope is highlighted in orange), SpyCatcher is colored in blue and additional linkers and histidine tag are colored in black. In the RBD-SC sequence, the Spike Receptor Binding Domain of SARS-CoV-2 is colored in grey (N and O-glycosites are highlighted, respectively, in green and red), SpyCatcher is colored in blue and additional linkers and histidine tag are colored in black.

3.3. ADD A2L and ADD MelA Are Differently Internalized by DC Subsets

To investigate the ability of human DC subsets to fix by adhesion at the cell surface, or internalize ADDomers, fluorescent ADD A2L and ADD MelA labeled with Alexa Fluor 647 (AF 647) were incubated for 1 h with PBMC containing the three major human DC subsets: plasmacytoid DC (pDC), conventional DC1 (cDC1) and conventional DC2 (cDC2). Plasmacytoid DC are specialized to sense and respond to viruses, whereas conventional DC are more specialized in cross presentation via MHC class I to activate CD8⁺ T cells [21]. Cells were then either washed and directly analyzed by flow cytometry or coated on microscope slides and stained with specific DC subsets markers. No “cell-scraping” treatment was performed, meaning that the flow cytometry experiment would reveal ADDomers fixed on the cell surfaces as well as ADDomers internalized. Confocal microscopy was used to decipher the internalization of ADDomers by the DC subsets.

Analysis by flow cytometry shows that both ADDomers are fixed/internalized by all DCs but revealed distinct efficiency between subsets. Whereas cDC2s strongly fixed/internalized ADDomers, cDC1s were a little less efficient, and pDCs even less (Figure 2A, Supplementary Figure S3). There is also a dose response effect for both ADDomers suggesting specific behavior of the ADDomers (Figure 2B). Interestingly, ADD MelA is less fixed/internalized than ADD A2L by all DC subsets. Such a decrease in fixation can be caused by the shielding of ADDomer’s integrin binding motif (RGD motif in the RGD loop) by the MelanA-SC on the ADDomer’s surface, since this motif has been shown to promote internalization in cells [22,23]. Confocal microscopy images further revealed that cDC2s massively engulfed ADDomers, whereas fluorescent ADDomers looked less internalized and more localized on the surface of cDC1s. Very few ADDomers looked localized on the surface of pDCs (Figure 2C). These observations suggest that ADDomers are not only fixed but also internalized by the DC subsets cDC2s and cDC1s.

3.4. ADDomer Triggers a Strong Activation of All DC Subsets Together with Cytokine Secretion

We then wanted to investigate the impact of ADDomer on DC subsets, especially their ability to activate them. Thus, PBMC (containing all DC subsets) were cultured either with a mixture of TLR ligands (TLR3-L, TLR7/8-L, TLR9-L) that stimulate cDC1s, cDC2s and pDCs, or peptide MelA_{26–35} (10 μM), ADD Ø (i.e., ADDomer which does not display any epitope) or ADD A2L (1 μM). TLR (Toll-Like-Receptors) are pathogen-recognition receptors that dimerize after the binding of their ligand (TLR-L) and become activated. Through the signaling pathway, they will stimulate the DCs, leading to a higher cross presentation, triggering a better cross priming.

Within alive CD45⁺ cells, DCs were defined as HLA-DR⁺ and the absence of Lin. cDC2s were gated as CD11c⁺ BDCA1⁺. pDCs were defined as CD11c negative and BDCA2⁺, while cDC1s were depicted as CD11c⁺/BDCA3⁺. The viability of DC subsets was first assessed using live&dead labeling. We observed that both ADDomers were not toxic for DCs within PBMCs, as the percentage of living cells was above 90% whatever the conditions (Figure 3A). The activation status of DC subsets was further depicted by investigating the expression of costimulatory molecules (CD40, CD80 and CD86) by flow cytometry. As expected, the TLR-L mix (positive control) up-regulated CD80, CD40 and/or CD86 molecules on each DC subset compared to the control condition, demonstrating their proper activation. Peptide MelA_{26–35} did not activate DCs, as there was no significant up-regulation of the costimulatory molecules (Figure 3B). Noteworthy, both ADDomers (ADD Ø and ADD A2L) triggered a strong activation of BDCA1 (cDC2s), BDCA2 (pDCs) and BDCA3 (cDC1s) subsets, highlighted by the up-regulation of the three costimulatory molecules (from 13 to 100% depending on the donor and the DCs subset). This up-regulation is as high as in TLR-L condition or even higher. This observation reveals the potent adjuvant properties of the ADDomer itself as even the ADD Ø can activate the DC subsets (Figure 3B). Furthermore, even if TLR-L stimulation leads to huge levels of cytokines secretion, ADD Ø and A2L triggered low level of IL28/IFN λ 2 secretion (maximum of 106 pg/mL for 1 donor compared to 24 pg/mL for the negative control) or low level of

IFN α 2 expression (maximum of 195 pg/mL for 1 donor compared to 102 pg/mL for the negative control) and IL29/IFN λ 1 (Figure 3C). These results suggest the weak but potent immune-stimulating potential of ADDomers on all DC subsets.

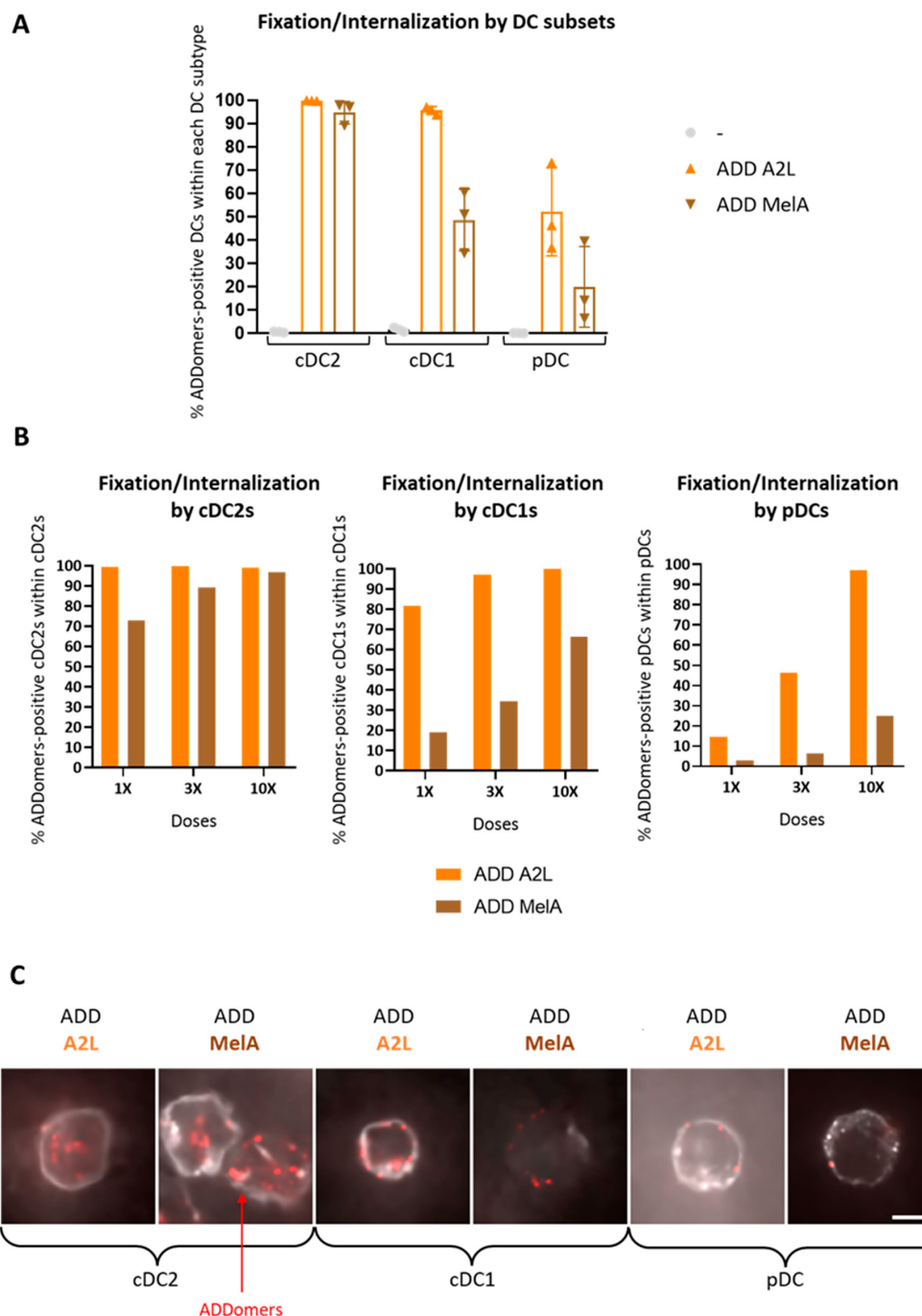


Figure 2. DC subsets efficiently fix and internalize ADDomers. PBMC (A,B) or PanDC (C) were incubated with different doses ($1\times$, $3\times$, $10\times$) of fluorescent A2L/MelA-ADDomer for 1 h (A,B) or 2 h (C). The fixation and internalization of ADDomer by DC subsets were then evaluated by flow cytometry and confocal microscopy. (A) Percentage of fixation of ADDomer ($3\times$) by each DC subset ($n = 3$ donors). (B) Dose response of ADDomer fixation by DC subsets ($n = 1$ donor). (C) Confocal imaging of ADDomer internalization by DC subsets. ADDomers are colored in red and the specific underlying BDCA1, BDCA2 or BDCA3 labeling is shown in gray. Scale bar is 5 microns and images are 18×18 microns.

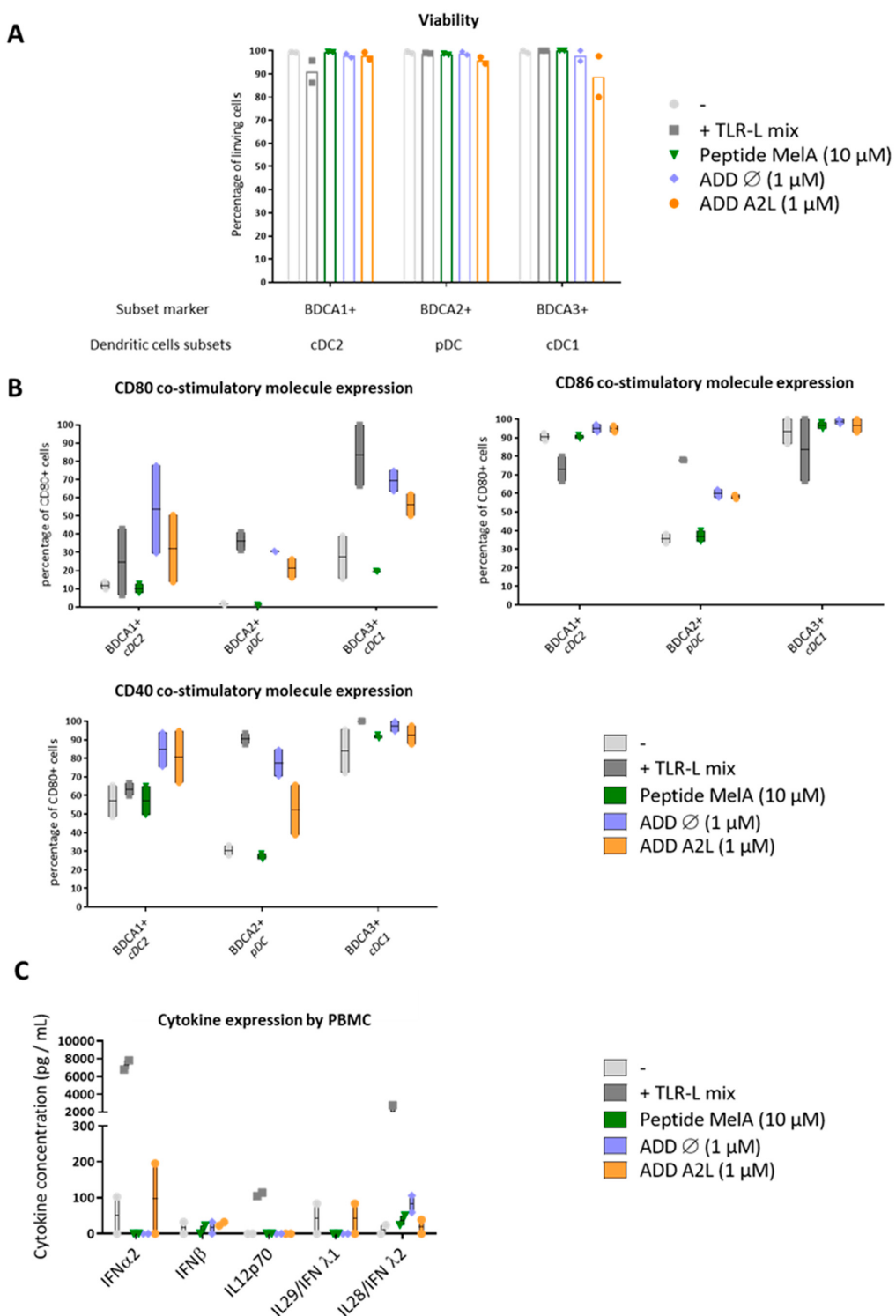


Figure 3. ADDomer triggers a strong activation of DC subsets together with cytokine secretion. PBMCs were cultured for 24 h in control conditions (−), or with either a mixture of TLR-L (Poly IC, R848, CpGA), MelA_{26–35} peptide (10 µM), empty ADDomer (ADD Ø) or displaying A2L (ADD A2L) both at 1 µM. The viability, activation and cytokine secretion by DC subsets were then evaluated. (A) Impact of ADDomer on DCs' viability assessed by measuring the percentage of alive cDC2s (BDCA1+), cDC1s (BDCA3+) and pDCs (BDCA2+) ($n = 2$ donors). (B) Impact of ADDomer on DCs' activation depicted by evaluating the percentage of CD40+, CD80+ and CD86+ DC subsets ($n = 2$ donors). (C) Cytokine secretion measured in the culture supernatants by Luminex ($n = 2$ donors).

3.5. DCs Efficiently Cross-Present the A2L Epitope from ADDomer Displaying the Full MelanA Antigen

To determine if the ADDomer could be cross-presented by human DCs, panDCs purified from HLA-A2+ PBMC (mix of cDC2s, cDC1s and pDCs) were pulsed with ADD Ø, ADD A2L, ADD MelA or peptide MelA_{26–35} as the positive control. Pulsed panDCs were then co-cultured with HLA-A2 restricted T cells containing pre-amplified anti-MelA_{26–35} CD8+ T cells. The production of IFN γ was analyzed by CBA (Cytometric Bead Array). The success of the cross presentation was revealed by the ability of T cells to produce IFN γ upon recognition of the complex peptide/HLA-A2 complex presented by the panDCs. The results show that ADD MelA seems to lead to a higher IFN γ production than ADD Ø and ADD A2L (Figure 4). This suggests that ADD MelA is cross-presented by dendritic cells.

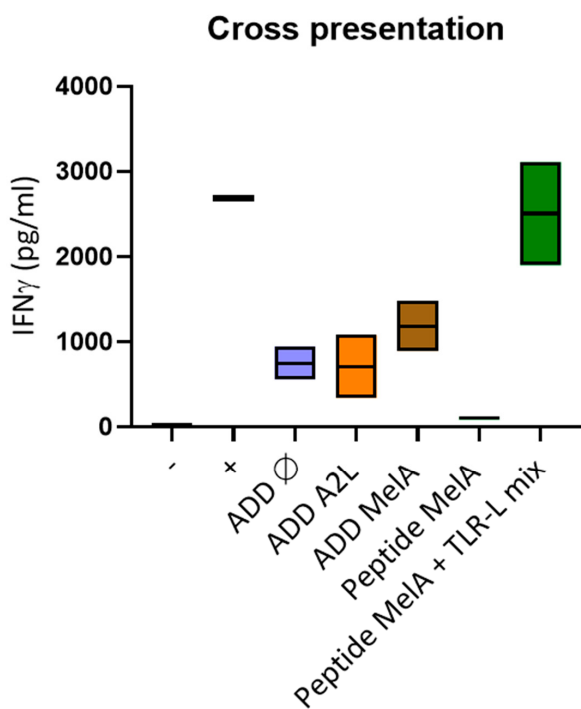


Figure 4. DCs efficiently cross-present the A2L epitope from ADDomer displaying MelA. Purified panDCs were incubated with ADD Ø, ADD A2L, ADD MelA, Peptide MelA and Peptide MelA + TLR-L for 1 h and cocultured 20 h with MelA_{26–35} specific CD8+ T cells. IFN γ secretion was then evaluated by CBA. T cells were also cultured alone (−) or with PMA/iono (+) ($n = 2$ donors).

3.6. ADDomer Displaying A2L Epitope Cross-Prime High Affinity Peptide-Specific CD8+ T Cells

Based on the previously observed ability of DC to fix, internalize and cross-present ADDomers, we further explored whether DCs could cross-prime peptide-specific CD8+ T cells from ADDomers displaying epitopes. To assess this point, PBMCs from 3 HLA-A2+ donors (containing < 0.03% of naïve MelA_{26–35}-specific CD8+ T cells) were incubated in control conditions (negative control), or with peptide MelA_{26–35} (positive control), or with ADD Ø or with ADD A2L (0.15 μ M). These conditions were performed in the presence or absence of a mixture of TLR ligands (TLR3-L, TLR7/8-L, TLR9-L) that stimulate cDC1s, cDC2s and pDCs. As described before TLR will stimulate the DCs leading to a higher cross presentation, triggering a better cross priming. Dextramer staining was performed to measure the percentage of anti-MelA_{26–35} dextramer+ CD8+ T cells at days 0, 7, 13 and 20 (Supplementary Figure S4), the relative amplification of Ag-specific T cells as well as the affinity of the amplified dextramer+ CD8+ T cells.

As expected, there is no triggering of anti-MelA_{26–35} CD8+ T cells in control conditions until D20 (percentage below 0.1%), whereas an amplification of dextramer+ CD8+ T cells (from 0.09% up to 22%) is observed for the 3 donors with the peptide MelA_{26–35} (positive control) with and without the TLR-L mix. Concerning the ADD Ø, we noticed negligible

or no elicitation (percentage below 0.4% of dextramer+ CD8+ T cells for the 3 donors) (Figure 5A), revealing that the ADDomer itself does not trigger anti-MelA_{26–35} CD8+ T cells, even though it strongly activated DCs.

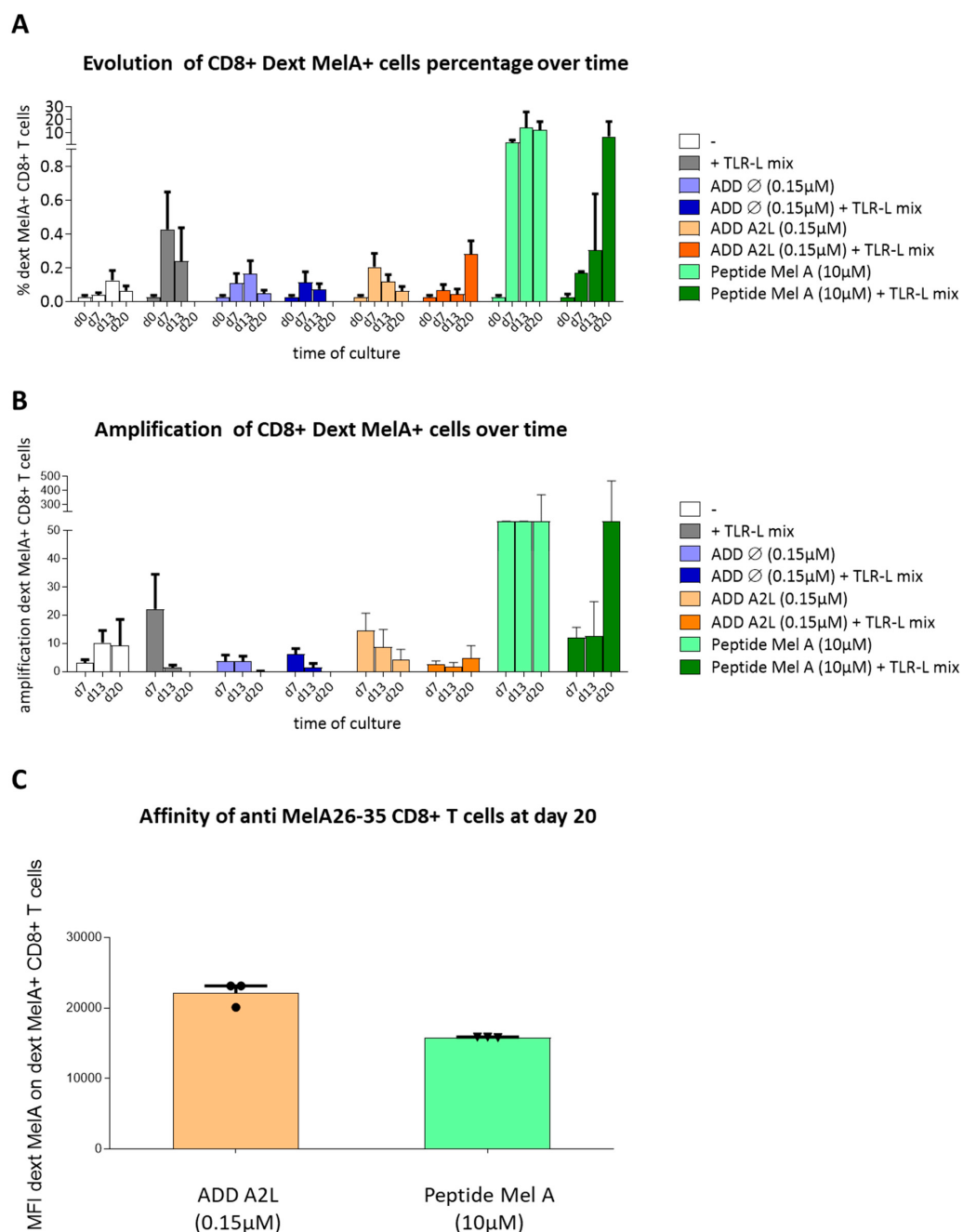


Figure 5. ADDomer displaying A2L epitope efficiently cross-prime peptide-specific CD8+ T cells dotted with a high affinity. PBMC were cultured in control conditions or with empty ADDomer (ADD Ø) or ADD A2L in the presence or not of a mixture of TLR-L. Cultures were restimulated every 7 days for 3 weeks. The elicitation of MelA-specific CD8 T cells was then evaluated by dextramer staining. (A) Evolution of Dext MelA+ CD8 T cells over time in the different conditions ($n = 3$ donors). (B) Amplification of Dext MelA+ CD8+ T cells over time. The amplification of antigen-specific CD8+ T cells was calculated based on the ratio of absolute numbers of dextramer+ CD8+ T cells at day X/day 0 ($n = 3$ donors). (C) Affinity of Dext MelA+ CD8+ T cells at day 20 ($n = 3$ donors).

Notably, ADD A2L was able to trigger dextramer+ CD8 T cells optimally at day 7 in the absence of TLR-L, and at day 20 in the presence of TLR-L mix (maximum 0.359% of dextramer+ CD8+ T cells at D20). Therefore, the results suggest that TLR-L mix is required to optimally stimulate the DCs for triggering anti-MelA_{26–35} CD8+ T cells from ADD A2L (Figure 5A).

Furthermore, the amplification of anti-MelA_{26–35} CD8+ T cells was calculated as the ratio of absolute numbers of antigen specific CD8+ T cells from day 0 (Figure 5B). For the negative control, no significant amplification of anti-MelA_{26–35} CD8+ T cells was observed, whereas, for the peptide MelA_{26–35} in the absence of TLR-L mix (positive control), an amplification at day 20 was noticed. For the ADD Ø, a negligible amplification (maximum of 7.51 without TLR mix and 10.08 with the TLR mix at day 7) was detected. Notably, concerning the ADD A2L, there was no obvious amplification with TLR mix (maximum of 9.20). However, when stimulated without TLR mix we observed an amplification of 23.41 at day 7 (Figure 5B).

Finally, the affinity of the anti-MelA_{26–35} CD8+ T cells could be defined by using the MFI of the dextramer labeling, knowing that a higher MFI corresponds to a better affinity (Figure 5C). By comparing the affinity of the anti-MelA_{26–35} CD8+ T cells, it appears that the one triggered by ADD A2L is higher than the one elicited by the peptide MelA_{26–35} itself. Indeed, the MFI for the 3 donors tested tends to be 33% higher for the ADD A2L (~20,000) than for the peptide MelA_{26–35} (~15,000). This observation highlights the ability of ADD A2L to trigger high affinity anti-MelA_{26–35} CD8+ T cells (Figure 5C).

3.7. De-Targeting and Re-Targeting ADDomers Specifically to DC Subsets

ADDomers present a very specific integrin binding motif (RGD motif in the RGD loop [22,23]), allowing them to be internalized by most cells [22,23]. With the aim of limiting off-target effects, we mutated the RGD motif into KGE. To direct the ADDomers to dendritic cells, the Spike Receptor Binding Domain of SARS-CoV-2 (from K300 to E554) fused to the SpyCatcher (RBD-SC) was displayed on the ADDomer's surface via the SpyTag/SpyCatcher system [15]. The A2L epitope was then moved from the VL to the RGD loop next to the RGD/KGE motif (Figure 1A). RBD-SC is secreted by insect cells during its production in baculovirus expression system and is therefore glycosylated (mostly poly-mannoses [24,25]). Indeed, 3 putative N-glycosites (N331, N334 and N343 highlighted in green) and 2 putative O-glycosites (T323 and S325 highlighted in red) are present in the RBD-SC sequence [26] (Figure 1C). The glycosylation of RBD-SC has already been assessed in Chevillard et al., 2022 [15]. These N-Glycan motifs can be recognized by different C-type lectin receptors (CLRs) present on the dendritic cell surface [27] as a function of the nature of the N-Glycan and its level of processing. Indeed, high-mannose or hybrid type N-glycan, which both expose terminal mannose residue, will be recognized by CLRs such as DC-SIGN, while MGL may binds either Hybrid or Complex-type N-Glycan, exposing terminal galactose. The covalent binding of RBD-SC to ADD-ST was assessed by SDS-PAGE. As expected, an adduct of a higher molecular weight corresponding to the RBD-SC bound to the ADD KGE or ADD RGD monomer (both bearing the ST motif) was clearly seen (Figure 1B, lower panel).

3.8. Functional De-Targeting of ADD KGE Compared to ADD RGD on A549 Cells

To assess ADDomer's de-targeting via the KGE motif, A549 adherent cells were incubated for 1h with ADD KGE and ADD RGD, both labeled with identic quantities of AF 488. Both ADDomer's internalization inside the A549 cells was evaluated by flow cytometry, and microscopy. A549 adherent cells (lung epithelium cell line) were used as a model of epithelial cells which can participate in off-target effects. For the flow cytometry analysis, after incubation with the fluorescent ADDomers, cells were treated with trypsin in order to remove the ADDomers fixed on cell surfaces while not affecting the ADDomers internalized by the cells. The total duration of this treatment was 20 min, as described in materials and methods. Thanks to the trypsin treatment, the fluorescence intensities represented in

Figure 6A correspond to ADD KGE and ADD RGD, which have been internalized. The fluorescence intensities at $t = 20$ min (1 h of incubation + 20 min of treatment for flow cytometry analysis) corresponding to the ADDomers (represented in blue for ADD KGE and in red for ADD RGD) (are both higher than the one corresponding to the negative control (in green), strongly suggesting they have been both internalized. Moreover, as both ADDomers are stoichiometrically labeled with AF 488 (data not shown), we can infer that the difference in fluorescence intensities between the 2 ADDomers corresponds to their respective internalization levels, suggesting internalization levels by A549 are higher for ADD RGD than for ADD KGE reflecting a partial de-targeting of this latter.

For the microscopy analysis, cells were incubated for 1 h with the fluorescent ADDomers at 37°C , 5% CO_2 , and then monitored for another hour using a spinning disk confocal microscope. The Figure 6B shows that at $t = 0$ (1 h of incubation) both ADDomers (represented in green spots) are localized within the cells (underlined in red). At $t = 60$ min (2 h of incubation) however, ADD RGD are still clearly visible within the cells whereas ADD KGE are much less present. The quantitative analysis of mean fluorescent intensities in the cells (red regions of interest) in both cases (Figure 6C) shows that ADD RGD associated fluorescence is almost retained while ADD KGE fluorescence is lost after 2 h. This suggests that ADD KGE but not ADD RGB is degraded during this lap time. As both moieties are internalized, this latter finding suggests that ADD RGD and ADD KGE might use different internalization mechanisms.

3.9. Assessment of ADDomer Targeting to C-Type Lectin Receptors (CLRs) by SPR

DCs especially cDC2s express C-type lectin receptors, such as DC-SIGN and MGL. ADD KGE, ADD KGE RBD and RBD-SC interaction with DC-SIGN and MGL receptors (tetrameric and trimeric protein, respectively) was measured by SPR. To do so, these ADDomers were injected over streptavidin surfaces functionalized with the extracellular domains (ECD) of DC-SIGN or MGL receptors modified with a biotin at their N-terminus (respectively called DC-SIGN Biot-ECD and MGL Biot-ECD). This specific N-terminal biotinylation allows the surface functionalization in an oriented manner, thus mimicking the membrane orientation of the DC-SIGN ECD and MGL-ECD. This allows an optimal access to the carbohydrates recognition domain (CRD)s of these multimeric receptors [28]. These 2 receptors can recognize glycosylation patterns [29,30] present on the RBD-SC. For ADD KGE, the sensorgrams revealed that the interaction is negligible and thus no relevant: the K_{Dapp} could therefore not be determined (Figure 7). On the contrary, the addition of RBD to ADD KGE (ADD KGE RBD) resulted in very strong and reliable interactions for both lectin receptors. However, a strong preference for DC-SIGN over MGL have been observed with respective K_{Dapp} of 0.34 ± 0.005 nM and 66.1 ± 4.6 nM, respectively.

Finally, the RBD-SC alone shows significant interactions with the two receptors and like with ADD KGE RBD the interaction is stronger for DC-SIGN ($K_{\text{Dapp}} = 601 \pm 90$ nM), than for MGL ($K_{\text{Dapp}} = 982 \pm 31$ nM) (Figure 7). When comparing, for both lectins, the K_{Dapp} of the ADD KGE RBD with the ones of the single RBD-SC, a tremendous increase in affinity by a factor of about 1800 times was observed towards DC-SIGN and of “only” 15 times for MGL. This underlines the great enhancement of avidity, and thus targeting efficiency, that can be achieved thanks to the avidity generated by the multivalent RBD presentation within the ADD context. Moreover, the higher interaction increase observed with DC-SIGN compared to MGL, suggests that the RBD harbor more particularly N-Glycan specific to DC-SIGN.

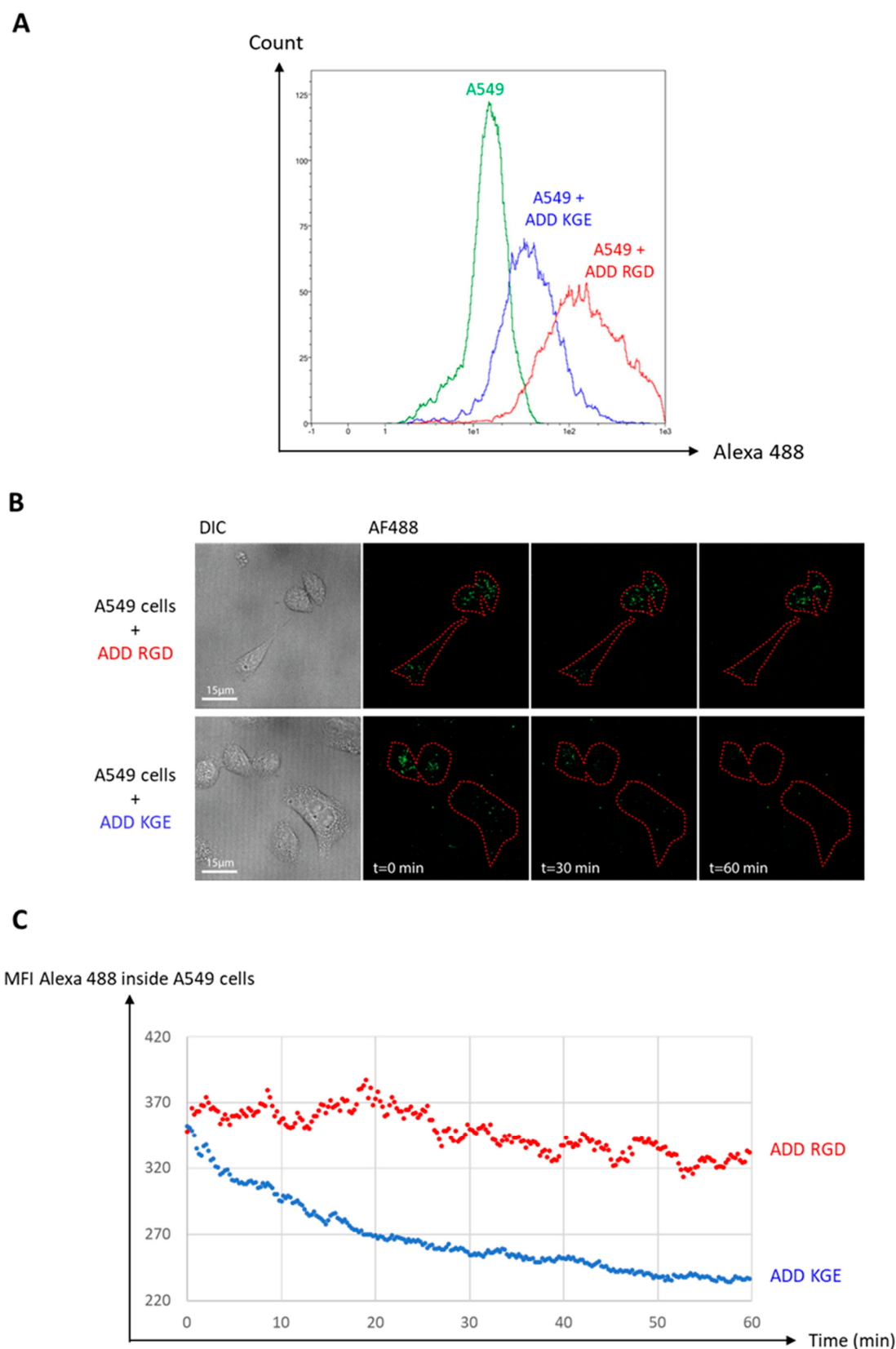
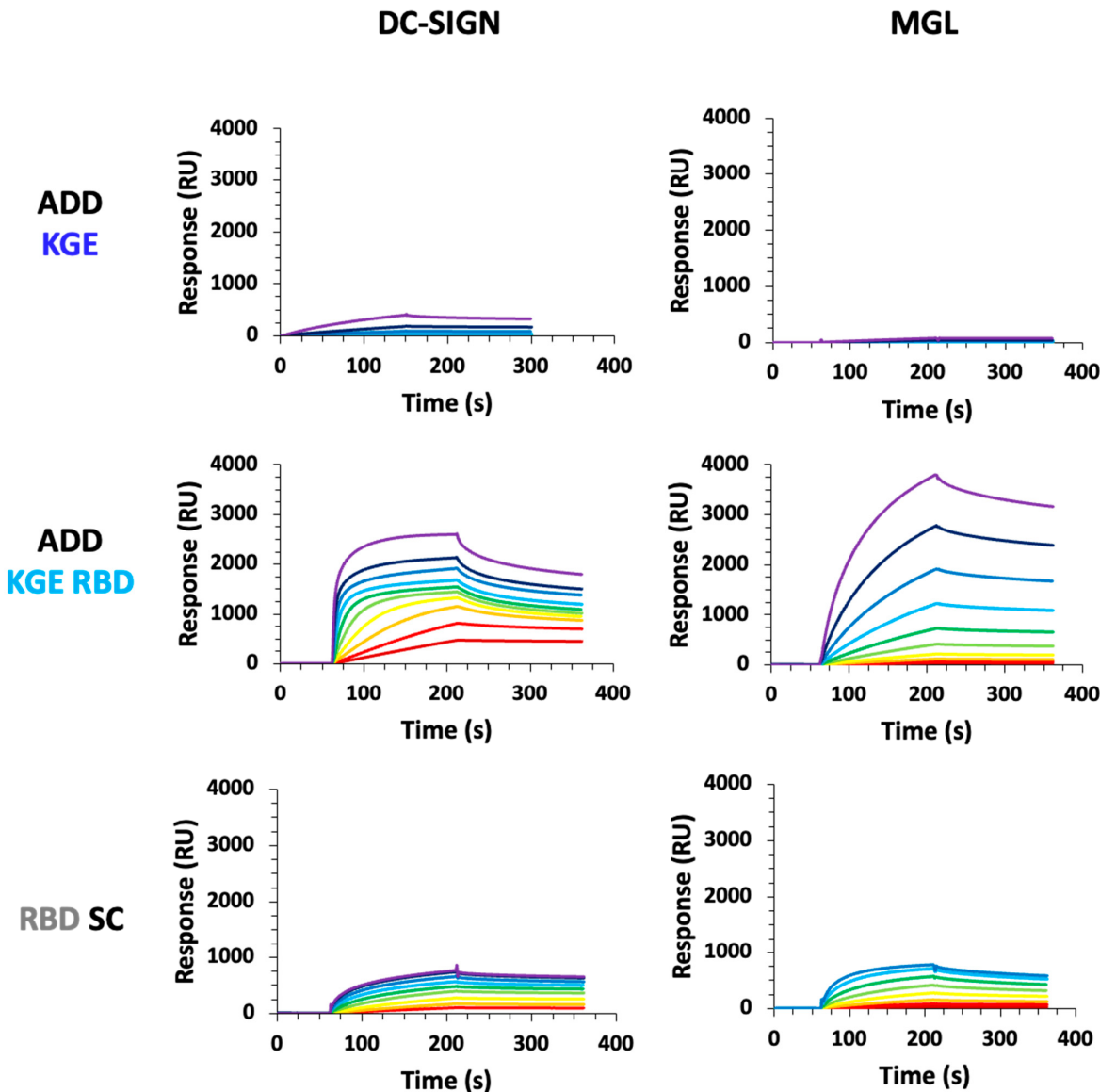


Figure 6. ADD KGE and ADD RGD internalization by lung epithelial cell line A549. (A) ADD KGE AF 488 and ADD RGD AF 488 internalization by lung epithelial cell line A549 evaluated by flow cytometry at $t = 20$ min. (B) Time lapse imaging by confocal microscopy of ADD KGE AF 488 and ADD RGD AF 488 internalization by lung epithelial cell line A549. (C) Mean Fluorescence Intensity (MFI) of ADD KGE AF 488 and ADD RGD AF 488 within cells over time.

A**B**

	$K_{D\ app}$ for DC SIGN surface	$K_{D\ app}$ for MGL surface
ADD KGE	N/A	N/A
ADD KGE RBD	0.34 nM +/- 0.046 nM	66.11 nM +/- 4.6 nM
RBD SC	601.3 nM +/- 89 nM	981.6 nM +/- 31 nM

Figure 7. ADD KGE, ADD KGE RBD and RBD-SC binding evaluation on DC-SIGN and MGL receptors by surface plasmon resonance. (A) Sensorgrams of the interaction of the ADD-KGE constructs and RBD-SC onto DC-SIGN or MGL oriented surface. For ADD KGE and ADD KGE RBD, injected concentrations range from 136 nM to 0.2 nM by cascade dilution by a factor of 2. For RBD SC, concentration used range from 14.4 μ M down to 56 nM by cascade dilution by 2. (B) Table of apparent K_D calculated using steady state analysis in the BIAEval software.

3.10. ADD KGE/RGD and ADD KGE/RGD RBD Are Successfully Fixed/Internalized by DC Subsets but Differentially Depending on the Subset

In addition, for ADD A2L and ADD MelA (Figure 2), we observed that all ADDomers are better fixed/internalized by cDC2s, than cDC1s than pDCs (Figure 8A,B, Supplementary Figure S5). Indeed, whereas cDC2s strongly fix/internalize ADDomers, cDC1s were a little less efficient, and pDCs even less. There is also a dose response effect for all ADDomers suggesting specific fixation/internalization (Figure 8B). Similar to ADD MelA, the addition of RBD-SC on both ADD KGE and ADD RGD seemed to decrease the fixation/internalization, even though it was less obvious than for ADD MelA and it varied between donors. This decrease in fixation/internalization can also be caused (for the ADD RGD versus ADD RGD RBD) by the shielding of ADDomer's integrin binding motif [22,23] (RGD motif in the RGD loop) by the RBD-SC on the ADDomer's surface. As mentioned for A549 cells, ADD KGE seems to be fixed/internalized by a non-RGD-dependent-integrin-mediated mechanism. One can imagine that this mechanism involves recognition of other molecular patterns present on the ADDomer's surface which are also shielded by the RBD-SC.

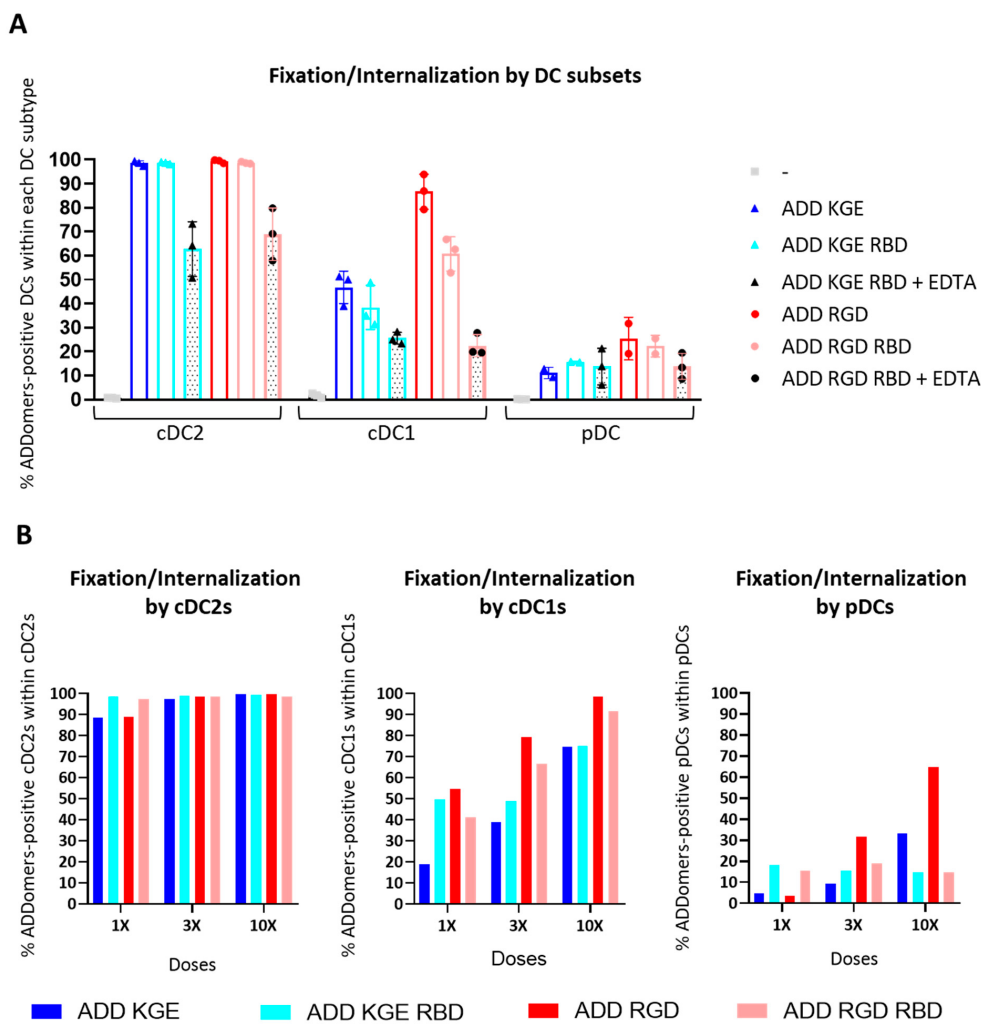


Figure 8. ADD KGE/RGD (with or without RBD-SC and EDTA) fixation/internalization by DC subsets. PBMC pre-incubated or not with EDTA were incubated with fluorescent KGE/RBD ADDomer for 1 h. The fixation of ADDomer by DC subsets was then evaluated by flow cytometry. (A) Fixation and internalization evaluation of ADD KGE/RGD (with or without RBD-SC and EDTA) (0.5 μ M i.e., 3 \times) on DC subsets using flow cytometry ($n = 3$ donors). (B) Fixation and internalization evaluation of ADD KGE/RGD (with or without RBD-SC and EDTA) (0.15 μ M i.e., 1 \times or 0.5 μ M i.e., 3 \times or 1.5 μ M i.e., 10 \times) on DC subsets using flow cytometry ($n = 1$ donor).

3.11. ADD KGE/RGD RBD Fixation/Internalization by Dendritic Cells Might Involve Binding to a CLR

As SPR data showed a binding of glycosylated RBD to the CLRs DC-SIGN and MGL, CLR binding was investigated on DC subsets. To do this, ADDomers AF647 were incubated for 1h with PBMC containing DC subsets and internalization was evaluated by flow cytometry. The PBMC were previously incubated in the absence or in the presence of EDTA. EDTA chelates Ca^{2+} ions are involved in CLR-ligand binding as well as in the integrin mediated internalization. We hypothesized that an internalization decrease observed in the presence of EDTA for the ADD KGE RBD would suggest a non-integrin mediated internalization mechanism requiring Ca^{2+} is involved. According to the SPR data, this mechanism might involve CLRs such as DC-SIGN or MGL. This hypothesis was validated as a strong internalization decrease was noticed for ADD KGE RBD + EDTA compared to ADD KGE RBD (Figure 8A).

3.12. Only ADD RGD Is Cross-Presented by Dendritic Cells

A cross presentation experiment was performed similarly to the ADD MelA cross presentation experiment (Figure 4). The results show that only ADD RGD seems to lead to a higher $\text{IFN}\gamma$ production than ADD Ø (Figure 9). This suggests that only ADD RGD is cross-presented by dendritic cells.

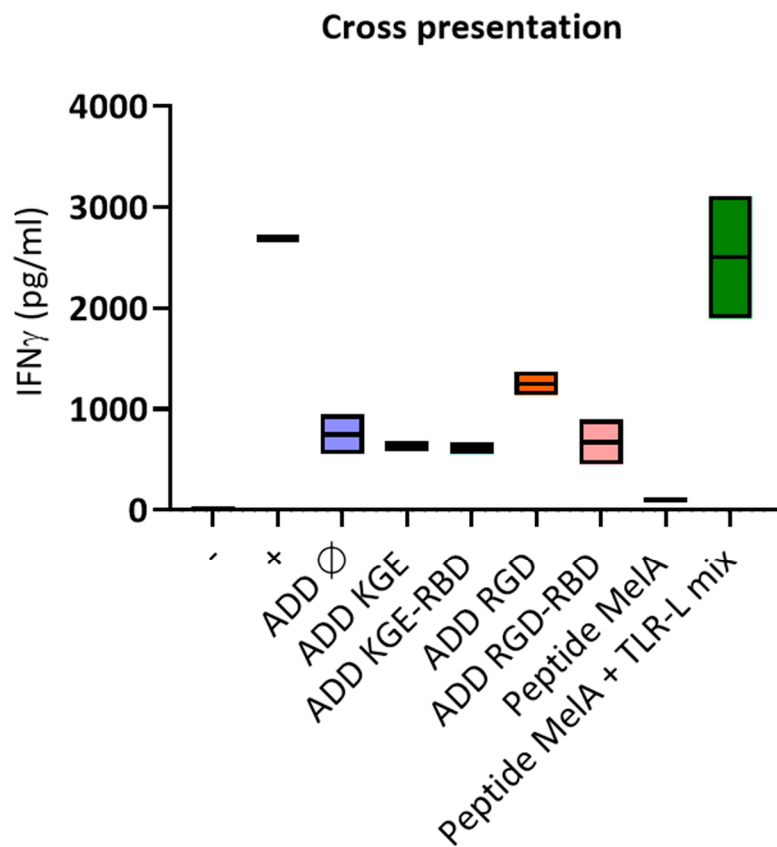


Figure 9. DCs efficiently cross-present the A2L epitope only when displayed by ADD RGD. Purified panDCs were incubated with ADD Ø, ADD KGE/RGD +/- RBD, Peptide MelA and Peptide MelA + TLR-L for 1 h and cocultured 20 h with MelA_{26–35} specific CD8+ T cells. $\text{IFN}\gamma$ secretion was then evaluated by CBA. T cells were also cultured alone (−) or with PMA/iono (+) ($n = 2$ donors).

4. Discussion

In this work we assessed in vitro the immunogenicity on human PBMC from healthy donors of an “adenovirus-inspired” non-infectious VLP displaying a human melanoma tumor epitope or antigen and the impact of ADDomers on human DCs’ features. The VLP used results from the spontaneous assembly of twelve homopentameric penton bases from

the human adenovirus of type 3 (HAdV-B3). The engineering of this 60-mer VLP named ADDomer (Adenovirus dodecamer) enabled an easy and rapid genetic insertion of short epitopes at two different locations of the particle surface. This vaccine platform displaying ovalbumin model antigen or epitopes was already proven to control melanoma tumor growth in mice bearing B16 OVA tumors [16].

MelanA (MelA) is a well-characterized melanoma differentiation antigen containing the immunodominant MHC class I A2L epitope (ELAGIGILTV). These MelanA and A2L antigen and epitopes are often used in preclinical and clinical studies evaluation of vaccine candidates against melanoma [31–34]. To bind the MHC-I proteins, class I epitopes must be processed by the proteasome into 8–10 amino-acids peptides. With the cleavage efficiency being influenced by the flanking regions [35,36], special attention must be paid to the epitope directly neighboring. It is known that small amino-acid residues such as glycine or alanine favor the antigen processing by the proteasome [37]. Here, we genetically inserted the MHC-I A2L epitope flanked on both sides by “GSGG” linkers in the “VL” exposed loop for ADD A2L or in the “RGD” exposed loop for ADD KGE/RGD +/− RBD.

After demonstrating that ADDomers could be internalized differentially by dendritic cells depending on their design as well as on the DC subset (Figure 2), we studied the impact of ADD Ø and ADD A2L on human DCs subsets in order to determine whether ADDomers could activate them (Figure 3). It was observed that both ADDomers were not toxic for DCs from healthy donors. Both of them also trigger a high activation of BDCA1, BDCA2 and BDCA3 subsets, highlighted by the up-regulation of the three costimulatory molecules (CD40, CD80, CD86), revealing the potent adjuvant properties of the ADDomer itself. Once activated, DCs express costimulatory molecules at their surface which are required for the activation of T cells. CD40 interacts with CD40 ligand on CD4 T cells surface, and CD80/CD86 interact with CD28 on CD8 T cells. Since the ADDomer derives from adenovirus, it could bind to existing receptors as well as trigger receptor cross-linking, which could explain the very high activation of DCs. Regarding cytokine expression, ADDomers (mostly ADD A2L) triggered a slight production of DC-specific cytokines, especially IFN α , IL28, IL29, which are crucial for subsequent antitumor effector elicitation.

Next, we explored the induction of tumor-antigen specific immune response in vitro in human with ADD A2L in other words, we investigated the ability of ADDomers to trigger anti-MelA_{26–35} CD8+ T cells from PBMCs, over 20 days (3 stimulations—one per week) by measuring the percentage of anti-MelA_{26–35} CD8+ T cells every 7 days using dextramer labeling.

This result highlighted the ability of ADD A2L to trigger anti-MelA_{26–35} CD8+ T cells amplification. Moreover, the amplified anti-MelA_{26–35} CD8+ T cells showed a high affinity for the HLA/MelA_{26–35} complex (Figure 5), highlighting their ability to kill target cells with low levels of peptide/MHC complexes.

It was shown in previous work that the genetic insertion of short epitopes in the two exposed loops of ADDomer did not affect the overall particle structure [12]. However, an epitope-based vaccine presents a major limitation for human use: HLA restriction. Indeed, the encoded epitopes are specific to a certain HLA allele. In our case, the epitope A2L is specific to the HLA A2, which is present in only 40% of the Caucasian population. To overcome this limitation, developing a full antigen-based vaccine enabling epitope presentation in all individuals is preferable (i.e., developing an off-the-shelf vaccine) [38]. Unfortunately, genetic insertion of large-folded antigens results in subunit misfolding and insolubility [39]. In a previous study, Villegas et al. have shown that OVA_{248–376} antigen could be fused to WW-domains, allowing interactions with the adenovirus PPxY sequences included in the adenovirus penton base [16,40]. However, this non-covalent interaction relies on a relatively low K_D (65 nM) [41] that could not warrant a homogenous batch required for clinical trials. To overcome this limitation, insertion of a SpyTag (13 residues) in the exposed loops of ADDomer has been reported to permit the spontaneous and covalent attachment of large and correctly folded antigens such as the SARS-CoV-2 Receptor Binding Domain or ovalbumine to the particle [15,42]. Fusion of melanoma tumor antigen

(MelA) to the SpyCatcher successfully resulted in the display of this antigen to the vaccine platform (Figure 1A,B).

Comparison of ADD MelA versus ADD A2L internalization by DCs subsets was then verified. Indeed, one known mechanism of ADDomers inside cells relies on the binding of integrins with the RGD motif exposed on ADDomer's "RGD" loops [22,23]. These "RGD" motifs could be shielded by the addition of MelA-SC on the ADDomer's surface. The results showed that ADD MelA is less but still internalized by all DC subsets compared to ADD A2L (Figure 2). Interestingly, whereas cDC2s strongly fix/capture both ADDomers, cDC1s were a little less efficient, and pDCs even less.

Cross presentation comparison between ADD MelA and ADD A2L was also performed, revealing that ADD MelA seems to be more cross-presented than ADD A2L (Figure 4). This suggests that displaying a protein antigen containing multiple MHC-I and MHC-II epitopes instead of a single epitope only favors the cross presentation of this epitope. An explication to this finding could be the activation of the CD4 immune response by the full-length antigen MelanA, which potentializes the CD8 response against the A2L epitope.

The second part of this study was to specifically address the ADDomers to the dendritic cells via ADDomer's design modifications. The aim is to limit off-target effects and to enhance cross priming via enhanced ADDomer uptake by DCs.

The de-targeting was performed by mutating the specific integrin binding motif "RGD" motif in the RGD loop into "KGE", therefore limiting an RGD-dependent-integrin-mediated ADDomer uptake by epithelial cells, which has been observed in previous studies [22].

The re-targeting was achieved by displaying on the ADDomer's surface the Spike Receptor Binding Domain of SARS-CoV-2 fused to the SpyCatcher (RBD-SC). This was carried out via the SpyTag/SpyCatcher system described earlier [15]. RBD-SC is secreted by insect cells during its production in baculovirus expression system and is therefore glycosylated, mostly by poly-mannoses [24–26], which can be recognized by C-type lectin receptors (CLRs) such as DC-SIGN and MGL present on the dendritic cell surface [29,30]. The A2L epitope was then moved from the VL to the RGD loop next to the RGD/KGE motif (Figure 1A).

To evaluate first de-targeting efficacy, A549 adherent cells were incubated with ADD KGE and ADD RGD for 1h. Internalization was evaluated by flow cytometry and microscopy. Both techniques show that ADD KGE is less but still internalized by A549 cells than ADD RGD suggesting an efficient de-targeting (Figure 6). Moreover, the microscope experiment suggests that ADD RGD and ADD KGE might use different internalization mechanisms. ADD KGE seems therefore to be internalized by a non-RGD-dependent-integrin-mediated mechanism.

Secondly, the re-targeting via the interaction of the RBD-SC with CLRs was evaluated by SPR. RBD binding to captured DC-SIGN and MGL CLRs via the glycosylation patterns was measured. This experiment revealed that compared to ADD KGE RBD and RBD-SC, ADDomer not harboring RBD (ADD KGE) has very poor interaction with the surfaces. On the contrary, the compounds containing RBD interact strongly with the surfaces, thanks to strong affinities to CLRs. We also observed a logical higher affinity for ADD KGE RBD due to the more important avidity brought by the multivalent presentation of RBD by the ADDomer platform (Figure 7). The affinity of DC-SIGN for these compounds is logically stronger than for MGL, since glycosylations are principally composed of poly-mannoses (present on the RBD N-glycosites when produced in insect cells) [24–26], which are the natural ligands of DC-SIGN [29]. MGL, however, has a better affinity for N-acetyl galactosamine (putatively present on the RBD O-glycosites when produced in insect cells) [26,30].

When we looked at the re-targeting at a cellular level, we observed that the addition of RBD did not enhance ADDomer's uptake as expected and on the contrary, reduced the proportion of ADDomers internalized by the dendritic cells (Figure 8). For ADD RGD versus ADD RGD RBD, just as for ADD MelA, this decrease in internalization can be caused by the shielding of ADDomer's integrin binding motif (RGD motif in the RGD

loop) by the RBD-SC on the ADDomer's surface. For ADD KGE versus ADD KGE RBD, as mentioned for A549 cells, internalization seems to take place via a non-RGD-dependent-integrin-mediated mechanism. One can imagine that this mechanism involves recognition of other molecular patterns present on the ADDomer's surface which are also shielded by the RBD-SC. However, in both cases (KGE versus RGD), the internalization seems to be mediated by an unknown receptor (putatively a CLR) present on the dendritic cell surfaces (Figure 7). In terms of cross-presentation, our results showed that ADD RGD is cross-presented by dendritic cells contrary to ADD KGE, ADD KGE RBD and ADD RGD RBD. This suggests that the RGD-dependent-integrin mediated internalization might play a role in the cross-presentation process of the ADDomer' displayed epitope A2L. This is also consistent with the observation that the ADDomer RGD is fixed in a higher level by cDC1s compared to ADDomer KGE and RBD, and cDC1s are the subset of DCs exhibiting the highest cross-presentation capacities.

Altogether, our results show that ADDomer could be a promising cancer vaccine platform displaying tumor antigens and epitopes. Epitopes can be genetically inserted into the ADDomers loops without degrading the ADDomer structure. On the other hand, antigen insertion requires the expression of both ADDomer SpyTag and the antigen fused to the SpyCatcher. This covalent and autocatalytic binding allows the production of a "ready to use" cancer vaccine applicable to a large population and to different types of cancers with known epitopes and antigens. Currently, cancer vaccines use either tumor-associated antigens or more personalized neo-antigens which could both be displayed by the ADDomer platform. Moreover, the multiple epitopes and antigens could be displayed at the same time on ADDomers, allowing a multi-specific immune response and therefore limiting treatment failure or resistance.

Supplementary Materials: The following supporting information can be downloaded at: <https://www.mdpi.com/article/10.3390/biomedicines10112881/s1>, Figure S1: Separation of the complex ADD-mCherry from the left over mCherry-SC. (A) SDS PAGE gel of boiled and reduced samples showing left over mCherry-SC after incubation of ADD ST with mCherry-SC. (B) SDS PAGE gel of boiled and reduced samples and sucrose gradient image showing the separation of the complex ADD mCherry and the left over mCherry-SC; Figure S2: Preparation of ADDomers labeled with Alexa 647 for ADDomers internalization evaluation by DC subsets. (A) Workflow of ADDomers AF647 preparation and purification. (B) Agarose gel of labeled and non-labeled ADD mCherry; Figure S3. Dotplots of ADDomer fixation on DC subsets. (A) Gating strategy of DC subsets. (B) ADDomer fixation on DC subsets; Figure S4: ADD Ø and ADD A2L cross priming evaluation. (A) dextramer. (B) Workflow of ADD Ø and ADD A2L cross priming evaluation. (C) Dot blots showing the percentage of CD8+ Dext MelA+ T cells at D0 and at D20 for each condition (dot plots pre-gated on CD45+ CD3+ CD8+ T cells); Figure S5: Zoom on ADD KGE RBD binding evaluation on DC-SIGN by surface plasmon resonance. Separate fitting of ADD KGE RBD with DC-SIGN.

Author Contributions: Conceptualization, S.B., C.A., D.L. and P.F.; investigations, S.B., C.A., C.C., D.L., M.T., J.-P.K., M.P., F.F. and O.M.; funding acquisition, S.B., C.A. and P.F.; with input from all authors, S.B. wrote the manuscript. All authors have read and agreed to the published version of the manuscript.

Funding: This work was supported by 'Fondation d'Entreprise SILAB—Jean Paufique' and EFS AuRA. Solène Besson was the recipient of the SILAB price 2020–2022 dedicated to skin cancer research. S.B. was granted by a 'bourse doctorale' from the University Grenoble Alpes. This work used the platforms of the Grenoble Instruct-ERIC centre (ISBG; UAR 3518 CNRS-CEA-UGA-EMBL) within the Grenoble Partnership for Structural Biology (PSB), supported by FRISBI (ANR-10-INBS-05-02) and GRAL, financed within the University Grenoble Alpes graduate school (Ecole Universitaire de Recherche) CBH-EUR-GS (ANR-17-EURE-0003). F.F. is supported by the French Agence Nationale de la Recherche (ANR) PIA for Glyco@Alps (ANR-15-IDEX-02).

Institutional Review Board Statement: The study was conducted in accordance with the Declaration of Helsinki, and approved by the French Blood Service's (EFS-AuRA) Institutional Review Board and declared under the reference #DC-2008-787. Written informed consent was acquired from all participants prior to their participation in this study.

Informed Consent Statement: Informed consent was obtained from all subjects involved in the study.

Data Availability Statement: Data are available upon request.

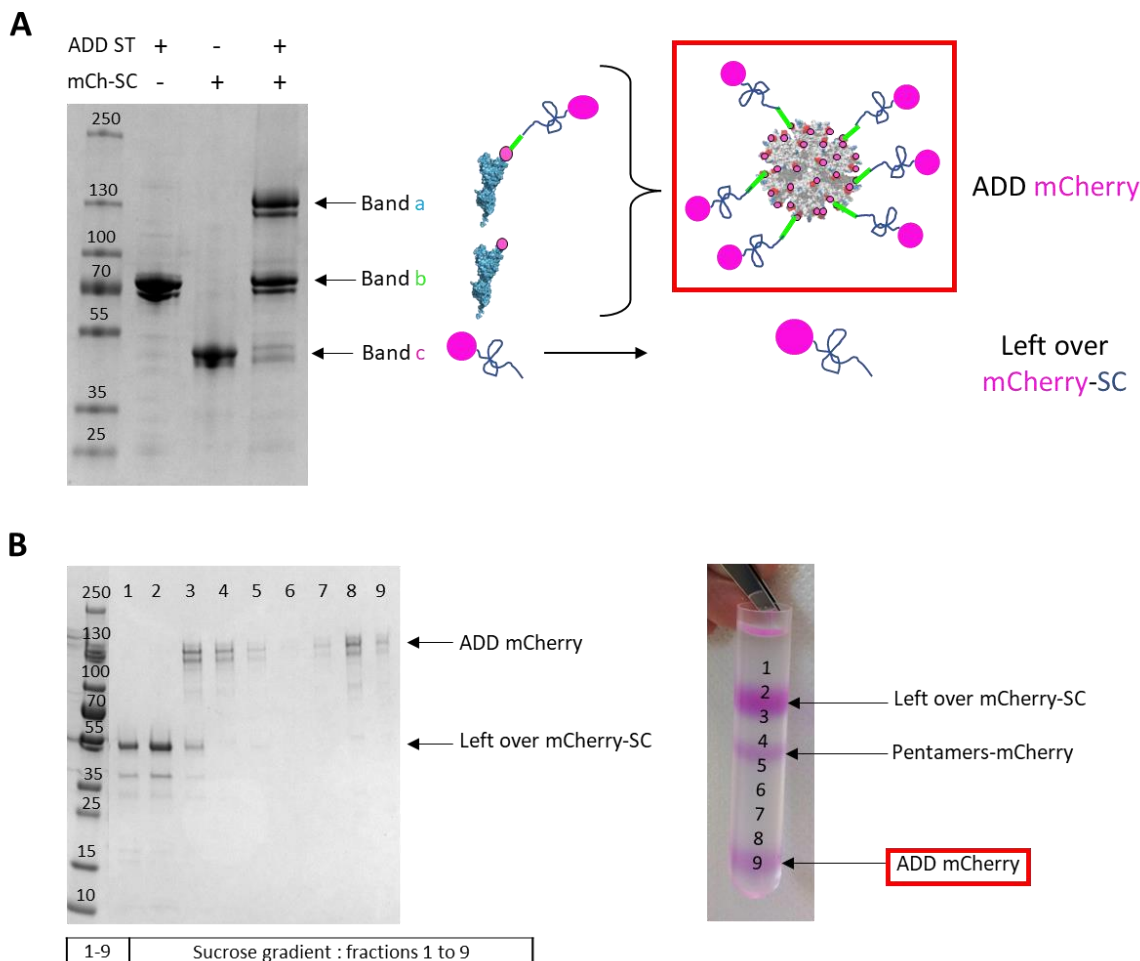
Acknowledgments: We warmly thank Jean Paufique and Brigitte Closs from the Fondation d’Entreprise SILAB for their scientific and financial support which enabled us to perform this work. We warmly thank the Microcell core facility (Univ. Grenoble Alpes, Inserm U 1209, CNRS UMR 5309, Institute for Advanced Biosciences) as well as Rose-Laure Revel-Goyet, Françoise Lacroix and Oleksandr Glushonkov for the support and access to the M4D Cell imaging Platform (Institut de Biologie Structurale, Grenoble). We are indebted to Emilie Stermann, Marie-Claire Dagher, Christopher Chevillard and Laurence Chaperot for their help and advices. Flow cytometry experiments and part of confocal imaging were performed on Microcell core facility (Univ. Grenoble Alpes, Inserm U 1209, CNRS UMR 5309, Institute for Advanced Biosciences), member of the Life Science Imaging—In vitro (ISdV) platform and partly supported by the French network GIS-IBISA.

Conflicts of Interest: The authors declare no conflict of interest.

References

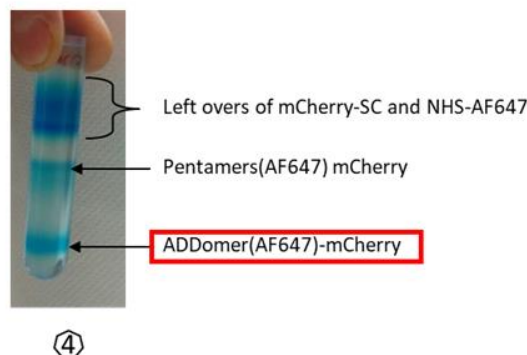
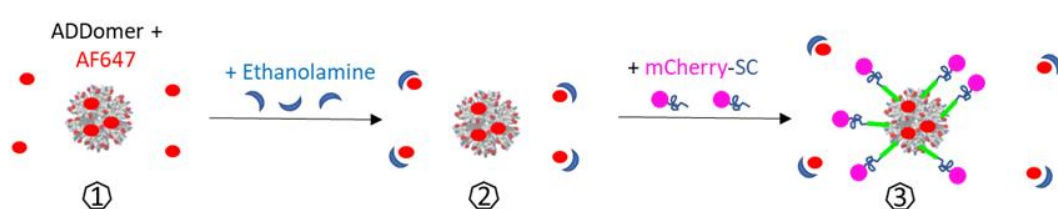
1. Hu, Z.; Ott, P.A.; Wu, C.J. Towards personalized, tumour-specific, therapeutic vaccines for cancer. *Nat. Rev. Immunol.* **2018**, *18*, 168–182. [[CrossRef](#)] [[PubMed](#)]
2. Galluzzi, L.; Vacchelli, E.; Bravo-San Pedro, J.M.; Buqué, A.; Senovilla, L.; Baracco, E.E.; Bloy, N.; Castoldi, F.; Abastado, J.-P.; Agostinis, P.; et al. Classification of current anticancer immunotherapies. *Oncotarget* **2014**, *5*, 12472–12508. [[CrossRef](#)]
3. Lichty, B.D.; Breitbach, C.J.; Stojdl, D.F.; Bell, J.C. Going viral with cancer immunotherapy. *Nat. Rev. Cancer* **2014**, *14*, 559–567. [[CrossRef](#)] [[PubMed](#)]
4. Chen, D.S.; Mellman, I. Oncology meets immunology: The cancer-immunity cycle. *Immunity* **2013**, *39*, 1–10. [[CrossRef](#)] [[PubMed](#)]
5. Stevenson, F.K.; Palucka, K. Understanding and activating immunity against human cancer. *Curr. Opin. Immunol.* **2010**, *22*, 212–214. [[CrossRef](#)]
6. Guo, C.; Manjili, M.H.; Subjeck, J.R.; Sarkar, D.; Fisher, P.B.; Wang, X.Y. Therapeutic cancer vaccines: Past, present, and future. *Adv. Cancer Res.* **2013**, *119*, 421–475.
7. Guo, Y.; Lei, K.; Tang, L. Neoantigen Vaccine Delivery for Personalized Anticancer Immunotherapy. *Front. Immunol.* **2018**, *9*, 1499. [[CrossRef](#)]
8. Niemann, J.; Kühnel, F. Oncolytic viruses: Adenoviruses. *Virus Genes* **2017**, *53*, 700–706. [[CrossRef](#)]
9. Hemminki, O.; Bauerschmitz, G.; Hemmi, S.; Lavilla-Alonso, S.; Diaconu, I.; Guse, K.; Koski, A.; Desmond, R.A.; Lappalainen, M.; Kanerva, A.; et al. Oncolytic adenovirus based on serotype 3. *Cancer Gene Ther.* **2011**, *18*, 288–296. [[CrossRef](#)]
10. Hemminki, O.; dos Santos, J.M.; Hemminki, A. Oncolytic viruses for cancer immunotherapy. *J. Hematol. Oncol.* **2020**, *13*, 84. [[CrossRef](#)]
11. Seymour, L.W.; Fisher, K.D. Oncolytic viruses: Finally delivering. *Br. J. Cancer* **2016**, *114*, 357–361. [[CrossRef](#)] [[PubMed](#)]
12. Vrignau, C.; Bufton, J.C.; Garzoni, F.; Stermann, E.; Rabi, F.; Terrat, C.; Guidetti, M.; Josserand, V.; Williams, M.; Woods, C.J.; et al. Synthetic self-assembling ADDomer platform for highly efficient vaccination by genetically encoded multipeptope display. *Sci. Adv.* **2019**, *5*, eaaw2853. [[CrossRef](#)] [[PubMed](#)]
13. Fender, P.; Ruigrok, R.W.; Gout, E.; Buffet, S.; Chroboczek, J. Adenovirus dodecahedron, a new vector for human gene transfer. *Nat. Biotechnol.* **1997**, *15*, 52–56. [[CrossRef](#)] [[PubMed](#)]
14. Besson, S.; Vrignau, C.; Vassal-Stermann, E.; Dagher, M.C.; Fender, P. The Adenovirus Dodecahedron: Beyond the Platonic Story. *Viruses* **2020**, *12*, 718. [[CrossRef](#)]
15. Chevillard, C.; Amen, A.; Besson, S.; Hannani, D.; Bally, I.; Dettling, V.; Gout, E.; Moreau, C.J.; Buisson, M.; Gallet, S.; et al. Elicitation of potent SARS-CoV-2 neutralizing antibody responses through immunization with a versatile adenovirus-inspired multimerization platform. *Mol. Ther.* **2022**, *30*, 1913–1925. [[CrossRef](#)]
16. Villegas-Mendez, A.; Garin, M.I.; Pineda-Molina, E.; Veratti, E.; Bueren, J.A.; Fender, P.; Lenormand, J.-L. In vivo delivery of antigens by adenovirus dodecahedron induces cellular and humoral immune responses to elicit antitumor immunity. *Mol. Ther. J. Am. Soc. Gene Ther.* **2010**, *18*, 1046–1053. [[CrossRef](#)]
17. Reina, J.J.; Maldonado, O.S.; Tabarani, G.; Fieschi, F.; Rojo, J. Mannose Glycoconjugates Functionalized at Positions 1 and 6. Binding Analysis to DC-SIGN Using Biosensors. *Bioconjug. Chem.* **2007**, *18*, 963–969. [[CrossRef](#)]
18. Bulteau, F.; Thépaut, M.; Henry, M.; Hurbin, A.; Vanwonterghem, L.; Vivès, C.; Le Roy, A.; Ebel, C.; Renaudet, O.; Fieschi, F.; et al. Targeting Tn-Antigen-Positive Human Tumors with a Recombinant Human Macrophage Galactose C-Type Lectin. *Mol. Pharm.* **2021**, *19*, 235–245. [[CrossRef](#)]
19. Achilli, S.; Monteiro, J.T.; Serna, S.; Mayer-Lambertz, S.; Thépaut, M.; Le Roy, A.; Ebel, C.; Reichardt, N.-C.; Lepenies, B.; Fieschi, F.; et al. TETRALEC, Artificial Tetrameric Lectins: A Tool to Screen Ligand and Pathogen Interactions. *Int. J. Mol. Sci.* **2020**, *21*, 5290. [[CrossRef](#)]
20. Schindelin, J.; Arganda-Carreras, I.; Frise, E.; Kaynig, V.; Longair, M.; Pietzsch, T.; Preibisch, S.; Rueden, C.; Saalfeld, S.; Schmid, B.; et al. Fiji: An open-source platform for biological-image analysis. *Nat. Methods* **2012**, *9*, 676–682. [[CrossRef](#)]

21. Collin, M.; Bigley, V. Human dendritic cell subsets: An update. *Immunology* **2018**, *154*, 3–20. [CrossRef] [PubMed]
22. Gout, E.; Schoehn, G.; Fenel, D.; Lortat-Jacob, H.; Fender, P. The Adenovirus Type 3 Dodecahedron's RGD Loop Comprises an HSPG Binding Site That Influences Integrin Binding. *J. Biomed. Biotechnol.* **2010**, *2010*, e541939. [CrossRef] [PubMed]
23. Wickham, T.J.; Mathias, P.; Cheresh, D.A.; Nemerow, G.R. Integrins $\alpha v\beta 3$ and $\alpha v\beta 5$ promote adenovirus internalization but not virus attachment. *Cell* **1993**, *73*, 309–319. [CrossRef]
24. Shi, X.; Jarvis, D.L. Protein N-Glycosylation in the Baculovirus-Insect Cell System. *Curr. Drug Targets* **2007**, *8*, 1116–1125. [CrossRef] [PubMed]
25. Harrison, R.L.; Jarvis, D.L. Protein N-glycosylation in the baculovirus-insect cell expression system and engineering of insect cells to produce 'mammalianized' recombinant glycoproteins. *Adv. Virus Res.* **2006**, *68*, 159–191.
26. Gong, Y.; Qin, S.; Dai, L.; Tian, Z. The glycosylation in SARS-CoV-2 and its receptor ACE2. *Signal Transduct. Target. Ther.* **2021**, *6*, 396. [CrossRef]
27. Thépaut, M.; Luczkowiak, J.; Vivès, C.; Labiod, N.; Bally, I.; Lasala, F.; Grimoire, Y.; Fenel, D.; Sattin, S.; Thielens, N.; et al. DC/L-SIGN recognition of spike glycoprotein promotes SARS-CoV-2 trans-infection and can be inhibited by a glycomimetic antagonist. *PLOS Pathog.* **2021**, *17*, e1009576. [CrossRef]
28. Porkolab, V.; Pifferi, C.; Sutkeviciute, I.; Ordanini, S.; Taouai, M.; Thépaut, M.; Vivès, C.; Benazza, M.; Bernardi, A.; Renaudet, O.; et al. Development of C-type lectin-oriented surfaces for high avidity glycoconjugates: Towards mimicking multivalent interactions on the cell surface. *Org. Biomol. Chem.* **2020**, *18*, 4763–4772. [CrossRef]
29. van Liempt, E.; Bank, C.M.; Mehta, P.; Garcí'a-Vallejoa, J.J.; Kawai, Z.S.; Geyer, R.; Alvarez, R.A.; Cummings, R.D.; van Kooyk, Y.; van Die, I. Specificity of DC-SIGN for mannose- and fucose-containing glycans. *FEBS Lett.* **2006**, *580*, 6123–6131. [CrossRef]
30. Zizzari, I.G.; Napoletano, C.; Battisti, F.; Rahimi, H.; Caponnetto, S.; Pierelli, L.; Nuti, M.; Rughetti, A. MGL Receptor and Immunity: When the Ligand Can Make the Difference. *J. Immunol. Res.* **2015**, *2015*, 450695. [CrossRef]
31. Boscheinen, J.B.; Thomann, S.; Knipe, D.M.; DeLuca, N.; Schuler-Thurner, B.; Gross, S.; Dörrie, J.; Schaft, N.; Bach, C.; Rohrhofer, A.; et al. Generation of an Oncolytic Herpes Simplex Virus 1 Expressing Human MelanA. *Front. Immunol.* **2019**, *10*, 2. [CrossRef] [PubMed]
32. Tuettenberg, A.; Becker, C.; Huter, E.; Knop, J.; Enk, A.H.; Jonuleit, H. Induction of strong and persistent MelanA/MART-1-specific immune responses by adjuvant dendritic cell-based vaccination of stage II melanoma patients. *Int. J. Cancer* **2006**, *118*, 2617–2627. [CrossRef] [PubMed]
33. Connio, J.; Scomparin, A.; Peres, C.; Yeini, E.; Pozzi, S.; Matos, A.I.; Kleiner, R.; Moura, L.I.F.; Zupančič, E.; Viana, A.S.; et al. Immunization with mannosylated nanovaccines and inhibition of the immune-suppressing microenvironment sensitizes melanoma to immune checkpoint modulators. *Nat. Nanotechnol.* **2019**, *14*, 891–901. [CrossRef] [PubMed]
34. Chauvin, J.-M.; Larrieu, P.; Sarrabayrouse, G.; Prevost-Blondel, A.; Lengagne, R.; Desfrançois, J.; Labarrière, N.; Jotereau, F.; Shin, J.H.; Park, J.-Y.; et al. HLA anchor optimization of the melan-A-HLA-A2 epitope within a long peptide is required for efficient cross-priming of human tumor-reactive T cells. *J. Immunol. Baltim. Md 1950* **2012**, *188*, 2102–2110. [CrossRef]
35. Del Val, M.; Schlicht, H.-J.; Ruppert, T.; Reddehase, M.J.; Koszinowski, U.H. Efficient processing of an antigenic sequence for presentation by MHC class I molecules depends on its neighboring residues in the protein. *Cell* **1991**, *66*, 1145–1153. [CrossRef]
36. Kloetzel, P.-M. Antigen processing by the proteasome: Ubiquitin and proteasomes. *Nat. Rev. Mol. Cell Biol.* **2001**, *2*, 179–188. [CrossRef]
37. Nussbaum, A.K.; Dick, T.P.; Keilholz, W.; Schirle, M.; Stevanović, S.; Dietz, K.; Heinemeyer, W.; Groll, M.; Wolf, D.H.; Huber, R.; et al. Cleavage motifs of the yeast 20S proteasome β subunits deduced from digests of enolase 1. *Proc. Natl. Acad. Sci. USA* **1998**, *95*, 12504–12509. [CrossRef]
38. Zhao, W.; Wu, J.; Chen, S.; Zhou, Z. Shared neoantigens: Ideal targets for off-the-shelf cancer immunotherapy. *Pharmacogenomics* **2020**, *21*, 637–645. [CrossRef]
39. Vragniau, C. Modification des Dodécaèdres Bases de L'adénovirus de Sérotype 3: Design et Caractérisation d'un Nouveau Vecteur Multi-épitopique Polyvalent. Ph.D. Thesis, Université Grenoble Alpes, Grenoble, France, 20 September 2018. Available online: <https://hal.archives-ouvertes.fr/tel-02110396> (accessed on 20 September 2018).
40. Villegas-Méndez, A.; Fender, P.; Garín, M.I.; Rothe, R.; Liguori, L.; Marques, B.; Lenormand, J.-L. Functional Characterisation of the WW Minimal Domain for Delivering Therapeutic Proteins by Adenovirus Dodecahedron. *PLoS ONE* **2012**, *7*, e45416. [CrossRef]
41. Galinier, R.; Gout, E.; Lortat-Jacob, H.; Wood, J.; Chroboczek, J. Adenovirus Protein Involved in Virus Internalization Recruits Ubiquitin-Protein Ligases. *Biochemistry* **2002**, *41*, 14299–14305. [CrossRef]
42. Zakeri, B.; Fierer, J.O.; Celik, E.; Chittock, E.C.; Schwarz-Linek, U.; Moy, V.T.; Howarth, M. Peptide tag forming a rapid covalent bond to a protein, through engineering a bacterial adhesin. *Proc. Natl. Acad. Sci. USA* **2012**, *109*, E690–E697. [CrossRef] [PubMed]

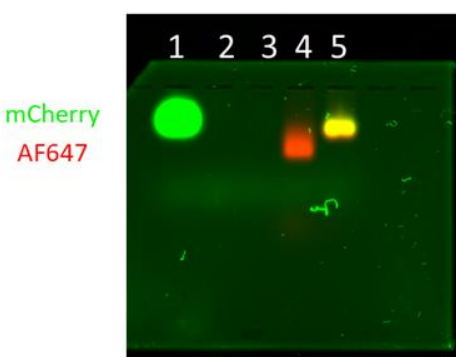


Supplementary figure S1: Separation of the complex ADD-mCherry from the left over mCherry-SC

(A) SDS PAGE gel of boiled and reduced samples showing left over mCherry-SC after incubation of ADD ST with mCherry-SC (B) SDS PAGE gel of boiled and reduced samples and sucrose gradient image showing the separation of the complex ADD mCherry and the left over mCherry-SC

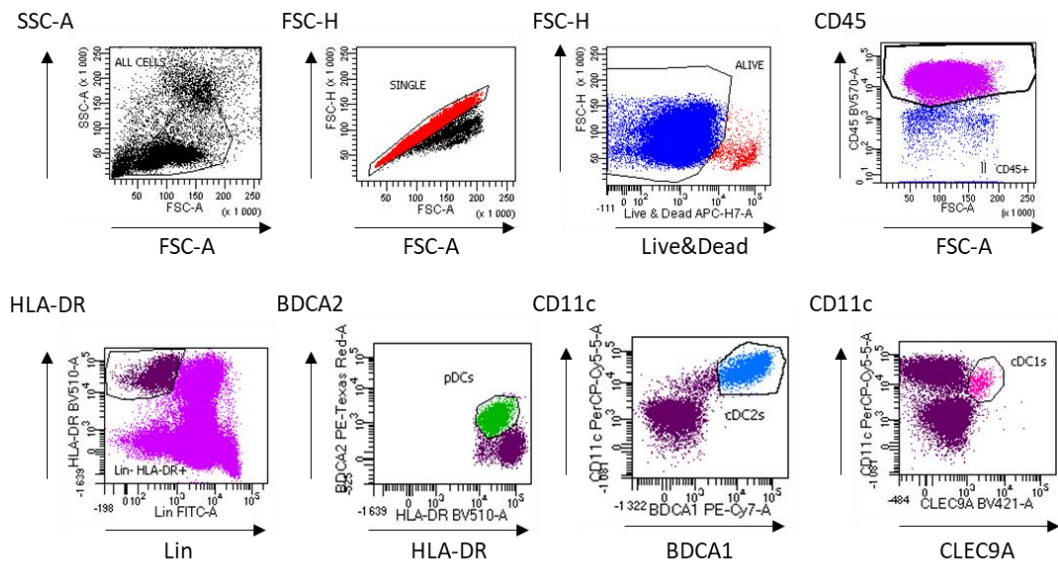
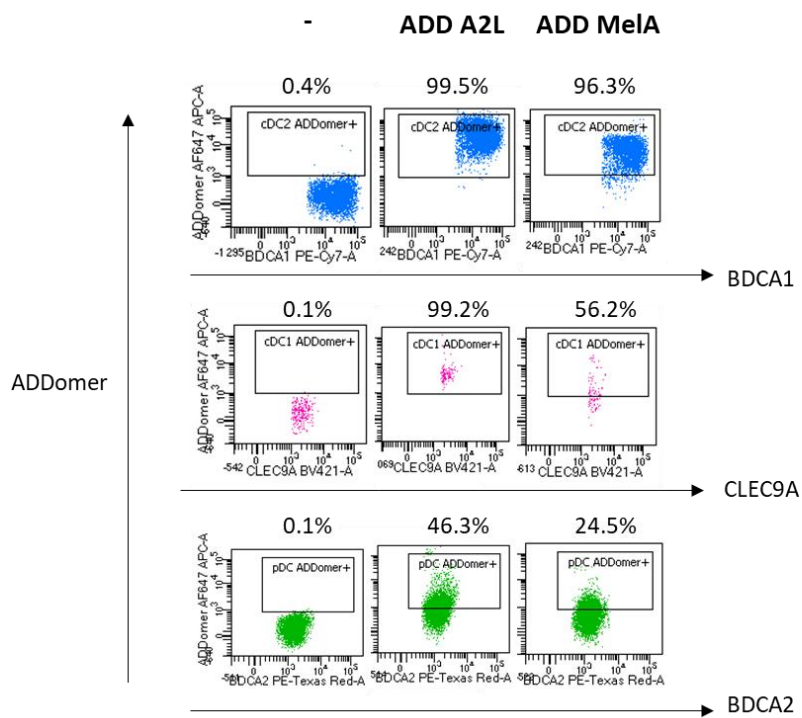
A**B**

1	2	3	4	5
mCherry-SC Crt +	RBD-SC Crt -	MelanA-SC Crt -	ADD ST (AF647)	ADD ST (AF647) mCherry



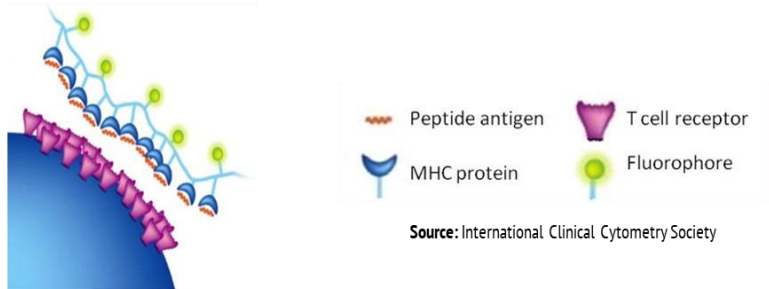
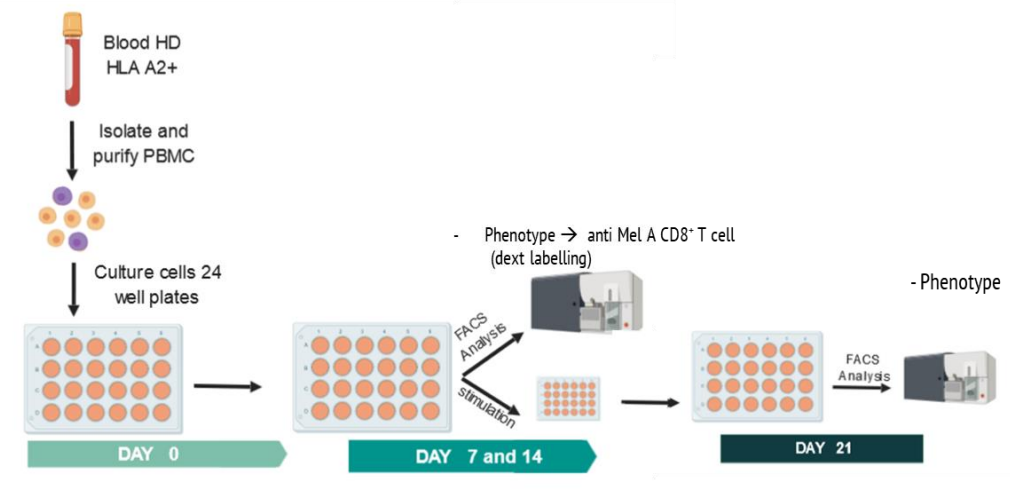
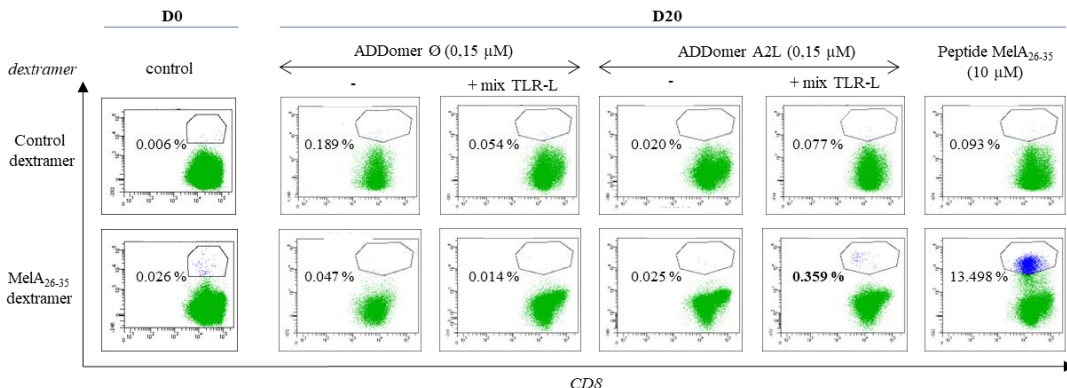
Supplementary figure S2: Preparation of ADDomers labelled with Alexa 647 for ADDomers internalisation evaluation by DC subsets

(A) Workflow of ADDomers AF647 preparation and purification (B) Agarose gel of labelled and non-labelled ADD mCherry.

A**B**

Supplementary figure S3: Dotplots of ADDomer fixation on DC subsets

(A) Gating strategy of DC subsets (B) ADDomer fixation on DC subsets.

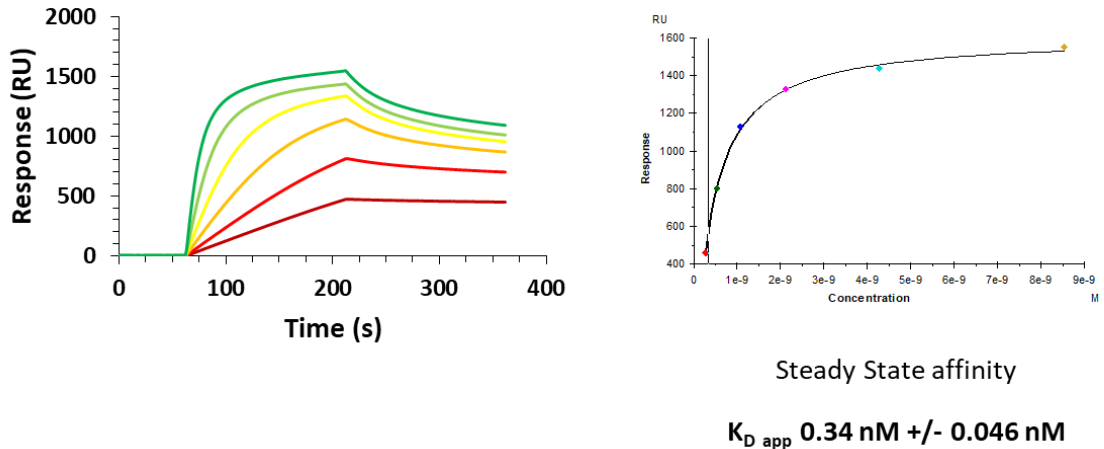
A**B****C**

Supplementary figure S4: ADD Ø and ADD A2L cross priming evaluation

(A) dextramer (B) Workflow of ADD Ø and ADD A2L cross priming evaluation (C)

Dot blots showing the percentage of CD8+ Dext MelA+ T cells at D0 and at D20 for each condition (dot plots pre-gated on CD45+ CD3+ CD8+ T cells).

ADD KGE RBD interaction with DC-SIGN



Supplementary figure S5: Zoom on ADD KGE RBD binding evaluation on DC-SIGN by surface plasmon resonance

Separate fitting of ADD KGE RBD with DC-SIGN.

Conclusion du chapitre :

Pour conclure, les travaux exposés dans ce chapitre montrent que les ADDomers présentant des épitopes et antigènes du mélanome sont capables d'induire une réponse immunitaire anti-tumorale *in vitro* sur des cellules dendritiques humaines de donneurs sains. Pour aller plus loin, il serait intéressant d'évaluer l'efficacité anti-tumorale de ces ADDomers chez un organisme vivant entier. Etant donné le fait que nous n'avons pas accès à des modèles animaux présentant un système immunitaire humain (souris humanisées par exemple) l'épitope A2L ainsi que l'antigène MelanA du mélanome humain ne peuvent plus être utilisés pour une évaluation chez l'animal. Le modèle chez la souris qui est communément utilisé pour le mélanome est le modèle B16 OVA. La lignée B16 OVA est une lignée de mélanome de souris exprimant l'antigène de poulet ovalbumine et est utilisée chez la souris pour l'étude de cancers de la peau. Ainsi, afin de pouvoir utiliser ce modèle nous avons remplacé les épitopes/antigènes de mélanome humain (A2L et MelanA) par des épitopes et antigènes de l'ovalbumine (OT-I, OT-II et ovalbumine). Ce travail *in vivo* est présenté dans le chapitre suivant.

Chapitre VI : Evaluation *in vivo* d'ADDomers présentant des épitopes et antigènes modèles du mélanome

Introduction du chapitre :

Dans ce chapitre nous présenterons les caractérisations *in vivo* qui ont été réalisées sur des souris C57bl6J greffées avec des cellules B16 OVA. Ces souris ont été injectées avec différents ADDomers présentant des épitopes ou antigènes modèles (ovalbumine) du mélanome.

Dans un premier temps plusieurs adjuvants ont été testés avec l'ADDomer afin de mettre en évidence celui induisant la meilleure réponse immunitaire. Puis, dans un deuxième temps la croissance tumorale a été évaluée dans différents schémas vaccinaux (prophylactique et thérapeutique).

Stimulation of the immune system by a tumor antigen-bearing adenovirus-inspired VLP allows control of melanoma growth

Solène Besson,¹ Emilie Boucher,² David Laurin,^{3,4} Olivier Manches,^{3,4} Caroline Aspord,^{3,4} Dalil Hannani,² and Pascal Fender¹

¹CNRS, University Grenoble Alpes, CEA, UMR5075, Institut de Biologie Structurale, 38042 Grenoble, France; ²University Grenoble Alpes, CNRS, UMR 5525, VetAgro Sup, Grenoble INP, TIMC, 38000 Grenoble, France; ³Institute for Advanced Biosciences, Immunobiology and Immunotherapy in Chronic Diseases, INSERM U 1209, CNRS UMR 5309, Université Grenoble Alpes, 38000 Grenoble, France; ⁴R&D Laboratory, Etablissement Français du Sang Auvergne-Rhône-Alpes, 38000 Grenoble, France

Virus-like particles (VLPs) are versatile protein-based platforms that can be used as a vaccine platform mainly in infectiology. In the present work, we compared a previously designed, non-infectious, adenovirus-inspired 60-mer dodecahedric VLP to display short epitopes or a large tumor model antigen. To validate these two kinds of platforms as a potential immunostimulating approach, we evaluated their ability to control melanoma B16-ovalbumin (OVA) growth in mice. A set of adjuvants was screened, showing that polyinosinic-polycytidylic acid (poly(I:C)) was well suited to generate a homogeneous cellular and humoral response against the desired epitopes. In a prophylactic setting, vaccination with the VLP displaying these epitopes resulted in total inhibition of tumor growth 1 month after vaccination. A therapeutic vaccination strategy showed a delay in grafted tumor growth or its total rejection. If the “simple” epitope display on the VLP is sufficient to prevent tumor growth, then an improved engineered platform enabling display of a large antigen is a tool to overcome the barrier of immune allele restriction, broadening the immune response, and paving the way for its potential utilization in humans as an off-the-shelf vaccine.

INTRODUCTION

Despite the genomic vaccine revolution seen during the coronavirus disease 2019 (COVID-19) pandemic,¹ protein-based vaccines remain attractive because of their low cost of production, ease of transport and storage, and better social acceptance. Virus-like-particles (VLPs) are non-infectious nanoparticles that assemble spontaneously, mimicking their corresponding virus and, thus, their immunogenicity. Two of the best known examples are the surface antigen of hepatitis B virus (HBV)² and the structural L1 protein of the human papillomavirus (HPV), which elicit antibodies preventing virus-induced cervical cancer from different HPV types.³ Beyond this, VLPs can be used as a scaffold for display of epitopes derived from other biological targets. The immunogenicity is highly increased through presentation to the immune system in a multimeric manner, and a number of vaccine platforms have been developed to this aim,

with various advantages and limitations.⁴ One advantage is that the small size of VLPs (less than 100 nm) permits efficient drainage to the lymph nodes, which can favor the immune response.^{5,6} Formulation with an adequate adjuvant, such as inorganic salts (alum), an oil emulsion (MF59), or a lipid A component (monophosphoryl lipid [MPL]) is often used and depends on the platform/antigen tandem and the targeted application.⁷

From a manufacturing point of view, two main approaches can be considered for presentation of epitopes at the VLP surface. Chemical cross-linking has been reported to induce a good titer of neutralizing antibodies but makes the manufacturing workflow more complex and increases the cost of production. Genetic insertion of the epitope into the VLP enables an easier way of production and purification but may face the risk of epitope misfolding and/or VLP self-assembly issues during production. Because this limitation increases with the size and complexity of the epitope to be inserted, large antigen display cannot be considered using this approach. To overcome this issue, a two-component system called SpyTag/SpyCatcher (ST/SC) has been developed. In this system, derived from *Streptococcus pyogenes*, an aspartate residue from the 13-amino-acid ST peptide genetically inserted in the VLP can spontaneously create a covalent bond with a lysine residue in the complementary SC module that can be fused to large antigens.^{8–11}

We have reported previously that a non-infectious VLP derived from the human adenovirus of type 3 and consisting of 60 identical penton base monomers could be exploited to display epitopes of interest on its surface.^{6,12,13} In this vaccine platform, called adenovirus dodecamer (ADDomer), exposed loops of the penton base protein were engineered to allow insertion of foreign peptides, such as a linear neutralizing epitope from chikungunya virus. However, this design did not permit insertion of structurally complex antigens. To

Received 31 August 2022; accepted 5 December 2022;
<https://doi.org/10.1016/j.omtm.2022.12.003>.

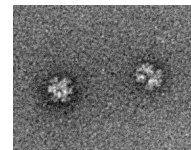
Correspondence: Pascal Fender, CNRS, University Grenoble Alpes, CEA, UMR5075, Institut de Biologie Structurale, 38042 Grenoble, France.
E-mail: pascal.fender@ibs.fr



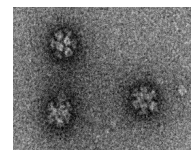
A



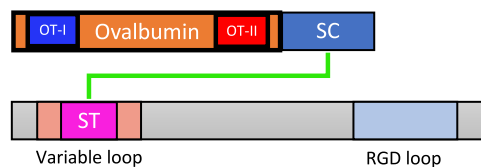
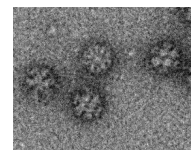
ADDomer Ø



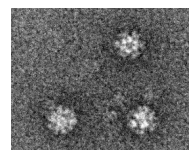
ADDomer Duo



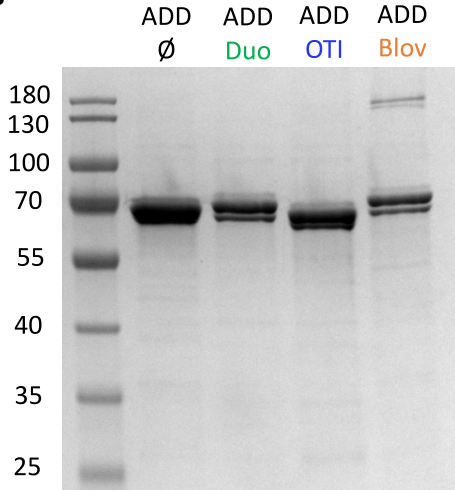
ADDomer OT I



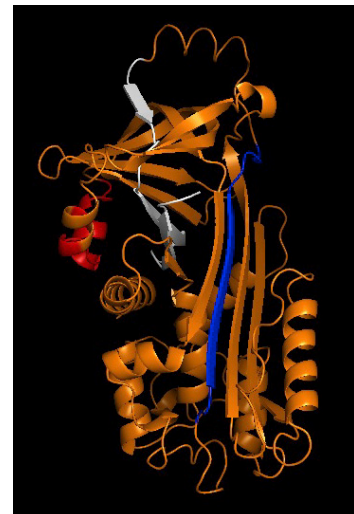
Blov SC
ADD ST
ADDomer Blov



B



C



D

GSIGAASMEFCDFVKELKVHHANETIFYCPIAIMSALAMVYLGAKDSTRTQINKVVRFDKLPFGFDSIEACQGTSVN VHSSLRDILNQITKPNDVYSF
SLASRLYAEERYPILPEYLOCVKELYRGGLEPINFQTAADQARELINSVVESQTNGIIRNLQPSVSDQTAAMLVNAIVFKGLWEKAFKDEDTQAMP
FRVTEQEKS PKPVQMMYQIGLFRVASMASEKM KILELPFASGTM SMLVLLPDEVSGLEQL ESIINFEKLT EWTSS NVMEERKIKVYLPRMKMEEKYNLT
FVL MAMGITDV FSS SANLS GISSAESLK ISQAVHAAHAEINEAGRE VVVGSAEAGVDAASV ASGGTVDTLSGLSSEQGQSGDMTIEEDSATHIKFSKRD
EDG KELAGATMELR DSSGKTISTWISDGQVKDFYLYPGKYTFVETAAPDGYEVATAITFTVNEQGQVTNGKATKGDAHIGSGHHHHHH

(legend on next page)

overcome this limitation while keeping the immunogenicity advantage of ADDomer, we redesigned this platform by genetically inserting an ST. Spontaneous display of large and structurally complex antigens with potential post-translational modifications, such as the severe acute respiratory syndrome coronavirus 2 (SARS-CoV-2) receptor binding domain (RBD) fused to the SC was achieved. This system has proven to be highly effective to elicit potent neutralizing antibodies against SARS-CoV-2.¹⁴

In this work, we assess the potential of these two vaccine platforms (direct epitope display and large antigen fusion via SC) in the context of cancer immunotherapy, using the melanoma B16-ovalbumin (OVA) model in mice. An investigation of the cellular immune response underlying tumor growth control is also performed.

RESULTS

MHC class I and class II OVA epitopes can be displayed successfully on the ADDomer surface

The ADDomer is a non-infectious nanoparticle formed of 12 bricks of the homopentameric penton base from the human adenovirus type 3. Two exposed loops can be used for insertion of epitopes: the variable loop (VL) and the RGD (Arg-Gly-Asp) loop (RGD-L). The major histocompatibility complex (MHC) class I epitope (SIINFEKLTEWTSS, called OT-I) and the MHC class II epitope (ISQAVHAAHAEI NEAGR, called OT-II) from the OVA were genetically inserted into the RGD-L and VL respectively. These two epitopes have been chosen to initiate a CD8⁺ T lymphocyte immune response (via the epitope OT-I presented to CD8 by dendritic cells) as well as a CD4⁺ T lymphocyte immune response (via the epitope OT-II presented to CD4⁺ T cells by dendritic cells). Because of the spontaneous homooligomerization of the 12-pentameric penton bases, 60 copies of each epitope are exposed on the surface of the ADDomer particle, called ADDomer-Duo (ADD-Duo) (Figure 1A). The ADD-Duo was successfully produced in a baculovirus expression system and purified in two steps (Figure 1B). Negative-stain electron microscopy showed that particles harboring these two epitopes were well folded (Figure 1A). An ADDomer displaying only the OT-I epitope was also generated.

Immunization with ADD-Duo in combination with the poly(I:C) adjuvant elicits a potent cellular and humoral anti-OVA response compared with the other adjuvants used

We aimed to define the best adjuvant to use in combination with the ADDomer vaccine. To do so, mice were vaccinated with ADD-Duo without or with a different set of adjuvants according to a prime-boost schedule (Figures 2A and 2B). Mice vaccinated with an “empty”

ADDomer (ADD-Ø; i.e., an ADDomer that does not display any OVA epitopes) were used as a control. For the adjuvant screening, three different adjuvants were screened separately or in combination (i.e., the three adjuvants together). These different adjuvants aim to target different Toll-like receptors (TLRs) on the three human dendritic cells subtypes (Figure 2B), each of them being representative of one subset. MPLA targets the TLR4 mostly present on cDC2, poly(I:C) (polyinosinic-polycytidylic acid) targets the TLR3 mostly present on cDC1, and ODN 2395 (oligodeoxynucleotide containing an unmethylated CpG motif) targets the TLR9 mostly present on pDC (plasmacytoid Dendritic Cell). To define the best ADD-Duo/adjuvant combination, mice were split into 6 groups (Figure 2B). On day 14, mice were sacrificed, and their immune response was analyzed in their circulating blood, spleen, and injection site-draining lymph nodes (Figure 2A).

The frequency of antigen-specific CD8⁺ T cells has been determined in the draining lymph nodes and the spleen using a dextramer staining. Poly(I:C) alone was the adjuvant that gave the most homogeneous anti OT-I immune response in the draining lymph nodes (Figure 2C). In the spleen, it was more difficult to determine the best combination because two mice of three in group 5 (poly(I:C)) showed a similar response as the other groups. However, the third mouse of this group showed the highest percentage of specific CD8⁺ T lymphocytes compared with all other mice of all groups.

Humoral response against the OT-II peptide was also investigated by ELISA (Figure 2D). Again, poly(I:C) gave the highest responses, and the combination of the three adjuvants together did not significantly improve the response compared with poly(I:C) alone (Figure 2D).

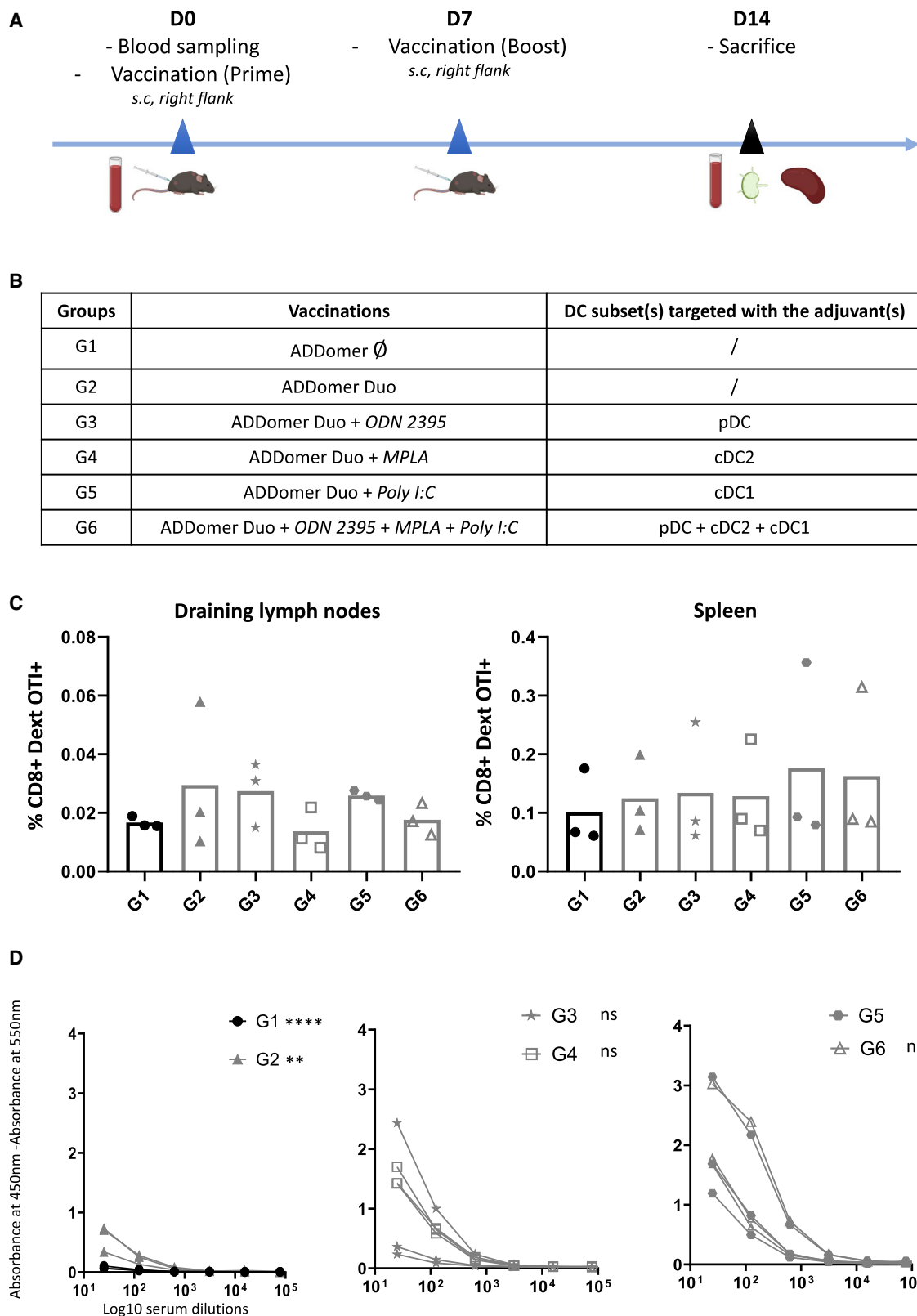
The results show that the association of the three adjuvants did not give a better response (cellular and humoral) than poly(I:C) alone. In particular, in the draining lymph nodes, the response obtained with the association of the three adjuvants is lower than the one obtained for poly(I:C) alone. This suggests that the cDC1 subset was probably the main dendritic cell (DC) subset involved in mounting an immune response against the epitopes displayed by the ADDomer. Poly(I:C) is thus a well-suited adjuvant for ADDomer vaccination *in vivo*. This is in line with other studies using poly(I:C) for therapeutic anti-cancer vaccines.^{15,16}

Immunization with ADDDuo+poly(I:C) protects against B16-OVA tumor challenge

To assess the functionality of antigen-specific T cells induced by ADDomer vaccination, vaccinated mice were challenged with a

Figure 1. Design and characterization of ADD-Ø, ADD-Duo, ADD-OT-I, and ADD-Blov

(A) Diagram showing the insertion of epitopes (OT-I, blue; OT-II, red) and SpyTag (ST; pink) in the 2 loops of the ADDomer monomer. ST (pink) can make an isopeptidic bond with SpyCatcher (SC; blue) fused to the OVA protein (orange) containing the OT-I and OT-II epitopes. Negative-stain electron micrographs of ADD-Ø, ADD-Duo, ADD-OT-I, and ADD-Blov (bar, 30 nm) are shown on the right. (B) SDS-PAGE profile of reduced and boiled samples of ADD-Ø, ADD-Duo, ADD-OT-I, and ADD-Blov, showing a higher-molecular weight (MW) covalent adduct for the ADD-Blov (ADD-ST/Blov-SC). (C) Structure of the OVA protein with the epitopes OT-I and OT-II highlighted, respectively, in blue and red. The protein structure colored in white was removed and replaced by the SC to give the Blov-SC protein. (D) Sequence of Blov-SC with OVA (orange; OT-I and OT-II epitopes highlighted, respectively, in blue and red), SC (blue), and additional linkers and histidine tag (black).



(legend on next page)

subcutaneous OVA-expressing tumor inoculation (prophylactic setting). Mice were vaccinated 5 times every 2 or 3 days with ADD-Duo+poly(I:C) (Figure 3A). ADD-Ø was used as a control (Figure 3B). Nearly 4 weeks (25 days) after the last injection, mice were challenged with subcutaneous implantation of the tumor cell line B16-OVA. This cell line expresses the OVA antigen containing the two epitopes OT-I and OT-II, which are displayed on ADD-Duo.

Tumor growth was monitored, and mice were sacrificed on day 17, when the first tumor reached the ethical tumor size limit. Mice that received ADD-Ø developed tumors, whereas mice that received ADD-Duo did not have visible tumors on day 17. (Figure 3C). This result shows that the immune response induced by vaccination was specific to the tumor antigens borne by the vehicle and not due to an indirect stimulating response triggered by the vehicle itself. Remarkably, even though a gap of nearly 4 weeks passed between the last vaccination and the challenge, none of the mice showed tumor growth, reflecting that a robust response was mounted during this immunization period.

Large OVA antigen can be successfully displayed on the ADDomer's surface

To get rid of the allelic restriction and elicit a multi-specific anti-tumor response, display of large antigens rather than small epitopes on the ADDomer surface is desirable. To do so, an ADDomer displaying the ST peptide (ADD-ST) on its surface was used to spontaneously make an isopeptidic bond with an SC fused to the OVA protein (1–355), called binder long OVA (Blov), containing the OT-I and OT-II epitopes (Figures 1A and 1D). The OVA C terminus sequence (356–396, colored white in Figure 1C) buried in the protein was removed and replaced with the SC prolonged with a histidine tag. This OVA C-terminus deletion aimed to make the SC more accessible to the ST to favor Blov-SC assembly to ADD-ST. A melittin signal peptide was added to Blov fused to SC (Blov-SC) to allow protein post-translational modifications (PTMs), such as glycosylations and secretion from insect cells. ADD-ST and Blov-SC were produced separately in insect cells using the baculovirus expression system.

Covalent binding of Blov-SC to ADD-ST was assessed by SDS-PAGE. As expected, an adduct of a higher molecular weight corresponding to Blov-SC bound to the ADD-ST monomer was clearly seen (Figure 1B). This faint band, observed around 180 kDa, reflects weak binding of Blov-SC to ADD-ST (3 Blov-SCs per ADD-ST particle), which is lower than the theoretical ratio used for incubation (ratio of 4:1, meaning 15 Blov-SCs per ADD-ST particle). Electron micrographs showed that particles remained intact after antigen binding (Figure 1A).

Therapeutic vaccination with ADD-Duo, ADD-OT-I, and ADD-Blov drastically decreases tumor growth and improves mouse survival

To assess the efficacy of the ADDomer vaccine in a therapeutic setting, mice were vaccinated 5 times every 2–3 days with ADD-Duo, ADD-OT-I, and ADD-Blov from 1 day after tumor inoculation. ADD-Ø was used as a control, and all ADDomers were injected with poly(I:C) (Figures 4A and 4B). Each group was composed of 12 mice; 6 were euthanized on day 15 to evaluate immunological responses and the others (5 or 6 per group according to the success of tumor implantation) when the maximal ethical tumor size was reached to investigate the long-term clinical response.

On day 15, mice vaccinated with ADD-Duo, ADD-OT-I, and ADD-Blov had a significantly smaller tumor than mice vaccinated with ADD-Ø. For example, on day 15, the mean tumor size for the ADD-Ø group was 81.7 mm² versus 16.8 mm² for the ADD-Duo group (Figure 4C). Visual inspection showed a massive difference in tumor size between the ADD-Ø and ADD-OT-I groups (Figure 4D, center panel). Macroscopic observation showed a well-vascularized tumor in mice vaccinated with ADD-Ø, whereas a much smaller and very poorly vascularized tumor was seen in mice vaccinated with ADD-OT-I (Figure 4D, left and right panel, respectively).

Cellular response was investigated (Figures 5 and S2). In the spleen, a higher OVA-specific CD8⁺ T cell frequency was observed with the ADD-Duo and ADD-OT-I groups compared with the ADD-Ø group. However, the difference between the ADD-Blov and ADD-Ø groups was not significant (Figure 5A, left). In the tumor, tumor-infiltrating OVA-specific CD8⁺ T cell frequency was higher with the ADD-Duo, ADD-OT-I, and ADD-Blov groups versus the ADD-Ø group (Figures 5A, right, and 5B). This observation could only be made on one tumor for the treated groups (ADD-Duo, ADD-OT-I, and ADD-Blov) because only one tumor was available for analysis as a result of the high efficiency of the vaccination regarding tumor growth. A similar trend was observed in the spleen and in the tumor when looking at the absolute number of OVA-specific CD8⁺ T lymphocytes (Figure 5C).

Therapeutic vaccination improves mouse survival in all vaccinated groups and notably for the group of mice vaccinated with ADD-OT-I and ADD-Blov (Figure 6A). Individual tumor growth experiments showed that all tumors were well controlled, even over 60 days of follow up, and only one mouse from two groups escaped from immunological control (Figure 6B, groups ADD-OT-I and ADD-Blov).

DISCUSSION

In this study, we assessed the potential use of an adenovirus-inspired non-infectious VLP as a potential therapeutic anticancer vaccine. The

Figure 2. ADD-Ø and ADD-Duo immunogenicity evaluation and adjuvant screening

(A) Immunization schedule, blood sampling, and organ collection for all groups. s.c., subcutaneous. (B) Different groups were evaluated regarding the immunogenicity of ADD-Ø (G1), ADD-Duo (G2), ADD-Duo + 1 adjuvant (G3, G4, G5), and ADD-Duo + 3 adjuvants (G6). (C) Percentage of CD8⁺ dextramer OT-I⁺ T lymphocytes in the draining lymph nodes and spleen for all groups (n = 3). (D) Ab response against OT-II peptide on day 14 (n = 3).

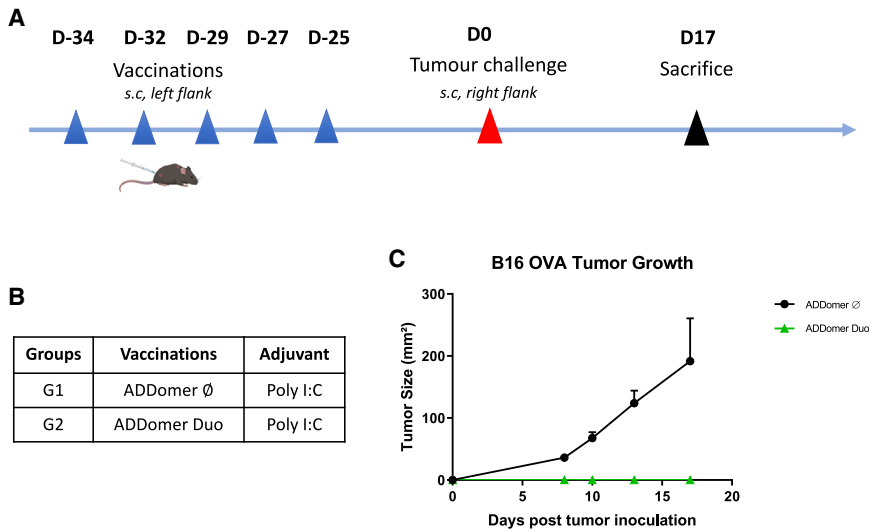


Figure 3. Tumor challenge of mice vaccinated previously with ADD-Ø and ADD-Duo

(A) Immunization and tumor challenge schedule for all groups. (B) Different groups were evaluated regarding the protective effect of ADD-Ø (G1) and ADD-Duo (G2) against a tumor challenge. Both ADDomers were injected with the poly(I:C) adjuvant, and the tumor challenge was performed using the B16-OVA cell line. (C) Tumor size evolution days after tumor inoculation (n = 3).

investigated VLP originally results from spontaneous assembly of 12 homopentameric penton bases from a human adenovirus of type 3 (HAdV-B3).¹⁷ Engineering of this 60-mer VLP, called ADDomer, enabled easy and rapid genetic insertion of short epitopes at two different locations of the particle surface. This vaccine platform has been shown recently to trigger a significant neutralizing humoral response against a 19-amino-acid epitope from chikungunya virus.⁶

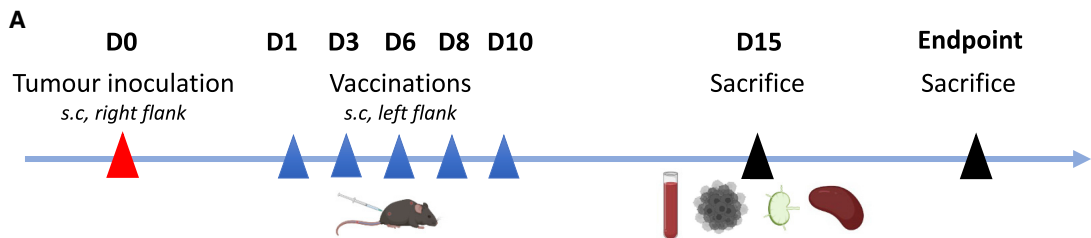
OVA is a well-characterized antigen encompassing the immunodominant MHC class I-restricted OVA_{257–264} (SIINFEKL) and the MHC class II-restricted OVA_{323–339} (ISQAVHAAHAEINEAGR) epitopes. This OVA system is often used to investigate the immunization potential of novel vaccine platforms or vaccine candidates against different cancers, including melanoma.^{18–20} To bind the MHC class I proteins, class I epitopes must be processed by the proteasome into 8- to 10-amino-acid peptides. Because the cleavage efficiency is influenced by the flanking regions,^{21,22} special attention must be paid to the directly neighboring epitope. It is known that small amino acid residues, such as glycine or alanine, favor antigen processing by the proteasome.²³ Here we genetically inserted the MHC class I OVA epitope flanked by GSGG linkers alone in the RGD-L or in combination with an MHC class II OVA epitope in the VL (Figure 1A). In both cases, the VLPs displaying MHC class I alone or both epitopes at once resulted in nicely folded VLPs, as seen by transmission electron microscopy (Figure 1A).

To obtain an optimized vaccine formulation, it is often necessary to combine an adjuvant to the vaccine platform/antigen tandem. Adjuvants enhance the magnitude, breadth, and durability of the immune response and can orient the balance between the humoral and cellular response.²⁴ Despite identification of TLRs expressed on DCs sensing the different pathogen-associated molecular patterns (PAMPs),^{25,26} the choice of adjuvant is still empirical. The immune response triggered by ADD-Duo occurred in the absence or presence of a set of adjuvants known to activate different subsets of DCs. ODN 2395, MPLA,

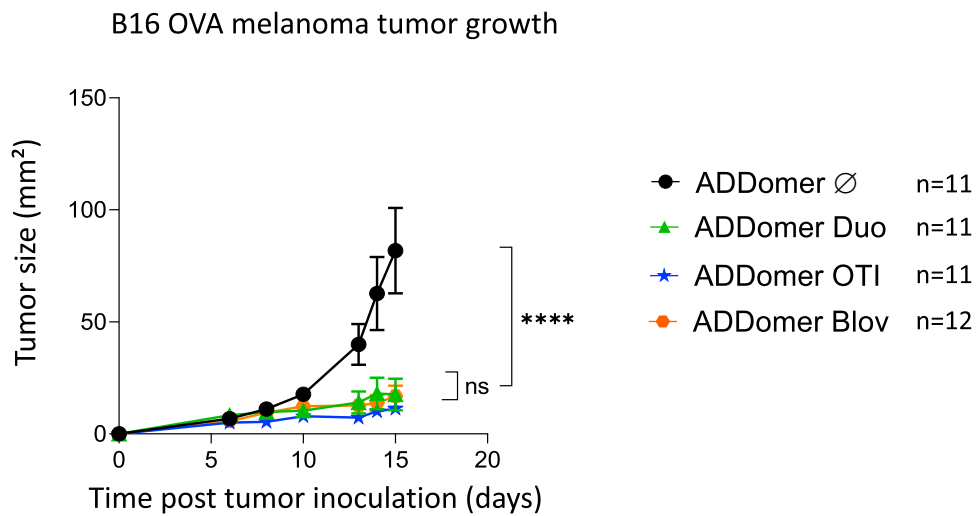
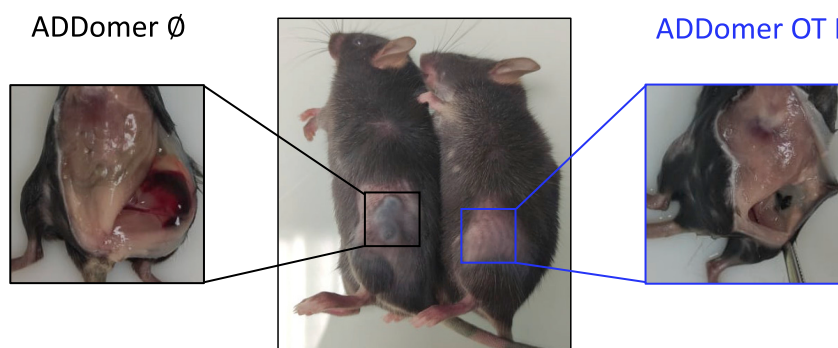
and poly(I:C), activating pDC, cCD2, and cCD1, respectively, were tested (Figure 2). Poly(I:C) gave the most homogeneous OVA-specific CD8 response in the draining lymph nodes and spleen as well as a good humoral response against the MHC class II OVA epitope. Poly(I:C) has been reported to interact with TLR3²⁷ and is often used in cancer immunotherapy trials²⁸ because it triggers potent Th1-mediated anti-tumor immunity through cDC1 targeting.

In a first attempt, we studied the possibility of preventing tumor growth in vaccinated mice. For this purpose, immunizations were performed with ADD-DUO in the presence of poly(I:C) with a delay of 25 days between the last injection and tumor implantation. Tumor growth was monitored until the ethical endpoint was reached. Contrary to the rapid increase in tumor size seen in the group vaccinated with the empty ADDomer (i.e., vehicle not displaying OVA epitopes), no tumors were seen in mice vaccinated with ADD-Duo (Figure 3C). This result shows that the anti-tumor effect was indeed due to the epitope displayed by the vector and not due to non-specific activation of the immune system. This protection seems to last for a long time because there was a delay of 25 days between the last immunization and tumor implantation, suggesting elicitation of a potent memory CD8⁺ T cell response.

Genetic insertion of sequences coding short epitopes, such as OT-I and OT-II (14 and 17 residues, respectively), in the two exposed loops of the ADDomer did not affect the overall particle structure (Figure 1A), and the slightly faster migration of OT-I compared to ADDomer-Ø is likely due to its sequence composition²⁹ because mass spectroscopy analyses confirmed the exact molecular weight of these two constructs. In humans, an epitope-based vaccine would represent an important limitation because use is restricted to a particular HLA-bearing population (for instance an HLA-A2-restricted epitope-based vaccine would be suitable only for around 40% of the European population). It would be desirable to overcome this limitation by developing a fully protein-based vaccine, enabling epitope presentation in all individuals (i.e., developing an off-the-shelf vaccine).³⁰ Thus, displaying large antigens rather than short epitopes would be valuable. Unfortunately, genetic insertion of large folded antigens results in subunit misfolding and insolubility.³¹ Villegas et al.^{20,32} have shown that the OVA_{248–376} antigen could be fused to

**B**

Groups	Mice number	Vaccinations	Adjuvant	Mice sacrificed at D15	Mice sacrificed at endpoint
G1	12	ADDomer Ø	Poly I:C	6	6
G2	12	ADDomer Duo	Poly I:C	6	6
G3	12	ADDomer OTI	Poly I:C	6	6
G4	12	ADDomer Blov	Poly I:C	6	6

C**D**

(legend on next page)

WW domains (containing two conserved tryptophans) to make interactions with the adenovirus PPxY sequences in the adenovirus penton base. However, this non-covalent interaction relied on a relatively low K_D (65 nM)³³ that did not warrant a homogeneous batch required for clinical trials. To overcome this limitation, insertion of an ST (13 residues) in the exposed loops of the ADDomer has been reported to permit spontaneous and covalent attachment of large and correctly folded antigens, such as the SARS-CoV-2 RBD, to the particle.^{8,14} Fusion of OVA₁₋₃₅₅ (Blov) to the SC successfully resulted in display of this antigen to the vaccine platform (Figures 1A and 1B).

Therapeutic vaccination where tumor implantation occurred prior to vaccination has been performed using an ADDomer with genetic epitope insertion and large OVA antigen display using the ST/SC system. Both systems were efficient at preventing B16-OVA tumor growth (Figure 4C). The different OVA-bearing VLPs (30 nm for the undecorated particle) are within the size range (20–200 nm) of particles readily drained to lymph nodes, potentiating uptake by antigen-presenting cells and cross-presentation.^{34,35} These immunizations seemed to elicit robust and sustained immune responses capable of rejecting the highly aggressive B16-OVA melanoma in prophylactic and therapeutic strategies (Figures 3 and 4).

Because CD8⁺ T cells are key players in immuno-oncology, most efforts in vaccine development focus on generation of this response by improving antigen delivery and presentation on the DC surface for the initial T cell encounter.³⁶

In our experiments, immunological characterization showed a significant OVA-specific CD8⁺ T cell response in the spleen of mice vaccinated with ADD-Duo and ADD-OT-I (Figures 5A and 5C). A similar tendency was also observed in the only residual tumor where this analysis was feasible (Figures 5B and 5C). However, because of the low number of mice presenting a tumor with a size suitable for this analysis, we cannot draw a solid conclusion regarding this observation. Surprisingly, the anti-OT-I CD8⁺ T cell response in the spleen of mice vaccinated with ADD-Blov was not significant compared with control ADD-Ø. By contrast, this response seemed to be significant compared with the control group within the tumor (4.08% versus 0.28%). Despite the low amount of tumor material that could be analyzed in the ADD-Blov group, this tendency is highly supported by tumor growth control as well as long-term mouse survival (Figures 4C and 6A, respectively). In Blov mice, multi-specific immune responses could have been triggered, improving the tumor control, even though such multi-specific responses were not investigated here (only response against a single epitope was investigated). Such

multi-specific responses could be investigated through cytokine production upon *ex vivo* T cell restimulation with APC loaded with OVA.

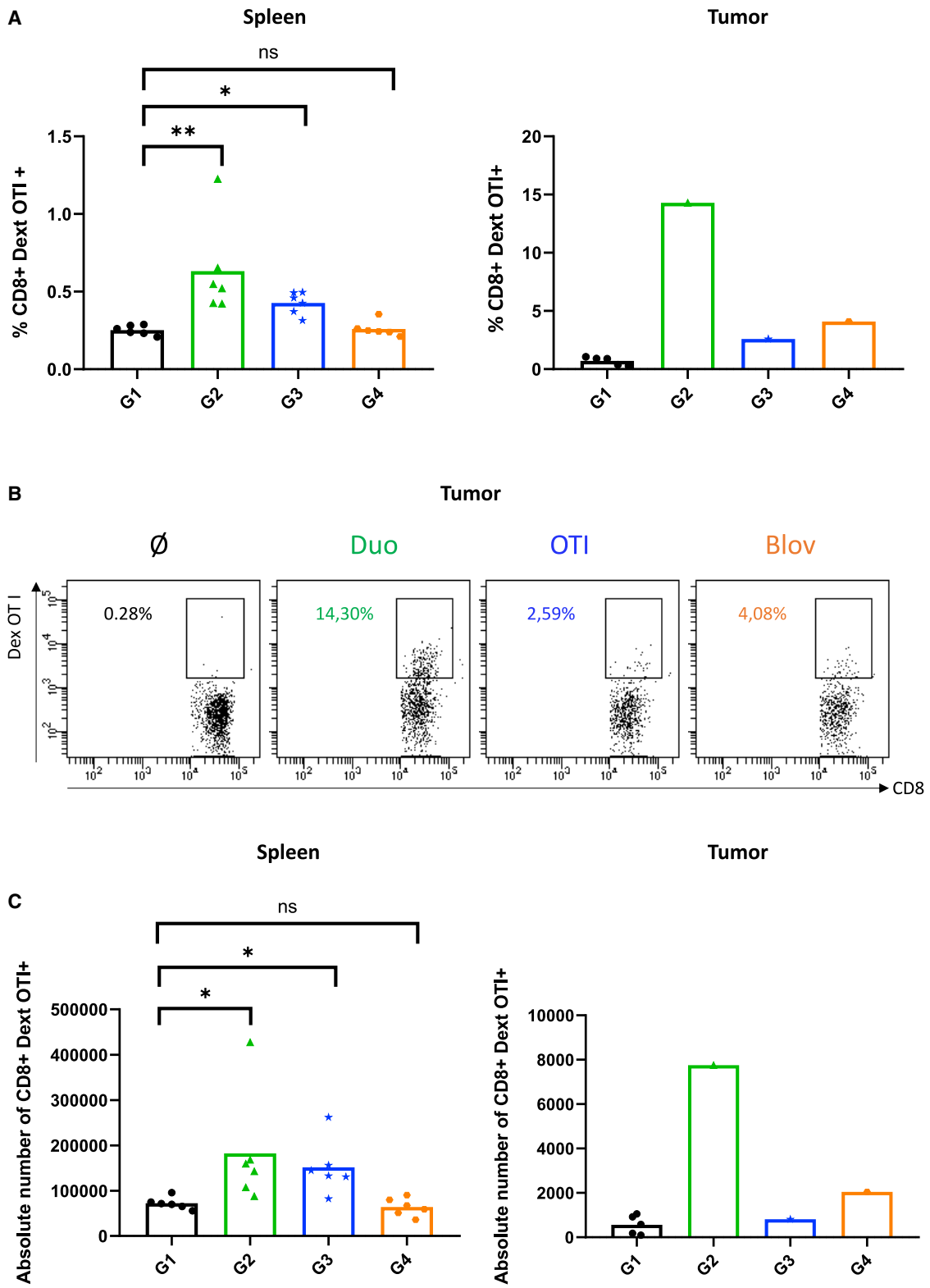
Another unexpected feature was the presence of a strong, anti-OVA CD8⁺ T cell response in the spleen and in measurable tumors of mice vaccinated with ADD-Duo, which was not correlated with the long-term survival curves. We propose two possible hypotheses to explain these data: generation of regulatory T cells and/or tumor escape. It is conceivable that addition of a unique CD4⁺ T cell epitope, as opposed to ADDomer-OT-I or full OVA protein, triggered a regulatory T cell response which, in turn, impaired efficient anti-tumor immunity despite a high proportion of anti-OVA CD8⁺ T cells. Another explanation could be tumor escape from anti-OVA CD8⁺ T cells by MHC class I loss and/or strong immune checkpoint expression. The ADD-Duo vaccine triggered the highest immunization in spleen and tumor (Figure 5). One can imagine that, upon strong immune pressure, tumor cell clones lacking MHC class I expression were selected and/or that OVA-specific T cell-derived interferon γ (IFN γ) triggered high PD-L1 expression by tumor cells, leading to their inhibition and subsequent tumor escape. To address these hypotheses, fluorescence-activated cell sorting (FACS) analysis of OVA-specific FoxP3 regulatory T cells as well as MHC class I, PD-L1, and PD-1 expression would be required.

Our data show that the ADDomer is well suited to mount an efficient anti-tumoral response. Genetic insertion of epitopes directly in the ADDomer loops is based on single-particle expression but limited to short epitopes, thus restricting its use to personalized medicine or stratified patients. Display of large antigen required expression of ADD-ST and the large cargo fused to the SC. Because of the autocatalytic reaction, simple addition of both components resulted in “ready-to-use” immunotherapy applicable to a large population. With this latter strategy, a mosaic vaccine displaying several different antigens at once can be produced,^{37,38} paving the way for next-generation products with a broader immunological spectrum for off-the-shelf cancer immunotherapy.

Improvement of the technology can be envisioned to combine our platform with other therapeutic strategies, such as oncolytic viruses (OVs). Indeed, a similar approach has already been reported with oncolytic adenovirus encoding OVA or melanoma epitopes directly into the tumor.³⁹ It could be feasible to combine the respective advantages of OVs and particle display by designing an oncolytic adenovirus encoding the ADDomer-ST and the antigen of interest fused to an SC to benefit from tumor lysis and *in situ* immune stimulation.

Figure 4. Effect of therapeutic vaccination with ADDomers on B16-OVA tumor growth

(A) Tumor inoculation, immunization, blood sampling, and organ collection for all groups. (B) Different groups were evaluated regarding the therapeutic effect of ADD-Ø (G1), ADD-Duo (G2), ADD-OT-I (G3), and ADD-Blov (G4). ADDomers were injected with the poly(I:C) adjuvant, and tumor inoculation was performed using the B16-OVA cell line. Each group is composed of 12 mice; 6 were sacrificed on day 15 to evaluate the short-term clinical and immunological response, and the remaining mice ($n = 5$ for ADD-Ø/Duo/OT-I, $n = 6$ for ADD-Blov) were sacrificed when the endpoint was reached to investigate a long-term response. (C) Tumor size evolution days after tumor inoculation ($n = 11$ for ADD-Ø/Duo/OT-I, $n = 12$ for ADD-Blov). (D) Photographs showing the difference in tumor size and aspect on mice vaccinated with ADD-Ø or ADD-OT-I.



(legend on next page)

MATERIALS AND METHODS

Baculovirus production

The baculovirus expression system was used for production of the different ADDomers (ADD-Ø, ADD OT-I, ADD-Duo, and ADD-ST) and for OVA fused to SC (Blov-SC). Synthetic DNA (Genscript) was cloned in pACEBac1 using the restriction sites BamHI and HindIII. For Blov-SC, the OVA sequence (1–355) was cloned upstream of the SC, and a His₆ tag was added to the C-terminus of SC. This fusion protein was secreted using the melittin signal peptide in the vector. Recombinant baculoviruses were made by transposition with an in-house bacmid expressing yellow fluorescent protein, as described previously.⁶ The baculovirus was amplified on Sf21 cells at a low multiplicity of infection (MOI), and after two amplification cycles, it was used to infect insect cells for 64–72 h at a high MOI. For ADDomer production, the infected cells were pelleted and recovered, whereas for Blov-SC, cells were discarded, and the supernatant was saved.

Protein purification

ADDomer purification

The ADDomers were purified according to a classic protocol.⁴⁰ Briefly, after lysis of the insect cell pellet by three cycles of freezing-thawing in the presence of Complete protease inhibitor cocktail (Roche) and removal of debris, the lysate was loaded onto a 20%–40% sucrose density gradient. The gradient was centrifuged for 18 h at 4°C at 41,000 rpm on an SW41 rotor in a Beckman XPN-80 ultracentrifuge. The dense collected fractions at the bottom of the tubes were dialyzed against HEPES (10 mM, pH 7.4) and NaCl (150 mM) and then loaded onto a Macroprep Q cartridge (Bio-Rad). After elution by a 150–600 mM linear NaCl gradient in HEPES (10 mM, pH 7.4), ADDomer-containing fractions were checked by SDS-PAGE and concentrated on Amicon (MWCO, 100 kDa) with buffer exchange to HEPES (10 mM, pH 7.4) and NaCl (150 mM).

Blov-SC purification

The insect cell supernatant was centrifuged after thawing for 15 min at 5,000 × g for 30 min. The new supernatant was supplemented with 10 mM imidazole-HCl and Complete protease inhibitor cocktail EDTA free (Roche). The His-tagged Blov-SC protein was then purified by loading the supernatant onto a 1-mL His GraviTrap prepacked column (GE Healthcare), pre-equilibrated with 20 column volumes (CVs) of 500 mM sodium chloride, 10 mM HEPES (pH 7.4), and 10 mM imidazole. Columns were then washed with 20 CVs of the same buffer to remove non-specifically bound material. A second wash was performed at 12.5 mM imidazole in a similar buffer. Proteins were eluted with 10 CVs of buffer containing 200 mM imidazole.

Blov-SC-containing fractions were checked by SDS-PAGE and concentrated on Amicon (MWCO, 30 kDa) with buffer exchange to HEPES (10 mM, pH 7.4) and NaCl (150 mM).

ADD-Blov complex formation for characterization and mouse immunization experiments

Covalent complex formation was obtained by incubation of purified ADD-ST with purified Blov protein fused to SC (Blov-SC). Incubation was performed at 25°C under agitation on a Thermomixer at 300 rpm. The Blov-SC ratio per ADD-ST was fixed to 1:4 (1 Blov-SC for 4 monomers) to avoid steric hindrance between the Blov-SC proteins on the ADDomer surface. For immunization experiments, a ratio of 3 copies of Blov-SC per ADD-ST was chosen to leave minimal free Blov-SC. This ratio was calculated on SDS-PAGE using ImageLab software (Bio-Rad). The integrity of ADD-Blov was checked by negative-stain electron microscopy.

B16-OVA culture and preparation for tumor challenge in mice

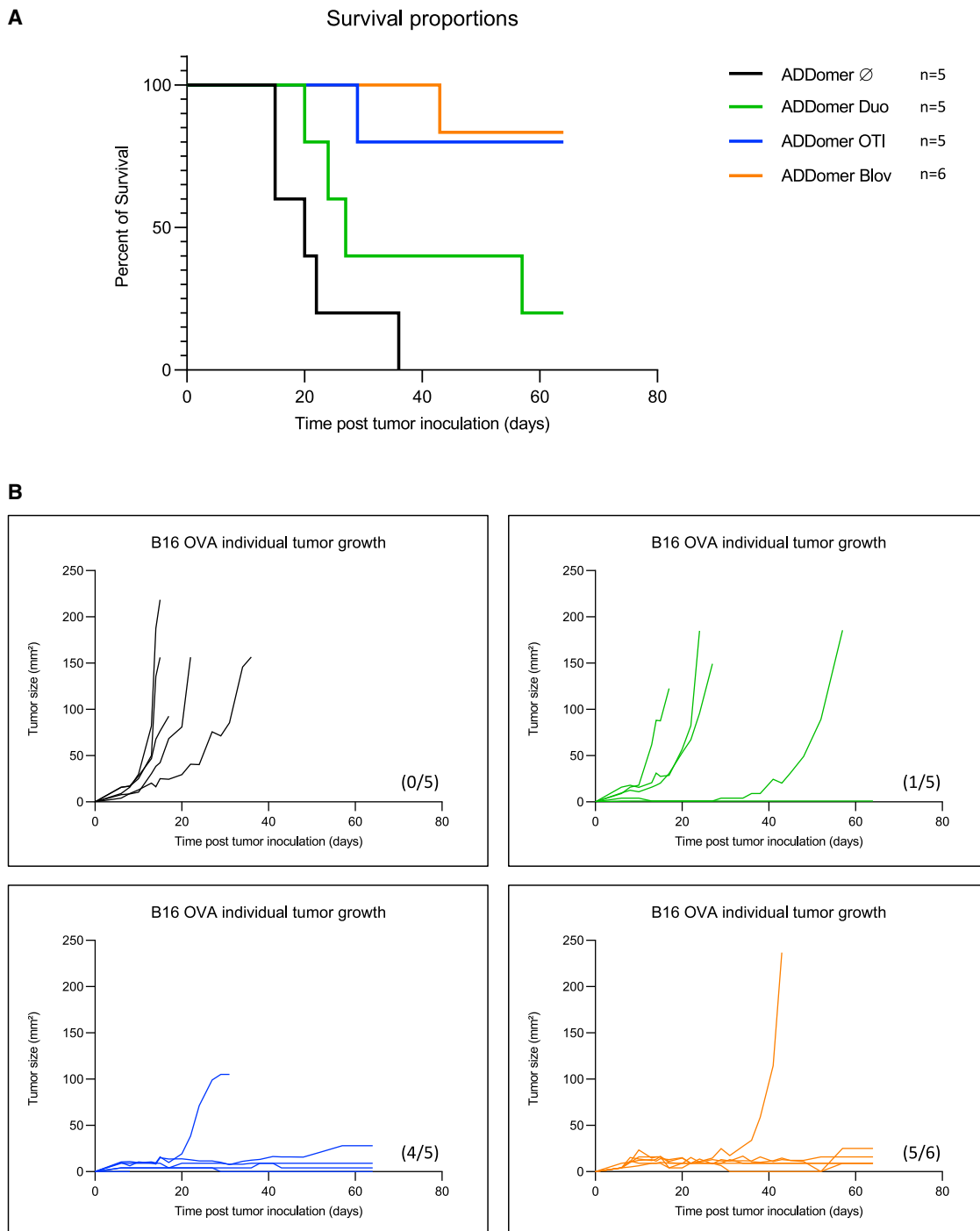
B16 melanoma cells stably expressing chicken OVA (B16-OVA) were provided by Dr. Dalil Hannani (TIMC Laboratory, Université Grenoble Alpes, France). The cells were tested for OVA expression (Figure S1) and for pathogens (mouse essential panel and PVM (Pneumonia Virus of Mice) PCR, Charles River Laboratories). The cell lines were maintained in RPMI-1640 Glutamax (Gibco) containing 10% fetal bovine serum (Gibco), 5,000 U/100 mL of penicillin-streptomycin (Gibco), and 500 µg/mL Geneticin at 37°C in 5% CO₂. Cells were cultivated in T75 flasks, washed with PBS, and passaged with trypsin. For mouse injection, cells were resuspended at 2.10⁶/mL in PBS.

In vivo experiments and vaccination

Animals were housed and bred at the Plateforme de Haute Technologie Animale (PHTA) core facility (Grenoble, France; EU0197, Agreement C38-51610006) under specific pathogen-free conditions in a temperature-controlled environment with a 12-h light/dark cycle and *ad libitum* access to water and food. Animal housing and procedures were in accordance with the recommendations from the Direction des Services Vétérinaires, Ministry of Agriculture of France, according to European Communities Council Directives 2010/63/EU and according to recommendations for health monitoring from the Federation of European Laboratory Animal Science Associations. Protocols involving animals were reviewed by the local ethics committee (Comité d'Ethique pour l'Expérimentation Animale no. 12, Cometh-Grenoble) and approved by the Ministry of Research (APAFIS 2021032418404959_v3, APAFIS 2018062601109404_v2, and APAFIS 2020112016376739_v1).

Figure 5. Short-term immunological responses

(A) Percentage of CD8⁺ dextramer OT-I⁺ T lymphocytes in the spleen ($n = 6$) and in the tumor ($n = 5$ for ADD-Ø, $n = 1$ for the other groups) for all groups. (B) Dot plot representation of the percentage of CD8⁺ dextramer OT-I⁺ T lymphocytes in the tumor of one mouse per group. (C) Absolute number of CD8⁺ dextramer OT-I⁺ T lymphocytes in the spleen ($n = 6$) and in the tumor ($n = 5$ for ADD-Ø, $n = 1$ for the other groups) for all groups.

**Figure 6. Tumor growth and survival monitoring for therapeutic vaccination**

(A) Kaplan-Meier survival analysis showing the percentage of surviving mice. (B) Tumor growth curves for individual mice of each group. The numbers of tumor-free mice are shown in parentheses.

Vaccination experiments were performed according to ethics guidelines. Five-week-old female C57Bl/6J mice were purchased from Janvier (Le Genest-Saint-Isle, France).

Adjuvant screening

Each mouse (6 groups of 3 mice each) received 100 µL of vaccine: 50 µL of ADDomer (40 µg per mouse) in HEPES (10 mM) and

NaCl (150 mM) adjuvanted with an equivalent volume of ODN 2395 (50 µg per mouse), MPLA (20 µg per mouse), or poly(I:C) (50 µg per mouse) (VacciGrade-InvivoGen). Mice were injected subcutaneously in the right flank twice (days 0 and 7) and sacrificed on day 14 for organ harvest (spleen and injection site draining lymph nodes [axillary, brachial, and inguinal lymph nodes on the right flank]). Blood was collected by retro-orbital sampling on day 0 and day 14 under anesthesia using 4% isoflurane.

Prophylactic vaccination

Mice received 5 doses, injected subcutaneously in the left flank, of the poly(I:C) adjuvanted ADDomer vaccine on days 0, 2, 5, 7, and 9. On day 34 (i.e., 25 days after the last vaccination), the mice were challenged with inoculation of B16-OVA cells (2.10^5 cells/mice in a total volume of 100 µL of PBS, right flank). Tumor growth was monitored for 17 days after the challenge.

Therapeutic vaccination

Mice received the first tumor inoculation (B16-OVA, 2.10^5 cells, right flank) before receiving 5 doses of the therapeutic poly(I:C)-adjuvanted ADDomer vaccine on days 1, 3, 6, 8, and 10. On day 15, 6 of the 12 animals were sacrificed, and the blood, tumor, spleen, and tumor side draining lymph nodes (axillary, brachial, and inguinal lymph nodes on the right flank) were collected for immune analyses. The 5 or 6 remaining vaccinated and tumor-bearing mice were then monitored for survival until the ethical endpoint was reached.

Flow cytometry analyses of the CD8⁺ dextramer OT-I⁺ response

After collection, organs (lymph nodes, spleens, and tumors) were resuspended, washed, and filtered using a 100-µm cell strainer. For spleens and tumors, Red Blood Lysis Buffer (1-min incubation, 1181438900, Merck) and RPMI-1640 Glutamax (Gibco) supplemented with 25 µg/mL of Liberase (20-min incubation, Liberase Research Grade, 5401119001, Merck), respectively, were used during this process. Two million cells were then incubated at room temperature (RT) in the dark for 30 min with the dextramer OT-I (H-2 Kb [SIINFEKL], JD2163-PE, Immudex). CD45, Live/Dead, CD3, CD4, and CD8 antibodies (BD Biosciences) were then added for 20 min at 4°C in the dark. Cells were then washed and analyzed on a flow cytometer (LSRII Analyzer, BD Biosciences).

ELISA

The peptide OT-II (peptide OVA_{23–339}, InvivoGen) was diluted at 2 µg/mL in PBS, and 50 mL was coated overnight at 4°C in a 96-well plate (Maxisorp Nunc Immunoplate, 442404). Plates were washed using a Thermo Scientific microplate washer (5165040). After three washes with 100 µL of PBS-Tween (0.05%), plates were blocked with PBS-BSA (3%) for 1 h. Mouse serum was serially diluted in PBS and incubated for 1 h (50 mL/well) at RT. After five washes with PBS-Tween (0.05%), a goat anti-mouse immunoglobulin G (IgG) (H + L) secondary antibody linked to horseradish peroxidase (JIR 115-035-062) diluted at 1:2,500 in PBS-Tween (0.05%) was added for 1 h. After five washes, 50 mL of transmembrane domain substrate

was distributed per well. The enzymatic reaction was stopped after 70 s by addition of 50 mL of H₂S04 (1 M), and plates were read at 450 nm with a Tecan Spark 10M plate reader.

Electron microscopy: Negative staining

Samples of 3.5 mL were adsorbed on the clean side of a carbon film evaporated previously on mica and then stained using 2% (w/v) sodium silicotungstate (pH 7.4) for 30 s. The sample/carbon ensemble was then transferred to a grid and air dried. Images were acquired under low-dose conditions (<30 e⁻/Å²) on an F20 electron microscope operating at 120 kV using a CETA camera.

Statistical analyses

Because percentages and absolute numbers of CD8⁺ dextramer OT-I⁺ T lymphocytes datasets followed a non-normal, heteroscedastic distribution, a non-parametric test was used for comparison of the different groups. Kruskal-Wallis tests were performed, followed by a Dunn's multiple comparison test for each figure. Differences were considered significant when the p value was below 0.05. Statistics were performed using GraphPad software v.8.

DATA AVAILABILITY

Data are available upon request.

SUPPLEMENTAL INFORMATION

Supplemental information can be found online at <https://doi.org/10.1016/j.omtm.2022.12.003>.

ACKNOWLEDGMENTS

We thank Jean Paufique and Brigitte Closs from the Fondation d'Entreprise SILAB for scientific and financial support, which enabled us to perform this work. We are grateful to Daphna Fenel and Guy Schoehn for electron microscopy. We are indebted to Emilie Stermann, Marie-Claire Dagher, Christopher Chevillard, Axelle Amen, Pascal Poignard, and Laurence Chaperot for help and advice. We thank the zootechnicians of the PHTA facility for animal housing and care. This work was supported by Fondation d'Entreprise SILAB - Jean PAUFIQUE. S.B. was the recipient of the SILAB price 2020–2022 dedicated to skin cancer research. S.B. was granted by a “bourse doctorale” from the Université Grenoble Alpes. D.H. is supported by GEFLUC Dauphiné-Savoie, Ligue Contre le Cancer Comité Isère, Ligue Contre le Cancer Comité Savoie, Université Grenoble Alpes IDEX Initiatives de Recherche Stratégiques, and Fondation du Souffle-Fonds de Recherche en Santé Respiratoire (FdS-FRSR). This work used the platforms of the Grenoble Instruct-ERIC Centerre (ISBG; UAR 3518 CNRS-CEA-UGA-EMBL) within the Grenoble Partnership for Structural Biology (PSB), supported by FRISBI (ANR-10-INBS-05-02) and GRAL, financed within the Université Grenoble Alpes graduate school (Ecole Universitaire de Recherche) CBH-EUR-GS (ANR-17-EURE-0003). The electron microscope facility is supported by the Auvergne-Rhône-Alpes region, the Fondation pour la Recherche Médicale (FRM), the Fonds

FEDER, and the GIS-Infrastructures en Biologie Sante et Agronomie (IBISA).

AUTHOR CONTRIBUTIONS

Conceptualization, S.B., C.A., D.H., and P.F.; investigation, S.B., E.B., O.M., D.L., C.A., and D.H.; animal experiments, S.B., C.A., D.L., E.B., and D.H.; funding acquisition, S.B. and P.F. S.B. and P.F wrote the manuscript.

DECLARATION OF INTERESTS

The authors declare no competing interests.

REFERENCES

- Bok, K., Sitar, S., Graham, B.S., and Mascola, J.R. (2021). Accelerated COVID-19 vaccine development: milestones, lessons, and prospects. *Immunity* 54, 1636–1651. <https://doi.org/10.1016/j.jimmuni.2021.07.017>.
- Ho, J.K.-T., Jeevan-Raj, B., and Netter, H.-J. (2020). Hepatitis B virus (HBV) subviral particles as protective vaccines and vaccine platforms. *Viruses* 12, 126. <https://doi.org/10.3390/v12020126>.
- Villa, L.L., Costa, R.L.R., Petta, C.A., Andrade, R.P., Ault, K.A., Giuliano, A.R., Wheeler, C.M., Koutsy, L.A., Malm, C., Lehtinen, M., et al. (2005). Prophylactic quadrivalent human papillomavirus (types 6, 11, 16, and 18) L1 virus-like particle vaccine in young women: a randomised double-blind placebo-controlled multicentre phase II efficacy trial. *Lancet Oncol.* 6, 271–278. [https://doi.org/10.1016/S1470-2045\(05\)70101-7](https://doi.org/10.1016/S1470-2045(05)70101-7).
- Nguyen, B., and Tolia, N.H. (2021). Protein-based antigen presentation platforms for nanoparticle vaccines. *NPJ Vaccines* 6, 70. <https://doi.org/10.1038/s41541-021-00330-7>.
- Reddy, S.T., van der Vlies, A.J., Simeoni, E., Angeli, V., Randolph, G.J., O’Neil, C.P., Lee, L.K., Swartz, M.A., and Hubbell, J.A. (2007). Exploiting lymphatic transport and complement activation in nanoparticle vaccines. *Nat. Biotechnol.* 25, 1159–1164. <https://doi.org/10.1038/nbt1332>.
- Vragniau, C., Bufton, J.C., Garzoni, F., Stermann, E., Rabi, F., Terrat, C., Guidetti, M., Josserand, V., Williams, M., Woods, C.J., et al. (2019). Synthetic self-assembling ADDomer platform for highly efficient vaccination by genetically encoded multipeptope display. *Sci. Adv.* 5, eaaw2853. <https://doi.org/10.1126/sciadv.aaw2853>.
- Caldeira, J.C., Perrine, M., Pericile, F., and Cavallo, F. (2020). Virus-like particles as an immunogenic platform for cancer vaccines. *Viruses* 12, 488. <https://doi.org/10.3390/v12050488>.
- Zakeri, B., Fierer, J.O., Celik, E., Chittock, E.C., Schwarz-Linek, U., Moy, V.T., and Howarth, M. (2012). Peptide tag forming a rapid covalent bond to a protein, through engineering a bacterial adhesin. *Proc. Natl. Acad. Sci. USA* 109, E690–E697. <https://doi.org/10.1073/pnas.1115485109>.
- Brune, K.D., Leneghan, D.B., Brian, I.J., Ishizuka, A.S., Bachmann, M.F., Draper, S.J., Biswas, S., and Howarth, M. (2016). Plug-and-Display: decoration of Virus-Like Particles via isopeptide bonds for modular immunization. *Sci. Rep.* 6, 19234. <https://doi.org/10.1038/srep19234>.
- Li, L., Fierer, J.O., Rapoport, T.A., and Howarth, M. (2014). Structural analysis and optimization of the covalent association between SpyCatcher and a peptide tag. *J. Mol. Biol.* 426, 309–317. <https://doi.org/10.1016/j.jmb.2013.10.021>.
- Keeble, A.H., and Howarth, M. (2020). Power to the protein: enhancing and combining activities using the Spy toolbox. *Chem. Sci.* 11, 7281–7291. <https://doi.org/10.1039/D0SC01878C>.
- Fender, P., Ruigrok, R.W., Gout, E., Buffet, S., and Chroboczek, J. (1997). Adenovirus dodecahedron, a new vector for human gene transfer. *Nat. Biotechnol.* 15, 52–56. <https://doi.org/10.1038/nbt0197-52>.
- Besson, S., Vragniau, C., Vassal-Stermann, E., Dagher, M.C., and Fender, P. (2020). The adenovirus dodecahedron: beyond the platonic story. *Viruses* 12, 718. <https://doi.org/10.3390/v12070718>.
- Chevillard, C., Amen, A., Besson, S., Hannani, D., Bally, I., Dettling, V., Gout, E., Moreau, C.J., Buisson, M., Gallet, S., et al. (2022). Elicitation of potent SARS-CoV-2 neutralizing antibody responses through immunization with a versatile adenovirus-inspired multimerization platform. *Mol. Ther.* 30, 1913–1925. <https://doi.org/10.1016/j.ymthe.2022.02.011>.
- Martins, K.A.O., Bavari, S., and Salazar, A.M. (2015). Vaccine adjuvant uses of poly-IC and derivatives. *Expert Rev. Vaccines* 14, 447–459. <https://doi.org/10.1586/14760584.2015.966085>.
- Liu, C., Chu, X., Sun, P., Feng, X., Huang, W., Liu, H., and Ma, Y. (2018). Synergy effects of Polyinosinic-polycytidylc acid, CpG oligodeoxynucleotide, and cationic peptides to adjuvant HPV E7 epitope vaccine through preventive and therapeutic immunization in a TC-1 grafted mouse model. *Hum. Vaccin. Immunother.* 14, 931–940. <https://doi.org/10.1080/21645515.2017.1420446>.
- Fender, P., Hall, K., Schoehn, G., and Blair, G.E. (2012). Impact of human adenovirus type 3 dodecahedron on host cells and its potential role in viral infection. *J. Virol.* 86, 5380–5385. <https://doi.org/10.1128/JVI.07127-11>.
- Bellone, M., Cantarella, D., Castiglioni, P., Crosti, M.C., Ronchetti, A., Moro, M., Garancini, M.P., Casorati, G., and Dellabona, P. (2000). Relevance of the tumor antigen in the validation of three vaccination strategies for melanoma. *J. Immunol.* 165, 2651–2656. <https://doi.org/10.4049/jimmunol.165.5.2651>.
- Epaulard, O., Toussaint, B., Quenee, L., Derouazi, M., Bosco, N., Villiers, C., Le Berre, R., Guery, B., Filopon, D., Crombez, L., et al. (2006). Anti-tumor immunotherapy via antigen delivery from a live attenuated genetically engineered *Pseudomonas aeruginosa* type III secretion system-based vector. *Mol. Ther.* 14, 656–661. <https://doi.org/10.1016/j.ymthe.2006.06.011>.
- Villegas-Mendez, A., Garin, M.I., Pineda-Molina, E., Veratti, E., Bueren, J.A., Fender, P., and Lenormand, J.-L. (2010). In vivo delivery of antigens by adenovirus dodecahedron induces cellular and humoral immune responses to elicit antitumor immunity. *Mol. Ther.* 18, 1046–1053. <https://doi.org/10.1038/mt.2010.16>.
- Del Val, M., Schlicht, H.-J., Ruppert, T., Reddehase, M.J., and Koszinowski, U.H. (1991). Efficient processing of an antigenic sequence for presentation by MHC class I molecules depends on its neighboring residues in the protein. *Cell* 66, 1145–1153. [https://doi.org/10.1016/0092-8674\(91\)90037-Y](https://doi.org/10.1016/0092-8674(91)90037-Y).
- Kloetzel, P.-M. (2001). Antigen processing by the proteasome: ubiquitin and proteasomes. *Nat. Rev. Mol. Cell Biol.* 2, 179–187. <https://doi.org/10.1038/35056572>.
- Nussbaum, A.K., Dick, T.P., Keilholz, W., Schirle, M., Stevanović, S., Dietz, K., Heinemeyer, W., Groll, M., Wolf, D.H., Huber, R., et al. (1998). Cleavage motifs of the yeast 20S proteasome β subunits deduced from digests of enolase 1. *Proc. Natl. Acad. Sci. USA* 95, 12504–12509. <https://doi.org/10.1073/pnas.95.21.12504>.
- Pulendran, B., Arunachalam, P.S., and O’Hagan, D.T. (2021). Emerging concepts in the science of vaccine adjuvants. *Nat. Rev. Drug Discov.* 20, 454–475.
- Beutler, B. (2004). Inferences, questions and possibilities in Toll-like receptor signaling. *Nature* 430, 257–263. <https://doi.org/10.1038/nature02761>.
- Kawai, T., and Akira, S. (2010). The role of pattern-recognition receptors in innate immunity: update on Toll-like receptors. *Nat. Immunol.* 11, 373–384. <https://doi.org/10.1038/ni.1863>.
- Alexopoulou, L., Holt, A.C., Medzhitov, R., and Flavell, R.A. (2001). Recognition of double-stranded RNA and activation of NF-κappaB by Toll-like receptor 3. *Nature* 413, 732–738. <https://doi.org/10.1038/35099560>.
- Ammi, R., De Waele, J., Willemen, Y., Van Brussel, I., Schrijvers, D.M., Lion, E., and Smits, E.L.J. (2015). Poly(I:C) as cancer vaccine adjuvant: knocking on the door of medical breakthroughs. *Pharmacol. Ther.* 146, 120–131. <https://doi.org/10.1016/j.pharmthera.2014.09.010>.
- Rath, A., Glibowicka, M., Nadeau, V.G., Chen, G., and Deber, C.M. (2009). Detergent binding explains anomalous SDS-PAGE migration of membrane proteins. *Proc. Natl. Acad. Sci. USA* 106, 1760–1765. <https://doi.org/10.1073/pnas.0813167106>.
- Zhao, W., Wu, J., Chen, S., and Zhou, Z. (2020). Shared neoantigens: ideal targets for off-the-shelf cancer immunotherapy. *Pharmacogenomics* 21, 637–645. <https://doi.org/10.2217/pgs-2019-0184>.

31. Vragniau, C. (2018). Modification des dodécaèdres bases de l'adénovirus de sérotype 3: Design et caractérisation d'un nouveau vecteur multi-épitopique polyvalent. In PhD Thesis, <https://hal.archives-ouvertes.fr/tel-02110396>.
32. Villegas-Méndez, A., Fender, P., Garin, M.I., Rothe, R., Liguori, L., Marques, B., and Lenormand, J.-L. (2012). Functional characterisation of the WW minimal domain for delivering therapeutic proteins by adenovirus dodecahedron. *PLoS One* 7. e45416. <https://doi.org/10.1371/journal.pone.0045416>.
33. Galinier, R., Gout, E., Lortat-Jacob, H., Wood, J., and Chroboczek, J. (2002). Adenovirus protein involved in virus internalization recruits Ubiquitin–Protein ligases. *Biochemistry* 41, 14299–14305. <https://doi.org/10.1021/bi020125b>.
34. Bachmann, M.F., and Jennings, G.T. (2010). Vaccine delivery: a matter of size, geometry, kinetics and molecular patterns. *Nat. Rev. Immunol.* 10, 787–796. <https://doi.org/10.1038/nri2868>.
35. Zabel, F., Kündig, T.M., and Bachmann, M.F. (2013). Virus-induced humoral immunity: on how B cell responses are initiated. *Curr. Opin. Virol.* 3, 357–362. <https://doi.org/10.1016/j.coviro.2013.05.004>.
36. Shibagaki, N., and Udey, M.C. (2002). Dendritic cells transduced with protein antigens induce cytotoxic lymphocytes and elicit antitumor immunity. *J. Immunol.* 168, 2393–2401. <https://doi.org/10.4049/jimmunol.168.5.2393>.
37. Cohen, A.A., Gnanapragasam, P.N.P., Lee, Y.E., Hoffman, P.R., Ou, S., Kakutani, L.M., Keeffe, J.R., Wu, H.-J., Howarth, M., West, A.P., et al. (2021). Mosaic nanoparticles elicit cross-reactive immune responses to zoonotic coronaviruses in mice. *Science* 371, 735–741.
38. Cohen, J. (2021). The dream vaccine. *Science* 372, 227–231. <https://doi.org/10.1126/science.372.6539.227>.
39. Feola, S., Russo, S., Martins, B., Lopes, A., Vandermeulen, G., Fluhler, V., De Giorgi, C., Fusciello, M., Pesonen, S., Ylösmäki, E., et al. (2022). Peptides-coated oncolytic vaccines for cancer personalized medicine. *Front. Immunol.* 13, 826164. <https://doi.org/10.3389/fimmu.2022.826164>.
40. Fender, P. (2014). Use of dodecahedron “VLPs” as an alternative to the whole adenovirus. *Methods Mol. Biol.* 1089, 61–70. https://doi.org/10.1007/978-1-62703-679-5_4.

Supplemental information

**Stimulation of the immune system
by a tumor antigen-bearing adenovirus-inspired
VLP allows control of melanoma growth**

Solène Besson, Emilie Boucher, David Laurin, Olivier Manches, Caroline Aspord, Dalil Hannani, and Pascal Fender

A

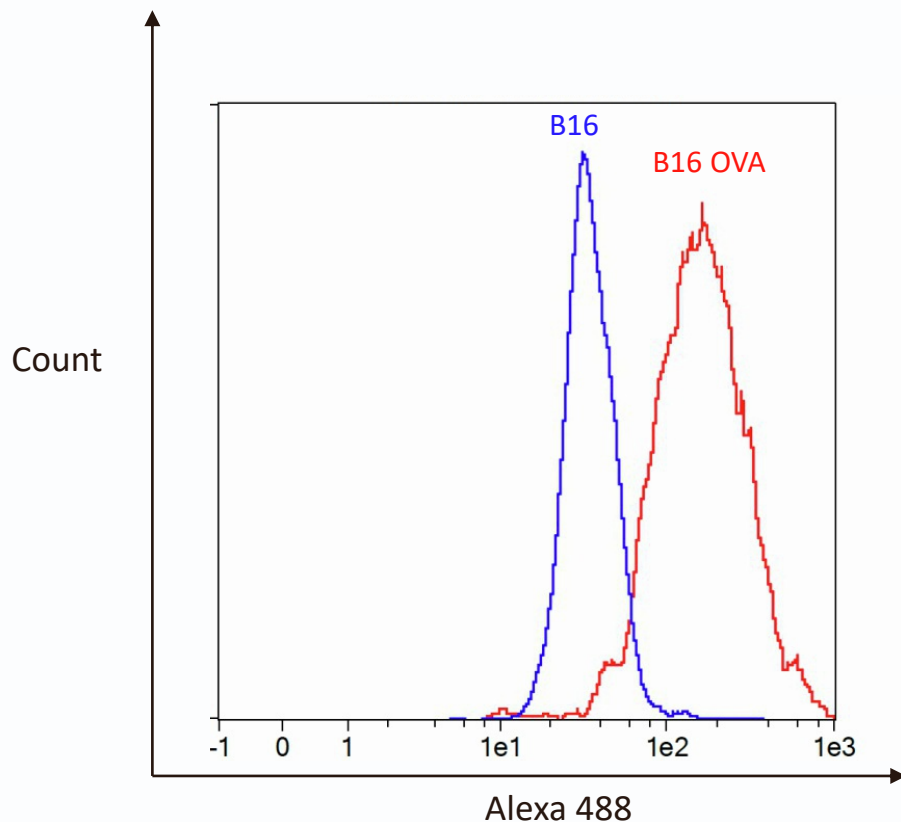
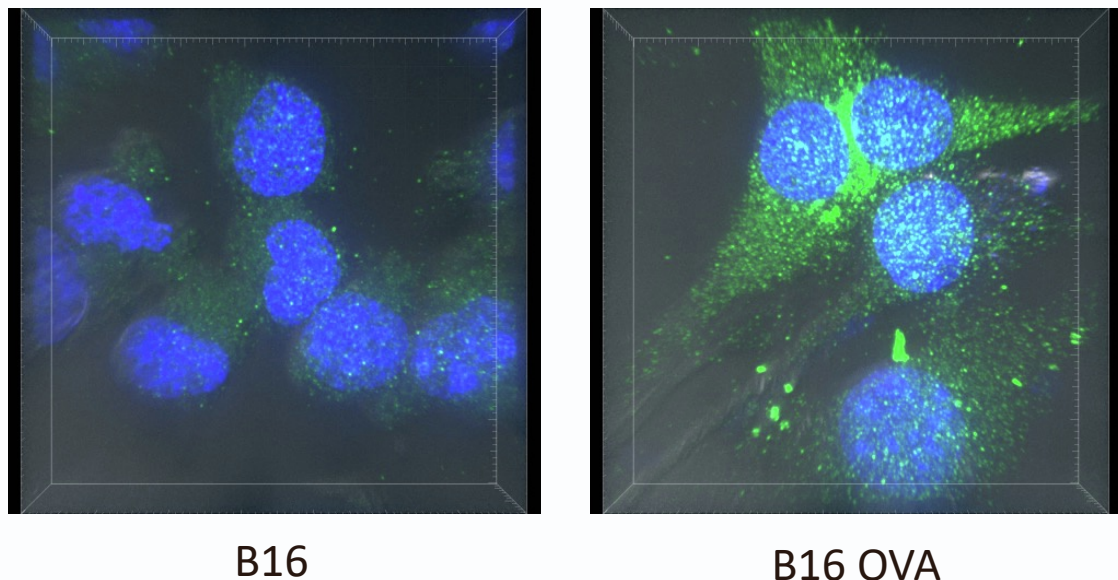
Ø	MRRRAVLGGAVVYPEGPPPSYESVMQQQAAMIQPPLAEPVPPRYLAPTEGRNSIRYSELSPLYDTTKLYLVDNKSADIASLNYQNDHSNFLTTVVQNNDF
Duo	MRRRAVLGGAVVYPEGPPPSYESVMQQQAAMIQPPLAEPVPPRYLAPTEGRNSIRYSELSPLYDTTKLYLVDNKSADIASLNYQNDHSNFLTTVVQNNDF
OTI	MRRRAVLGGAVVYPEGPPPSYESVMQQQAAMIQPPLAEPVPPRYLAPTEGRNSIRYSELSPLYDTTKLYLVDNKSADIASLNYQNDHSNFLTTVVQNNDF
ST	MRRRAVLGGAVVYPEGPPPSYESVMQQQAAMIQPPLAEPVPPRYLAPTEGRNSIRYSELSPLYDTTKLYLVDNKSADIASLNYQNDHSNFLTTVVQNNDF
Ø	TPTEASTQTINFDERSRWGGQLKTIIMHTNMPNVNEY MFSNKFKARVMVSRAPEGEFVTVNDG -----PVNDTYDHKEDI
Duo	TPTEASTQTINFDERSRWGGQLKTIIMHTNMPNVNEY MFSNKFKARVMVSRAPEGEFGSGG ISQAVHAAHAEINEAGR GGSGGGG PVNDTYDHKEDI
OTI	TPTEASTQTINFDERSRWGGQLKTIIMHTNMPNVNEY MFSNKFKARVMVSRAPEGEFVTVNDG -----PVNDTYDHKEDI
ST	TPTEASTQTINFDERSRWGGQLKTIIMHTNMPNVNEY MFSNKFKARVMVSRAPEGEFGSG AHIVMVDAYKPTK GSGGG -----PVNDTYDHKEDI
Ø	LKYEWFEFILPE GNFSATMTIDLMNNAIIDNYLEIGRQNGVLES DIGVKFDTRNFR LGWD PETKLIMP G VYT YEAFHPD ILLPGCGV DFTESRLS NLLGIRK
Duo	LKYEWFEFILPE GNFSATMTIDLMNNAIIDNYLEIGRQNGVLES DIGVKFDTRNFR LGWD PETKLIMP G VYT YEAFHPD ILLPGCGV DFTESRLS NLLGIRK
OTI	LKYEWFEFILPE GNFSATMTIDLMNNAIIDNYLEIGRQNGVLES DIGVKFDTRNFR LGWD PETKLIMP G VYT YEAFHPD ILLPGCGV DFTESRLS NLLGIRK
ST	LKYEWFEFILPE GNFSATMTIDLMNNAIIDNYLEIGRQNGVLES DIGVKFDTRNFR LGWD PETKLIMP G VYT YEAFHPD ILLPGCGV DFTESRLS NLLGIRK
Ø	RHPFQEGFKIMYEDLEGGNIPALLDVTAYEESKKDTTARETTT LAVA EETSED-----VDDDIRGDTYITELEKQKREAAA EVSRKKELKI QPLEK
Duo	RHPFQEGFKIMYEDLEGGNIPALLDVTAYEESKKDTTARGSGG SIINFEKLTEWTSS GGSGVDDDIRGDTYITELEKQKREAAA EVSRKKELKI QPLEK
OTI	RHPFQEGFKIMYEDLEGGNIPALLDVTAYEESKKDTTARGSGG SIINFEKLTEWTSS GGSGVDDDIRGDTYITELEKQKREAAA EVSRKKELKI QPLEK
ST	RHPFQEGFKIMYEDLEGGNIPALLDVTAYEESKKDTTARETTT LAVA EETSED-----VDDDIRGDTYITELEKQKREAAA EVSRKKELKI QPLEK
Ø	DSKRSYNVLEDKINTAYRSWYLSNYGNPEKGIRSWLTTSDVTCAEQVYWSLPDMMQDPVTFRSTRQVN NYPVVGAE LMPVFSKF YNEQAVY
Duo	DSKRSYNVLEDKINTAYRSWYLSNYGNPEKGIRSWLTTSDVTCAEQVYWSLPDMMQDPVTFRSTRQVN NYPVVGAE LMPVFSKF YNEQAVY
OTI	DSKRSYNVLEDKINTAYRSWYLSNYGNPEKGIRSWLTTSDVTCAEQVYWSLPDMMQDPVTFRSTRQVN NYPVVGAE LMPVFSKF YNEQAVY
ST	DSKRSYNVLEDKINTAYRSWYLSNYGNPEKGIRSWLTTSDVTCAEQVYWSLPDMMQDPVTFRSTRQVN NYPVVGAE LMPVFSKF YNEQAVY
Ø	SQQLRQATSLTHVFNRF PENQILIRPPAPTITVSENPALTDHGTLPLRSSIRGVQRVTVTDARRRTCPYVYKALGIVAPRVLSSRTF
Duo	SQQLRQATSLTHVFNRF PENQILIRPPAPTITVSENPALTDHGTLPLRSSIRGVQRVTVTDARRRTCPYVYKALGIVAPRVLSSRTF
OTI	SQQLRQATSLTHVFNRF PENQILIRPPAPTITVSENPALTDHGTLPLRSSIRGVQRVTVTDARRRTCPYVYKALGIVAPRVLSSRTF
ST	SQQLRQATSLTHVFNRF PENQILIRPPAPTITVSENPALTDHGTLPLRSSIRGVQRVTVTDARRRTCPYVYKALGIVAPRVLSSRTF

B

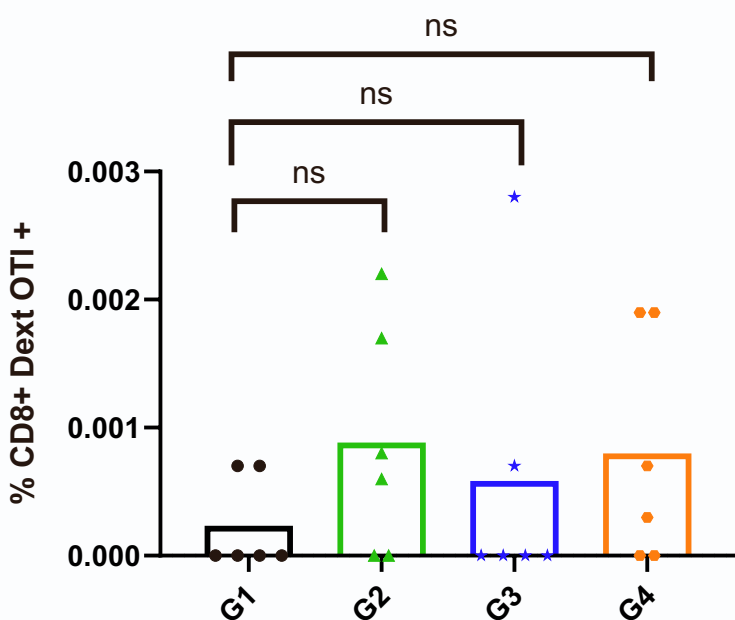
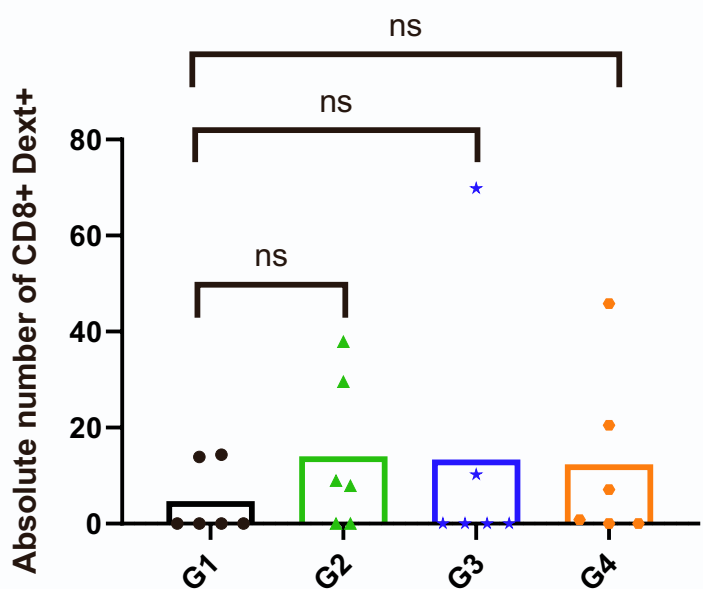
Blov-SC	MKFLVNVALVFMVVYISYY GSIGAASMEFCDFVKELKHANETIFYCPIAIMSALAMVYLGAKDSTRQINKVVRFDKLPGFGDSIEACQCGTSVN VHSSLRDILNQITKPN DVYFSL ASR LYAEERYPILPEYLQCVKELYRGGLEPINFQTAADQARELINSWVESQ TNGIIRNV LQPSSVDSQTAMVLVNAI VF KGLWEKA FKD EDTQAMPFRVTEQESKP VQMMYQIGLFRV ASMASEKM KILELPFASGTMSMLVLLPDEVSGLEQLE SIINFEKLTEWTSS NVM EERIKVYLP RMK MEE KYNLT FVLMAMG ITDV FSSA NL SG ISSAESLK ISQAVHAAHAEINEAGR EVVGS AEGVDA ASV ASGGTVDTL SGL SEQ GQSGDMTIEEDSAT HIKFSKR DEDG KELAG ATMEL RDSSGKTISTWISDGQVKDFYLYPGKYTFVETAAPDGYEVATAITFTVNEQGQVTVNGKATK GDAH IGSGHHHHHH
---------	--

Figure S1 : ADDomers and Blov-SC sequences

(A) ADDomers sequences: Variable and RGD loops are written in red and blue, respectively. Epitopes (OT-I and OT-II) and SpyTag are highlighted in light blue, light red and pink, respectively. In the SpyTag the reactive aspartate is indicated by a green triangle. Linkers are depicted in green. (B) Blov-SC sequence: The melittin secretion peptide is written in black. The ovalbumin protein is depicted in orange with epitopes OT-I and OT-II highlighted in light blue and light red, respectively. SpyCatcher is written in blue and the reactive lysine is indicated by a green triangle. Linkers and Histidine-Tag are represented in green and purple, respectively.

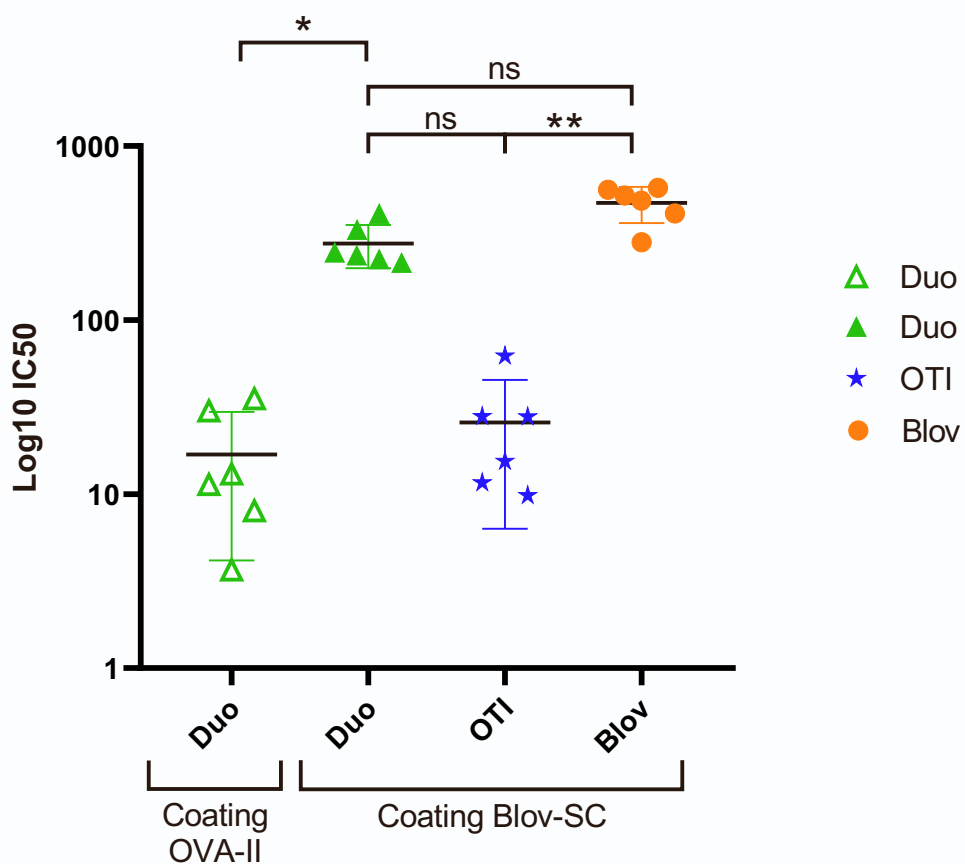
Figure S2**A****B****Figure S2 : Validation of ovalbumin expression by the B16 OVA cells.**

(A) FACS analysis using antibody against OVA. B16 and B16-OVA cells were scraped then fixed with 2% PFA and permeabilized with 0,1% triton X-100. After treatment with 1/500 anti-OVA antibody (abcam #ab181688) and 1/500 Goat anti-Rabbit AlexaFluor 488 secondary antibody, cells were read using MACSQuant VYB Flow Cytometer, (Miltenyi Biotech). (B) Same as in (A) on adherent cells with nucleus counterstained using Hoechst. Images were taken on confocal microscope (Olympus GATACA).

A**Draining lymph nodes****B****Draining lymph nodes****Figure S3: Short-term immunological responses in draining lymph nodes**

(A) Percentage of CD8+ Dextramer OVA-I+ T lymphocytes in the draining lymph nodes (n=6) for all groups. (B) Absolute number of CD8+ Dextramer OVA-I+ T lymphocytes in the draining lymph nodes (n=6) for all groups.

A



B

	Log 10 IC50 Coating OVA-II peptide	Log 10 IC50 Coating Blov-SC protein
ADDomer Ø	NA	NA
ADDomer Duo	16.9	275.7
ADDomer OTI	NA	25.8
ADDomer Blov	NA	472.2

Figure S4: Humoral response against ovalbumin antigen or epitope in vaccinated mice

(A) Graph showing the Log₁₀ IC₅₀ of antibodies against the OVA-II epitope or the Blov-SC antigen. The distribution of the data does not follow a normal distribution, therefore non-parametric tests were used. For paired sample comparisons (Duo coating OVA-II versus coating Blov-SC), the Wilcoxon test was used. For multiple comparisons on unpaired samples (Duo versus OTI versus Blov with coating Blov-SC), the Kruskall Wallis test was used. (B) Table showing the Log₁₀ IC₅₀ mean values for each group.

Conclusion du chapitre :

Pour conclure, nous avons vu que la plateforme ADDomer était prometteuse pour l'élaboration d'un vaccin thérapeutique efficace en oncologie du mélanome. La suite immédiate du projet serait de tester cette technologie avec des épitopes et antigènes humains sur des souris humanisées par exemple afin de vérifier les effets protecteurs mais surtout thérapeutiques de la vaccination avec des ADDomers. Il serait également intéressant d'analyser l'effet thérapeutique en faisant varier le temps entre l'implantation tumorale et la vaccination afin de voir potentiellement jusqu'à quel stade de la croissance tumorale la vaccination thérapeutique est toujours efficace. Par ailleurs, nous avons vu qu'il était possible de présenter différents antigènes sur le même ADDomer (*cf* Chapitre IV) ce qui pourrait permettre de maximiser les chances de succès thérapeutique. Il serait également possible d'afficher sur cette plateforme des néo-antigènes de patients dans le cadre de vaccins personnalisés. La technologie ADDomer représente donc une plateforme vaccinale prometteuse, polyvalente et facilement adaptable qui montre des résultats encourageants pour le traitement du mélanome.

La polyvalence et facilité d'adaptation de cette plateforme ont pu être démontrées au cours de cette thèse lors de la pandémie de la Covid-19. Cette pandémie est arrivée en France à la fin des optimisations de la plateforme permettant l'affichage d'antigènes entiers *via* le système SpyTag/SpyCatcher (voir chapitre IV). Afin d'évaluer la polyvalence de la plateforme, notre laboratoire a choisi de l'adapter au SARS-CoV-2. Nous avons ainsi affiché le RBD (domaine de liaison au récepteur) de la protéine 'Spike' du SARS-CoV-2 à l'ADDomer, et ce travail auquel j'ai pu participer est présenté en annexe de ce manuscrit.

Conclusion générale et perspectives

Malgré les récents progrès en matière de thérapie pour le traitement du mélanome avec notamment les immunothérapies, le mélanome et plus particulièrement le mélanome métastatique présente encore un faible taux de survie. De nombreuses équipes à travers le monde poursuivent les recherches dans l'optique d'améliorer les réponses aux traitements actuels, de stratifier les patients afin d'administrer le traitement le plus approprié à chaque patient mais également de trouver d'autres thérapies qui pourront être utilisées en combinaison avec les thérapies actuelles. Parmi les nouvelles thérapies proposées, les vaccins thérapeutiques sont une option encore en développement mais prometteuse. Après de nombreux échecs en phases cliniques en tant que monothérapies, un ré-engouement pour les vaccins s'est développé ces dernières années. Ces vaccins sont proposés en combinaison avec d'autres thérapies et plus particulièrement avec les anticorps bloqueurs de points de contrôle immunitaires.

Parmi les vaccins thérapeutiques, les vaccins d'origine virale sont largement utilisés pour délivrer les antigènes tumoraux (antigènes associés aux tumeurs ou néo-antigènes) de par leur immunogénicité intrinsèque.

Le vaccin développé dans cette thèse est une particule pseudo-virale non-infectieuse dérivée de l'adénovirus de sérotype 3. Cette particule nommée ‘dodécaèdre de l'adénovirus’ est constituée de 60 monomères d'une protéine unique de la surface des adénovirus : la base du penton. De manière remarquable, ces bases du penton ‘homo-pentamériques’ peuvent s'assembler par 12 (dodécameriser) donnant naissance au ‘dodécaèdre de l'adénovirus’. Au sein de cette particule quasi sphérique d'environ 30nm de diamètre il a été possible de déterminer trois régions dans les monomères qui pouvaient être modifiées sans altérer la structure globale de ce dodécaèdre. Cette découverte a ouvert la voie à l'insertion d'épitopes étrangers dans cette particule donnant

naissance à une nouvelle technologie vaccinale nommée ADDomer (Adenovirus Dodecamer). Cette technologie brevetée a déjà prouvé son efficacité en infectiologie (virus du Chikungunya) et le but de cette thèse était de prouver son efficacité en oncologie pour le traitement du mélanome.

1) Production et optimisation des ADDomers

Dans un premier temps, nous avons dessiné, produit, purifié et optimisé les vecteurs ADDomers afin qu'ils présentent des antigènes et des épitopes modèles ou réels de mélanome humain. Les épitopes ont pu être insérés génétiquement dans les boucles exposées de l'ADDomer (boucle variable ou boucle RGD). Cependant, les antigènes trop volumineux et structurés n'ont pas pu être insérés de cette manière à la surface de l'ADDomer en raison de problèmes de mauvais repliements des monomères ainsi générés empêchant la formation correcte des particules. Pour pallier à ce problème, les antigènes ont été affichés à la surface de l'ADDomer *via* le système SpyTag/SpyCatcher. Le peptide SpyTag a été inséré génétiquement dans la boucle variable de l'ADDomer et la protéine SpyCatcher a été fusionnée aux antigènes d'intérêt. Par simple incubation, le SpyCatcher portant l'antigène forme spontanément une liaison covalente avec le SpyTag porté par l'ADDomer fixant ainsi de manière irréversible l'antigène à l'ADDomer. Nous avons montré que ces rendements d'assemblage étaient meilleurs lorsque le cargo (antigène/épitope) était du côté N-terminal du SpyCatcher. De plus, nous avons mis en évidence que l'ADDomer était capable de présenter en même temps à sa surface différents antigènes de tailles et formes différentes allant d'un petit peptide de 17 acides aminés à une protéine d'environ 50kDa très structurée.

2) Evaluation *in vitro* des vaccins ADDomers

a. Comparaison des vaccins ADD A2L et ADD MelA

Dans une seconde partie, les différents ADDomers présentant des épitopes et antigènes humains du mélanome sont évalués *in vitro* sur des cellules dendritiques (DC) humaines de patients sains.

Nous avons montré que les ADDomers pouvaient être internalisés en proportions différentes en fonction du sous types de cellules dendritiques (cDC2, cDC1, pDC). En effet, alors que les cDC2s fixent/capturent fortement les ADDomers, les cDC1s sont un peu moins efficaces, et les pDCs encore moins. Par ailleurs nous avons observé un effet dose-réponse, ce qui suggère une internalisation spécifique des ADDomers. Enfin, les ADDomers présentant des antigènes (MelanA) à leur surface *via* le système ST/SC sont moins bien internalisés que les ADDomers présentant seulement l'épitope A2L inséré dans une des boucles (boucle variable pour ADD MelA). Cette diminution de l'internalisation pourrait être causée par le fait que l'antigène MelanA masque le motif 'RGD' permettant la liaison de l'ADDomer aux intégrines, nécessaire à son entrée dans les cellules *via* les intégrines.

Il a également été observé que les ADDomers n'étaient pas toxiques pour les DCs de donneurs sains et qu'ils étaient capables de déclencher leur activation. Cela a été mis en évidence par la régulation à la hausse des trois molécules de costimulation (CD40, CD80, CD86) ainsi que par une légère production de cytokines spécifiques aux DC, en particulier IFN α , IL28, IL29. De plus, de par son origine virale, l'ADDomer vide (ne présentant aucun épitopes ou antigène) est également capable d'activer les DC ce qui révèle les puissantes propriétés adjuvantes de l'ADDomer lui-même.

Nous avons ensuite évalué la capacité des DCs à cross présenter les ADDomers. La cross présentation décrit la capacité des DC à absorber, traiter et présenter aux lymphocytes T naïfs un agent exogène (dans notre cas cela correspondra aux épitopes et antigènes apportés par les

ADDomers) chargé dans des molécules du complexe majeur d'histocompatibilité (CMH) de classe I. Suite à cette présentation, l'étape de cross-priming, c'est-à-dire l'activation des cellules T CD8+ spécifiques des épitopes/antigènes présentés, sera amorcée. Les molécules du CMH de classe I ne présentent généralement que les antigènes endogènes, tandis que les antigènes exogènes sont présentés par les molécules du CMH de classe II, d'où le nom de cross présentation (ou présentation croisée). Nous avons comparé la cross présentation entre l'ADD MelA et l'ADD A2L. L'ADD MelA semble être plus cross présenté que l'ADD A2L. Cela suggère que l'affichage d'un antigène entier contenant un épitope au lieu d'un épitope seul favorise la cross présentation de cet épitope. Une explication de ce résultat pourrait être l'activation de la réponse immunitaire CD4 par l'antigène MelanA complet qui potentialise la réponse CD8 contre l'épitope A2L.

Enfin, nous avons exploré l'induction d'une réponse immunitaire spécifique de l'antigène tumoral *in vitro* chez l'homme avec l'ADD A2L (cross priming). Ce résultat a mis en évidence la capacité de l'ADDA2L à déclencher l'amplification des cellules T CD8+ anti-MelA₂₆₋₃₅ (anti A2L). De plus, les cellules T CD8+ anti-MelA₂₆₋₃₅ amplifiées ont montré une forte affinité pour le complexe HLA/MelA₂₆₋₃₅.

b. Dé-ciblage et re-ciblage des ADDomers

La deuxième partie de ce travail *in vitro* consistait à dé-cibler les cellules non cibles (cellules épithéliales) et à recibler les cellules cibles (cellules dendritiques) par le biais de modifications sur les ADDomers. L'objectif était de limiter les effets hors cible et d'améliorer l'adressage des ADDomers aux cellules dendritiques.

Le dé-ciblage a été effectué en mutant le motif spécifique de liaison aux intégrines dans la boucle RGD. Ce motif 'RGD' a été muté en 'KGE', limitant ainsi l'absorption de l'ADDomer par les cellules épithéliales, ce qui avait été observé dans des travaux précédents.

Le re-ciblage a été réalisé en affichant à la surface de l'ADDomer le domaine de liaison au récepteur (RBD) du Spike du SARS-CoV-2 fusionné au SpyCatcher (RBD-SC). Cette opération a été réalisée grâce au système SpyTag/SpyCatcher décrit précédemment. Cette protéine a été choisie suite à la pandémie de la Covid-19 durant laquelle notre laboratoire a été amené à évaluer la capacité de la technologie ADDomer présentant le RBD à provoquer une réponse humorale anti-Spike chez la souris. Le RBD-SC est sécrété par les cellules d'insectes lors de sa production en système baculovirus et est par conséquent glycosylé, principalement par des poly-mannoses. Ces glycosylations peuvent être reconnues par les récepteurs de type lectine de type C (CLR) tels que DC-SIGN et MGL présents à la surface des cellules dendritiques. L'épitope A2L a été placé dans la boucle RGD à côté du motif RGD/KGE. L'incubation de cellules adhérentes A549 avec ADD KGE et ADD RGD a montré que l'ADD KGE était moins bien internalisé que l'ADD RGD, ce qui suggère un dé-ciblage efficace. De plus, il semblerait que l'ADD KGE serait tout de même partiellement internalisé par un mécanisme non médié par les intégrines.

Le re-ciblage via le RBD-SC a d'abord été évalué par résonance plasmonique de surface (SPR). La liaison du RBD aux CLR DC-SIGN et MGL *via* les motifs poly-mannose a été mesurée. Les résultats montrent que l'ADD KGE RBD se lie aux deux récepteurs mais plus fortement à DC-SIGN.

Au niveau de l'internalisation par les cellules dendritiques, nous avons vu que l'ajout de RBD n'avait pas augmenté mais diminué l'absorption des ADDomers par les cellules dendritiques contrairement à ce que nous avions supposé. Pour l'ADD RGD RBD, nous supposons tout comme pour l'ADD MelA, que cette diminution pourrait être causée par le masquage du motif de liaison à l'intégrine 'RGD' de l'ADDomer par le RBD-SC. Pour les ADD KGE +/- RBD en raison de l'absence du motif 'RGD' comme mentionné pour les cellules A549, l'internalisation semble avoir lieu *via* un mécanisme non médié par les intégrines. On peut imaginer que ce

mécanisme implique la reconnaissance d'autres motifs moléculaires présents à la surface de l'ADDomer qui sont également masqués par le RBD-SC ce qui expliquerait la diminution de l'absorption des ADDomers par les cellules dendritiques en présence du RBD-SC. Par ailleurs, nous avons montré que l'internalisation semblait être également médiée par un CLR présent à la surface des cellules dendritiques. Enfin, nos résultats montrent que seul l'ADD RGD est cross présenté aux cellules dendritiques contrairement aux ADD KGE, ADD KGE RBD et ADD RGD RBD. Si on transpose ces données aux vaccins anti-mélanome, ceci suggère que l'internalisation médiée par les intégrines serait primordiale dans le processus de cross présentation de l'épitope A2L.

*3) Evaluation *in vivo* chez la souris des vaccins ADDomers*

Les différents ADDomers présentant des épitopes et des antigènes modèles du mélanome sont évalués *in vivo* chez des souris C57bl6J inoculées avec des cellules tumorales de la lignée B16 OVA, lignée communément utilisée dans l'évaluation *in vivo* du mélanome chez la souris. L'immunogénicité des ADDomers ainsi que leur effet préventif et thérapeutique sur la tumeur ont été évalués. L'antigène utilisé est l'ovalbumine avec les épitopes CMH-I et II notés respectivement OVA-I et OVA-II.

Dans un premier temps, la réponse immunitaire déclenchée par ADD-Duo (ADDomer présentant les épitopes OVA-I et II) a été réalisée en l'absence ou en présence d'une série d'adjuvants connus pour activer différents sous-ensembles de CD. Les adjuvants ODN, MPLA et Poly I:C activant respectivement les pDC, cCD2 et cCD1 ont été testés. Nous avons observé que le Poly I:C était l'adjuvant qui aboutissait à la réponse CD8 spécifique dirigée contre l'épitope OVA-I la plus homogène, que ce soit dans les ganglions lymphatiques drainant le site d'injection ou la rate. De plus, cet adjuvant a également induit une bonne réponse humorale contre l'épitope OVA-II. Ces résultats sont en lien avec les données de la littérature rapportant que le Poly I:C, souvent utilisé dans les essais d'immunothérapie contre le cancer, interagit avec

TLR327 et qu'il déclenche une puissante immunité anti-tumorale à médiation Th1 par le ciblage des cDC1s. Nous avons donc décidé de poursuivre nos évaluations *in vivo* avec cet adjuvant. Ensuite, nous avons étudié la possibilité de prévenir la croissance tumorale chez les souris vaccinées. Des immunisations (5 injections espacées de 2 à 3 jours) ont été réalisées avec l'ADD-Duo en présence de poly I:C avec un délai de 25 jours entre la dernière injection et l'implantation de la tumeur (B16-OVA). La croissance tumorale a été suivie jusqu'à ce que le point éthique soit atteint et nous avons mis en évidence que contrairement à l'augmentation rapide de la taille des tumeurs observée dans le groupe vacciné avec l'ADD Ø, aucune tumeur n'a été observée chez les souris vaccinées avec ADD-Duo. Ce résultat montre que l'effet anti-tumoral est bien dû à l'épitope affiché par le vecteur et non à une activation non spécifique du système immunitaire. De plus, cette protection semble être de longue durée puisqu'un délai de 25 jours s'est écoulé entre la dernière immunisation et l'implantation de la tumeur, suggérant l'induction d'une puissante réponse cellulaire CD8+ mémoire.

Comme évoqué précédemment, l'exposition d'antigènes tumoraux au lieu de simples épitopes est primordiale dans la conception d'un vaccin thérapeutique afin de s'affranchir de la restriction allélique. Nous avons donc conçu à la fois des ADDomers comportant un ou deux épitopes de l'ovalbumine (ADD-OTI présentant l'épitope OVA-I et l'ADD-Duo présentant les 2 épitopes OVA-I et OVA-II) ainsi qu'un ADDomer présentant l'antigène ovalbumine entier (ADD Blov) grâce au système SpyTag/SpyCatcher.

De manière intéressante, nous avons observé que les deux systèmes ont été efficaces pour empêcher la croissance de la tumeur B16-OVA lors d'un schéma vaccinal thérapeutique où les souris sont vaccinées avec les ADDomers après l'implantation tumorale.

Dans nos expériences, la caractérisation immunologique a montré une réponse significative des cellules T CD8+ spécifiques de l'OVA dans la rate des souris vaccinées avec l'ADD-Duo et l'ADD-OTI. Une tendance similaire a également été observée dans la seule tumeur résiduelle

où cette analyse était possible. Cependant, en raison du faible nombre de souris présentant une tumeur d'une taille adaptée à cette analyse, nous ne pouvons pas tirer de conclusion solide sur cette observation. Par ailleurs et de manière surprenante, la réponse des cellules T CD8+ anti-OVA-I dans la rate des souris vaccinées avec l'ADD-Blov n'était pas significative par rapport au contrôle ADD-Ø mais cette réponse semblait être significative par rapport au groupe contrôle dans la tumeur (4,08% vs 0,28%). Malgré le faible nombre de matériel tumoral qui a pu être analysé dans le groupe ADD-Blov, cette tendance est fortement soutenue par le contrôle de la croissance tumorale ainsi que par la survie à long terme des souris. Chez les souris Blov, des réponses immunitaires multi-spécifiques ont pu être déclenchées, améliorant ainsi le contrôle de la tumeur, même si ces réponses multi-spécifiques n'ont pas été étudiées ici (seule la réponse contre un seul épitope a été étudiée). Ces réponses multi-spécifiques pourraient être étudiées par la production de cytokines lors de la re-stimulation *ex vivo* des cellules T avec des APC chargés d'OVA.

Une autre caractéristique inattendue était la présence d'une forte réponse des cellules T CD8+ anti-OVA dans la rate et dans la tumeur mesurable des souris vaccinées avec l'ADD-Duo qui n'était pas corrélée avec les courbes de survie à long terme. Nous proposons deux hypothèses possibles pour expliquer ces données, la génération de cellules T régulatrices et/ou un échappement tumoral. En effet, il est concevable que l'ajout d'un épitope de cellules T CD4+ (OVA-II) seul (non inclus dans l'antigène entier ovalbumine) ait déclenché l'induction de cellules T régulatrices qui sont venues altérer l'immunité anti-tumorale malgré une proportion élevée de cellules T CD8+ anti-OVA. Une autre explication pourrait être que la tumeur échappe aux cellules T CD8+ anti-OVA par la perte du CMH de classe I et/ou par une forte expression des points de contrôle immunitaire. En effet, le vaccin ADD-Duo est celui qui a déclenché la plus forte réponse immunitaire à la fois dans la rate et dans la tumeur. On peut imaginer qu'en présence d'une forte pression immunitaire, les clones de cellules tumorales dépourvus

d'expression du CMH-I ont été sélectionnés et/ou que l'IFNy dérivé des cellules T spécifiques de l'OVA a déclenché une forte expression de PD-L1 par les cellules tumorales, conduisant à leur inhibition et à l'échappement tumoral. Pour répondre à ces hypothèses, une analyse FACS des cellules T régulatrices FoxP3 spécifiques de l'OVA, ainsi que de l'expression du CMH de classe I, de PD-L1 et de PD-1 serait nécessaire.

Pour conclure, dans ces travaux de thèse, nous avons démontré que notre technologie nous permettait d'afficher des épitopes et antigènes entiers de mélanome à la surface des ADDomers. Ces ADDomers ont montré leur capacité à induire une réponse immunitaire anti-tumorale efficace contre les épitopes/antigènes apportés par le vaccin d'abord *in vitro* sur des cellules dendritiques humaines de patients sains puis *in vivo* chez des souris. Une meilleure compréhension de la réponse immunitaire engendrée permettrait d'améliorer l'efficacité thérapeutique de ces vaccins, en améliorant par exemple le ciblage des cellules dendritiques. L'utilisation de ligands CLR plus spécifique des CLRs présents à la surface des différents sous-types de cellules dendritiques pourrait être prometteur. Ces ligands oligosaccharides pourraient être obtenus de manière commerciale puis fonctionnalisés chimiquement avec un groupement NHS (N-hydroxysuccinimide) permettant la liaison à l'ADDomer via les chaînes latérales des lysines (fonctions amines). L'insertion génétique d'épitopes directement dans les boucles des ADDomers est peu compatible avec une utilisation en médecine personnalisée ou avec des patients stratifiés. Pour y remédier, l'utilisation du système SpyTag/SpyCatchher, qui consiste en la simple addition des deux composants (ADDomer + antigène-SC) permet d'obtenir une immunothérapie "prête à l'emploi" applicable à une large population. En outre, cette dernière stratégie permet de produire des vaccins mosaïques présentant plusieurs antigènes différents à la fois, ouvrant la voie à une nouvelle génération de produits pour l'immunothérapie du cancer.

mais également pour la prévention des maladies infectieuses comme nous l'avons montré pour la Covid-19.

Comparé à d'autre systèmes d'affichage d'antigènes et d'épitopes, l'ADDomer présente de nombreux avantages. Dans un récent travail, le groupe du Pr Cerullo²⁶⁹ rapporte une stratégie combinée utilisant un virus oncolytique et l'expression/affichage d'antigènes tumoraux *in situ*. La technologie PeptiCRAc a été développée pour afficher l'épitope par interaction électrostatique avec les capsomères de l'hexon (240 copies donc 720 monomères). Par rapport à ces travaux, notre plateforme vaccinale codant génétiquement ou affichant des épitopes/antigènes (60 ou 120 copies) présente certains avantages et inconvénients. Parmi les avantages, nous pouvons affirmer que notre plateforme inspirée des adénovirus n'est pas infectieuse et donc plus sûre que les virus oncolytiques qui sont réplicatifs. Par rapport à PeptiCRAc qui affiche les épitopes en utilisant des interactions électrostatiques, dans la technologie ADDomer, les épitopes sont soit insérés génétiquement, soit liés de manière covalente, ce qui permet un meilleur contrôle de la stœchiométrie. Dans les deux cas, les deux technologies sont rapidement adaptables à n'importe quel épitope tumoral. Dans le cas d'ADDomer, nous montrons ici que de grands antigènes peuvent également être affichés. Cependant, contrairement aux virus oncolytiques qui se lysent et se répliquent *in situ*, notre plateforme n'a pas d'effet direct contre la tumeur et est donc passive après inoculation.

Il pourrait être envisagé de combiner les avantages respectifs des deux approches en concevant un adénovirus oncolytique codant l'ADDomer-ST et l'antigène d'intérêt fusionné à un SpyCatcher afin de bénéficier à la fois de la lyse tumorale et de la stimulation immunitaire *in situ*.

Par ailleurs, au vu des nombreux vaccins à ARN se développant actuellement, il est intéressant de comparer la réponse immunitaire générée par des vaccins codant ou affichant des antigènes tumoraux. Dans un travail récent, Anchim et al.²⁷⁰ compare la capacité de vaccins dérivés de la

capside d'adénovirus de sérotype 5 à susciter des réponses anticorps anti-ovalbumine. Ces vaccins affichent l'antigène d'intérêt ovalbumine soit dans l'hexon (AdH-3OVA2) soit dans la fibre (AdF-3OVA2) de la capsid ou codent pour la protéine entière de l'ovalbumine en tant que transgène (AdOVA). Il a été observé que dans le cas de souris naïves les réponses Ab anti-ovalbumine étaient plus élevées suite à une vaccination avec l'AdOVA par rapport au AdH-3OVA2 puis au AdF-3OVA2 (AdOVA > AdH-3OVA2 > AdF-3OVA2). En revanche, dans le cas de souris immune c'est-à-dire ayant déjà été immunisées avec le vecteur vide (mimant ainsi la pré-immunité adénovirale présente chez une grande partie de la population) les tendances s'inversent. Nous observons alors des réponses Ab anti-ovalbumine étaient plus élevées suite à une vaccination avec l'AdF-3OVA2 par rapport au AdH-3OVA2 puis au AdOVA (AdF-3OVA2 > AdH-3OVA2 > AdOVA).

Ces résultats montrent qu'il pourrait y avoir un avantage à afficher des antigènes à la surface d'une particule adénovirale par rapport à coder ces antigènes comme transgène.

Annexe

Introduction :

Le travail présenté dans cette annexe a été initié lors de la pandémie de la Covid-19. Le travail réalisé pendant les premiers mois de ma thèse sur l'optimisation des ADDomers (voir chapitre IV) ont pu être utilisées rapidement pour le développement d'un vaccin contre le SARS-CoV-2. L'équipe avait pour projet de décorer l'ADDomer avec le domaine de liaison au récepteur (RBD) du Spike du SARS-CoV-2 afin de provoquer une réponse humorale anti-Spike. Après vaccination, les anticorps neutralisants produits devraient empêcher le virus de pénétrer dans les cellules par inhibition de la fixation de celui-ci à son récepteur cellulaire ACE2. La réPLICATION virale ne sera donc plus possible et l'infection stoppée. Cette publication décrit le développement d'un vaccin ADDomer affichant un antigène du SARS-CoV-2 ainsi que l'évaluation de la réponse humorale induite chez des souris vaccinées.



Molecular Therapy

Original Article

Elicitation of potent SARS-CoV-2 neutralizing antibody responses through immunization with a versatile adenovirus-inspired multimerization platform

Christopher Chevillard,^{1,5} Axelle Amen,^{1,3,5} Solène Besson,^{1,5} Dalil Hannani,² Isabelle Bally,¹ Valentin Dettling,¹ Evelyne Gout,¹ Christophe J. Moreau,¹ Marlyse Buisson,¹ Salomé Gallet,¹ Daphna Fenel,¹ Emilie Vassal-Stermann,¹ Guy Schoehn,¹ Pascal Poignard,^{1,3,4} Marie-Claire Dagher,¹ and Pascal Fender¹

¹CNRS, Univ. Grenoble Alpes, CEA, UMR5075, Institut de Biologie Structurale, 38042 Grenoble, France; ²University Grenoble Alpes, CNRS, UMR 5525, VetAgro Sup, Grenoble INP, TIMC, 38000 Grenoble, France; ³CHU Grenoble Alpes, 38000 Grenoble, France; ⁴Department of Immunology and Microbiology, The Scripps Research Institute, La Jolla, CA 92037, USA

Virus-like particles (VLPs) are highly suited platforms for protein-based vaccines. In the present work, we adapted a previously designed non-infectious adenovirus-inspired 60-mer dodecahedric VLP (ADDomer) to display a multimeric array of large antigens through a SpyTag/SpyCatcher system. To validate the platform as a potential COVID-19 vaccine approach, we decorated the newly designed VLP with the glycosylated receptor binding domain (RBD) of SARS-CoV-2. Cryoelectron microscopy structure revealed that up to 60 copies of this antigenic domain could be bound on a single ADDomer particle, with the symmetrical arrangements of a dodecahedron. Mouse immunization with the RBD decorated VLPs already showed a significant specific humoral response following prime vaccination, greatly reinforced by a single boost. Neutralization assays with SARS-CoV-2 spike pseudo-typed virus demonstrated the elicitation of strong neutralization titers, superior to those of COVID-19 convalescent patients. Notably, the presence of pre-existing immunity against the adenoviral-derived particles did not hamper the immune response against the antigen displayed on its surface. This plug and play vaccine platform represents a promising new highly versatile tool to combat emergent pathogens.

INTRODUCTION

Although genomic vaccines have recently demonstrated their capacity to elicit protective immune responses,¹ protein-based vaccines remain highly attractive due to their lower cost, and ease of transport and storage, crucial to reach developing countries and remote locations, as well as better social acceptance, as recently highlighted by hesitancy regarding COVID-19 RNA vaccines. Protein immunogenicity is highly increased through presentation to the immune system in a multimeric manner, and a number of vaccine platforms have been developed to this aim, with various advantages and limitations.² We have previously reported that a non-infectious virus-like particle (VLP) derived from human adenovirus of type 3 and consisting of 60 identical penton base

monomers could be exploited to display epitopes of interest on its surface.^{3–5} In this vaccine platform, named ADDomer, exposed loops of the penton base protein were engineered to allow insertion of foreign peptides such as a linear neutralizing epitope from Chikungunya virus. However, this design did not permit the insertion of structurally complex antigens. To overcome this limitation while keeping the immunogenicity advantage of ADDomer, we describe here a redesigned platform offering a highly versatile capacity to display large and structurally complex antigens with potential post-translational modifications. In order to decorate the adenovirus-based VLPs with large antigens, the SpyTag/SpyCatcher system^{6–9} was combined with the ADDomer technology. In this system, derived from *Streptococcus pyogenes*, an aspartate residue from the 13 amino acid SpyTag peptide (ST) can spontaneously create a covalent bond with a lysine residue encompassed in the complementary SpyCatcher module (SC). We thus genetically inserted the sequence coding for the ST peptide into the “variable loop” of the ADDomer that was previously used for small antigen insertion, yielding a VLP with 60 potential attachment sites for complex antigens engineered with an SC anchor.

In order to assess the newly developed platform, we decided to first test it as a potential candidate vaccine to elicit neutralizing antibodies (NABs) against the severe acute respiratory syndrome coronavirus 2 (SARS-CoV-2). SARS-CoV-2 is an enveloped positive strand RNA virus belonging to the beta-coronavirus genus from the Coronaviridae family. It is the etiological agent of coronavirus disease 2019

Received 28 October 2021; accepted 7 February 2022;
<https://doi.org/10.1016/j.ymthe.2022.02.011>.

⁵These authors contributed equally

Correspondence: Pascal Fender, CNRS, Univ. Grenoble Alpes, CEA, UMR5075, Institut de Biologie Structurale, 38042 Grenoble, France

E-mail: pascal.fender@ibs.fr

Correspondence: Pascal Poignard, CNRS, Univ. Grenoble Alpes, CEA, UMR5075, Institut de Biologie Structurale, 38042 Grenoble, France

E-mail: pascal.poignard@ibs.fr

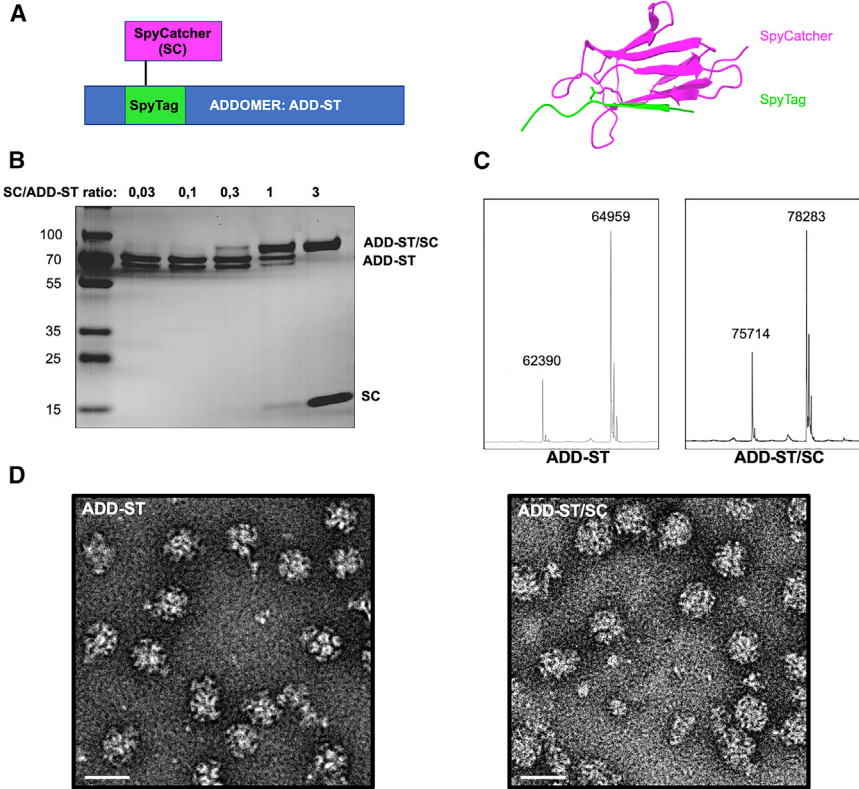


Figure 1. Application of the SpyTag/SpyCatcher cross-linking method to the ADDomer technology

(A) Diagram showing the internal insertion of SpyTag in the internal loop of an ADDomer monomer. Spytag (in green) can make an isopeptidic bond with SpyCatcher (in purple). Structure of a SpyTag covalently linked to a SpyCatcher is shown on the right (PDB code: 4MLI). (B) SDS-PAGE profile of reduced and boiled samples of ADD-ST after interaction with incremental ratio of SC showing the apparition of a higher MW covalent adduct (ADD-ST/SC). (C) Electrospray ionization graphs of ADD-ST and ADD-ST/SC showing the shift of the peaks by 13.3 kDa. The doublet is due to an alternative start of translation in ADD-ST and display the same mass shift of 13.3 kDa. (D) Negative staining electron micrographs of ADD-ST and ADD-ST/SC (bar, 30 nm).

can successfully be decorated with SARS-CoV-2 RBD and is highly immunogenic in mice, eliciting high neutralizing Ab titers.

RESULTS

Internal insertion of ST in ADDomer results in efficient SC cross-linking

ADDomer is a non-infectious 30-nm nanoparticle, formed from 12 bricks of the homo-pentameric penton base from the human adenovirus type 3. The ST sequence was inserted in the

ADDomer gene in a region coding for the exposed flexible loop called the variable loop (Figure 1A). Due to the spontaneous homo-oligomerization of the 12-pentameric penton base, 60 copies of ST are exposed on the surface of the ADDomer-ST (ADD-ST) particle. To assess whether the newly inserted ST sequence was accessible and functional on ADD-ST, incubation with a different ratio of SC was performed. After boiling of samples, SDS-PAGE profile clearly showed that the incremental SC/ADD-ST ratio is correlated with the apparition of a band of higher molecular weight and the decrease of the intensity of bands related to unlinked moieties. Importantly, there was no remaining signal for un-decorated ADD-ST after SC addition at the highest ratio, thus reflecting the full decoration of the nanoparticle (Figure 1B). This result suggests an efficient and concentration-dependent formation of the ADD-ST/SC complex. Mass spectroscopy analysis confirmed that the ADD-ST doublet shifted by 13.3 kDa (Figure 1C), which corresponds to the molecular weight (MW) of SC. The two peaks observed in mass spectroscopy is due to a second initiation codon in ADD-ST (starting at Methionine 25) without affecting the particle stability,²⁸ and SC can bind to each form indifferently, as shown by a similar shift of their MW corresponding to the addition of SC. Negative staining electron microscopy imaging performed on ADD-ST alone and ADD-ST fully decorated by SC showed that the integrity of the particle was not affected by the presence of SC and the grainy appearance of ADD-ST/SC likely reflects the presence of SC at the particle surface (Figure 1D). Altogether, these data show that SC cross-linking to ADD-ST is operational and can result in saturated decoration of the nanoparticle.

(COVID-19), and at the origin of the pandemic that started in December 2019, leading to 5,542,359 deaths as of January 19, 2022 (<https://covid19.who.int/>), and vast socio-economic consequences.¹⁰ Protection against SARS-CoV-2 infection and COVID-19 can be mediated by neutralizing Abs targeting the envelope trimeric glycoprotein spike (S) exposed at the surface of the virus.^{11,12} Accordingly, spike-based vaccine approaches eliciting SARS-CoV-2 NAb responses have been successful at preventing COVID-19.^{13–15} The ecto-domain of the S protein is divided into the S1 and S2 domains. The Spike protein binds to the host angiotensin-converting enzyme 2 (ACE2), which serves as an entry receptor, as previously reported with SARS-CoV, responsible for the 2002–2004 SARS outbreak.^{16–19} A subdomain of S1, named receptor binding domain (RBD), is the contact interface between the virus and the ACE2 receptor. Numerous studies have shown that the RBD comprises multiple distinct antigenic sites and is a prime target for NAb in COVID-19 convalescent patients.^{20–23} These NAb²⁴ strongly inhibit cell infection by SARS-CoV-2 by competing with the RBD-ACE2 interaction. Moreover, anti-RBD NAb have been shown to confer protection against SARS-CoV-2 challenge in animal models of COVID-19, as well as to prevent COVID-19 in humans, thus confirming the interest of using RBD as a vaccine immunogen.^{25–27}

This prompted us to use the RBD as the antigen to be displayed on our newly designed VLP platform in order to engineer a novel COVID-19 vaccine approach. Here, we report that the newly designed platform

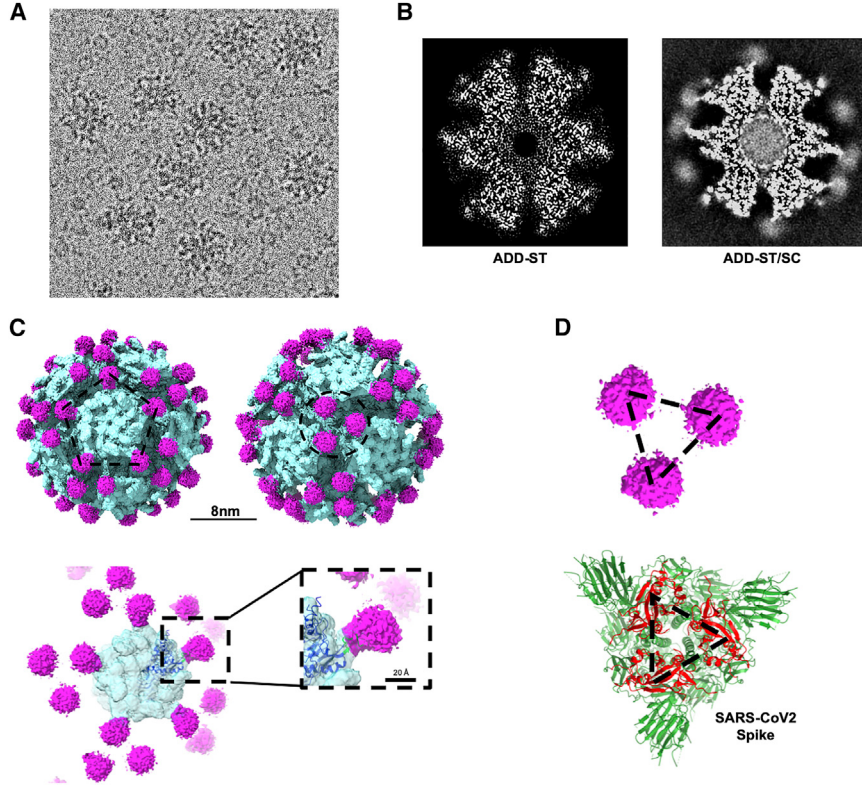


Figure 2. Cryo-EM reconstruction of ADD-ST decorated with SC

(A) Representative 2D picture of the particles frozen on ice (bar, 30 nm). (B) Section through the density of the 3D reconstruction without (ADD-ST) or with SC (ADD-ST/SC). (C) Isosurface representation of the ADDomer-ST/SC 3D structure showing the extra density of SC in purple onto the non-decorated ADD-ST scaffold in light blue. The particle is represented along either the 5- or 3-fold-axis (left and right, upper panel; bars, 80 and 20 Å, respectively). Focus on a pentameric complex of ADD-ST/SC with a close-up view onto a single SC/ST interaction (dashed line boxes in the lower panel). The atomic resolution structure (dark blue) of the HAd3 penton base (PDB 4AQQ) has been fitted into the ADDomer EM density (light blue). (D) Organization of SC along the 3-fold axis of the particle (upper panel) and comparison with SARS-CoV-2 RBD architecture (in red) within the Spike protein structure (in green, PDB 6VXX) at the same scale.

Cryoelectron microscopy analysis enables visualization of SC decoration on ADD-ST

In order to visualize the SC arrangement around the ADDomer particle, a structural study by cryoelectron microscopy (cryo-EM) was used. Fully decorated ADD-ST/SC particles were imaged on a Glacios electron microscope (Figure 2A). Image analysis was performed and the obtained 3D structure was compared with the structure of an un-decorated ADDomer particle (EMD-0198). An extra-density corresponding to SC bound to the ADDomer “variable loop” was clearly visible in ADD-ST/SC both in the density slice of the 3D map (Figure 2B) and in the isosurface representation of the structure (Figure 2C, purple density and supplementary movie). The resolution of the ADDomer particle is around 2.8 Å, allowing to clearly see the aminopeptidic chain. However, the ST/SC part is not rigidly attached to the ADDomer, which explains why the corresponding density is fuzzy, and the structure not better defined (Figure S1). The ADDomers have 2, 3, and 5 axes of symmetry (the latter two are shown in Figure 2C), which is a characteristic of a dodecahedron, meaning that SCs are distributed accordingly. Interestingly, along the 3-fold axis, SCs are ~4.7 nm apart, which is close to the RBD in the trimeric spike protein of SARS-CoV-2 (~4.1 nm), suggesting that the decorated particles would closely mimic the natural trimeric arrangement of RBDs (Figure 2D). Both the multivalency of SC displayed by the particle and the arrangements they have around the different symmetry axis could be an asset for vaccination purpose if an antigen is fused to this module.

Secreted RBD fused to SC is glycosylated and can be displayed at different ratios on the ADD-ST particle

To take advantage of the spontaneous and covalent linking of SC to ADD-ST, we reasoned that SC could be used as a versatile carrier to easily and efficiently fuse antigens, like in this SARS-CoV-2 vaccine development (Figure 3A), and in broader perspectives to diverse soluble proteins

of interest. In the present study, the SARS-CoV-2 RBD was fused to the N-terminus of the SC (RBD-SC) and a melittin signal peptide was added to allow protein post-translational modifications (PTMs) such as glycosylations and secretion from insect cells. To assess whether the secreted and purified RBD-SC was glycosylated, it was treated with N-glycosidase (PNGaseF), and the result showed a shift in the migration of the related band in SDS-PAGE gel, indicating that RBD-SC was indeed glycosylated (Figure 3B). As previously performed with unfused SC (Figure 1B), incremental amounts of RBD-SC were added to ADD-ST in order to decorate the particle with different ratio of cargos (from 0.03 to 3 copies of SC per particle monomers). The SDS-PAGE gel profile (Figure 3C) showed the correlated apparition of a band at higher MW with increased concentrations of RBD-SC. This result reflects the covalent linking of RBD-SC to the ADD-ST monomers, whereas the band corresponding to non-decorated ADD-ST monomer progressively faded away, disappearing when the particle is fully decorated. This result showed that the ADDomer platform can be decorated with different numbers of antigen copies exposed on its surface. Altogether, these experiments demonstrated that SC fusion to large antigens (~40 kDa for RBD-SC) with post-translational modifications enable their covalent linking to the ADDomer platform and that the ratio of decoration can be adjusted according to desired applications.

ADDomers decorated of glycosylated RBD bind to ACE2

RBD is the subdomain of the SARS-CoV-2 spike protein that binds to the human ACE2 receptor. To assess the function of RBDs

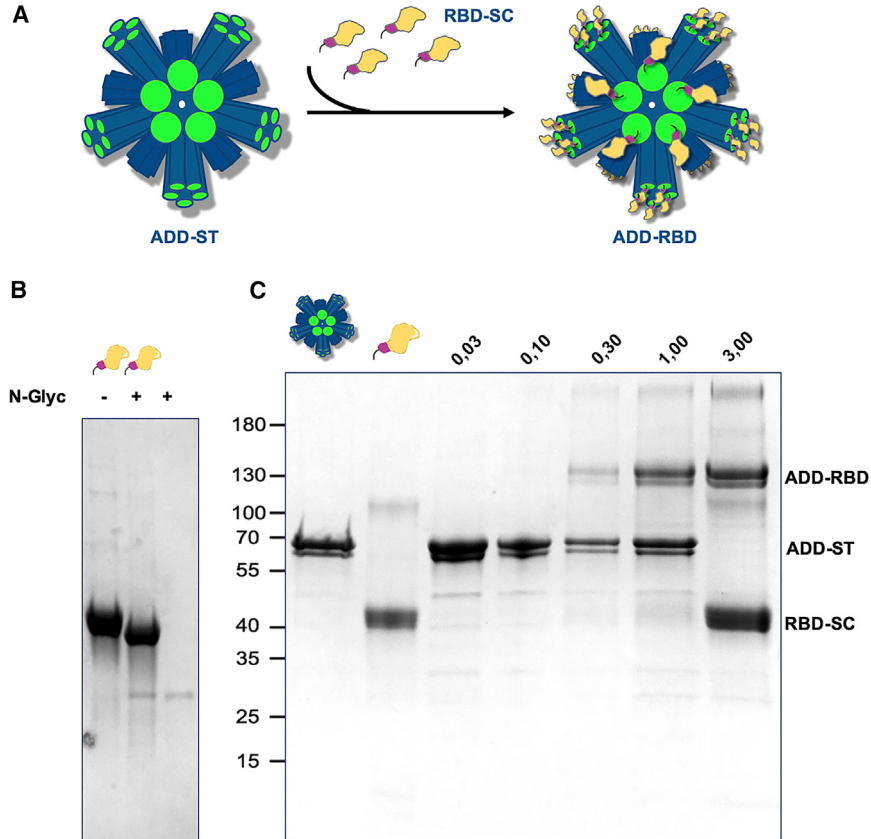


Figure 3. Fusion of SARS-CoV-2 RBD to SC enables its surface presentation on ADDomer particles

(A) Schematic representation of the spontaneous RBD-SC binding to ADD-ST to give ADD-RBD. (B) SDS-PAGE gel with RBD-SC before (−) and after (+) treatment with N-glycosidase and in absence of SC-RBD. The decrease of the molecular weight of SC-RBD after treatment indicates that it is glycosylated. (C) SDS-PAGE gel of reduced and boiled samples showing from left to right, the marker, bands of ADD-ST alone, SC-RBD alone and a fix amount of ADD-ST incubated with different ratio of RBD-SC (*per* particle monomer). The additional upper bands reflect the covalent adduct between ADD-ST and RBD-SC and thus the apparition of ADD-RBD. As expected, the increasing intensities of the ADD-RBD bands correlate with a decrease of non-decorated ADD-ST monomer.

pseudo-typed virus harboring the SARS-CoV-2 spike and either RBD-SC or ADD-RBD was performed. Negative control was made with undecorated ADD-ST alone. As expected, both RBD-SC alone and ADD-RBD were able to compete with the pseudo-typed virus with a slightly higher efficiency for the RBD-decorated particle (Figure 4C). Altogether, these experiments showed that RBD-SC is properly folded and can bind the ACE2 receptor at the molecular and cellular

scales when applied alone (RBD-SC) or linked to the ADDomer particles (ADD-RBD).

RBD-decorated ADDomer elicits rapid anti-CoV2 Ab responses in mice, not negatively impacted by adenovirus pre-immunity

Multivalent exposition of RBD antigens at the surface of the particle is likely to result in a better activation of the humoral system than RBD alone. However, one cannot exclude that ADDomer itself could also play an indirect role in the anti-SARS-CoV-2 response, especially in a population with pre-existing adenovirus immunity. To address these two points, four groups of 10 mice were designed (Figure 5A). The two first control groups were injected with RBD-SC alone in group 1 or with the same amount of unlinked RBD-SC plus naked-ADDomer (i.e., not displaying the antigen) in group 2. The two other groups (groups 3 and 4) were vaccinated with ADD-RBD (i.e., RBD displayed at the particle surface) but group 4 was pre-immunized with naked-ADDomer 2 weeks before the injection of ADD-RBD, in order to investigate whether anti-HAdV-3 penton base antibodies, as may possibly be found in individuals previously infected with adenovirus type 3, may impact the immunogenicity of ADD-RBD (Figure 5B). The presence of anti-ADDomer (i.e., HAdV-3 penton base adenovirus) antibodies in group 4 was checked by ELISA 1 day before the first immunization with ADD-RBD. The results (Figure S3) show that all group 4 mice did mount an antibody response against naked-ADDomer. Then, the immune response against RBD

linked to the ADDomer particles, three different approaches were used. First, binding experiments at the molecular scale were performed using surface plasmon resonance (SPR) on immobilized dimeric human ACE2 fused to the Fc domain of human immunoglobulin (Ig)G.²⁹ Sensorgrams of ADD-RBD binding to immobilized human ACE2 showed a clear concentration-dependent binding of the RBD-decorated particles on ACE2 and a stable interaction with no visible dissociation at the end of injections (Figure 4A). The extremely slow dissociation rate ($4.57 \times 10^{-4} \text{ s}^{-1}$) agreed with a sub-nanomolar “apparent” K_D ($3.09 \times 10^{-10} \text{ M}$). This apparent K_D is the result of an avidity with the decorated particle effect since the K_D of RBD-SC alone is slightly higher ($1.53 \times 10^{-8} \text{ M}$; Figure S2). In any case, this result showed that the RBD is functional and that our platform somehow mimics viruses that evolved to take advantage of multivalent interactions with cellular receptors. In a second experiment at the cell scale, the direct binding of ADD-RBD onto HeLa cells stably expressing ACE2 was visualized by immunofluorescence using anti-ADDomer antibodies. The green signal seen at the periphery of HeLa-ACE2 cells in the presence of ADD-RBD contrasted with the absence of signal observed with the same cells but in presence of undecorated ADD-ST particles. This result demonstrated that RBD at the surface of the particles induced the interaction with ACE2 present at the surface of the HeLa-Ace2 cells (Figure 4B). Finally, a competition experiment between a

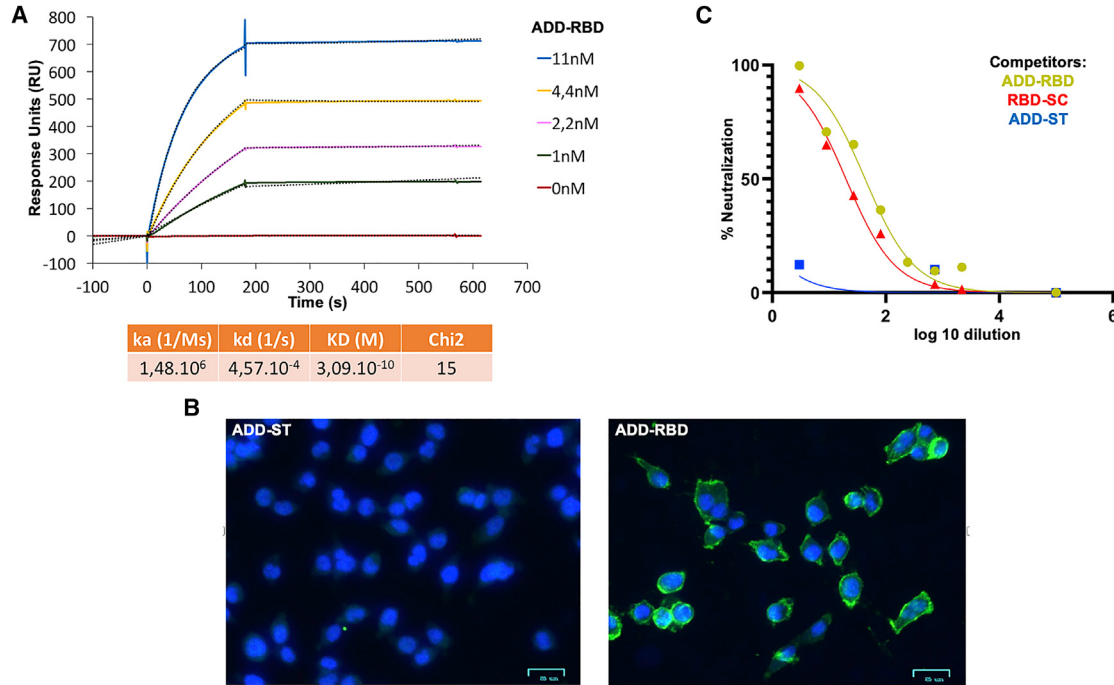


Figure 4. Functional characterization of the ADDomer particles decorated with SARS-CoV-2 RBD

(A) Surface plasmon resonance sensorgrams obtained by injection of different amounts of ADD-RBD to the immobilized ectodomain of the human ACE2 receptor fused to IgG Fc constant domain²⁹ and kinetic analysis. (B) Immunofluorescence microscopy images of HeLa-ACE2 cell at 4°C with double staining with Hoechst (blue) and anti-ADDomer Ab and an Alexa 488-conjugated secondary Ab (green) in presence of non-decorated ADD-ST (left) or ADD-RBD (right) particles. (C) Competition of pseudotyped SARS-CoV-2 virus encoding luciferase with either ADD-ST (blue), RBD-SC (red) and ADD-RBD (gold) at different dilutions.

was monitored by ELISA at days 13 (post first immunization), 27, and 41 (post second immunization). The RBD-decorated particles induced a significant anti-SARS-CoV-2 response after the first immunization (day 13, Figure 5C), whereas no response was detectable in controls of group 1 (RBD-SC alone) or group 2 (ADDomer with not displayed SC-RBD). Interestingly, anti HAdV-3 penton base pre-immunity did not negatively impact the anti-RBD response. A trend toward a stronger anti-RBD response was even observed at this stage.

Immunization boost increases both the amplitude and the duration of the response induced by ADD-RBD particles, independently of the anti-vector immunity

Two weeks after the second immunization (day 27), the anti-RBD response was clearly boosted for groups 3 and 4 that were injected with ADD-RBD, whereas the control groups 1 and 2 showed more heterogeneous responses (Figure 6A). This observation confirms that our vaccine platform displaying multivalent RBD antigens yields a rapid and efficient humoral response. The ADDomer technology applied to RBD antigen also demonstrated a long-lasting immunogenic effect with anti-SARS-CoV-2 RBD antibodies remaining at the highest level at day 41 (Figure 6B). The difference between mice pre-immunized by ADDomer (group 4) or not (group 3) was less pronounced than after the first immunization, both groups reaching high and comparable levels. Altogether, these results showed that the sec-

ond immunization enabled a high and long-lasting Ab response against the SARS-CoV-2 RBD using the ADDomer platform and that anti-vector pre-immunity is possibly beneficial in particular to the initial responses (Figure 6C).

RBD-decorated ADDomer immunization elicits strong neutralizing Ab responses

Since the RBD is critical for binding to the SARS-CoV-2 receptor ACE2, antibodies elicited through immunization with the RBD (RBD-SC or ADDomer-RBD) can hinder the interaction between the Spike proteins and ACE2, blocking viral entry. The ability to neutralize the virus depends on the affinity of the antibodies for the RBD domain, as well as on the epitope recognized. To assess the potency and efficacy of the antibodies induced in the four immunized groups of mice, the neutralization potency of sera (day 41) from vaccinated mice was assessed using SARS-CoV-2 spike (Wuhan strain) pseudo-typed lentivirus and ACE2-expressing HeLa cells. Only a partial and heterogeneous neutralization was obtained from group 1 and 2 sera in which RBD-SC was not displayed on ADDomer, even after two immunizations (Figure 7A, upper panels). Of note, sera from mice immunized with RBD-decorated ADDomer (groups 3 and 4) showed a better neutralization titer after a single immunization than groups 1 and 2 after 2 immunizations (Figure S4). After the second immunization, strong virus neutralization was observed in all mice from groups 3 and 4

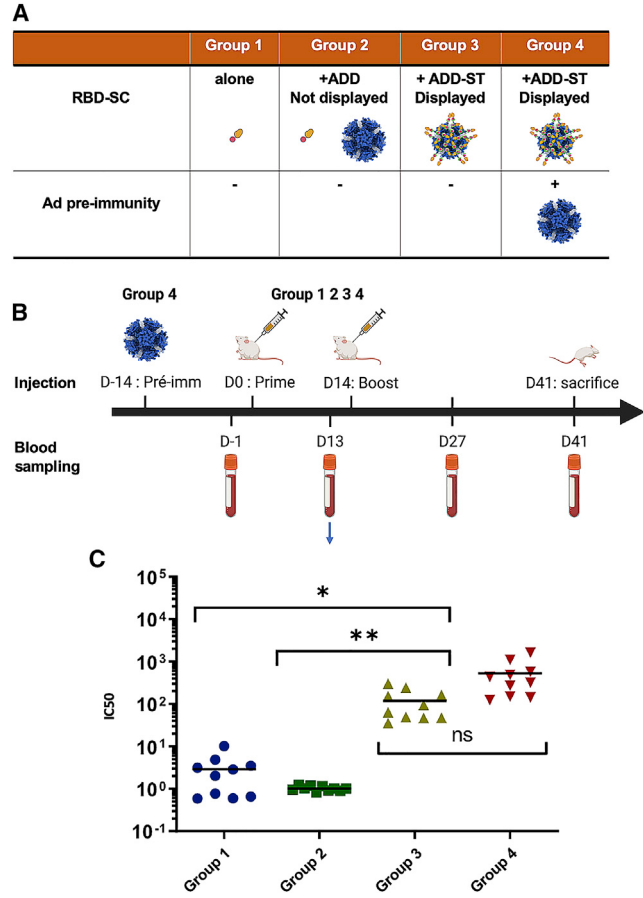


Figure 5. Immunization studies on mice inoculated with the same amount of RBD under different conditions

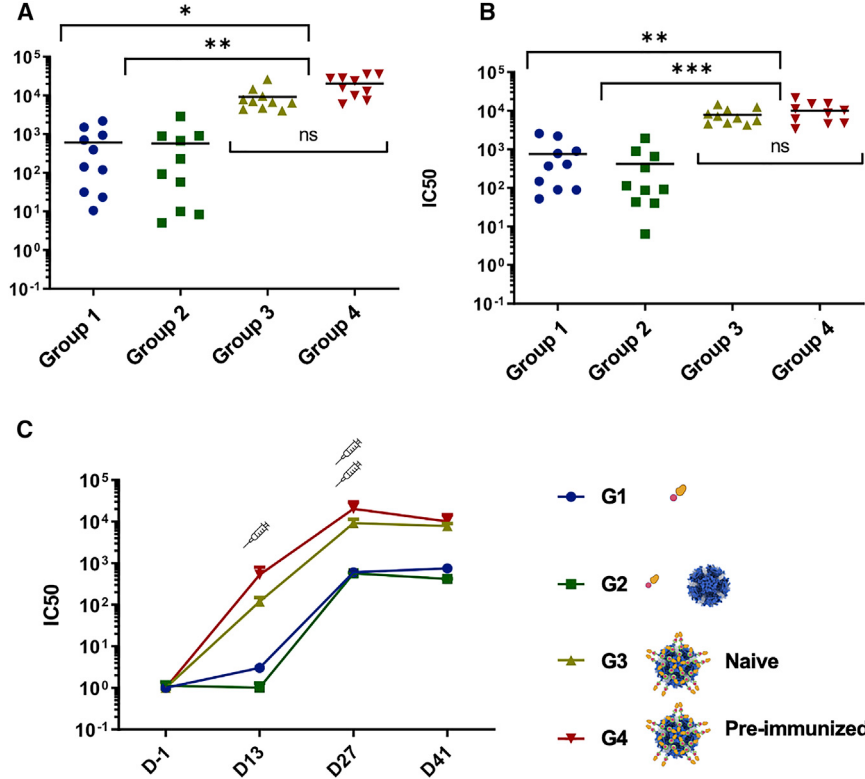
(A) Different groups were constituted to address the respective role of RBD-SC alone (group 1), RBD-SC in presence of naked-ADDomer (group 2), and RBD-SC displayed by ADDomer (ADD-RBD) either in adenovirus naïve or adenovirus pre-immunized mice (group 3 and 4 respectively). (B) Immunization schedule and blood sampling for all groups. (C) IC₅₀ of anti RBD response 13 days after the first immunization (n = 10). Lines are mean values and Kruskal-Wallis tests, were performed followed by a Dunn's multiple comparison tests.

(Figure 7A, lower panels). Neutralization titers (ND₅₀) clearly showed that mice vaccinated with RBD-decorated ADDomer had significantly higher neutralizing activity than mice immunized with the same amount of antigen when not displayed on the platform (Figure 7B). Moreover, in accordance with the ELISA results (Figure 5C), the anti-vector response (group 4) slightly increased the neutralization titer compared with the naïve group (group 3), which emphasizes that a pre-existing HAdV-3 penton base immunity could be beneficial for our novel vaccine platform (Figure 7B). The neutralizing Ab titers reached in groups 3 and 4 were overall superior to those from a cohort of convalescent COVID-19 patients composed of 50% mild (oxygen below 2 L/min) and 50% severe (intensive care unit) cases, and measured at 6 months after hospitalization (Figure 7B).³⁰

DISCUSSION

In this study, we designed a novel and highly versatile vaccine platform amenable to large antigens by adapting the ST/SC technology to ADDomer, an adenovirus-inspired VLP.^{5,6} This technology has already been described for designing VLP-derived vaccine; however, in these approaches, SC was the moiety grafted to the VLPs while the antigens were fused to the ST.^{7,31} In our novel vaccine technology, we used the opposite configuration with ST insertion in an internal loop of ADDomer, which minimized the risk of steric hindrance and functional impact on the spontaneous oligomerization of ADDomers. Insertion of ST in a surface-exposed loop of ADDomer did not impair the spontaneous assembly of 12 pentameric bricks (Figure 1D), thus creating a universal generic platform for multivalent antigen display. Experiments of saturating cross-linking with SC alone suggested that a full decoration (i.e., 60 copies) of the particle can be achieved (Figure 1B). Despite the flexibility of the loop in which ST was inserted, cryo-EM reconstruction of the ADD-ST/SC complex clearly showed an extra density corresponding to the SC interacting with ST fused to the ADDomer. The data thus strongly suggested that the ADDomer could be used to display a multimerized array of antigens, a property that is crucial for the elicitation of strong Ab responses.^{32–34} Interestingly, the characteristic 2-, 3-, and 5-fold symmetry axis of a dodecahedron are easily visible in the 3D structure (Figure 2C), this spatial configuration showing that the SCs are distributed at different distances from each other according to the symmetry axis. Such distribution of the antigen could potentially further favor the immunogenicity of the VLP by offering different patterns of presentation of the antigen at the particle surface.

The COVID pandemic led us to first evaluate our newly designed platform as an anti-SARS-CoV-2 vaccine to be displayed through fusion to the SC N-terminus. It is worth noting that in the 3-fold axis of ADDomer, the SC adopts a pseudo-trimeric arrangement, which on the RBD decorated VLP closely mimics the tridimensional configuration of this domain in the SARS-CoV-2 spike glycoprotein (Figure 2D). The distance between SC in such configuration is 4.7 nm, which is in the same range as that between RBDs in the trimeric Spike protein (4.1 nm). Expressing soluble RBD fused to SC in insect cells resulted in N-glycosylation as expected,³⁵ and did not affect the structure of SC, which retained its ability to cross-link to the ADD-ST vaccine platform in a dose-dependent manner (Figure 3C). The proper folding of the glycosylated RBD exposed at the surface of the particles and its ability to bind ACE2 were assessed in a functional viral entry assay via competition with SARS-CoV-2 Spike pseudo-typed virions (Figure 4C). An SPR experiment confirmed the high-affinity interaction of ADD-RBD to ACE2, the highly stable interaction observed suggesting an avidity effect of the multivalent particle exposing multiple copies of RBD (Figure 4A). Moreover, this experiment also shows that expressing RBD in insect cells leads to a functional SARS-CoV-2 glycoprotein domain. Several vaccines using the baculovirus expression system in insect cells have been approved, such as vaccines against papillomavirus or hepatitis B. The Novavax COVID-19 vaccine candidate, based on an insect cell-produced trimeric S protein, is also advancing toward approval trials.³⁶



The ability of the RBD-decorated ADDomer to elicit an anti-SARS-CoV-2 humoral response was then studied in mice. As expected, we confirmed that displaying the RBD in a multimerized manner led to a strong improvement in immunogenicity (groups 3 and 4 versus groups 1 and 2). Indeed, this was clearly apparent from the first injection, where the groups with decorated particles showed a significant anti-RBD response at day 13 as measured in ELISA (Figure 5C), whereas no response was observed for the other groups. This observation is in agreement with experiments reported with other vaccine platforms that showed that injection of RBD or S-trimer alone did not produce significant responses.^{31,37} In our experiment, we chose to inject 5 µg of RBD, but a dose-response study would be necessary to determine the optimal amount. As a comparison, similar experiments carried out with a similar 60-mer platform showed that 0.9 µg instead of 5 µg of RBD resulted in a similar immune response paving the way to dose-sparing.³⁸ After the second immunization, although a response was observed in the non-decorated groups, the titers attained in the decorated groups were about 10-fold greater (Figure 6A). Notably, the anti-RBD response in the latter groups endured over time with similar titers at 2 and 4 weeks following the second immunization (Figure 6B). The anti-SARS-CoV-2 RBD sera were further assessed for their capacity to neutralize S-protein pseudotyped lentivirus particles (Figure 7). As seen for binding responses, a neutralizing activity was observed in the RBD-decorated groups after the first immunization. Overall, a good correlation between ELISA and neutralizing titers was observed. Strong neutralizing titers were attained in all mice immunized with ADD-RBD after the boost immu-

Figure 6. Anti-RBD Ab in all groups of mice 2 and 4 weeks after the booster immunization

(A) IC50 of anti-RBD for each individual mice from all groups, 2 weeks after the booster injection. (B) Same data, 4 weeks after the booster injection. Lines are mean values. Kruskall-Wallis tests, were performed followed by a Dunn's multiple comparison tests. (C) Means of the anti-RBD response from all mice according to their groups and the time after the first immunization performed at day 0.

nization, superior to those of convalescent COVID-19 patients (Figure 7B), showing the ability of our vaccine platform to elicit functional Ab responses with a potential protective activity. The low titers obtained in mice immunized with RBD and naked ADDomer (no decoration) again demonstrated that the high immunogenicity achieved with decorated VLPs originated from the multimeric display of the antigen. A limitation of our study is that cellular responses were not measured. It is known that CD8 T cell responses likely play an important role in protecting against severe forms of COVID-19. In contrast to mRNA and viral vector vaccines, VLPs are not optimal platforms to elicit CD8 T cell responses, due to

the lack of endogenous antigen production. This hurdle may indeed represent a limitation for such vaccines, including our approach. However, CD8 responses may be elicited by VLPs under certain circumstances through cross-presentation following uptake by dendritic cells, and additional work will be necessary to evaluate whether ADDomer may potentially elicit specific CD8 T cells.

Overall, the data are in adequacy with results obtained with similar vaccine platforms using multimeric display of the SARS-CoV-2 RBD on scaffolds such as the 24-mer ferritin, the 60-mer dodecahedral thermophilic aldolase.^{31,39,40,41} In contrast to these latter vaccine platforms, our particles originate from a human virus, Adenovirus serotype 3 (HAd3), which is known to have a relatively high seroprevalence.^{42,43}

However, if HAdV-3 is globally among the most common types implicated in HAdV infections, a great variation is observed by geographic regions. Indeed, HAdV-3 accounts for 15% to 87% of adenoviral respiratory infections with a greater prevalence in Asia than in western countries.⁴⁴ Neutralizing antibodies against HAdV-3 are mainly directed against the hexon protein, which is not present in ADDomer made only of penton bases.

A potentially detrimental impact of pre-existing immunity on the immunogenicity of adenovirus-based viral vectors has been described,^{45,46} which thus led us to explore whether such effect may also be encountered with our adenovirus-derived VLP platform.

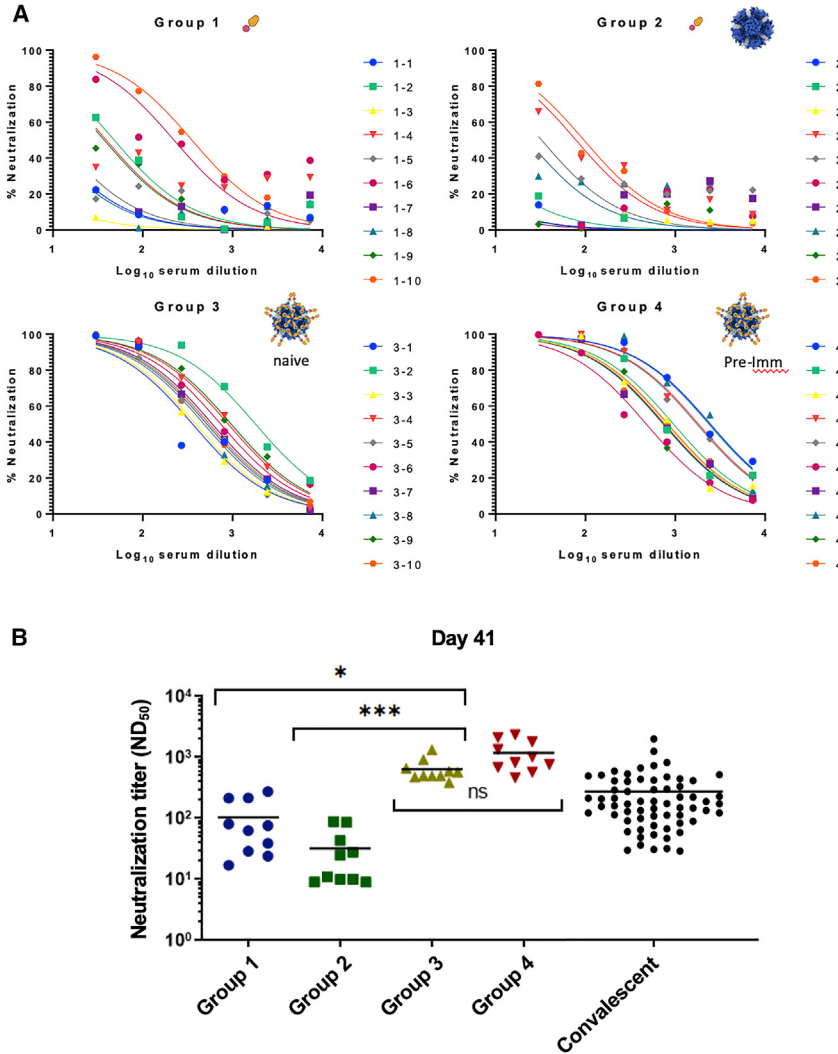


Figure 7. Neutralization study of mice sera on SARS-CoV-2 pseudo-typed virus and comparison with COVID-19 convalescent patients

(A) Curves showing the percentage of neutralization of individual sera of mice from all groups on viral infection by SARS-CoV-2 pseudo-typed virus. This pseudo-typed virus encodes luciferase as a reporter of cell infection and was preincubated with three-time serial dilutions of sera. Luciferase expression was compared to the one of non-neutralized virus. (B) Comparison of the neutralization titer at 50% of the maximal effect (ND_{50}) from all individual mice with the mean represented by a line. Statistical analysis using Kruskall-Wallis tests followed by a Dunn's multiple comparison tests demonstrates the superiority of neutralization of sera from mice immunized with RBD-decorated ADDomer particles versus both non-decorated particles and COVID-19 convalescent patients.

contrast to current platforms using the ST/SC system, we opted to engineer the ST on the VLP side, within the exposed VL. Thanks to this design, it can be envisaged to add another ST in a second exposed loop, such as the RGD (RGDL), to further increase stoichiometry (up to 120 attachment sites). Moreover, for mosaic vaccine approaches, the RGDL can be used to insert another orthogonal attachment site such as a snoop tag to display a second antigen. As an added value, the use of two different attachment tags/loops allows for differential antigenic stoichiometries and display patterns. Indeed, the RGDLs are more central on the pentameric building block of the ADDomer than the VLs, which are exposed on the periphery, resulting in a greater distance between the VLs than the RGDLs at the pentamer level.

Displaying antigens through attachment to these two loops will therefore lead to various patterns of antigen display at the VLP scale, as shown in Figure S5. This will offer a large range of combinations to vary the stoichiometry of decoration as well as the distance between the antigens to potentially optimize immunogenicity.⁴⁸ The versatility of the vaccine platform can thus be exploited to generate mosaic particles displaying RBDs from different betacoronaviruses or SARS-CoV-2 variants to broaden NAb responses and protect against current and future variants of concern. A recent work described that 60-mer mosaic nanoparticles with four to eight distinct RBDs from betacoronaviruses can be generated. Remarkably, the codisplay of the SARS-CoV-2 RBD along with other RBDs showed that the combination of antigens on the same particle did not affect the elicitation of neutralizing antibodies against a particular RBD.³⁷ Moreover, neutralization of both "matched" and "mismatched" strains was observed after mosaic priming, suggesting that such particles might protect against several betacoronaviruses at once after a single injection.

Interestingly, in contrast to adenovirus-viral vectors, pre-immunity against the VLP had no detrimental effect on the immunogenicity of our adenovirus-inspired VLP platform. Indeed, mice with immunity to ADDomer at the time of the first immunization appeared to respond with somehow greater Ab titers against RBD than naive mice, although the difference was not found significant (group 4 versus group 3, Figure 5C). This potential beneficial effect may be in particular explained by the formation of immune complexes leading to a better uptake by antigen-presenting cells, via Fc receptors, resulting in an increase in immunogenicity.⁴⁷ Of note, the prevalence, in individuals who have been infected with HAdV-3, of antibodies directed against the penton base, which is the only component of ADDomer, is not precisely known. Our present work anticipates that our platform could be used whatever the HAdV-3 immunological status of the patients, and the potential presence of anti-penton antibodies.

In conclusion, we designed a new adenovirus-inspired VLP platform that achieves high immunogenicity against the displayed antigen. In

www.moleculartherapy.org

More generally, our new versatile platform constitutes a putative tool in the preparedness to fight emerging pathogens that will remain to be investigated in viral challenge trials.

MATERIALS AND METHODS

Baculovirus production

The baculovirus expression system was used for both the production of ADDomer-SpyTag (ADD-ST) and for the RBD fused to SpyCatcher (RBD-SC). Synthetic DNA (Genscript) was cloned in the pACEBac1 using the restriction sites BamHI and HindIII. For RBD-SC, the SARS-CoV-2 spike sequence (320–554) was cloned upstream of the SC, and a hexa His-Tag was added in the C-terminus of SC. This fusion protein was secreted using the melittin signal peptide present in the vector. Recombinant baculoviruses were made by transposition with an in-house bacmid expressing yellow fluorescent protein, as previously described.⁵ Baculovirus was amplified on Sf21 cells at low multiplicity of infection (MOI) and after two amplification cycles was used to infect insect cells for 64 to 72 h at high MOI. For ADD-ST production, the infected cells were pelleted and recovered, whereas for RBD-SC, cells were discarded and the supernatant was saved.

Protein purification

ADDomer and ADD-ST purification

The ADDomer and ADD-ST were purified according to classical protocol.⁴⁹ Briefly, after lysis of the insect cell pellet by three cycles of freeze-thaw in the presence of Complete protease inhibitor cocktail (Roche), and removal of debris, the lysate was loaded onto a 20% to 40% sucrose density gradient. The gradient was centrifuged for 18 h at 4°C on an SW41 Rotor in a Beckman XPN-80 ultracentrifuge. The dense collected fractions at the bottom of the tubes were dialyzed against Hepes 10 mM pH 7.4, NaCl 150 mM, and then loaded onto a Macroprep Q cartridge (Bio-Rad). After elution by a 150- to 600-mM linear NaCl gradient in Hepes 10 mM pH 7.4, ADDomer-containing fractions were checked by SDS-PAGE and concentrated on Amicon (MWCO: 100 kDa) with buffer exchange to Hepes 10 mM pH 7.4, NaCl 150 mM.

SC purification

After lysis of the insect cell pellet as described above in the presence of Complete EDTA-free protease inhibitor cocktail, the clarified lysate was diluted five times in wash buffer (Hepes 10 mM pH 7.4, NaCl 150 mM, imidazole 10 mM) and loaded onto a His Gravitrapp column (Cytiva) by gravity, with two passages of the lysate onto the column. The column was washed with the same buffer, then eluted by 200 mM Imidazole. The fractions were analyzed by SDS-PAGE, pooled, and Imidazole was withdrawn by buffer exchange using Amicon ultrafiltration devices (MWCO: 4 kDa).

RBD-SC purification

The insect cell supernatant was centrifuged after thawing for 15 min at 7,500 g and loaded onto a Hepes 10 mM pH 7.4 pre-equilibrated Heparin column (Cytiva) of 5 mL for 500 mL of supernatant. The column was washed with Hepes 10 mM pH 7.4

for 25 mL then eluted for 10 mL with 0 to 500 mM linear NaCl gradient in Hepes 10 mM pH 7.4. The eluate was supplemented with 30 mM Imidazole-HCl and incubated with Ni-NTA beads (Qiagen), 2 mL of beads for 500 mL culture, for at least 1 h at 4°C under gentle agitation. The beads were then poured into an empty column and the protein was eluted by two column volumes of 250 mM Imidazole in Hepes 10 mM pH 7.4, NaCl 150 mM. It was then submitted to buffer exchange using an Amicon device (MWCO 30 kDa).

RBD purification

The following reagent was produced under HHSN272201400008C and obtained through BEI Resources, NIAID, NIH: Vector pCAGGS containing the SARS-CoV2, Wuhan-Hu-1 Spike Glycoprotein RBD, NR-52309. Vector NR-52309 from BEI Resources was used for mammalian expression of the RBD alone used for ELISA. EXPI293 cells grown in EXPI293 expression medium were transiently transfected with the vector according to the manufacturer's protocol (Thermo Fisher Scientific). Five days after transfection, the medium was recovered and filtered through a 0.45-mm filter. Two-step protein purification on Aktä Xpress, with a HisTrap HP column (GE Healthcare) and a Superdex 75 column (GE Healthcare) was performed using 20 mM Tris pH 7.5 and 150 mM NaCl buffer. For the HisTrap, a wash step in 75 mM imidazole was performed and RBD was eluted in buffer supplemented with 500 mM imidazole before loading onto the gel filtration column run in equilibration buffer.

N-glycosidase treatment

RBD-SC was incubated for 1 h at 37°C with the N-glycosidase PGNase F (kindly provided by Dr Nicole Thielens) at 1:100 ratio, then run on gel next to the same amount of untreated RBD-SC.

Complex formation

ADD-SpyTag + SpyCatcher (ADD-ST/SC) for Cryo-EM

The purified ADD-ST was mixed with an excess of purified SC (ratio 1:4). The protein mix was incubated overnight at 25°C under shaking in a Thermomixer (300 rpm). A purification step on a sucrose gradient was performed to remove the SC in excess and to recover only the fully decorated ADD-ST/SC at the bottom of the gradient. Buffer exchange was done in 10 mM Hepes, 150 mM NaCl, and the sample was concentrated to 1.5 mg/mL.

ADD-SpyTag + SpyCatcher-RBD (ADD-RBD) for characterization and mice immunization experiments

Covalent complex formation was obtained by incubation of purified ADD-ST with purified RBD protein fused to SC (RBD-SC). Incubation was performed at 25°C under agitation on a Thermomixer at 300 rpm. RBD-SC ratio per ADD-ST was varied according to the experiment, as indicated in the text. For immunization experiments, a ratio of 40 copies of RBD-SC per ADD-ST was chosen to leave minimal free RBD-SC. This ratio was calculated on SDS-PAGE using ImageLab software (Bio-Rad). Integrity of the ADD-RBD was checked by negative staining electron microscopy.

In vivo experiments and vaccination

Vaccination experiments were performed according to ethical guidelines, under a protocol approved by the Grenoble Ethical Committee for Animal Experimentation and the French Ministry of Higher Education and Research (reference number: APAFIS#27765-2020102114206782 v2). Five-week-old female Balb/c mice were purchased from Janvier (Le Genestet St. Isle, France). For all mice groups, vaccines were in PBS and adjuvanted with one volume of ADDavax (InvivoGen). All the mice received two vaccine doses at 2 weeks of interval (day 0 and day 14) starting at 8 weeks of age. Each mice group received subcutaneously the corresponding vaccine as indicated within the paper in 100 µL final volume, in the right flank. The pre-immunized group received 2 weeks before the first dose of vaccine (day -15) the ADDomer vector alone (5 µg in 100 µL final volume, in the right flank). The day before each vaccination, and 2 and 4 weeks after the last vaccination, 100 µL of blood was withdrawn for serologic tests. For retro-orbital blood sampling, mice were anesthetized with 4% Isoflurane.

ELISA

The antigens (either RBD or ADDomer) were diluted at 1 µg/mL in PBS, and 50 µL was coated overnight at 4°C, in a 96-well plate (Maxisorp NUNC Immunoplate, #442404). Plates were washed using a ThermoScientific Microplate washer (#5165040). After three washes with 100 µL of PBS-Tween 0.05%, plates were blocked with PBS-BSA 3% for 1 h. Mouse serum was serially diluted in PBS and incubated for 1 h (50 µL/well) at room temperature. After five washes with PBS-Tween 0.05%; a goat anti-mouse IgG (H + L) secondary Ab linked to horseradish peroxidase (JIR 115-035-062) diluted at 1:2,500 in PBS-Tween 0.05% was added for 1 h. After five washes, 50 µL of transmembrane domain substrate was distributed per well. The enzymatic reaction was stopped after 70 s by addition of 50 µL of H₂S₄ (1 M), and plates were read at 450 nm with a TECAN Spark 10M plate reader.

Electron microscopy

Negative staining

Samples of 3.5 µL were adsorbed on the clean side of a carbon film previously evaporated on mica and then stained using 2% (w/v) Sodium Silico Tungstate pH 7.4 for 30 s. The sample/carbon ensemble was then transferred to a grid and air-dried. Images were acquired under low-dose conditions (<30 e-/Å²) on an F20 electron microscope operated at 120 kV using a CETA camera.

Cryo-EM

Quantifoil grids (300 mesh, R 1.2/1.3) were negatively glow-discharged at 30 mA for 45 s; 3.5 µL of the sample were applied onto the grid, and excess solution was blotted away with a Vitrobot Mark IV (FEI) (blot time: 6 s, blot force: 0, 100% humidity, 20°C), before plunge-freezing in liquid ethane. The grid was transferred onto a 200-kV Thermo Fisher Glacios microscope equipped with a K2 summit direct electron detector for data collection. Automated data collection was performed with SerialEM, acquiring one image per hole, in counting mode. Micrographs were recorded at a nominal ×36,000 magnification, giving

a pixel size of 1.145 Å (calibrated using a β-galactosidase sample) with a defocus ranging from -0.6 to -2.35 µm. In total, 1,038 movies with 40 frames per movie were collected with a total exposure of 40 e-/Å².

Image processing and cryo-EM structure refinement

Movie drift correction was performed with Motioncor2⁵⁰ using frames from 2 to 40. CTF determination was performed with Relion 3.1.2 (Scheres 2012). A total of 939 movies of 1,038 were kept at this stage. Particle selection was done using the Laplacian filter with a diameter between 30 and 40 nm. A total of 77,323 particles were automatically selected, boxed into 480 × 480-pixel² boxes and submitted to 2D classification. After extensive selection and generation of an initial model imposing I1 symmetry, 3D refinement followed by CTF Refine and post-processing generated a final reconstruction including 10,163 particles with a resolution of 2.76 Å (Fourier Shell = 0.143) (applied B-factor -82)

Immunofluorescence microscopy

HeLa-ACE2 cells (kindly provided by Dr David Nemazee) were seeded on polylysine-coated glass coverslips the day before the experiment. Coverslips were incubated for 1 h at 4°C with 0.75 µg of either ADD-ST or ADD-RBD in 50 µL of pre-chilled DMEM. Coverslips were washed three times in cold PBS then fixed for 10 min with -20°C methanol. Fixed cells were blocked for 1 h in PBS supplemented by 3% normal goat serum, then incubated for 1 h with 1:1,000 rabbit HAd3 anti penton base serum. After three PBS washes, cells were incubated with 1/250 antiRabbit Alexa 488 Ab (ThermoFisher A32721), washed three times in PBS, then nuclei were counterstained with Hoechst 33258 for 3 min before mounting. Observations were done on a Zoe microscope (Bio-Rad).

Surface plasmon resonance

Surface plasmon resonance experiment was performed on a T200 instrument. Anti-human Fc polyclonal antibody (Jackson Immunoresearch, 109-005-008) diluted at 25 µg/mL in 10 mM sodium acetate pH 5 was immobilized on CM5 sensor chips using the amine coupling chemistry according to the manufacturer's instructions (Cytiva) to get an immobilization level of 14,000 RU. ACE-2 -Fc (GenScript Z033484) was diluted at 1.2 µg/mL in HBS P+ (Cytiva) to get an capture level of 100 RU. For interaction measurements, ADD-RBD (ranging from 1 nM to 11nM in HBSP+) was injected over captured ACE-2 Fc in HBS P+ buffer at 30 µL/min. Anti-human Fc polyclonal antibody flow cell was used for correction of the binding response. Regeneration of the surfaces was achieved by 10 mM Glycine pH2. Binding curves were analyzed using BIAEvaluation software (GE Healthcare) and data was fit to a 1:1 Langmuir with drifting baseline interaction model.

Neutralization assays and pseudo-typed SARS-CoV-2 virion production

Pseudovirus production and titration

Neutralization assays were performed using lentiviral pseudotypes harboring the SARS-CoV-2 spike and encoding luciferase. Briefly,

www.moleculartherapy.org

gag/pol and luciferase plasmids were co-transfected with a SARS-CoV-2 spike plasmid with a C-term deletion of 18aa at 1:0.4:1 ratio on adherent HEK293T cells. Supernatants containing the produced pseudoviruses were harvested 72 h after transfection, centrifuged, filtered through 0.45 µm and concentrated 50 times on Amicon Ultra (MWCO 100kDa), aliquoted and stored at -80°C. Before use, supernatants were tittered using HeLa ACE-2 cells to determine the appropriate dilution of pseudovirus necessary to obtain about 150,000 relative light units (RLU) per well in a 48-well plate.

Neutralization assay

Serial 3-fold dilutions starting from 1/10 dilution (serum), or 6 µg/mL (known bNabs) were let in contact with the pseudoviruses for 1 h at 37°C in 96-w white plates (Greiner #675083), before addition of HeLa ACE2 cells. Plates were incubated 24 h at 37°C, protected from evaporation, then cells were fed with 60 µL of DMEM (Gibco 11,966-025) supplemented with 10% FBS (VWR 97068-086), and incubated for another 24 h. Medium in each well was aspirated and replaced by 45 µL of 1X cell lysis buffer (OZ Bioscience # LUC1000) for a 60-min incubation under agitation; 30 µL of luciferin substrate was then added and RLU was measured instantly by a luminometer. For competition with ADD-ST, ADD-RBD, and RBD-SC, the same protocol was used with initial concentration of 150 µg/mL for ADD-ST, 200 µg/mL and ADD-RBD and 50 µg/mL for RBD-SC alone. Serums from a cohort of Grenoble region hospitalized convalescent patients were obtained with their consent, 6 to 8 months following COVID-19 diagnosis. The study was approved by the "Comité de Protection des Personnes SUD-EST I" on 20 August 2020 (ref 2020-84).

Statistical analyses

As the half maximal inhibitory concentration (IC₅₀) and median effective dose (ED₅₀) datasets followed a non-normal, heteroscedastic distribution, a non-parametric test was used for comparison of the different groups. Kruskall-Wallis tests were performed followed by a Dunn's multiple comparison tests for each figure. Differences were considered significant when p value was below 0.05. Statistics were performed using GraphPad software, version 9.

SUPPLEMENTAL INFORMATION

Supplemental information can be found online at <https://doi.org/10.1016/j.ymthe.2022.02.011>.

ACKNOWLEDGMENTS

We are grateful to the "CNRS Prematuration program," to the "ANR-Flash COVID" and to "Région Auvergne-Rhône-Alpes, AuRA" for the financial support to this work. This project has received funding from the European Research Council (ERC) under the European Union's Horizon 2020 research and innovation program (grant agreement No 682286). D.H. is supported by GEFLUC Dauphiné-Savoie, Ligue contre le Cancer Comité Isère, Université Grenoble Alpes IDEX Initiatives de Recherche Stratégiques and Fondation du Souffle-Fonds de recherche en santé respiratoire (FdS-FRSR). We

thank Aymeric Peuch for help with the usage of the EM computing cluster and Emmanuelle Neumann for the training of C.C. in negative staining and Leandro Estrozi for help with image analysis. We thank Philippe Mas, Dr Matthieu Roustit, and Dr Sebastian Dergan-Dylon for help with statistical analysis. We thank David Nemazee for HeLa-ACE2 cells and SARS-CoV-2 spike expression plasmid, and Pierre Charneau for plasmids encoding for lentiviral proteins and luciferase. We thank Olivier Epaulard and Julien Lupo for the COVID-19 patients cohort study. This work used the platforms of the Grenoble Instruct-ERIC center (ISBG; UAR 3518 CNRS-CEA-UGA-EMBL) within the Grenoble Partnership for Structural Biology (PSB), supported by FRISBI (ANR-10-INBS-05-02) and GRAL, financed within the University Grenoble Alpes graduate school (Écoles Universitaires de Recherche) CBH-EUR-GS (ANR-17-EURE-0003). The electron microscope facility is supported by the Auvergne-Rhône-Alpes Region, the Fondation Recherche Medicale (FRM), the fonds FEDER and the GIS-Infrastructures en Biologie Santé et Agronomie (IBISA). I.B.S. acknowledges integration into the Interdisciplinary Research Institute of Grenoble (IRIG, CEA). V.D. has an internship of Master de Biologie, École Normale Supérieure de Lyon, Université Claude Bernard Lyon I, Université de Lyon, 69342 Lyon Cedex 07, France.

AUTHOR CONTRIBUTIONS

P.F., M.C.D., and P.P. conceived the experiments. Vector production and purification were performed by C.C., V.D., and S.G. Structural analysis was performed by G.S., D.F., and C.C. Animal experiments were performed by D.H. and S.B. Molecular interaction studies was performed by E.G., C.M., and E.V.S. Immunological characterization and virus neutralization was performed by A.A., I.B., and M.B. With input from all authors, P.F. and P.P. wrote the manuscript.

DECLARATION OF INTERESTS

We declare no competing interests.

REFERENCES

1. Bok, K., Sitar, S., Graham, B.S., and Mascola, J.R. (2021). Accelerated COVID-19 vaccine development: milestones, lessons, and prospects. *Immunity* 54, 1636–1651.
2. Nguyen, B., and Tolia, N.H. (2021). Protein-based antigen presentation platforms for nanoparticle vaccines. *NPJ Vaccin.* 6, 70.
3. Fender, P., Ruigrok, R.W., Gout, E., Buffet, S., and Chroboczek, J. (1997). Adenovirus dodecahedron, a new vector for human gene transfer. *Nat. Biotechnol.* 15, 52–56.
4. Besson, S., Vrignau, C., Vassal-Sternmann, E., Dagher, M.C., and Fender, P. (2020). The adenovirus dodecahedron: beyond the platonic story. *Viruses* 12, 718.
5. Vrignau, C., Bufton, J.C., Garzoni, F., Sternmann, E., Rabi, F., Terrat, C., Guidetti, M., Josserand, V., Williams, M., Woods, C.J., et al. (2019). Synthetic self-assembling ADDomer platform for highly efficient vaccination by genetically encoded multipeptope display. *Sci. Adv.* 5, eaaw2853.
6. Zakeri, B., Fierer, J.O., Celik, E., Chittcock, E.C., Schwarz-Linek, U., Moy, V.T., and Howarth, M. (2012). Peptide tag forming a rapid covalent bond to a protein, through engineering a bacterial adhesin. *Proc. Natl. Acad. Sci.* 109, E690–E697.
7. Brune, K.D., Leneghan, D.B., Brian, I.J., Ishizuka, A.S., Bachmann, M.F., Draper, S.J., Biswas, S., and Howarth, M. (2016). Plug-and-Display: decoration of Virus-Like Particles via isopeptide bonds for modular immunization. *Sci. Rep.* 6, 19234.
8. Li, L., Fierer, J.O., Rapoport, T.A., and Howarth, M. (2014). Structural analysis and optimization of the covalent association between SpyCatcher and a peptide tag. *J. Mol. Biol.* 426, 309–317.

9. Keeble, A.H., and Howarth, M. (2020). Power to the protein: enhancing and combining activities using the Spy toolbox. *Chem. Sci.* **11**, 7281–7291.
10. Zhou, P., Yang, X.-L., Wang, X.-G., Hu, B., Zhang, L., Zhang, W., Si, H.-R., Zhu, Y., Li, B., Huang, C.-L., et al. (2020). A pneumonia outbreak associated with a new coronavirus of probable bat origin. *Nature* **579**, 270–273.
11. Khoury, D.S., Cromer, D., Reynaldi, A., Schlub, T.E., Wheatley, A.K., Juno, J.A., Subbarao, K., Kent, S.J., Triccas, J.A., and Davenport, M.P. (2021). Neutralizing antibody levels are highly predictive of immune protection from symptomatic SARS-CoV-2 infection. *Nat. Med.* **27**, 1205–1211.
12. McMahan, K., Yu, J., Mercado, N.B., Loos, C., Tostanoski, L.H., Chandrashekhar, A., Liu, J., Peter, L., Atyeo, C., Zhu, A., et al. (2021). Correlates of protection against SARS-CoV-2 in rhesus macaques. *Nature* **590**, 630–634.
13. Polack, F.P., Thomas, S.J., Kitchin, N., Absalon, J., Gurtman, A., Lockhart, S., Perez, J.L., Pérez Marc, G., Moreira, E.D., Zerbini, C., et al. (2020). Safety and efficacy of the BNT162b2 mRNA covid-19 vaccine. *N. Engl. J. Med.* **383**, 2603–2615.
14. Jackson, L.A., Anderson, E.J., Roushaphal, N.G., Roberts, P.C., Makhene, M., Coler, R.N., McCullough, M.P., Chappell, J.D., Denison, M.R., Stevens, L.J., et al. (2020). An mRNA vaccine against SARS-CoV-2 — preliminary report. *N. Engl. J. Med.* **383**, 1920–1931.
15. Heath, P.T., Galiza, E.P., Baxter, D.N., Boffito, M., Browne, D., Burns, F., Chadwick, D.R., Clark, R., Cosgrove, C., Galloway, J., et al. (2021). Safety and efficacy of NVX-CoV2373 covid-19 vaccine. *N. Engl. J. Med.* **385**, 1172–1183.
16. Shang, J., Ye, G., Shi, K., Wan, Y., Luo, C., Aihara, H., Geng, Q., Auerbach, A., and Li, F. (2020). Structural basis of receptor recognition by SARS-CoV-2. *Nature* **581**, 221–224.
17. Yan, R., Zhang, Y., Li, Y., Xia, L., Guo, Y., and Zhou, Q. (2020). Structural basis for the recognition of SARS-CoV-2 by full-length human ACE2. *Science* **367**, 1444–1448.
18. Lan, J., Ge, J., Yu, J., Shan, S., Zhou, H., Fan, S., Zhang, Q., Shi, X., Wang, Q., Zhang, L., et al. (2020). Structure of the SARS-CoV-2 spike receptor-binding domain bound to the ACE2 receptor. *Nature* **581**, 215–220.
19. Starr, T.N., Greaney, A.J., Hilton, S.K., Ellis, D., Crawford, K.H.D., Dingens, A.S., Navarro, M.J., Bowen, J.E., Tortorici, M.A., Walls, A.C., et al. (2020). Deep mutational scanning of SARS-CoV-2 receptor binding domain reveals constraints on folding and ACE2 binding. *Cell* **182**, 1295–1310.e21.
20. Piccoli, L., Park, Y.-J., Tortorici, M.A., Czudnochowski, N., Walls, A.C., Beltramello, M., Silacci-Fregnii, C., Pinto, D., Rosen, L.E., Bowen, J.E., et al. (2020). Mapping neutralizing and immunodominant sites on the SARS-CoV-2 spike receptor-binding domain by structure-guided high-resolution serology. *Cell* **183**, 1024–1042.e21.
21. Barnes, C.O., West, A.P., Huey-Tubman, K.E., Hoffmann, M.A.G., Sharaf, N.G., Hoffman, P.R., Koranda, N., Grisick, H.B., Gaebler, C., Muecksch, F., et al. (2020). Structures of human antibodies bound to SARS-CoV-2 spike reveal common epitopes and recurrent features of antibodies. *Cell* **182**, 828–842.e16.
22. Robbiani, D.F., Gaebler, C., Muecksch, F., Lorenzi, J.C.C., Wang, Z., Cho, A., Agudelo, M., Barnes, C.O., Gazumyan, A., Finkin, S., et al. (2020). Convergent antibody responses to SARS-CoV-2 in convalescent individuals. *Nature* **584**, 437–442.
23. Brouwer, P.J.M., Caniels, T.G., van der Straten, K., Snitselaar, J.L., Aldon, Y., Bangaru, S., Torres, J.L., Okba, N.M.A., Claireaux, M., Kerster, G., et al. (2020). Potent neutralizing antibodies from COVID-19 patients define multiple targets of vulnerability. *Science* **369**, 643–650.
24. Barnes, C.O., Jette, C.A., Abernathy, M.E., Dam, K.-M.A., Esswein, S.R., Grisick, H.B., Malyutin, A.G., Sharaf, N.G., Huey-Tubman, K.E., Lee, Y.E., et al. (2020). SARS-CoV-2 neutralizing antibody structures inform therapeutic strategies. *Nature* **588**, 682–687.
25. Alsoussi, W.B., Turner, J.S., Case, J.B., Zhao, H., Schmitz, A.J., Zhou, J.Q., Chen, R.E., Lei, T., Rizk, A.A., McIntire, K.M., et al. (2020). A potently neutralizing antibody protects mice against SARS-CoV-2 infection. *J. Immunol.* **205**, 915–922.
26. Zost, S.J., Gilchuk, P., Case, J.B., Binshtein, E., Chen, R.E., Nikolola, J.P., Schäfer, A., Reidy, J.X., Trivette, A., Nargi, R.S., et al. (2020). Potently neutralizing and protective human antibodies against SARS-CoV-2. *Nature* **584**, 443–449.
27. O'Brien, M.P., Forleo-Neto, E., Musser, B.J., Isa, F., Chan, K.-C., Sarkar, N., Bar, K.J., Barnabas, R.V., Barouch, D.H., Cohen, M.S., et al. (2021). Subcutaneous REGEN-COV antibody combination to prevent covid-19. *N. Engl. J. Med.* **385**, e70.
28. Fuschiotti, P., Schoehn, G., Fender, P., Fabry, C.M.S., Hewat, E.A., Chroboczek, J., Ruigrok, R.W.H., and Conway, J.F. (2006). Structure of the dodecahedral penton particle from human adenovirus type 3. *J. Mol. Biol.* **356**, 510–520.
29. Lei, C., Qian, K., Li, T., Zhang, S., Fu, W., Ding, M., and Hu, S. (2020). Neutralization of SARS-CoV-2 spike pseudotyped virus by recombinant ACE2-Ig. *Nat. Commun.* **11**, 2070.
30. Epaulard, O., Buisson, M., Nemoz, B., Maréchal, M.L., Terzi, N., Payen, J.-F., Froidure, M., Blanc, M., Mounayar, A.-L., Quénard, F., et al. (2021). Persistence at one year of neutralizing antibodies after SARS-CoV-2 infection: influence of initial severity and steroid use. *J. Infect.* <https://doi.org/10.1016/j.jinf.2021.10.009>.
31. Tan, T.K., Rijal, P., Rahikainen, R., Keeble, A.H., Schimanski, L., Hussain, S., Harvey, R., Hayes, J.W.P., Edwards, J.C., McLean, R.K., et al. (2021). A COVID-19 vaccine candidate using SpyCatcher multimerization of the SARS-CoV-2 spike protein receptor-binding domain induces potent neutralising antibody responses. *Nat. Commun.* **12**, 542.
32. Kanekiyo, M., Wei, C.-J., Yassine, H.M., McTamney, P.M., Boyington, J.C., Whittle, J.R.R., Rao, S.S., Kong, W.-P., Wang, L., and Nabel, G.J. (2013). Self-assembling influenza nanoparticle vaccines elicit broadly neutralizing H1N1 antibodies. *Nature* **499**, 102–106.
33. Kanekiyo, M., Bu, W., Joyce, M.G., Meng, G., Whittle, J.R.R., Baxa, U., Yamamoto, T., Narlapa, S., Todd, J.-P., Rao, S.S., et al. (2015). Rational design of an epstein-barr virus vaccine targeting the receptor-binding site. *Cell* **162**, 1090–1100.
34. Bachmann, M.F., and Zinkernagel, R.M. (1997). Neutralizing antiviral B cell responses. *Annu. Rev. Immunol.* **15**, 235–270.
35. Watanabe, Y., Allen, J.D., Wrapp, D., McLellan, J.S., and Crispin, M. (2020). Site-specific glycan analysis of the SARS-CoV-2 spike. *Science* **369**, 330–333.
36. Shinde, V., Bhikha, S., Hoosain, Z., Archary, M., Bhorat, Q., Fairlie, L., Laloo, U., Masilela, M.S.L., Moodley, D., Hanley, S., et al. (2021). Efficacy of NVX-CoV2373 covid-19 vaccine against the B.1.351 variant. *N. Engl. J. Med.* **385**, 1172–1183.
37. Cohen, A.A., Gnanapragasam, P.N.P., Lee, Y.E., Hoffman, P.R., Ou, S., Kakutani, L.M., Keefe, J.R., Wu, H.-J., Howarth, M., West, A.P., et al. (2021). Mosaic nanoparticles elicit cross-reactive immune responses to zoonotic coronaviruses in mice. *Science* **371**, 735–741.
38. Walls, A.C., Fiala, B., Schäfer, A., Wrenn, S., Pham, M.N., Murphy, M., Tse, L.V., Shehata, L., O'Connor, M.A., Chen, C., et al. (2020). Elicitation of potent neutralizing antibody responses by designed protein nanoparticle vaccines for SARS-CoV-2. *Cell* **183**, 1367–1382.e17.
39. He, L., Lin, X., Wang, Y., Abraham, C., Sou, C., Ngo, T., Zhang, Y., Wilson, I.A., and Zhu, J. (2021). Single-component, self-assembling, protein nanoparticles presenting the receptor binding domain and stabilized spike as SARS-CoV-2 vaccine candidates. *Sci. Adv.* **7**, eabf1591.
40. Salzer, R., Clark, J.J., Vaysburd, M., Chang, V.T., Albecka, A., Kiss, L., Sharma, P., Gonzalez Llamazares, A., Kipar, A., Hiscox, J.A., et al. (2021). Single-dose immunisation with a multimerised SARS-CoV-2 receptor binding domain (RBD) induces an enhanced and protective response in mice. *FEBS Lett.* **595**, 2323–2340.
41. Saunders, K.O., Lee, E., Parks, R., Martinez, D.R., Li, D., Chen, H., Edwards, R.J., Gobeil, S., Barr, M., Mansouri, K., et al. (2021). Neutralizing antibody vaccine for pandemic and pre-emergent coronaviruses. *Nature* **594**, 553–559.
42. Vogels, R., Zuidgeest, D., van Rijnsoever, R., Hartkoorn, E., Damen, I., de Béthune, M.-P., Kostense, S., Penders, G., Helmus, N., Koudstaal, W., et al. (2003). Replication-deficient human adenovirus type 35 vectors for gene transfer and vaccination: efficient human cell infection and bypass of preexisting adenovirus immunity. *JVI* **77**, 8263–8271.
43. Arnborg, N. (2012). Adenovirus receptors: implications for targeting of viral vectors. *Trends Pharmacol. Sci.* **33**, 442–448.
44. Haque, E., Banik, U., Monwar, T., Anthony, L., and Adhikary, A.K. (2018). Worldwide increased prevalence of human adenovirus type 3 (HAdV-3) respiratory infections is well correlated with heterogeneous hypervariable regions (HVRs) of hexon. *PLoS ONE* **13**, e0194516.
45. Lanzi, A., Ben Youssef, G., Perricaudet, M., and Benihoud, K. (2011). Anti-adenovirus humoral responses influence on the efficacy of vaccines based on epitope display on adenovirus capsid. *Vaccine* **29**, 1463–1471.

www.moleculartherapy.org

46. Anchim, A., Raddi, N., Zig, L., Perrieau, P., Le Goffic, R., Ryffel, B., and Benihoud, K. (2018). Humoral responses elicited by adenovirus displaying epitopes are induced independently of the infection process and shaped by the toll-like receptor/MyD88 pathway. *Front Immunol.* **9**, 124.
47. Heyman, B. (2003). Feedback regulation by IgG antibodies. *Immunol. Lett.* **88**, 157–161.
48. Veneziano, R., Moyer, T.J., Stone, M.B., Wamhoff, E.-C., Read, B.J., Mukherjee, S., Shepherd, T.R., Das, J., Schief, W.R., Irvine, D.J., et al. (2020). Role of nanoscale antigen organization on B-cell activation probed using DNA origami. *Nat. Nanotechnol.* **15**, 716–723.
49. Fender, P. (2014). Use of dodecahedron “VLPs” as an alternative to the whole adenovirus. *Methods Mol. Biol.* **1089**, 61–70.
50. Zheng, S.Q., Palovcak, E., Armache, J.-P., Verba, K.A., Cheng, Y., and Agard, D.A. (2017). MotionCor2: anisotropic correction of beam-induced motion for improved cryo-electron microscopy. *Nat. Methods* **14**, 331–332.

Références

1. Pierre Agache. *Physiologie de la peau et explorations fonctionnelles cutanées*. (2000).
2. Nestle, F. O., Di Meglio, P., Qin, J.-Z. & Nickoloff, B. J. Skin immune sentinels in health and disease. *Nat. Rev. Immunol.* **9**, 679–691 (2009).
3. Tobin, D. J. Biochemistry of human skin—our brain on the outside. *Chem. Soc. Rev.* **35**, 52–67 (2006).
4. Sommerville, I. F., Collins, W. P., Flamigni, C., Koullapis, E. & Dewhurst, C. J. Androgen metabolism in human skin. *Proc. R. Soc. Med.* **64**, 845–847 (1971).
5. J. Kanitis. *biologie de la peau humaine chapter Structure histologique de la peau humaine*. (1997).
6. Flacher, V. *et al.* Epidermal Langerhans cells rapidly capture and present antigens from C-type lectin-targeting antibodies deposited in the dermis. *J. Invest. Dermatol.* **130**, 755–762 (2010).
7. Friedrich Merkel. Tastzellen und tastkörperchen bei den haustieren und beim menschen. in (1875).
8. Maricich, S. M. *et al.* Merkel cells are essential for light-touch responses. *Science* **324**, 1580–1582 (2009).
9. Ortonne, J. P. & Benedetto, J. P. Mélanocytes épidermiques et mélanocytes folliculaires. 11.
10. Démarchez, M. Le mélanocyte et la pigmentation. <https://biologiedelapeau.fr> <https://biologiedelapeau.fr/spip.php?article12> (2019).

11. Fitzpatrick, T. B. & Breathnach, A. S. [THE EPIDERMAL MELANIN UNIT SYSTEM].
Dermatol. Wochenschr. **147**, 481–489 (1963).
12. Singh, S. K. *et al.* Melanin transfer in human skin cells is mediated by filopodia--a model for homotypic and heterotypic lysosome-related organelle transfer. *FASEB J. Off. Publ. Fed. Am. Soc. Exp. Biol.* **24**, 3756–3769 (2010).
13. Riley, P. A. Melanin. *Int. J. Biochem. Cell Biol.* **29**, 1235–1239 (1997).
14. Alaluf, S., Heinrich, U., Stahl, W., Tronnier, H. & Wiseman, S. Dietary carotenoids contribute to normal human skin color and UV photosensitivity. *J. Nutr.* **132**, 399–403 (2002).
15. François Aubin, P. H. *Rayonnement ultraviolet et peau*. (John Libbey Eurotext, 2001).
16. Patrick Varrendo, J.-J. G. *Biologie de la peau humaine, chapitre Réparation d'ADN et cancers : incidences sur le mélanome*. (2000).
17. Wood, R. D. Nucleotide excision repair in mammalian cells. *J. Biol. Chem.* **272**, 23465–23468 (1997).
18. Kwa, R. E., Campana, K. & Moy, R. L. Biology of cutaneous squamous cell carcinoma. *J. Am. Acad. Dermatol.* **26**, 1–26 (1992).
19. Mac-Mary, S. *et al.* Assessment of cumulative exposure to UVA through the study of asymmetrical facial skin aging. *Clin. Interv. Aging* **5**, 277–284 (2010).
20. Moro, N., Mauch, C. & Zigrino, P. Metalloproteinases in melanoma. *Eur. J. Cell Biol.* **93**, 23–29 (2014).
21. Chiriboga, L. *et al.* Endothelin-1 in the tumor microenvironment correlates with melanoma invasion. *Melanoma Res.* **26**, 236–244 (2016).

22. Sandri, S. *et al.* Vemurafenib resistance increases melanoma invasiveness and modulates the tumor microenvironment by MMP-2 upregulation. *Pharmacol. Res.* **111**, 523–533 (2016).
23. Falzone, L. *et al.* MMP-9 overexpression is associated with intragenic hypermethylation of MMP9 gene in melanoma. *Aging* **8**, 933–944 (2016).
24. Lee, K. R., Lee, J. S., Kim, Y. R., Song, I. G. & Hong, E. K. Polysaccharide from Inonotus obliquus inhibits migration and invasion in B16-F10 cells by suppressing MMP-2 and MMP-9 via downregulation of NF-κB signaling pathway. *Oncol. Rep.* **31**, 2447–2453 (2014).
25. Guarneri, C. *et al.* NF-κB inhibition is associated with OPN/MMP-9 downregulation in cutaneous melanoma. *Oncol. Rep.* **37**, 737–746 (2017).
26. Haass, N. K. & Herlyn, M. Normal human melanocyte homeostasis as a paradigm for understanding melanoma. *J. Investigig. Dermatol. Symp. Proc.* **10**, 153–163 (2005).
27. Lázár-Molnár, E., Hegyesi, H., Tóth, S. & Falus, A. Autocrine and paracrine regulation by cytokines and growth factors in melanoma. *Cytokine* **12**, 547–554 (2000).
28. Knudsen, K. A., Frankowski, C., Johnson, K. R. & Wheelock, M. J. A role for cadherins in cellular signaling and differentiation. *J. Cell. Biochem. Suppl.* **30–31**, 168–176 (1998).
29. Puliafito, A. *et al.* Collective and single cell behavior in epithelial contact inhibition. *Proc. Natl. Acad. Sci. U. S. A.* **109**, 739–744 (2012).
30. Huttenlocher, A. *et al.* Integrin and cadherin synergy regulates contact inhibition of migration and motile activity. *J. Cell Biol.* **141**, 515–526 (1998).
31. Janmey, P. A. & McCulloch, C. A. Cell mechanics: integrating cell responses to mechanical stimuli. *Annu. Rev. Biomed. Eng.* **9**, 1–34 (2007).

32. Haass, N. K., Smalley, K. S. M. & Herlyn, M. The role of altered cell-cell communication in melanoma progression. *J. Mol. Histol.* **35**, 309–318 (2004).
33. O. Berthier-Vergnes. *Biologie de la peau, chapitre Mécanismes d'invasion et de métastase du mélaocyte malin*, pages 133–145. (INSERM, 1995).
34. Isola, A. L., Eddy, K. & Chen, S. Biology, Therapy and Implications of Tumor Exosomes in the Progression of Melanoma. *Cancers* **8**, 110 (2016).
35. Wilkins, D. K. & Nathan, P. D. Review: Therapeutic opportunities in noncutaneous melanoma. *Ther. Adv. Med. Oncol.* **1**, 29–36 (2009).
36. Curtin, J. A. *et al.* Distinct Sets of Genetic Alterations in Melanoma. *N. Engl. J. Med.* **353**, 2135–2147 (2005).
37. Kuk, D. *et al.* Prognosis of Mucosal, Uveal, Acral, Nonacral Cutaneous, and Unknown Primary Melanoma From the Time of First Metastasis. *The Oncologist* **21**, 848–854 (2016).
38. Bennett, D. R., Wasson, D., MacArthur, J. D. & McMillen, M. A. The effect of misdiagnosis and delay in diagnosis on clinical outcome in melanomas of the foot. *J. Am. Coll. Surg.* **179**, 279–284 (1994).
39. Wu, X.-C. *et al.* Racial and ethnic variations in incidence and survival of cutaneous melanoma in the United States, 1999-2006. *J. Am. Acad. Dermatol.* **65**, S26-37 (2011).
40. Cress, R. D. & Holly, E. A. Incidence of cutaneous melanoma among non-Hispanic whites, Hispanics, Asians, and blacks: an analysis of California cancer registry data, 1988-93. *Cancer Causes Control CCC* **8**, 246–252 (1997).
41. Cormier, J. N. *et al.* Ethnic differences among patients with cutaneous melanoma. *Arch. Intern. Med.* **166**, 1907–1914 (2006).

42. Cancer Genome Atlas Network. Genomic Classification of Cutaneous Melanoma. *Cell* **161**, 1681–1696 (2015).
43. Hayward, N. K. *et al.* Whole-genome landscapes of major melanoma subtypes. *Nature* **545**, 175–180 (2017).
44. Krauthammer, M. *et al.* Exome sequencing identifies recurrent somatic RAC1 mutations in melanoma. *Nat. Genet.* **44**, 1006–1014 (2012).
45. Eddy, K. & Chen, S. Overcoming Immune Evasion in Melanoma. *Int. J. Mol. Sci.* **21**, 8984 (2020).
46. Shain, A. H. & Bastian, B. C. From melanocytes to melanomas. *Nat. Rev. Cancer* **16**, 345–358 (2016).
47. Pollock, P. M. *et al.* High frequency of BRAF mutations in nevi. *Nat. Genet.* **33**, 19–20 (2003).
48. Menzies, A. M. *et al.* Distinguishing Clinicopathologic Features of Patients with V600E and V600K BRAF-Mutant Metastatic Melanoma. *Clin. Cancer Res.* **18**, 3242–3249 (2012).
49. Bradford, P. T., Goldstein, A. M., McMaster, M. L. & Tucker, M. A. Acral lentiginous melanoma: incidence and survival patterns in the United States, 1986-2005. *Arch. Dermatol.* **145**, 427–434 (2009).
50. Huang, K., Fan, J. & Misra, S. Acral Lentiginous Melanoma: Incidence and Survival in the United States, 2006-2015, an Analysis of the SEER Registry. *J. Surg. Res.* **251**, 329–339 (2020).
51. Rabbie, R., Ferguson, P., Molina-Aguilar, C., Adams, D. J. & Robles-Espinoza, C. D. Melanoma subtypes: genomic profiles, prognostic molecular markers and therapeutic possibilities. *J. Pathol.* **247**, 539–551 (2019).

52. Moon, K. R. *et al.* Genetic Alterations in Primary Acral Melanoma and Acral Melanocytic Nevus in Korea: Common Mutated Genes Show Distinct Cytomorphological Features. *J. Invest. Dermatol.* **138**, 933–945 (2018).
53. Liang, W. S. *et al.* Integrated genomic analyses reveal frequent TERT aberrations in acral melanoma. *Genome Res.* **27**, 524–532 (2017).
54. de Lima Vazquez, V. *et al.* Molecular profiling, including TERT promoter mutations, of acral lentiginous melanomas. *Melanoma Res.* **26**, 93–99 (2016).
55. Curtin, J. A., Busam, K., Pinkel, D. & Bastian, B. C. Somatic activation of KIT in distinct subtypes of melanoma. *J. Clin. Oncol. Off. J. Am. Soc. Clin. Oncol.* **24**, 4340–4346 (2006).
56. Rossi, E. *et al.* Immunological Backbone of Uveal Melanoma: Is There a Rationale for Immunotherapy? *Cancers* **11**, 1055 (2019).
57. Johansson, P. *et al.* Deep sequencing of uveal melanoma identifies a recurrent mutation in PLCB4. *Oncotarget* **7**, 4624–4631 (2015).
58. Van Raamsdonk, C. D. *et al.* Mutations in GNA11 in Uveal Melanoma. *N. Engl. J. Med.* **363**, 2191–2199 (2010).
59. Van Raamsdonk, C. D. *et al.* Frequent somatic mutations of GNAQ in uveal melanoma and blue naevi. *Nature* **457**, 599–602 (2009).
60. Khalili, J. S. *et al.* Combination small molecule MEK and PI3K inhibition enhances uveal melanoma cell death in a mutant GNAQ- and GNA11-dependent manner. *Clin. Cancer Res. Off. J. Am. Assoc. Cancer Res.* **18**, 4345–4355 (2012).
61. Moore, A. R. *et al.* Recurrent activating mutations of G-protein-coupled receptor CYSLTR2 in uveal melanoma. *Nat. Genet.* **48**, 675–680 (2016).
62. Mihajlovic, M., Vlajkovic, S., Jovanovic, P. & Stefanovic, V. Primary mucosal melanomas: a comprehensive review. *Int. J. Clin. Exp. Pathol.* **5**, 739–753 (2012).

63. Lerner, B. A., Stewart, L. A., Horowitz, D. P. & Carvajal, R. D. Mucosal Melanoma: New Insights and Therapeutic Options for a Unique and Aggressive Disease. *Oncol. Williston Park N* **31**, e23–e32 (2017).
64. Kabbarah, O. & Chin, L. Revealing the genomic heterogeneity of melanoma. *Cancer Cell* **8**, 439–441 (2005).
65. Hintzsche, J. D. *et al.* Whole-exome sequencing identifies recurrent SF3B1 R625 mutation and comutation of NF1 and KIT in mucosal melanoma. *Melanoma Res.* **27**, 189–199 (2017).
66. Furney, S. J. *et al.* Genome sequencing of mucosal melanomas reveals that they are driven by distinct mechanisms from cutaneous melanoma. *J. Pathol.* **230**, 261–269 (2013).
67. Sheng, X. *et al.* GNAQ and GNA11 mutations occur in 9.5% of mucosal melanoma and are associated with poor prognosis. *Eur. J. Cancer* **65**, 156–163 (2016).
68. Si, L., Wang, X. & Guo, J. Genotyping of mucosal melanoma. *Chin. Clin. Oncol.* **3**, 11–11 (2014).
69. Braun, R. P., Rabinovitz, H. S., Oliviero, M., Kopf, A. W. & Saurat, J.-H. Dermoscopy of pigmented skin lesions. *J. Am. Acad. Dermatol.* **52**, 109–121 (2005).
70. Friedman, R. J., Rigel, D. S. & Kopf, A. W. Early detection of malignant melanoma: the role of physician examination and self-examination of the skin. *CA. Cancer J. Clin.* **35**, 130–151 (1985).
71. An Atlas of Dermoscopy | Ashfaq Marghoob, Ralph Braun | Taylor & Francis. *Taylor & Francis* <https://www.taylorfrancis.com/books/edit/10.3109/9781841847627/atlas-dermoscopy-ashfaq-marghoob-ralph-braun>.
72. Chatelain, C. Morphogenèse du mélanome in situ. 169.

73. Pehamberger, H., Steiner, A. & Wolff, K. In vivo epiluminescence microscopy of pigmented skin lesions. I. Pattern analysis of pigmented skin lesions. *J. Am. Acad. Dermatol.* **17**, 571–583 (1987).
74. M. Dawid, R. P. Braun, H. Rabinovitz & H. Pehamberger. *Précis illustré de dermoscopie, chapitre Analyse des patrons, pages 118–127.* vol. 21 (2007).
75. Argenziano, G. et al. Dermoscopy of pigmented skin lesions: results of a consensus meeting via the Internet. *J. Am. Acad. Dermatol.* **48**, 679–693 (2003).
76. Gershenwald, J. E. et al. Melanoma staging: Evidence-based changes in the American Joint Committee on Cancer eighth edition cancer staging manual. *CA. Cancer J. Clin.* **67**, 472–492 (2017).
77. Breslow, A. Thickness, cross-sectional areas and depth of invasion in the prognosis of cutaneous melanoma. *Ann. Surg.* **172**, 902–908 (1970).
78. Bønnelykke-Behrndtz, M. L. & Steiniche, T. Ulcerated Melanoma: Aspects and Prognostic Impact. *Exon Publ.* 67–75 (2017) doi:10.15586/codon.cutaneousmelanoma.2017.ch5.
79. Clark, W. H. et al. A study of tumor progression: The precursor lesions of superficial spreading and nodular melanoma. *Hum. Pathol.* **15**, 1147–1165 (1984).
80. Damsky, W. E., Rosenbaum, L. E. & Bosenberg, M. Decoding Melanoma Metastasis. *Cancers* **3**, 126–163 (2011).
81. Naik, P. P. Cutaneous Malignant Melanoma: A Review of Early Diagnosis and Management. *World J. Oncol.* **12**, 7–19 (2021).
82. Perera, E., Gnaneswaran, N., Jennens, R. & Sinclair, R. Malignant Melanoma. *Healthcare* **2**, 1–19 (2014).
83. Strojan, P. Role of radiotherapy in melanoma management. *Radiol. Oncol.* **44**, 1–12 (2010).

84. Shi, W. Radiation Therapy for Melanoma. *Exon Publ.* 101–120 (2017)
doi:10.15586/codon.cutaneousmelanoma.2017.ch8.
85. Postow, M. A. *et al.* Immunologic Correlates of the Abscopal Effect in a Patient with Melanoma. *N. Engl. J. Med.* **366**, 925–931 (2012).
86. D'Andrea, M. A. & Reddy, G. K. Systemic Antitumor Effects and Abscopal Responses in Melanoma Patients Receiving Radiation Therapy. *Oncology* **98**, 202–215 (2020).
87. Mishra, H. *et al.* Melanoma treatment: from conventional to nanotechnology. *J. Cancer Res. Clin. Oncol.* **144**, 2283–2302 (2018).
88. Luke, J. J., Flaherty, K. T., Ribas, A. & Long, G. V. Targeted agents and immunotherapies: optimizing outcomes in melanoma. *Nat. Rev. Clin. Oncol.* **14**, 463–482 (2017).
89. Menzies, A. M. & Long, G. V. Systemic treatment for BRAF-mutant melanoma: where do we go next? *Lancet Oncol.* **15**, e371–e381 (2014).
90. Chapman, P. B. *et al.* Improved survival with vemurafenib in melanoma with BRAF V600E mutation. *N. Engl. J. Med.* **364**, 2507–2516 (2011).
91. Tsai, J. *et al.* Discovery of a selective inhibitor of oncogenic B-Raf kinase with potent antimelanoma activity. *Proc. Natl. Acad. Sci. U. S. A.* **105**, 3041–3046 (2008).
92. Søndergaard, J. N. *et al.* Differential sensitivity of melanoma cell lines with BRAFV600E mutation to the specific Raf inhibitor PLX4032. *J. Transl. Med.* **8**, 39 (2010).
93. Ravnan, M. C. & Matalka, M. S. Vemurafenib in patients with BRAF V600E mutation-positive advanced melanoma. *Clin. Ther.* **34**, 1474–1486 (2012).
94. Hauschild, A. *et al.* Dabrafenib in BRAF-mutated metastatic melanoma: a multicentre, open-label, phase 3 randomised controlled trial. *The Lancet* **380**, 358–365 (2012).

95. Daud, A. & Tsai, K. Management of Treatment-Related Adverse Events with Agents Targeting the MAPK Pathway in Patients with Metastatic Melanoma. *The Oncologist* **22**, 823–833 (2017).
96. Sanchez, J. N., Wang, T. & Cohen, M. S. BRAF and MEK Inhibitors: Use and Resistance in BRAF-Mutated Cancers. *Drugs* **78**, 549–566 (2018).
97. Robert, C. *et al.* Five-year outcomes from a phase 3 METRIC study in patients with BRAF V600 E/K-mutant advanced or metastatic melanoma. *Eur. J. Cancer Oxf. Engl. 1990* **109**, 61–69 (2019).
98. Eroglu, Z. & Ribas, A. Combination therapy with BRAF and MEK inhibitors for melanoma: latest evidence and place in therapy. *Ther. Adv. Med. Oncol.* **8**, 48–56 (2016).
99. Long, G. V. *et al.* Combined BRAF and MEK inhibition versus BRAF inhibition alone in melanoma. *N. Engl. J. Med.* **371**, 1877–1888 (2014).
100. Robert, C. *et al.* Improved overall survival in melanoma with combined dabrafenib and trametinib. *N. Engl. J. Med.* **372**, 30–39 (2015).
101. Larkin, J. *et al.* Combined vemurafenib and cobimetinib in BRAF-mutated melanoma. *N. Engl. J. Med.* **371**, 1867–1876 (2014).
102. Ascierto, P. A. *et al.* Cobimetinib combined with vemurafenib in advanced BRAFV600-mutant melanoma (coBRIM): updated efficacy results from a randomised, double-blind, phase 3 trial. *Lancet Oncol.* **17**, 1248–1260 (2016).
103. Dummer, R. *et al.* Encorafenib plus binimatinib versus vemurafenib or encorafenib in patients with BRAF-mutant melanoma (COLUMBUS): a multicentre, open-label, randomised phase 3 trial. *Lancet Oncol.* **19**, 603–615 (2018).

104. Dummer, R. *et al.* Overall survival in patients with BRAF-mutant melanoma receiving encorafenib plus binimetinib versus vemurafenib or encorafenib (COLUMBUS): a multicentre, open-label, randomised, phase 3 trial. *Lancet Oncol.* **19**, 1315–1327 (2018).
105. Beadling, C. *et al.* KIT Gene Mutations and Copy Number in Melanoma Subtypes. *Clin. Cancer Res.* **14**, 6821–6828 (2008).
106. Shtivelman, E. *et al.* Pathways and therapeutic targets in melanoma. *Oncotarget* **5**, 1701–1752 (2014).
107. Guo, J. *et al.* Efficacy and safety of nilotinib in patients with KIT-mutated metastatic or inoperable melanoma: final results from the global, single-arm, phase II TEAM trial. *Ann. Oncol. Off. J. Eur. Soc. Med. Oncol.* **28**, 1380–1387 (2017).
108. Hodi, F. S. *et al.* Imatinib for Melanomas Harboring Mutationally Activated or Amplified KIT Arising on Mucosal, Acral, and Chronically Sun-Damaged Skin. *J. Clin. Oncol.* **31**, 3182–3190 (2013).
109. Lebbe, C. *et al.* Phase II multicentric uncontrolled national trial assessing the efficacy of nilotinib in the treatment of advanced melanomas with c-KIT mutation or amplification. *J. Clin. Oncol.* **32**, 9032–9032 (2014).
110. Dahl, C. *et al.* KIT is a frequent target for epigenetic silencing in cutaneous melanoma. *J. Invest. Dermatol.* **135**, 516–524 (2015).
111. Slipicevic, A. & Herlyn, M. KIT in melanoma: many shades of gray. *J. Invest. Dermatol.* **135**, 337–338 (2015).
112. Mourah, S. & Lebbé, C. Mécanismes de résistance aux inhibiteurs de BRAF et MEK. *Mis E Au Point* 6 (2017).
113. Green, J. & Ariyan, C. Update on immunotherapy in melanoma. *Surg. Oncol. Clin. N. Am.* **24**, 337–346 (2015).

114. Hou, B., Tang, Y., Li, W., Zeng, Q. & Chang, D. Efficiency of CAR-T Therapy for Treatment of Solid Tumor in Clinical Trials: A Meta-Analysis. *Dis. Markers* **2019**, 3425291 (2019).
115. Eisenhauer, E. A. *et al.* New response evaluation criteria in solid tumours: revised RECIST guideline (version 1.1). *Eur. J. Cancer Oxf. Engl.* **1990** *45*, 228–247 (2009).
116. Seymour, L. *et al.* iRECIST: guidelines for response criteria for use in trials testing immunotherapeutics. *Lancet Oncol.* **18**, e143–e152 (2017).
117. Wolchok, J. D. *et al.* Guidelines for the evaluation of immune therapy activity in solid tumors: immune-related response criteria. *Clin. Cancer Res. Off. J. Am. Assoc. Cancer Res.* **15**, 7412–7420 (2009).
118. Klocke, K., Sakaguchi, S., Holmdahl, R. & Wing, K. Induction of autoimmune disease by deletion of CTLA-4 in mice in adulthood. *Proc. Natl. Acad. Sci.* **113**, E2383–E2392 (2016).
119. Waterhouse, P. *et al.* Lymphoproliferative Disorders with Early Lethality in Mice Deficient in Ctla-4. *Science* **270**, 985–988 (1995).
120. Nishimura, H. *et al.* Autoimmune Dilated Cardiomyopathy in PD-1 Receptor-Deficient Mice. *Science* **291**, 319–322 (2001).
121. Ribas, A. & Wolchok, J. D. Cancer immunotherapy using checkpoint blockade. *Science* **359**, 1350–1355 (2018).
122. Azuma, M. *et al.* B70 antigen is a second ligand for CTLA-4 and CD28. *Nature* **366**, 76–79 (1993).
123. Linsley, P. S. *et al.* Human B7-1 (CD80) and B7-2 (CD86) bind with similar avidities but distinct kinetics to CD28 and CTLA-4 receptors. *Immunity* **1**, 793–801 (1994).

124. Chambers, C. A., Kuhns, M. S., Egen, J. G. & Allison, J. P. CTLA-4-mediated inhibition in regulation of T cell responses: mechanisms and manipulation in tumor immunotherapy. *Annu. Rev. Immunol.* **19**, 565–594 (2001).
125. Seidel, J. A., Otsuka, A. & Kabashima, K. Anti-PD-1 and Anti-CTLA-4 Therapies in Cancer: Mechanisms of Action, Efficacy, and Limitations. *Front. Oncol.* **8**, (2018).
126. Gun, S. Y., Lee, S. W. L., Sieow, J. L. & Wong, S. C. Targeting immune cells for cancer therapy. *Redox Biol.* **25**, 101174 (2019).
127. He, M. *et al.* Remarkably similar CTLA-4 binding properties of therapeutic ipilimumab and tremelimumab antibodies. *Oncotarget* **8**, 67129–67139 (2017).
128. Cha, E. *et al.* Improved Survival with T Cell Clonotype Stability After Anti-CTLA-4 Treatment in Cancer Patients. *Sci. Transl. Med.* **6**, 238ra70-238ra70 (2014).
129. Kvistborg, P. *et al.* Anti-CTLA-4 therapy broadens the melanoma-reactive CD8+ T cell response. *Sci. Transl. Med.* **6**, 254ra128-254ra128 (2014).
130. Simpson, T. R. *et al.* Fc-dependent depletion of tumor-infiltrating regulatory T cells co-defines the efficacy of anti-CTLA-4 therapy against melanoma. *J. Exp. Med.* **210**, 1695–1710 (2013).
131. Romano, E. *et al.* Ipilimumab-dependent cell-mediated cytotoxicity of regulatory T cells ex vivo by nonclassical monocytes in melanoma patients. *Proc. Natl. Acad. Sci. U. S. A.* **112**, 6140–6145 (2015).
132. Ingram, J. R. *et al.* Anti-CTLA-4 therapy requires an Fc domain for efficacy. *Proc. Natl. Acad. Sci. U. S. A.* **115**, 3912–3917 (2018).
133. Arce Vargas, F. *et al.* Fc Effector Function Contributes to the Activity of Human Anti-CTLA-4 Antibodies. *Cancer Cell* **33**, 649-663.e4 (2018).

134. Maio, M. *et al.* Five-Year Survival Rates for Treatment-Naive Patients With Advanced Melanoma Who Received Ipilimumab Plus Dacarbazine in a Phase III Trial. *J. Clin. Oncol.* **33**, 1191–1196 (2015).
135. Savoia, P., Astrua, C. & Fava, P. Ipilimumab (Anti-Ctla-4 Mab) in the treatment of metastatic melanoma: Effectiveness and toxicity management. *Hum. Vaccines Immunother.* **12**, 1092–1101 (2016).
136. Topalian, S. L. *et al.* Survival, Durable Tumor Remission, and Long-Term Safety in Patients With Advanced Melanoma Receiving Nivolumab. *J. Clin. Oncol.* **32**, 1020–1030 (2014).
137. Wolchok, J. D. *et al.* Overall Survival with Combined Nivolumab and Ipilimumab in Advanced Melanoma. *N. Engl. J. Med.* **377**, 1345–1356 (2017).
138. Cac, J., Jam, V., J, L. & Rm, L. Biomarkers for Response of Melanoma Patients to Immune Checkpoint Inhibitors: A Systematic Review. *Front. Oncol.* **7**, (2017).
139. de Azevedo, S. J. *et al.* First-line atezolizumab monotherapy in patients with advanced BRAFV600 wild-type melanoma. *Pigment Cell Melanoma Res.* **34**, 973–977 (2021).
140. De Sousa Linhares, A. *et al.* Therapeutic PD-L1 antibodies are more effective than PD-1 antibodies in blocking PD-1/PD-L1 signaling. *Sci. Rep.* **9**, 11472 (2019).
141. Gutzmer, R. *et al.* Atezolizumab, vemurafenib, and cobimetinib as first-line treatment for unresectable advanced BRAFV600 mutation-positive melanoma (IMspire150): primary analysis of the randomised, double-blind, placebo-controlled, phase 3 trial. *The Lancet* **395**, 1835–1844 (2020).
142. Kitano, S., Nakayama, T. & Yamashita, M. Biomarkers for Immune Checkpoint Inhibitors in Melanoma. *Front. Oncol.* **8**, (2018).

143. Ye, Y. *et al.* Sex-associated molecular differences for cancer immunotherapy. *Nat. Commun.* **11**, 1779 (2020).
144. Castro, A. *et al.* Strength of immune selection in tumors varies with sex and age. *Nat. Commun.* **11**, 4128 (2020).
145. Herbst, R. S. *et al.* Predictive correlates of response to the anti-PD-L1 antibody MPDL3280A in cancer patients. *Nature* **515**, 563–567 (2014).
146. Daud, A. I. *et al.* Programmed Death-Ligand 1 Expression and Response to the Anti-Programmed Death 1 Antibody Pembrolizumab in Melanoma. *J. Clin. Oncol. Off. J. Am. Soc. Clin. Oncol.* **34**, 4102–4109 (2016).
147. Taube, J. M. *et al.* Association of PD-1, PD-1 ligands, and other features of the tumor immune microenvironment with response to anti-PD-1 therapy. *Clin. Cancer Res. Off. J. Am. Assoc. Cancer Res.* **20**, 5064–5074 (2014).
148. Cottrell, T. R. & Taube, J. M. PD-L1 and Emerging Biomarkers in Immune Checkpoint Blockade Therapy. *Cancer J. Sudbury Mass* **24**, 41–46 (2018).
149. Zerde, I., Matikas, A., Bergh, J., Rassidakis, G. Z. & Foukakis, T. Genetic, transcriptional and post-translational regulation of the programmed death protein ligand 1 in cancer: biology and clinical correlations. *Oncogene* **37**, 4639–4661 (2018).
150. Madore, J. *et al.* PD-L1 expression in melanoma shows marked heterogeneity within and between patients: implications for anti-PD-1/PD-L1 clinical trials. *Pigment Cell Melanoma Res.* **28**, 245–253 (2015).
151. Wolf, Y. *et al.* UVB-Induced Tumor Heterogeneity Diminishes Immune Response in Melanoma. *Cell* **179**, 219-235.e21 (2019).
152. Gros, A. *et al.* Prospective identification of neoantigen-specific lymphocytes in the peripheral blood of melanoma patients. *Nat. Med.* **22**, 433–438 (2016).

153. Goodman, A. M. *et al.* Tumor Mutational Burden as an Independent Predictor of Response to Immunotherapy in Diverse Cancers. *Mol. Cancer Ther.* **16**, 2598–2608 (2017).
154. Chalmers, Z. R. *et al.* Analysis of 100,000 human cancer genomes reveals the landscape of tumor mutational burden. *Genome Med.* **9**, 34 (2017).
155. Panda, A. *et al.* Identifying a Clinically Applicable Mutational Burden Threshold as a Potential Biomarker of Response to Immune Checkpoint Therapy in Solid Tumors. *JCO Precis. Oncol.* 1–13 (2017) doi:10.1200/PO.17.00146.
156. Gopalakrishnan, V. *et al.* Gut microbiome modulates response to anti–PD-1 immunotherapy in melanoma patients. *Science* **359**, 97–103 (2018).
157. Sivan, A. *et al.* Commensal *Bifidobacterium* promotes antitumor immunity and facilitates anti–PD-L1 efficacy. *Science* **350**, 1084–1089 (2015).
158. Routy, B. *et al.* Gut microbiome influences efficacy of PD-1–based immunotherapy against epithelial tumors. *Science* **359**, 91–97 (2018).
159. Rossi, E. *et al.* Efficacy of immune checkpoint inhibitors in different types of melanoma. *Hum. Vaccines Immunother.* **17**, 4–13 (2021).
160. Liu, D. *et al.* Integrative molecular and clinical modeling of clinical outcomes to PD1 blockade in patients with metastatic melanoma. *Nat. Med.* **25**, 1916–1927 (2019).
161. Kaunitz, G. J. *et al.* Melanoma subtypes demonstrate distinct PD-L1 expression profiles. *Lab. Invest.* **97**, 1063–1071 (2017).
162. Waldman, A. D., Fritz, J. M. & Lenardo, M. J. A guide to cancer immunotherapy: from T cell basic science to clinical practice. *Nat. Rev. Immunol.* **20**, 651–668 (2020).
163. Perica, K., Varela, J. C., Oelke, M. & Schneck, J. Adoptive T cell immunotherapy for cancer. *Rambam Maimonides Med. J.* **6**, e0004 (2015).

164. Rohaan, M. W., Wilgenhof, S. & Haanen, J. B. A. G. Adoptive cellular therapies: the current landscape. *Virchows Arch.* **474**, 449 (2019).
165. Morgan, R. A., Dudley, M. E. & Rosenberg, S. A. Adoptive cell therapy: genetic modification to redirect effector cell specificity. *Cancer J. Sudbury Mass* **16**, 336–341 (2010).
166. Rosenberg, S. A. *et al.* Use of Tumor-Infiltrating Lymphocytes and Interleukin-2 in the Immunotherapy of Patients with Metastatic Melanoma. *N. Engl. J. Med.* **319**, 1676–1680 (1988).
167. Rosenberg, S. A. *et al.* Durable Complete Responses in Heavily Pretreated Patients with Metastatic Melanoma Using T-Cell Transfer Immunotherapy. *Clin. Cancer Res.* **17**, 4550–4557 (2011).
168. Besser, M. J. *et al.* Clinical Responses in a Phase II Study Using Adoptive Transfer of Short-term Cultured Tumor Infiltration Lymphocytes in Metastatic Melanoma Patients. *Clin. Cancer Res.* **16**, 2646–2655 (2010).
169. Rohaan, M. W., Berg, J. H. van den, Kvistborg, P. & Haanen, J. B. A. G. Adoptive transfer of tumor-infiltrating lymphocytes in melanoma: a viable treatment option. *J. Immunother. Cancer* **6**, 102 (2018).
170. Kumar, A., Watkins, R. & Vilgelm, A. E. Cell Therapy With TILs: Training and Taming T Cells to Fight Cancer. *Front. Immunol.* **12**, (2021).
171. Kageshita, T., Hirai, S., Ono, T., Hicklin, D. J. & Ferrone, S. Down-Regulation of HLA Class I Antigen-Processing Molecules in Malignant Melanoma: Association with Disease Progression. *Am. J. Pathol.* **154**, 745–754 (1999).
172. Hicklin, D. J. *et al.* beta2-Microglobulin mutations, HLA class I antigen loss, and tumor progression in melanoma. *J. Clin. Invest.* **101**, 2720–2729 (1998).

173. Morgan, R. A. *et al.* Cancer Regression in Patients After Transfer of Genetically Engineered Lymphocytes. *Science* **314**, 126–129 (2006).
174. Ott, P. A., Dotti, G., Yee, C. & Goff, S. L. An Update on Adoptive T-Cell Therapy and Neoantigen Vaccines. *Am. Soc. Clin. Oncol. Educ. Book* e70–e78 (2019)
doi:10.1200/EDBK_238001.
175. Catros, V. Les CAR-T cells , des cellules tueuses spécifiques d'antigènes tumoraux: De nouvelles générations pour le traitement des tumeurs solides. *médecine/sciences* **35**, 316–326 (2019).
176. Johnson, L. A. *et al.* Gene therapy with human and mouse T-cell receptors mediates cancer regression and targets normal tissues expressing cognate antigen. *Blood* **114**, 535–546 (2009).
177. Pfefferle, A. & Huntington, N. D. You Have Got a Fast CAR: Chimeric Antigen Receptor NK Cells in Cancer Therapy. *Cancers* **12**, E706 (2020).
178. Lauss, M. *et al.* Mutational and putative neoantigen load predict clinical benefit of adoptive T cell therapy in melanoma. *Nat. Commun.* **8**, 1738 (2017).
179. Roy, S., Sethi, T. K., Taylor, D., Kim, Y. J. & Johnson, D. B. Breakthrough concepts in immune-oncology: Cancer vaccines at the bedside. *J. Leukoc. Biol.* **108**, 1455–1489 (2020).
180. Loughlin, K. R. William B. Coley. *Urol. Clin. North Am.* **47**, 413–417 (2020).
181. Hall, S. S. *A commotion in the blood : life, death, and the immune system*. (New York : Henry Holt, 1997).
182. Sylvester, R. J., van der MEIJDEN, A. P. M. & Lamm, D. L. Intravesical bacillus Calmette-Guerin reduces the risk of progression in patients with superficial bladder

- cancer: a meta-analysis of the published results of randomized clinical trials. *J. Urol.* **168**, 1964–1970 (2002).
183. Kantoff, P. W. *et al.* Sipuleucel-T Immunotherapy for Castration-Resistant Prostate Cancer. *N. Engl. J. Med.* **363**, 411–422 (2010).
184. OPTiM: A randomized phase III trial of talimogene laherparepvec (T-VEC) versus subcutaneous (SC) granulocyte-macrophage colony-stimulating factor (GM-CSF) for the treatment (tx) of unresected stage IIIB/C and IV melanoma. | Journal of Clinical Oncology. https://ascopubs.org/doi/abs/10.1200/jco.2013.31.18_suppl.lba9008.
185. Hamid, O., Ismail, R. & Puzanov, I. Intratumoral Immunotherapy—Update 2019. *The Oncologist* **25**, theoncologist.2019-0438 (2019).
186. Curran, M. A. & Glisson, B. S. New Hope for Therapeutic Cancer Vaccines in the Era of Immune Checkpoint Modulation. *Annu. Rev. Med.* **70**, 409–424 (2019).
187. Powell, D. J. & Rosenberg, S. A. Phenotypic and functional maturation of tumor antigen-reactive CD8+ T lymphocytes in patients undergoing multiple course peptide vaccination. *J. Immunother. Hagerstown Md 1997* **27**, 36–47 (2004).
188. Berger, T. G. *et al.* Circulation and homing of melanoma-reactive T cells to both cutaneous and visceral metastases after vaccination with monocyte-derived dendritic cells. *Int. J. Cancer* **111**, 229–237 (2004).
189. Chiong, B. *et al.* Characterization of long-term effector-memory T-cell responses in patients with resected high-risk melanoma receiving a melanoma Peptide vaccine. *J. Immunother. Hagerstown Md 1997* **27**, 368–379 (2004).
190. Speiser, D. E. *et al.* Evaluation of melanoma vaccines with molecularly defined antigens by ex vivo monitoring of tumor-specific T cells. *Semin. Cancer Biol.* **13**, 461–472 (2003).

191. Rosenberg, S. A., Yang, J. C. & Restifo, N. P. Cancer immunotherapy: moving beyond current vaccines. *Nat. Med.* **10**, 909–915 (2004).
192. Hailemichael, Y. *et al.* Persistent antigen at vaccination sites induces tumor-specific CD8⁺ T cell sequestration, dysfunction and deletion. *Nat. Med.* **19**, 465–472 (2013).
193. Croft, M., Benedict, C. A. & Ware, C. F. Clinical targeting of the TNF and TNFR superfamilies. *Nat. Rev. Drug Discov.* **12**, 147–168 (2013).
194. Curran, M. A. *et al.* Systemic 4-1BB activation induces a novel T cell phenotype driven by high expression of Eomesodermin. *J. Exp. Med.* **210**, 743–755 (2013).
195. Michot, J. M. *et al.* Immune-related adverse events with immune checkpoint blockade: a comprehensive review. *Eur. J. Cancer Oxf. Engl. 1990* **54**, 139–148 (2016).
196. Badoual, C. *et al.* PD-1-expressing tumor-infiltrating T cells are a favorable prognostic biomarker in HPV-associated head and neck cancer. *Cancer Res.* **73**, 128–138 (2013).
197. Duraiswamy, J., Kaluza, K. M., Freeman, G. J. & Coukos, G. Dual blockade of PD-1 and CTLA-4 combined with tumor vaccine effectively restores T-cell rejection function in tumors. *Cancer Res.* **73**, 3591–3603 (2013).
198. Hurwitz, A. A. *et al.* Combination immunotherapy of primary prostate cancer in a transgenic mouse model using CTLA-4 blockade. *Cancer Res.* **60**, 2444–2448 (2000).
199. Rice, A. E. *et al.* An HPV-E6/E7 immunotherapy plus PD-1 checkpoint inhibition results in tumor regression and reduction in PD-L1 expression. *Cancer Gene Ther.* **22**, 454–462 (2015).
200. Soares, K. C. *et al.* PD-1/PD-L1 blockade together with vaccine therapy facilitates effector T-cell infiltration into pancreatic tumors. *J. Immunother. Hagerstown Md 1997* **38**, 1–11 (2015).

201. van Elsas, A., Hurwitz, A. A. & Allison, J. P. Combination immunotherapy of B16 melanoma using anti-cytotoxic T lymphocyte-associated antigen 4 (CTLA-4) and granulocyte/macrophage colony-stimulating factor (GM-CSF)-producing vaccines induces rejection of subcutaneous and metastatic tumors accompanied by autoimmune depigmentation. *J. Exp. Med.* **190**, 355–366 (1999).
202. Wada, S. *et al.* Sequencing CTLA-4 blockade with cell-based immunotherapy for prostate cancer. *J. Transl. Med.* **11**, 89 (2013).
203. Liu, J. *et al.* Cancer vaccines as promising immuno-therapeutics: platforms and current progress. *J. Hematol. Oncol. J Hematol Oncol* **15**, 28 (2022).
204. Jaffee, E. M. *et al.* Novel allogeneic granulocyte-macrophage colony-stimulating factor-secreting tumor vaccine for pancreatic cancer: a phase I trial of safety and immune activation. *J. Clin. Oncol. Off. J. Am. Soc. Clin. Oncol.* **19**, 145–156 (2001).
205. Nemunaitis, J. GVAX (GMCSF gene modified tumor vaccine) in advanced stage non small cell lung cancer. *J. Control. Release Off. J. Control. Release Soc.* **91**, 225–231 (2003).
206. Nemunaitis, J. Vaccines in cancer: GVAX, a GM-CSF gene vaccine. *Expert Rev. Vaccines* **4**, 259–274 (2005).
207. Le, D. T. *et al.* Evaluation of ipilimumab in combination with allogeneic pancreatic tumor cells transfected with a GM-CSF gene in previously treated pancreatic cancer. *J. Immunother. Hagerstown Md 1997* **36**, 382–389 (2013).
208. Le, D. T. *et al.* Safety and survival with GVAX pancreas prime and Listeria Monocytogenes-expressing mesothelin (CRS-207) boost vaccines for metastatic pancreatic cancer. *J. Clin. Oncol. Off. J. Am. Soc. Clin. Oncol.* **33**, 1325–1333 (2015).

209. Kwiatkowska-Borowczyk, E. *et al.* Whole cell melanoma vaccine genetically modified to stem cells like phenotype generates specific immune responses to ALDH1A1 and long-term survival in advanced melanoma patients. *Oncoimmunology* **7**, e1509821 (2018).
210. Mackiewicz, J., Burzykowski, T., Iżycki, D. & Mackiewicz, A. Re-induction using whole cell melanoma vaccine genetically modified to melanoma stem cells-like beyond recurrence extends long term survival of high risk resected patients - updated results. *J. Immunother. Cancer* **6**, 134 (2018).
211. Vreeland, T. J. *et al.* A Phase IIb Randomized Controlled Trial of the TLPLDC Vaccine as Adjuvant Therapy After Surgical Resection of Stage III/IV Melanoma: A Primary Analysis. *Ann. Surg. Oncol.* **28**, 6126–6137 (2021).
212. Scariot, D. B. *et al.* Oral treatment with T6-loaded yeast cell wall particles reduces the parasitemia in murine visceral leishmaniasis model. *Sci. Rep.* **9**, 20080 (2019).
213. Herbert, G. S. *et al.* Initial phase I/Ia trial results of an autologous tumor lysate, particle-loaded, dendritic cell (TLPLDC) vaccine in patients with solid tumors. *Vaccine* **36**, 3247–3253 (2018).
214. Ribas, A. *et al.* Dendritic cell vaccination combined with CTLA4 blockade in patients with metastatic melanoma. *Clin. Cancer Res. Off. J. Am. Assoc. Cancer Res.* **15**, 6267–6276 (2009).
215. Wilgenhof, S. *et al.* Phase II Study of Autologous Monocyte-Derived mRNA Electroporated Dendritic Cells (TriMixDC-MEL) Plus Ipilimumab in Patients With Pretreated Advanced Melanoma. *J. Clin. Oncol. Off. J. Am. Soc. Clin. Oncol.* **34**, 1330–1338 (2016).

216. Crosby, E. J. *et al.* Vaccine-Induced Memory CD8+ T Cells Provide Clinical Benefit in HER2 Expressing Breast Cancer: A Mouse to Human Translational Study. *Clin. Cancer Res. Off. J. Am. Assoc. Cancer Res.* **25**, 2725–2736 (2019).
217. Madan, R. A. *et al.* Ipilimumab and a poxviral vaccine targeting prostate-specific antigen in metastatic castration-resistant prostate cancer: a phase 1 dose-escalation trial. *Lancet Oncol.* **13**, 501–508 (2012).
218. Spira, A. *et al.* Multicenter, Open-Label, Phase I Study of DSP-7888 Dosing Emulsion in Patients with Advanced Malignancies. *Target. Oncol.* **16**, 461–469 (2021).
219. Chung, H. C. *et al.* Efficacy and Safety of Pembrolizumab in Previously Treated Advanced Cervical Cancer: Results From the Phase II KEYNOTE-158 Study. *J. Clin. Oncol. Off. J. Am. Soc. Clin. Oncol.* **37**, 1470–1478 (2019).
220. Youn, J. W. *et al.* Pembrolizumab plus GX-188E therapeutic DNA vaccine in patients with HPV-16-positive or HPV-18-positive advanced cervical cancer: interim results of a single-arm, phase 2 trial. *Lancet Oncol.* **21**, 1653–1660 (2020).
221. De Keersmaecker, B. *et al.* TriMix and tumor antigen mRNA electroporated dendritic cell vaccination plus ipilimumab: link between T-cell activation and clinical responses in advanced melanoma. *J. Immunother. Cancer* **8**, e000329 (2020).
222. Jansen, Y. *et al.* A randomized controlled phase II clinical trial on mRNA electroporated autologous monocyte-derived dendritic cells (TriMixDC-MEL) as adjuvant treatment for stage III/IV melanoma patients who are disease-free following the resection of macrometastases. *Cancer Immunol. Immunother. CII* **69**, 2589–2598 (2020).
223. Sahin, U. *et al.* Personalized RNA mutanome vaccines mobilize poly-specific therapeutic immunity against cancer. *Nature* **547**, 222–226 (2017).

224. Türeci, Ö. *et al.* Targeting the Heterogeneity of Cancer with Individualized Neoepitope Vaccines. *Clin. Cancer Res. Off. J. Am. Assoc. Cancer Res.* **22**, 1885–1896 (2016).
225. Yarchoan, M., Johnson, B. A., Lutz, E. R., Laheru, D. A. & Jaffee, E. M. Targeting neoantigens to augment antitumour immunity. *Nat. Rev. Cancer* **17**, 209–222 (2017).
226. Hu, Z., Ott, P. A. & Wu, C. J. Towards personalized, tumour-specific, therapeutic vaccines for cancer. *Nat. Rev. Immunol.* **18**, 168–182 (2018).
227. Klebanoff, C. A. & Wolchok, J. D. Shared cancer neoantigens: Making private matters public. *J. Exp. Med.* **215**, 5–7 (2018).
228. Guo, Y., Lei, K. & Tang, L. Neoantigen Vaccine Delivery for Personalized Anticancer Immunotherapy. *Front. Immunol.* **9**, 1499 (2018).
229. Dzwierzynski, W. W. Melanoma Risk Factors and Prevention. *Clin. Plast. Surg.* **48**, 543–550 (2021).
230. Vragniau, C. *et al.* Synthetic self-assembling ADDomer platform for highly efficient vaccination by genetically encoded multiepitope display. *Sci. Adv.* **5**, eaaw2853 (2019).
231. Zakeri, B. *et al.* Peptide tag forming a rapid covalent bond to a protein, through engineering a bacterial adhesin. *Proc. Natl. Acad. Sci. U. S. A.* **109**, E690–697 (2012).
232. Bok, K., Sitar, S., Graham, B. S. & Mascola, J. R. Accelerated COVID-19 vaccine development: milestones, lessons, and prospects. *Immunity* **54**, 1636–1651 (2021).
233. Ho, J. K.-T., Jeevan-Raj, B. & Netter, H.-J. Hepatitis B Virus (HBV) Subviral Particles as Protective Vaccines and Vaccine Platforms. *Viruses* **12**, 126 (2020).
234. Villa, L. L. *et al.* Prophylactic quadrivalent human papillomavirus (types 6, 11, 16, and 18) L1 virus-like particle vaccine in young women: a randomised double-blind placebo-controlled multicentre phase II efficacy trial. *Lancet Oncol.* **6**, 271–278 (2005).

235. Nguyen, B. & Tolia, N. H. Protein-based antigen presentation platforms for nanoparticle vaccines. *Npj Vaccines* **6**, 70 (2021).
236. Reddy, S. T. *et al.* Exploiting lymphatic transport and complement activation in nanoparticle vaccines. *Nat. Biotechnol.* **25**, 1159–1164 (2007).
237. Caldeira, J. C., Perrine, M., Pericle, F. & Cavallo, F. Virus-Like Particles as an Immunogenic Platform for Cancer Vaccines. *Viruses* **12**, 488 (2020).
238. Zakeri, B. *et al.* Peptide tag forming a rapid covalent bond to a protein, through engineering a bacterial adhesin. *Proc. Natl. Acad. Sci.* **109**, E690–E697 (2012).
239. Brune, K. D. *et al.* Plug-and-Display: decoration of Virus-Like Particles via isopeptide bonds for modular immunization. *Sci. Rep.* **6**, 19234 (2016).
240. Li, L., Fierer, J. O., Rapoport, T. A. & Howarth, M. Structural Analysis and Optimization of the Covalent Association between SpyCatcher and a Peptide Tag. *J. Mol. Biol.* **426**, 309–317 (2014).
241. Keeble, A. H. & Howarth, M. Power to the protein: enhancing and combining activities using the Spy toolbox. *Chem. Sci.* **11**, 7281–7291 (2020).
242. Fender, P., Ruigrok, R. W., Gout, E., Buffet, S. & Chroboczek, J. Adenovirus dodecahedron, a new vector for human gene transfer. *Nat. Biotechnol.* **15**, 52–56 (1997).
243. Besson, S., Vragniau, C., Vassal-Stermann, E., Dagher, M. C. & Fender, P. The Adenovirus Dodecahedron: Beyond the Platonic Story. *Viruses* **12**, 718 (2020).
244. Chevillard, C. *et al.* Elicitation of potent SARS-CoV-2 neutralizing antibody responses through immunization with a versatile adenovirus-inspired multimerization platform. *Mol. Ther.* **30**, 1913–1925 (2022).
245. Martins, K. A., Bavari, S. & Salazar, A. M. Vaccine adjuvant uses of poly-IC and derivatives. *Expert Rev. Vaccines* **14**, 447–459 (2015).

246. Liu, C. *et al.* Synergy effects of Polyinosinic-polycytidylic acid, CpG oligodeoxynucleotide, and cationic peptides to adjuvant HPV E7 epitope vaccine through preventive and therapeutic immunization in a TC-1 grafted mouse model. *Hum. Vaccines Immunother.* **14**, 931–940 (2018).
247. Fender, P., Hall, K., Schoehn, G. & Blair, G. E. Impact of human adenovirus type 3 dodecahedron on host cells and its potential role in viral infection. *J. Virol.* **86**, 5380–5385 (2012).
248. Bellone, M. *et al.* Relevance of the Tumor Antigen in the Validation of Three Vaccination Strategies for Melanoma. *J. Immunol.* **165**, 2651–2656 (2000).
249. Epaillard, O. *et al.* Anti-tumor Immunotherapy via Antigen Delivery from a Live Attenuated Genetically Engineered *Pseudomonas aeruginosa* Type III Secretion System-Based Vector. *Mol. Ther.* **14**, 656–661 (2006).
250. Villegas-Mendez, A. *et al.* In vivo delivery of antigens by adenovirus dodecahedron induces cellular and humoral immune responses to elicit antitumor immunity. *Mol. Ther. J. Am. Soc. Gene Ther.* **18**, 1046–1053 (2010).
251. Del Val, M., Schlicht, H.-J., Ruppert, T., Reddehase, M. J. & Koszinowski, U. H. Efficient processing of an antigenic sequence for presentation by MHC class I molecules depends on its neighboring residues in the protein. *Cell* **66**, 1145–1153 (1991).
252. Kloetzel, P.-M. Antigen processing by the proteasome: Ubiquitin and proteasomes. *Nat. Rev. Mol. Cell Biol.* **2**, 179–188 (2001).
253. Nussbaum, A. K. *et al.* Cleavage motifs of the yeast 20S proteasome β subunits deduced from digests of enolase 1. *Proc. Natl. Acad. Sci.* **95**, 12504–12509 (1998).
254. Pulendran, B., Arunachalam, P. S. & O'Hagan, D. T. Emerging concepts in the science of vaccine adjuvants. *Nat Rev Drug Discov* **20**, 454–475.

255. Beutler, B. Inferences, questions and possibilities in Toll-like receptor signalling. *Nature* **430**, 257–263 (2004).
256. Kawai, T. & Akira, S. The role of pattern-recognition receptors in innate immunity: update on Toll-like receptors. *Nat. Immunol.* **11**, 373–384 (2010).
257. Alexopoulou, L., Holt, A. C., Medzhitov, R. & Flavell, R. A. Recognition of double-stranded RNA and activation of NF- κ B by Toll-like receptor 3. *Nature* **413**, 732–738 (2001).
258. Ammi, R. *et al.* Poly(I:C) as cancer vaccine adjuvant: knocking on the door of medical breakthroughs. *Pharmacol. Ther.* **146**, 120–131 (2015).
259. Zhao, W., Wu, J., Chen, S. & Zhou, Z. Shared neoantigens: ideal targets for off-the-shelf cancer immunotherapy. *Pharmacogenomics* **21**, 637–645 (2020).
260. Vragniaux, C. Modification des dodécaèdres bases de l'adénovirus de sérotype 3: Design et caractérisation d'un nouveau vecteur multi-épitopique polyvalent. *PhD Thesis* <https://hal.archives-ouvertes.fr/tel-02110396>, (2018).
261. Villegas-Méndez, A. *et al.* Functional characterisation of the WW minimal domain for delivering therapeutic proteins by adenovirus dodecahedron. *PLoS One* **7**, e45416 (2012).
262. Galinier, R., Gout, E., Lortat-Jacob, H., Wood, J. & Chroboczek, J. Adenovirus Protein Involved in Virus Internalization Recruits Ubiquitin-Protein Ligases [†]. *Biochemistry* **41**, 14299–14305 (2002).
263. Bachmann, M. F. & Jennings, G. T. Vaccine delivery: a matter of size, geometry, kinetics and molecular patterns. *Nat. Rev. Immunol.* **10**, 787–796 (2010).
264. Zabel, F., Kündig, T. M. & Bachmann, M. F. Virus-induced humoral immunity: on how B cell responses are initiated. *Curr. Opin. Virol.* **3**, 357–362 (2013).

265. Shibagaki, N. & Udey, M. C. Dendritic Cells Transduced with Protein Antigens Induce Cytotoxic Lymphocytes and Elicit Antitumor Immunity. *J. Immunol.* **168**, 2393–2401 (2002).
266. Cohen, A. A. *et al.* Mosaic nanoparticles elicit cross-reactive immune responses to zoonotic coronaviruses in mice. *Science* **371**, 735–741 (2021).
267. Cohen, J. The dream vaccine. *Science* **372**, 227–231 (2021).
268. Fender, P. Use of dodecahedron ‘VLPs’ as an alternative to the whole adenovirus. *Methods Mol. Biol. Clifton NJ* **1089**, 61–70 (2014).
269. Feola, S. *et al.* Peptides-Coated Oncolytic Vaccines for Cancer Personalized Medicine. *Front. Immunol.* **13**, 826164 (2022).
270. Anchim, A. *et al.* Humoral Responses Elicited by Adenovirus Displaying Epitopes Are Induced Independently of the Infection Process and Shaped by the Toll-Like Receptor/MyD88 Pathway. *Front. Immunol.* **9**, 1 (2018).